Analysis of Reinforced Embankments and Foundations Overlying Soft Soils

by

Vernon Ray Schaefer

Dissertation submitted to the Faculty of the

Virginia Polytechnic Institute and State University

in partial fulfillment of the requirements for the degree of

Doctor of Philosophy

in

Civil Engineering

APPROVED:

J. M. Duncan

G. W. Clough

R. M. Jones

R. D. Krebs

T. Kuppusamy

June, 1987

Blacksburg, Virginia

Analysis of Reinforced Embankments and Foundations Overlying Soft Soils

by

Vernon Ray Schaefer

J. M. Duncan

Civil Engineering

(ABSTRACT)

The use of tensile reinforcement to increase the tensile strength and shear strength of soils has lead to many new applications of reinforced soil. The use of such reinforcing in embankments and foundations over weak soils is one of the most recent applications of this technology. The studies conducted were concerned with the development of and application of analytical techniques to reinforced soil foundations and embankments over weak soils.

A finite element computer program was modified for application to reinforced soil structures, including consolidation behavior of the foundation soil. Plane strain and axisymmetric versions of the program were developed and a membrane element developed which has radial stiffness but no flexural stiffness. The applicability of the program was verified by comparing analytical results to case histories of reinforced embankments and to model studies of reinforced foundations.

A simplified procedure for computing the bearing capacity of reinforced sand over weak clay was developed which is more general than those previously available. Good agreement with available experimental results was obtained, providing preliminary verification of the procedure.

Extensive analyses were made of a reinforced embankment successfully constructed with no sign of distress, and of two reinforced embankments constructed to failure. These analyses showed that good agreement can be obtained between measured and calculated reinforcement forces, settlements, and pore pressures for both working and failure conditions. The analyses further show that the use of the finite element method and limit equilibrium analyses provide an effective approach for the design of reinforced embankments on weak foundations.

Acknowledgements

I would like to thank Prof. Mike Duncan for his helpful guidance, patience and insights during the course of this study. I have learned a great deal from this remarkable educator.

I also thank the other members of my committee: Wayne Clough, Robert Jones, Robert Krebs and T. Kuppusamy. Prof. Kuppusamy was particularly helpful with certain aspects of the finite element analyses.

The friendship shown by my fellow graduate students has made this endeavor all the more worthwhile. My sincerest graditude goes to Al Sehn, office mate and friend, who, with his family, kept the Midwest alive for us among the Southerners. Barry Milstone, John Pappas, Bryan Sweeney, Jopan Sheng, Jotaro Iwabuchi, Phillippe Mayu and John Volk enriched life at Virginia Tech. The laughter of John Pappas will always ring in my ears.

The Tensar Corporation supported much of the studies conducted. Computer time was provided by the Virginia Tech Computer Center. The Huntington District of the US Army Corps of Engineers provided the instrumentation data for Mohicanville Dike No. 2. The author also received the Pratt Presidential Engineering Fellowship during his studies, which eased the burden.

The greatest debt of gratitude is owed to my family. Through it all they have been at my side with their love and support. For all their support, I dedicate this work

Table of Contents

List of Illustrations

List of Tables

CHAPTER I

INTRODUCTION

Soil is one of the cheapest and most effective construction materials. When compacted, it finds use as subgrades for our roads, abutments for our bridges, foundations for structures, and fills for embankments and retaining walls, to name just a few. Despite its wide application, soil has inherent shortcomings in its structural capabilities; namely, it is unable to sustain tension or high levels of shear. This limits its use in certain applications. Within the last 20 years, however, it has been shown that soil can be reinforced with systems of small structural elements, thereby providing the needed tensile and shear strength and stiffness. With the advent of this new technology, many new applications have been developed including reinforced soil retaining walls, embankments and foundations.

The concept of strengthening soil by the addition of reinforcing materials is very old. Indeed, the basic principles are demonstrated in nature by birds and animals in the construction of nests and lodges. The reinforcement of clay bricks using reeds or straw probably began very early in civilization. Jones (1985) provides a detailed account of the historical record of the use of reinforced soil.

One of the examples Jones cites is that of a ziggurrat of the ancient city of Dur-Kurigatzu, now known as Agar-Quf. The ziggurrat, which is an ancient temple tower, is located five kilometers north of Baghdad.

It was constructed of clay bricks varying in thickness between 130-400 mm, reinforced with woven mats of reed laid horizontally on a layer of sand and gravel at vertical spacings between 0.5 and 2.0 m. This structure is presently 45 m tall, although it is estimated that its original height was around 80 m. It is thought to be over 3000 years old.

Other examples include reed-reinforced earth levees built by the Romans along the Tiber River; the Great Wall of China containing mixtures of clay and gravel reinforced with tamarisk branches; fortifications of alternate layers of logs and earth fill constructed by the Gauls; and the construction of earth retaining walls in the U.S. using wooden reinforcement by Munster as early as 1925.

The modern concept of reinforcing soil to resist tensile forces by the use of an indigenous material was proposed in the 1930's by Arthur Casagrande who idealized the problem in the form of a weak soil reinforced by high-strength membranes laid in horizontal layers. Holtz (1977) reports that Casagrande envisioned the use of steel rods and plates to reinforce embankments on weak soils, but rejected their use as uneconomical. Westergaard (1938) proposed an analytical approach to the problem in a paper in the 60th Anniversary Volume on Solid Mechanics dedicated to Stephen Timoshenko.

It was not until the work of a Frenchman, Henri Vidal, in the 1960's, however, that the use of reinforcement in soils became a practical matter. Vidal developed a system of earth reinforcement using horizontal metal strips behind a facing to construct vertical reinforced earth walls. The design procedures espoused by Vidal (1969) are based on the development

of adhesion or interaction between the reinforcement and the soil due to friction of sufficient means to restrain the soil as if acted upon by a lateral force equivalent to the at-rest pressure.

Since Vidal's pioneering work many different reinforcing materials have been developed, notably in the area of polymer-based materials. Today the use of steel bars, wire meshes, high-density polyethylene grids, woven and non-woven textiles, root mats and various forms of wood as reinforcement are commonplace in the construction of retaining walls, bridge abutments, dams, highway embankments, landslide repair and road construction over soft soils.

Although the use of reinforcement in soils has been one of the leading new technologies in the area of geotechnical engineering, the development of rational design methods has not always kept pace with the new applications of reinforced soil or the new materials proposed for use as reinforcement. Since the 1960's, a wealth of literature on soil reinforcement has developed, much of it pertaining to the use of reinforced soil in retaining structures. It is only recently that attention has turned to the application of reinforced soil embankments and foundations overlying soft soils.

In this light, this study was directed to development of a rational understanding of the analysis and design of reinforced soil structures overlying weak or soft soils. To this end there are two numerical approaches which may be applied rationally - namely limit equilibrium methods and finite element methods. Both of these approaches have found considerable use in geotechnical engineering, yet advances and confidence

in their use has come only when the numerical results have been tested against actual behavior of geotechnical structures. Therefore, the analysis of well-documented case histories formed a significant part of the work performed in this study.

Chapter II reviews the literature on reinforced embankments and describes many of the factors which come into play when analyzing reinforced embankments. In this study, a finite element code was adapted for the analysis of reinforced soil structures over soft soils, and this is described in Chapter III. In Chapter IV, a brief review of reinforced foundations is presented and a method for determining the bearing capacity of reinforced foundations over soft clay is proposed and compared to available model test data. The applicability of the finite element method for analysis of reinforced foundations is also considered in Chapter IV. In Chapters V and VI, the finite element method is used to analyze case histories, and the calculated and measured behavior of reinforced embankments on weak soils are compared. A summary is presented in Chapter VII.

CHAPTER II

REINFORCED EMBANKMENTS

2.1 Introduction

Using reinforced soils in embankments is a relatively recent practice, springing from the need to construct haul roads and earth dams on relatively weak soils and road embankments in areas short on right-of-way. Reinforcement of soil allows construction of slopes and embankments having steep side slopes and over weak foundation soils. Early design procedures for embankments over good foundation subsoils followed the successful procedures used in the design of reinforced soil retaining walls (Jewell et al. 1984 and Leshchinsky 1984). It was a relatively straightforward matter to extend procedures for vertical retaining walls to those sloping from 30° to 80° from the horizontal. The analysis of reinforced embankments over weak subsoils is somewhat more complex owing to uncertainties introduced by the weak subsoils.

The successful design of a reinforced embankment must take account of the internal stability of the embankment, the overall stability of the embankment and foundation, and the stability of the foundation. These conditions are illustrated in Figure 2.1.

Internal stability can be evaluated by computing the resistance to sliding of the embankment over the reinforcement. This is accomplished by calculating the horizontal force exerted by the embankment and the

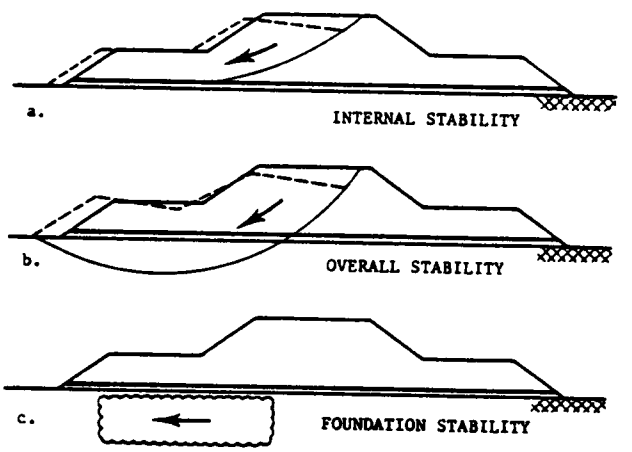

Figure 2.1 **Schematic of a reinforced embankment on a soft foundation and the three principal failure mechanisms (Jewell, 1982).**

resistance provided by the soil-reinforcement interface. Using a wedge analysis procedure, the factor of safety can be computed as:

$$F_s = \frac{\gamma H^2 K_a}{\gamma HL \tan \varphi_{sf}} \qquad [2.1]$$

where γ is the unit weight of the embankment soil, H is the height of the embankment, K_a is the active lateral earth pressure coefficient, L is the length of reinforcement from the crest to the toe, φ_{sf} is the angle to interaction between the soil and the reinforcement and F_s is the factor of safety with respect to sliding failure. Alternately, circular and noncircular limit equilibrium methods may be used to assess internal stability.

Foundation stability can be evaluated using conventional bearing capacity analysis methods assuming the embankment to be an infinitely long strip (Christopher and Holtz, 1984). Additionally, lateral squeeze of the foundation soil under a rigid embankment can be analyzed using a plastic flow method for squeeze between two plates as described by Jurgenson (1934).

Stability analysis of embankments on soft, weak soils has long proved to be a difficult task for geotechnical engineers. Bjerrum (1972) summarizes much of the effort spent on relating stability calculations to case histories and field and laboratory measured soil strengths. His summary shows that stability analyses do not always predict embankment behavior on soft soils accurately. Despite this, stability analyses are a useful and reliable tool for experienced geotechnical engineers and have

remained the dominant analysis procedure. In addition, finite element techniques have been used to gain further insight into embankment behavior (Duncan, 1972).

The procedures used for analysis and design of reinforced embankments have naturally followed those used for unreinforced embankments. Thus limit equilibrium and finite element analyses have been used to analyze and design reinforced embankments. The application of these procedures to reinforced embankments is more fully described below.

2.2 Limit Equilibrium Methods

2.2.1 General

The use of limit equilibrium techniques for analyzing unreinforced slopes and embankments is well accepted geotechnical engineering practice. The extension of these procedures to reinforced slopes and embankments is, however, not always straightforward. Uncertainties exist in the procedure used to incorporate the reinforcement strength into the stability analysis, the strength of the reinforcement to input into the analysis, the mechanism of soil-reinforcement interaction, all this in addition to the usual uncertainties in regard to construction on soft soils. An analysis of the stability of a reinforced soil slope or embankment requires consideration of both the external forces necessary to maintain stability and the internal forces necessary to ensure reinforcement integrity.

Several limit equilibrium approaches have been proposed for the analysis of reinforced embankments. While most of these methods involve some type of modification of common slip circle analysis, there are distinct differences in the details of the modifications proposed. Common to all of the methods is the assumption of rigid-plastic soil behavior. Additionally, most of these methods make no provision for embankment-reinforcement interaction and deformation behavior.

The details of several limit equilibrium techniques are summarized in Table 2.1. As may be seen, the approaches include extension of the Ordinary Method of Slices, extension of Bishop's Modified Method, the use wedge-type analyses, and the use of variational calculus combined with extremization.

The first extension of limit equilibrium methods to the design of reinforced embankments appears to be that of Wager (1968) who analyzed an anchored sheetpile wall used to reinforce a road embankment on a soft subsoil. The analysis consisted of adding a resisting moment due to the anchor force to the resisting moment along a circular slip surface in the foundation. The method was presented in English by Wager and Holtz (1976). Broms (1977) discussed Wager's procedure and how it could be applied to polyester fabric reinforced embankments. Christopher and Holtz (1984) report that the procedure has been successfully applied in 30 or so cases.

Christie and El-Hadi (1977) proposed an extension to the Ordinary Method of Slices (OMS) to account for horizontal forces necessary to maintain stability. In their formulation, the factor of safety applied

Table 2.1 Limit equilibrium techniques applied to reinforced embankments.

REFERENCE		METHOD
Wager	1968	Added the resisting moment due to an anchored sheetpile wall to resisting moment developed along a circular slip surface in the foundation. Resistance force in the anchor computed as full passive earth pressure. Procedure applied to edge failure of road embankments. Fill resistance calculated in terms of an equivalent active earth pressure.
Wager and Holtz	1976	English version of Wager (1968). Emphasized that a total stress analysis for end-of-construction conditions is critical. Full shearing strength of embankment is considered as it is unlikely that a crack will develop at failure due to presence of reinforcement.
Broms	1977	The factor of safety for the critical circle for the unreinforced embankment is found by conventional means. The required moment and required horizontal force necessary to raise the factor of safety to an acceptable value (1.3 to 1.5) are then determined to find the reinforcement strength.
Christie and El-Hadi	1977	Modified the Ordinary Method of Slices to include a resisting moment due to horizontal forces.
Bell	1980	Extended circular arc analyses to include resiting moment due to horizontal forces.
Brakel, Coppens, Maagdenberg and Risseeuw	1982	Modified the Ordinary Method of Slices to include a resisting moment due to horizontal forces. Used earth pressure theory to evaluate sliding mode of failure. Comparison to Almere, Netherlands test embankment showed good agreement using force in fabric of 80 kN/m. Measured force was 95 kN/m.

Table 2.1 Limit equilibrium techniques applied to reinforced embankments (cont.).

REFERENCE		METHOD
Fowler	1982	Used Bishop's Modified Method. Fabric is modelled as an equivalent cohesive layer with $\phi = 0$. Pinto Pass case history.
Jewell	1982	Modified equilibrium equations for slip circle analyses, i.e. F = Mr/Mo by $\Delta Mr = P \bullet yr$, P = mobilized reinforcement force, yr = moment arm. Add ΔMr to Mr to obtain Fr = $(Mr + \Delta Mr)/Mo$. Considers horizontal force only. Excludes strength of embankment in resisting moment, i.e., assumes a fully cracked section. Compared method to Almere, Netherlands and Pinto Pass, Alabama case histories and concluded that the results verify the procedure although no specific data are given to support the contention.
Ingold	1982	Modified Bishop's Modified Method to include resisting moment due to horizontal orientation of reinforcement. Proposed using horizontal orientation as it is a lower bound solution and thus is conservative.
Murray	1982	Used a bilineal slip plane and developed an expression for the factor of safety to include deformation criteria (extension of fabric). Is a wedge type analysis. Very mathematical.
Jewell, Paine and Woods	1984	Developed two-part wedge surface procedure for steep slope reinforced embankments over stable ground. Result is design charts for using Tensar geogrids. In the development of the charts, the bond angle is assumed to be one-half of design friction angle of the soil, and frictional resistance to sliding over geogrids is assumed to be 80% of design friction angle of the soil, thus incorporating factors of safety into the charts.

Table 2.1 Limit equilibrium techniques applied to reinforced embankments (cont.).

REFERENCE	METHOD
Milligan and La Rochelle 1984	Developed a circular arc analysis in dimensionless form. Included horizontal reinforcing force. Extended this to shallow translational failures. Considered fill resistance in the form of a Coulomb failure surface to be replaced by a single active force.
Leshchinsky 1984	Method based on limiting equilibrium combined with extremization using variational calculus. Mathematical.
Rowe and Soderman 1984	Modified Bishop's Modified Method to include resisting moment due to either horizontal or tangential orientation of the reinforcement. No details of the modifications made are presented. Verification of procedure is made by comparison to Almere, Netherlands case history for a fabric force of 80 kN/m.
McGown, Paine and DuBois 1984	Presents a discussion of strain compatibility between soil and geogrids. Provides guidelines on selection of soil and geogrid strengths, interlock friction, and factors of safety to apply to these values.
Jones 1985	Textbook. Reports method of Jewell, 1982. Includes procedures for evaluating internal stability, i.e., bond length.
Jewell 1985	Describes design philosophies. Based on locus of maximum required force and on locus of zero required force. Shows that equal length reinforcing causes shedding of force to lower layers due to bond stress limits. Describes compatibility curve for designing extensible reinforcing.

Table 2.1 Limit equilibrium techniques applied to reinforced embankments (cont.).

REFERENCE		METHOD
Low	1985	Modified Bishop's Modified Method to include resisting moment due to either horizontal or tangential orientation of the reinforcement. Verification of procedures by comparison to Almere, Netherlands case history.

to the soil strength is also applied to the reinforcement force. Bell (1980) also proposed extending circular arc analyses for horizontal reinforcement forces. Brakel et al. (1982) proposed adding a counteracting moment due to the reinforcement force acting tangential to the slip surface to the unreinforced OMS slip circle analysis.

Wedge type analyses have been developed by Murray (1982) and Jewell, Paine and Woods (1984). Murray (1982) used a bilineal slip plane and incorporated deformation criteria for the reinforcement in the analysis to arrive at expressions for the factor of safety. Jewell, Paine and Woods used two part wedge analysis to consider the slip surface development in reinforced embankments over stable foundations.

A procedure based on limiting equilibrium combined with extremization using variational calculus was developed by Leshchinsky (1984). Charts have been developed from this procedure and are applicable to reinforced embankments on stable foundations with slope angles varying from 30° to 90° (Leshchinsky and Volk, 1984).

Bishop's Modified Method (BMM) has been used extensively in the analysis of unreinforced embankments and has subsequently been used in the analysis of reinforced embankments. Fowler (1982) modelled the reinforcement as an equivalent cohesive layer with $\varphi = 0$ in a BMM analysis. Ingold (1982a) extended Bishop's Modified Method to account for horizontal orientation of reinforcement, but recognized that the assumption of horizontal orientation was conservative. Rowe and Soderman (1984) and Low (1985) have extended Bishop's Modified Method to include either hor-

izontal or tangential orientation of the reinforcement at the failure surface.

In these extensions, a restoring moment due to the fabric force is added to the unreinforced restoring moment, assuming the reinforcement force acts either parallel to the original reinforcement position (i.e., horizontal) or tangential to the slip surface at the point of intersection of the slip circle surface and the reinforcement. The subject of orientation of the reinforcement force at failure is discussed in more detail in Section 2.2.3. Low showed that the manner in which the factor of safety is defined is important. The effect of the reinforcement can be included in the definition of factor of safety in two ways: as an additional force resisting failure or as a reduction in the forces causing failure. This concept is explored in more detail below.

More recently Rowe and Soderman (1985) have extended their method to include a more rigorous treatment of the compatibility between soil strains and reinforcement strains. This is discussed in more detail in Section 2.2.4.

Milligan and La Rochelle (1984) have correctly pointed out that extending conventional limit equilibrium procedures to include the effects of reinforcement does not eliminate the errors and uncertainties which exist in current unreinforced stability analyses.

Chart solutions for simple configurations of embankment and foundation geometries and various reinforcement strengths have been prepared by Fowler (1982), Ingold (1982a), Rowe (1984), Leshchinsky and Volk (1984) and Low (1985).

2.2.2 Definition of Factor of Safety

The factor of safety without reinforcement may be defined as the factor by which the shear strength must be divided to bring the slope into a state of barely stable equilibrium:

$$F_o = \frac{\text{shear strength}}{\text{shear stress required for equilibrium}} \qquad [2.2]$$

To evaluate the shear stress required for equilibrium, the geometry of of the problem is divided into a number of slices as shown in Figure 2.2 and moments are summed about the center of the circular arc. By satisfying the equations of equilibrium, both the shear strength and the shear stress can be expressed in terms of the geometry of the slope and the properties of the soil. The resulting factor of safety may be expressed in terms of moments as:

$$F_o = \frac{M_R}{M_o} \qquad [2.3]$$

where M_R is the resisting moment of the soil and M_o is the overturning moment. Formulation of the Ordinary Method of Slices (OMS) and Bishop's Modified Method (BMM) are obtained by summing appropriate moments and are described in many soil mechanics textbooks, for example, see Lambe and Whitman (1979).

The factor of safety of a reinforced slope or embankment my be expressed as:

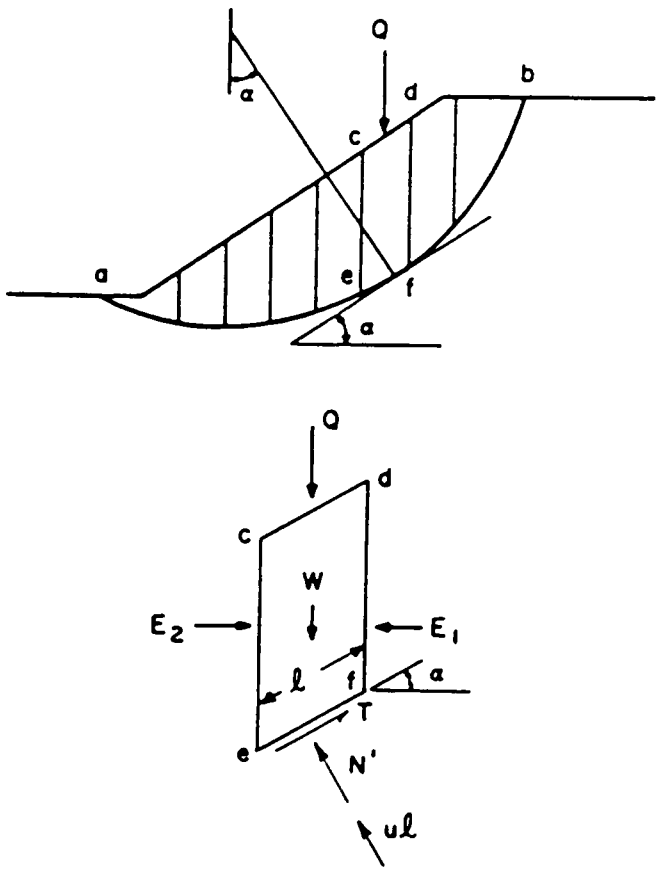

Bishop's Method;

$$FS = \frac{\Sigma(c'l + \tan\phi' \cdot N')}{\Sigma w \sin\alpha}$$

where: $N' = N'(FS, \ldots\ldots)$

Σ indicates summation over all the slices.

Figure 2.2 Method of slices.

$$F_R = \frac{(M_R + M_T)}{M_o} \qquad [2.4]$$

where M_T is the resisting moment of the reinforcement, and M_R and M_o are as previously defined. These definitions, as applied to a slip circle, are shown in Figure 2.3. An implicit assumption in this definition is that there are no interactions between the soil and reinforcement that change the individual contributions of M_R and M_T.

Equation 2.4 can be rearranged in the following form:

$$M_o = \frac{M_R}{F_R} + \frac{M_T}{F_R} \qquad [2.5]$$

from which it is evident that the definition of F_R as given by Equation 2.4 implies that both the soil resisting moment and the reinforcement resisting moment are divided by the same factor F_R to bring the slope or embankment to a condition of barely stable equilibrium.

It should be emphasized that the term M_T in Eqns. 2.4 and 2.5 represents the potential resisting moment that the reinforcement is capable of providing, given sufficient strain. The enhanced safety of a reinforced embankment may not be noticeable at working conditions if the mobilized force in the reinforcement is small. Nevertheless, the potential strength of the reinforcement is latent in the system and provides an added margin of safety. A reinforced embankment not close to failure might exhibit almost the same behavior as its unreinforced counterpart. However, if both embankment heights were increased gradually (or, equivalently, if foundation shear strength was decreased gradually), the re-

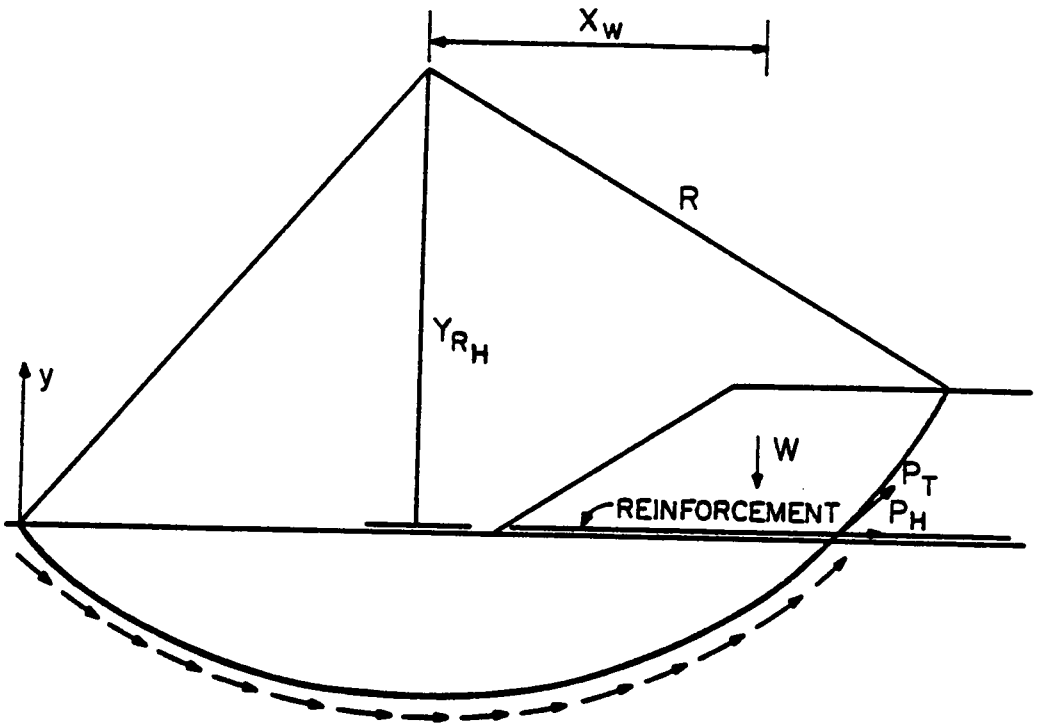

Disturbing moment : $M_o = W \cdot x_w$

Soil Resisting moment : $M_R = (\sum \tau_s . AL) \cdot Y_R$

Reinforcement Resisting moment : $M_{T_H} = P \cdot Y_R$

$M_{T_f} = P \cdot R$

P = reinforcement force , F/L

Figure 2.3 Definitions and forces for a slip circle analysis of a reinforced embankment.

inforced embankment would eventually reach a greater height (or withstand a smaller foundation shear strength) than the unreinforced embankment before a failure would occur.

The definition of F_R may also be considered in terms of the reinforcing moment playing the role of reducing the overturning moment. In this case the force is an external one and the factor of safety, with stabilizing force T, is defined as:

$$F'_R = \frac{M_R}{(M_O - M'_T)} \qquad [2.6]$$

where M'_T is the moment due to the force T. Equation 2.6 can be rearranged as follows:

$$M_O = \frac{M_R}{F'_R} + M'_T \qquad [2.7]$$

It is thus clear that in this case the externally applied reinforcing moment M'_T is not divided by F'_R in formulating the equilibrium condition.

A factor of safety can be applied to the soil resisting moment and the reinforcing resisting moment, thus obtaining a the factor of safety for the system. This is not the case in Equation 2.6 and thus the preceding discussions make it clear that the factor of safety as defined by Equation 2.4 is the more appropriate one for a reinforced embankment or slope.

The improvement in the factor of safety due to reinforcement may be incorporated in a stability analysis by adding $\frac{M_T}{M_O}$ to the factor of

safety for the same circle without reinforcement as calculated by the OMS or BMM, and results in

$$F_R = F_O + \frac{M_T}{M_O} \qquad [2.8]$$

where F_O is the unreinforced factor of safety calculated by Eqn. 2.2 or 2.3. The value of M_T is dependent upon the reinforcement orientation, which can be specified to be either horizontal or tangential to the slip surface, as discussed in the next section. M_T may then defined within a computer program as:

$$M_{Th} = \Sigma[T_i(Y_i - Y_c)] \qquad [2.9a]$$

or

$$M_{Tt} = \Sigma[T_i(\text{Radius of slip circle})] \qquad [2.9b]$$

where

M_{Th} = resisting moment due to reinforcement with horizontal orientation.
M_{Tt} = resisting moment due to reinforcement with tangential orientation.
T_i = force in i-th layer of reinforcement where it is intersected by the slip circle.
Y_i = Y coordinate of reinforcement.
Y_c = Y coordinate of circle center.

The force in a layer of reinforcement can be varied along the length of the reinforcement.

Two assumptions are inherent in the definition of the factor of safety:

1. The potential slip surface intersects the reinforcement far from the free end of the reinforcement so that if failure occurs, the full strength of the reinforcement can be developed. This is a requirement of sufficient anchorage to develop the full strength of the reinforcement.

2. The will be no relative slip between the reinforcement and the soil.

Thus, in practical application of the methods discussed above, a separate determination of the proper reinforcement force to use must be made, as well as checking that soil-reinforcement bond is sufficient. These concepts are explored in further detail in Sections 2.2.4 and 2.2.5, respectively.

2.2.3 Orientation of Reinforcement at the Slip Surface

The possibility of the reinforcement orientation being changed due to the relative movement of soil along the slip surface has been considered by Romstad et al. (1978), Rowe and Soderman (1984) and Leshchinsky (1984), Low (1985) and others. There are two directions commonly assumed. The first is that the reinforcement force acts horizontally as shown in Figure 2.4a. The second assumes a tangential orientation to the slip surface as depicted in Figure 2.4b. The need to consider reinforcement orientation arises because relative movement along the slip surface may change the orientation.

1) Reinforcement remains horizontal
at the slip surface

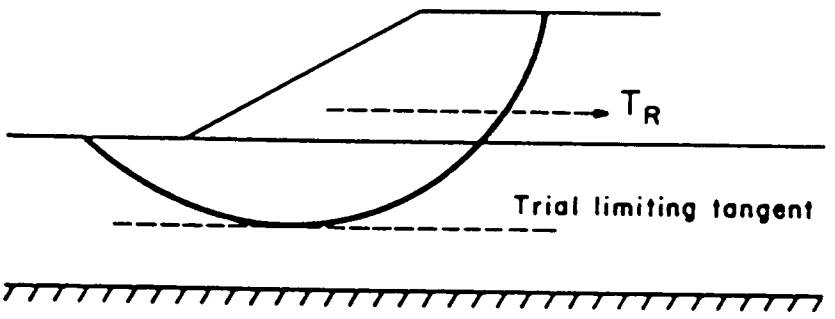

2) Reinforcement becomes tangential
at the slip surface

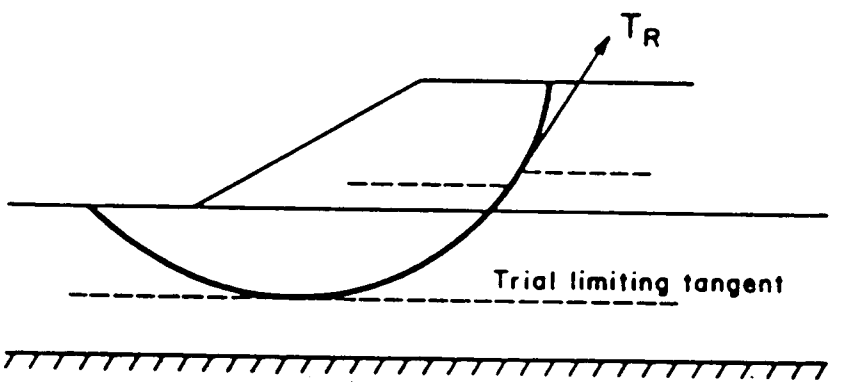

Figure 2.4 Orientation of reinforcement at the slip surface.

At working conditions with a factor of safety greater than unity the relative displacement of the soil along the slip surface may be too small to change the orientation of the reinforcement significantly. Nevertheless, since F_R is defined in terms of the potential strength of the reinforcement, it seems consistent with this notion to use potential orientation (the orientation that the reinforcement is likely to assume at failure) in combination with the potential strength of the reinforcement when computing the potential reinforcing moment, M_T for use in Equation 2.4.

The orientation at failure of an initially horizontal reinforcement naturally depends on the flexural rigidity of the reinforcement. The two diagrams in Figure 2.4 represent the extreme possible orientations of initially horizontal reinforcement at failure. The situation shown in the top diagram would be realistic in the extreme case of very stiff steel bar reinforcement whereas that shown in the bottom diagram is only possible in the case of reinforcement having negligible flexural rigidity.

It should be noted that when the reinforcement is tangentially oriented at the slip surface, it probably has less effect on the normal force acting on the slip surface than when the reinforcement remains horizontal. For the condition shown in Figure 2.4, the normal force and consequently the shear strength of the soil near the slip surface would be increased as a result of the normal component of the reinforcing force. This effect is ignored in conventional limit equilibrium analyses. In contrast, the orientation in the bottom diagram leads to a longer lever arm and hence greater potential resisting moment from the reinforcement, although the

normal force on the slip surface and the increase in the strength of the soil would likely be smaller in this case. There thus may be some compensating effects that would tend to keep the overall resistance about the same as the orientation of the reinforcement changes. The factor of safety calculated assuming tangentially oriented and horizontally oriented reinforcement are believed to represent reasonable values of the upper and lower bounds for the reinforced factor of safety.

A computer program based on Bishop's Modified Method and the definition of M_T described above has been developed and is capable of computing the factor of safety assuming either horizontally oriented reinforcement or tangentially oriented reinforcement, (Duncan et al. 1985). The approximate relationship between the ratio of $\frac{F_{Rt}}{F_{Rh}}$ and $\frac{D}{H}$ was developed by Low (1985) and is shown in Figure 2.5. In this figure, F_{Rt} is the increase in the factor of safety with tangential oriented reinforcement, and F_{Rh} is that corresponding to horizontal oriented reinforcement. It can be seen that the factor of safety due to tangential oriented reinforcement is always larger than that due to horizontal oriented reinforcement and that the ratio of the two increases as the depth of the weak foundation increases. The work by Low (1985) and Rowe and Soderman (1984, 1985) suggests that using the average of the factor of safety obtained from trials considering horizontal and tangential orientations yields satisfactory and conservative design results.

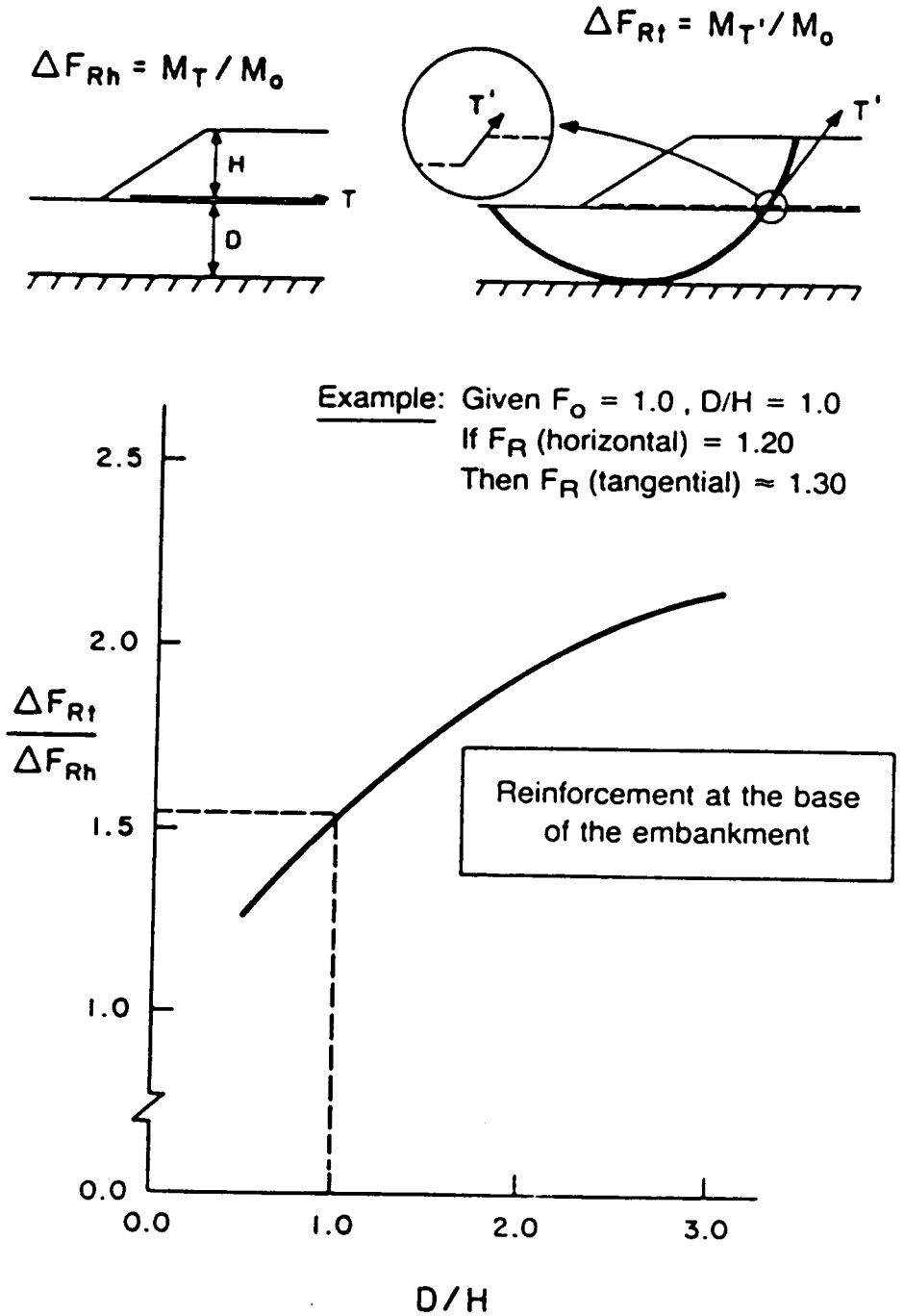

Figure 2.5 Approximate ratio of factor of safety calculated using tangential and horizontal orientations (after Low, 1985).

2.2.4 Selection of Reinforcement Forces for Design

The use of limit equilibrium procedures results in a factor of safety with respect to the ultimate limit state and is based on the potentially realizable strengths of both the soil and the reinforcement. For soil this strength is normally its peak value, however, for strain softening soils this may be its residual strength. The strength of tensile reinforcement which can be mobilized in a reinforced soil embankment is subject to the following limitations: (1) the ultimate strength of the reinforcement, (2) the minimum force required to cause failure of the reinforcement-soil interface, this may be either through pullout failure or through shearing failure of the interface, and (3) the force mobilized at a strain compatible with the strain occurring in the soil (Rowe and Soderman, 1984). Failure modes for the reinforcement-soil interface under field conditions are shown in Figure 2.6.

2.2.4.1 Ultimate Strength

If the reinforcement in an embankment is stressed to its ultimate strength and ruptures, a catastrophic failure may ensue. To avoid such an event, engineers are obliged to design reinforcement to ensure that its ultimate strength is not exceeded. For the plethora of man-made geotextiles and geogrids on the market today, it is necessary to ensure that the mobilized force at working conditions is below their long-term creep strength. This requires particularly close attention because the

(a) Pullout mode of failure

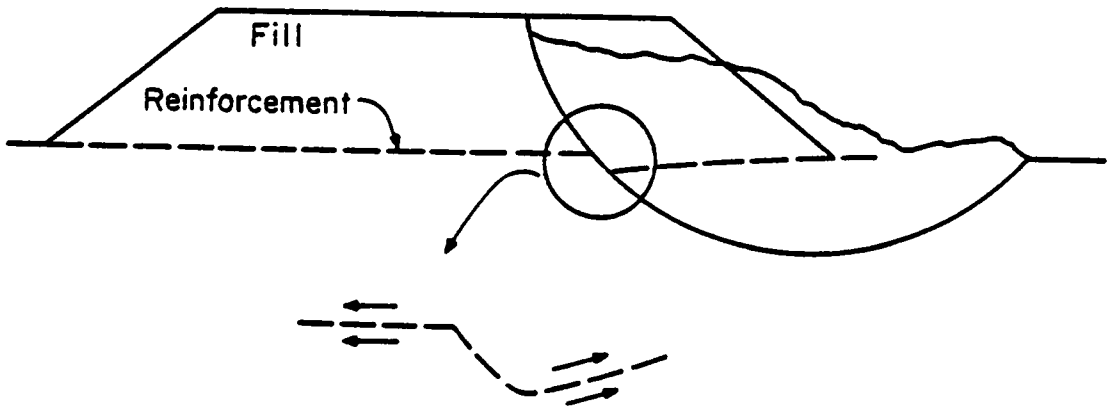

Pullout of reinforcement from fill due to inadequate interface strength.

(b) Direct Shear Mode.

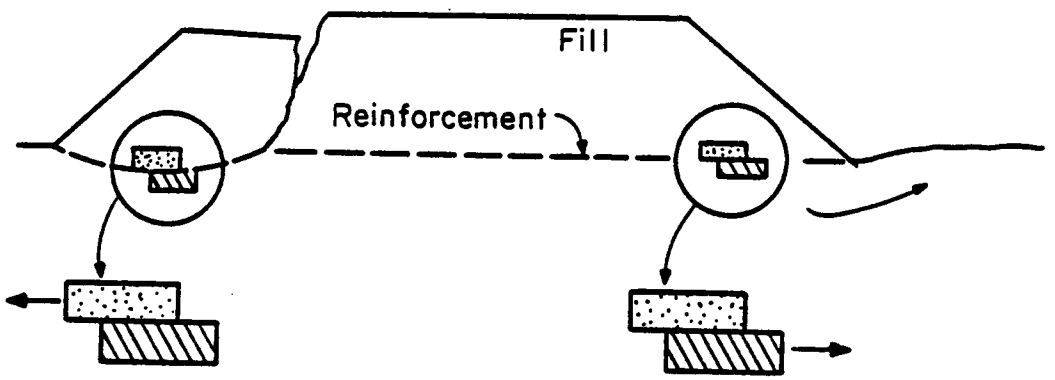

Fill can slide over reinforcement and foundation or if a slip surface develops in foundation the foundation can slide out from under the fill.

Figure 2.6 Failure modes for reinforcement-soil interface in the field.

creep strength (i.e., long-term ultimate strength) of these products can often be only 40 to 60 percent of the ultimate strength as measured in short-term laboratory tests (Rowe et al. 1984 and McGown et al. 1984).

Figure 2.7 shows the relationships which might exist between ductile and brittle soils and reinforcing having the same ultimate strength but different moduli. Reinforcement Types A, B and C represent, respectively, high, medium and low modulus geotextiles. For a structure built on a brittle soil and designed using a reasonable factor of safety, the system will not reach the limiting conditions but rather equilibrium will be maintained at a working level well below the peak strength of the soil, as shown in Figure 2.7. However, at working conditions, reinforcement Type A would be stressed above its allowable load (allowable load = ultimate strength/factor of safety). On the other hand, a lower modulus reinforcement, such as Type C, may be mobilized to a working force representing only a small fraction of its ultimate strength. Both cases are undesirable. The first case implies that more reinforcement would be needed to reduce the stress in the reinforcement at working conditions. The second case implies that the reinforcement would play a more significant role in stabilizing the embankment and in reducing deformations if it possessed a higher modulus. In fact, such restraining effects are desirable for a foundation material which tends to exhibit strain-softening behavior. A more desirable condition would therefore be obtained using reinforcement possessing the same strength but having an intermediate value of modulus such that at working conditions the re-

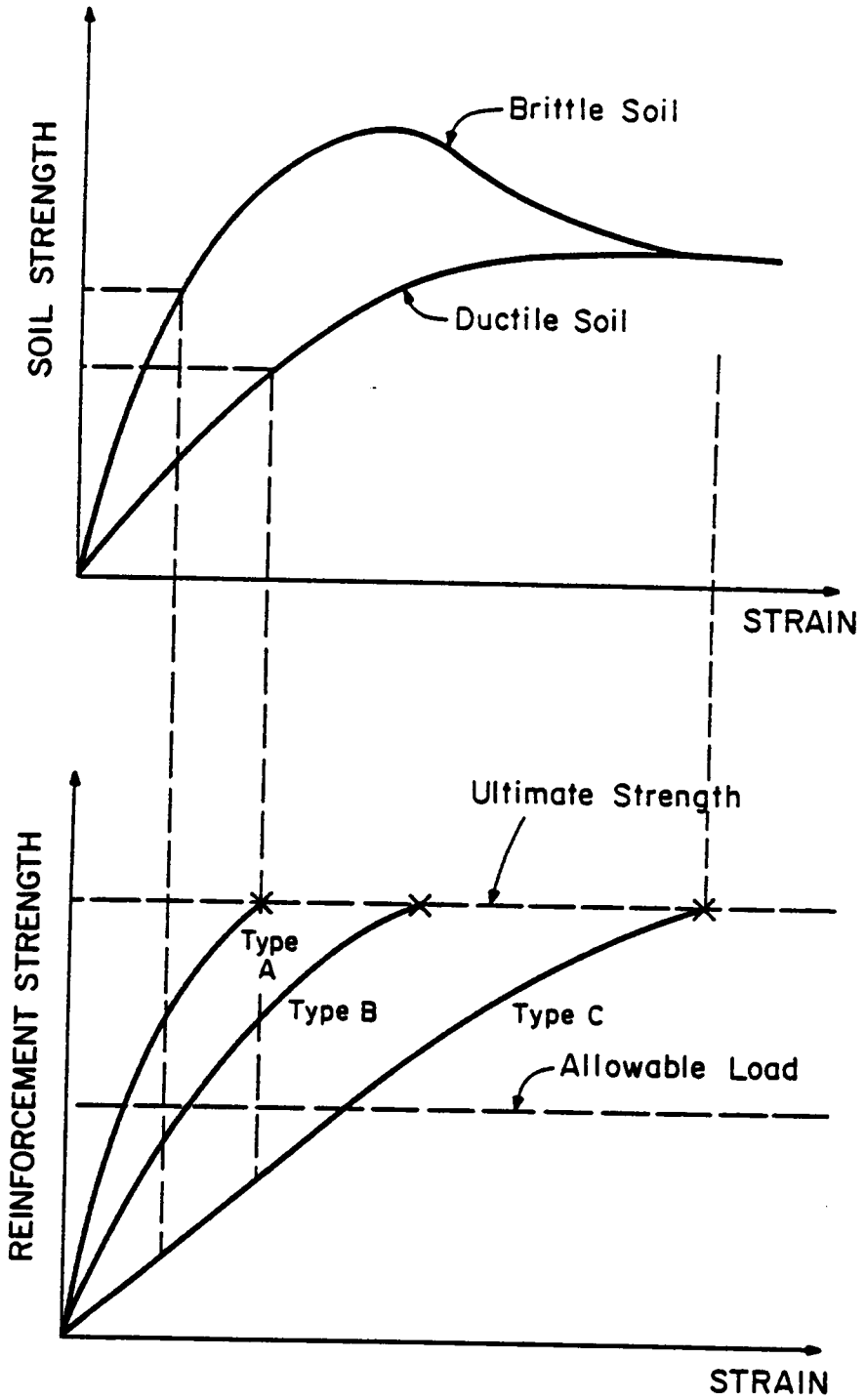

Figure 2.7 Consideration of mobilized soil strength and reinforcement forces under working conditions.

inforcement would be strained to give a high but allowable restraining force such as shown for Type B reinforcing.

For a ductile and less stiff soil similar comparisons may be made. Again consider a working stress level based on an adequate factor of safety. In Figure 2.7 it may be seen that both Type A and B reinforcement would be stressed above their allowable load and indeed the Type A reinforcement would be stressed to the point of rupture leading to a catastrophic failure to the structure. For this case only the low modulus reinforcement would be stressed to below its allowable load.

It should be emphasized that all three types of reinforcement shown give the same factor of safety with respect to ultimate limit state. However, the behavior of the reinforcements is much different under working conditions. These principles are intimately related to strain compatibility considerations and are discussed more in Section 2.2.4.2.

McGown et al. (1984) have proposed a procedure to develop the load-strain curve for materials which exhibit creep behavior which accounts for the long-term creep strength of the material. This procedure is shown in Figure 2.8. It consists of determining the strain-time relationship of a geotextile or a geogrid under a constant load as in a creep test (Figure 2.8a). From this plot, the load-strain relationship can be determined as a function of time, as in Figure 2.8b, and by extrapolation the long-term ultimate strength can be determined. Finally, the long-term stiffness can be determined as in Figure 2.8c.

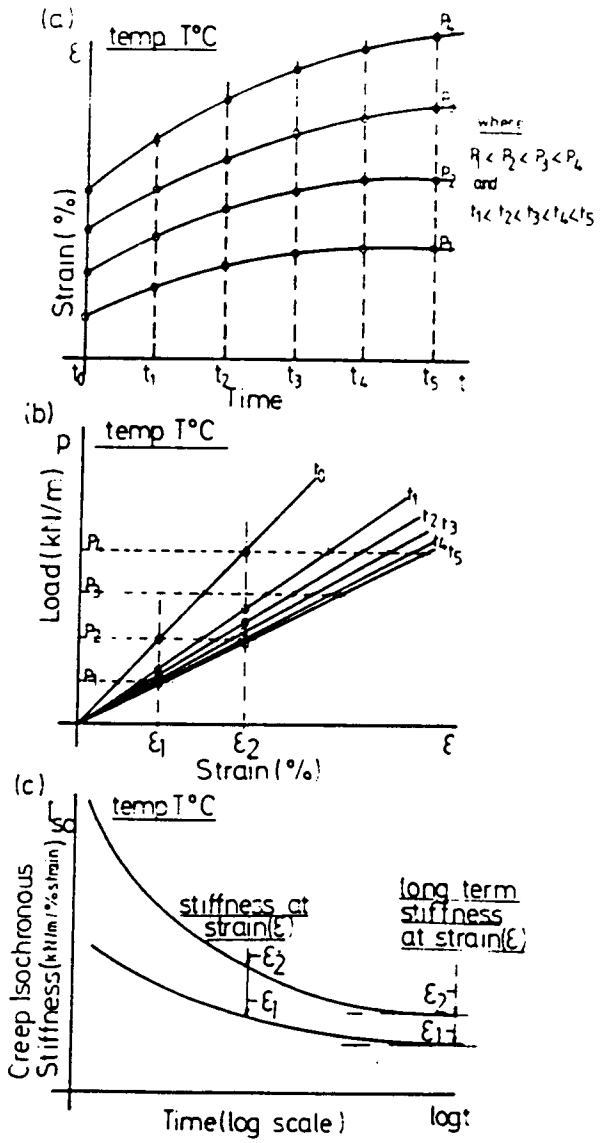

Figure 2.8 **Procedure for determining load-strain curves for creep sensitive reinforcing materials (McGown et al. 1984).**

2.2.4.2 Strength of the Reinforcement-Soil Interface

Under field conditions, reinforcement is subject to pullout forces and shear forces as shown in Figure 2.6. The strength of the reinforcement-soil bond at the interface may govern mobilization of this bond if the shear stresses at the reinforcement-soil interface exceed the bond strength which can develop. The bond strength which develops can fail in essentially two mechanisms: (1) failure in a pullout mode due to insufficient anchorage capacity and (2) sliding of the fill along either the upper or lower surface of the reinforcement in a direct shear mode. The field situations of these two modes of failure are shown in Figure 2.6.

The analogous laboratory test conditions for these two modes of failure are shown in Figure 2.9. In the pullout test, the two halves of the box are fixed and one end of the reinforcing sample is subjected to a horizontal load. In direct shear tests, one half of the box is fixed while the other half is subjected to a horizontal force. The reinforcement is anchored along an edge of the box to induce tensile forces in the reinforcement. During each test, the normal load is kept constant. This results in a constant normal stress:

$$\sigma = \frac{P}{A_b} \qquad [2.10]$$

where A_b = area of the box. Recording the horizontal force and displacements during the test allows determination of the ultimate shear stress.

In the direct shear test it is assumed that the shear stress, τ between the soil and the reinforcement are uniformly distributed. Hence, the shear stress is:

$$\tau = \frac{T}{A_r} \qquad [2.11]$$

where T is the applied horizontal force and A_r is the area of the reinforcement inside the box. Plotting the values of τ_{ult} corresponding to T_{ult} for a series of normal stresses allows determination of the bond strength or interface friction angle, δ as shown in Figure 2.10.

The shear stresses developed in pullout tests on geotextiles are not uniformly distributed due to the extensibility of the material (Holtz, 1977 and Collios et al. 1980). However, assuming a uniform distribution of the shear stresses leads to correct values of the average bond angle of the interface (Collios et al. 1980). Hence,

$$\tau = \frac{T}{2A_r} \qquad [2.12]$$

where T is the applied pullout force, A_r is the area of the reinforcement inside the box and the factor of 2 accounts for shear stress developed on both sides of the reinforcement. As in the direct shear test, plotting values of $\tau_{ult,}$ for a series of normal stresses allows determination of the bond strength or interface friction angle, δ

The mechanism of reinforcement-soil bond is little understood at present and available test data have indicated it is a function of several variables. These include normal stress on the reinforcement; soil

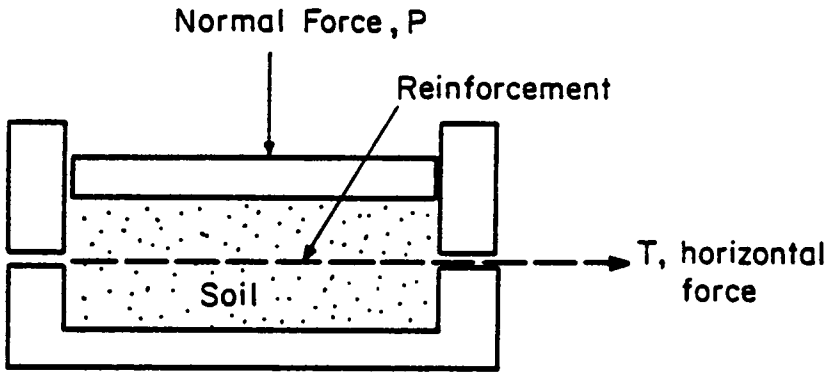

(a) Pullout Test

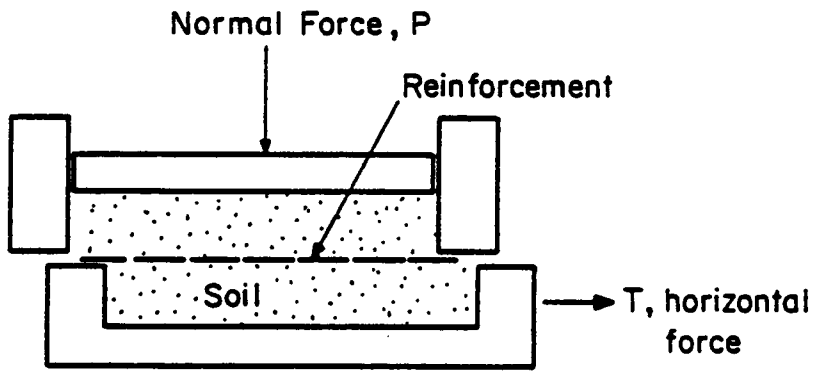

(b) Direct Shear Test

Figure 2.9 Schematic representation of laboratory pullout and direct shear tests.

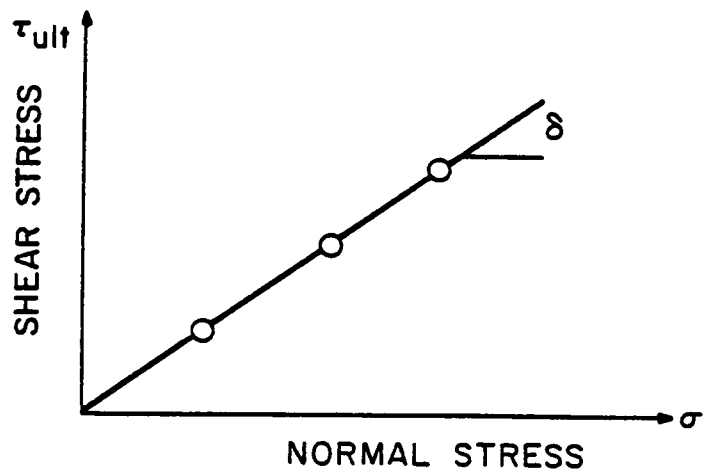

Figure 2.10 Determination of δ for tests over a range of normal stresses.

angularity, density and particle size; ratio of reinforcement opening size to soil particle size; and relative reinforcement-soil stiffness. Data by Collios et al. (1980) showed that as the size of reinforcement openings, measured as the size of mesh or as the space between fabric filaments, approaches the size of the soil particles, the bond angle increase due to interlock of the soil grains with the reinforcement. They also showed that interlock can occur if a geotextile deforms to the shape of the soil particles. This is a function of the stiffness of the geotextile, the size of the soil particles and the applied normal stress.

Typical results from pullout tests are shown in Figure 2.11. These data have been replotted from Ingold (1982b) and are for woven and nonwoven geotextiles and a geogrid. For the sand used, the bond angle varies with reinforcement type and with normal stress. Similar variations in bond angle with normal stress have been reported by Holtz (1977).

The bond angle or interface friction angle has been determined by a number of investigators on several geotextiles and geogrids over a wide range of sand density, strength, size and angularity. A summary of several of these is shown in Table 2.2 where δ is the bond angle and φ is the friction angle of the soil determined from direct shear or triaxial tests. It may be seen that for geotextiles and geogrids $\frac{\delta}{\varphi} \cong 1$.

Holtz (1977) recommends, for design purposes, assuming δ = conservative values of φ. The data in Table 2.2 would appear to substantiate this recommendation. However, caution must be exercised in such generalization in light of conflicting data. For instance, Rowe et al. (1985) conducted pullout tests on Tensar SR2 geogrids in loose sand with the

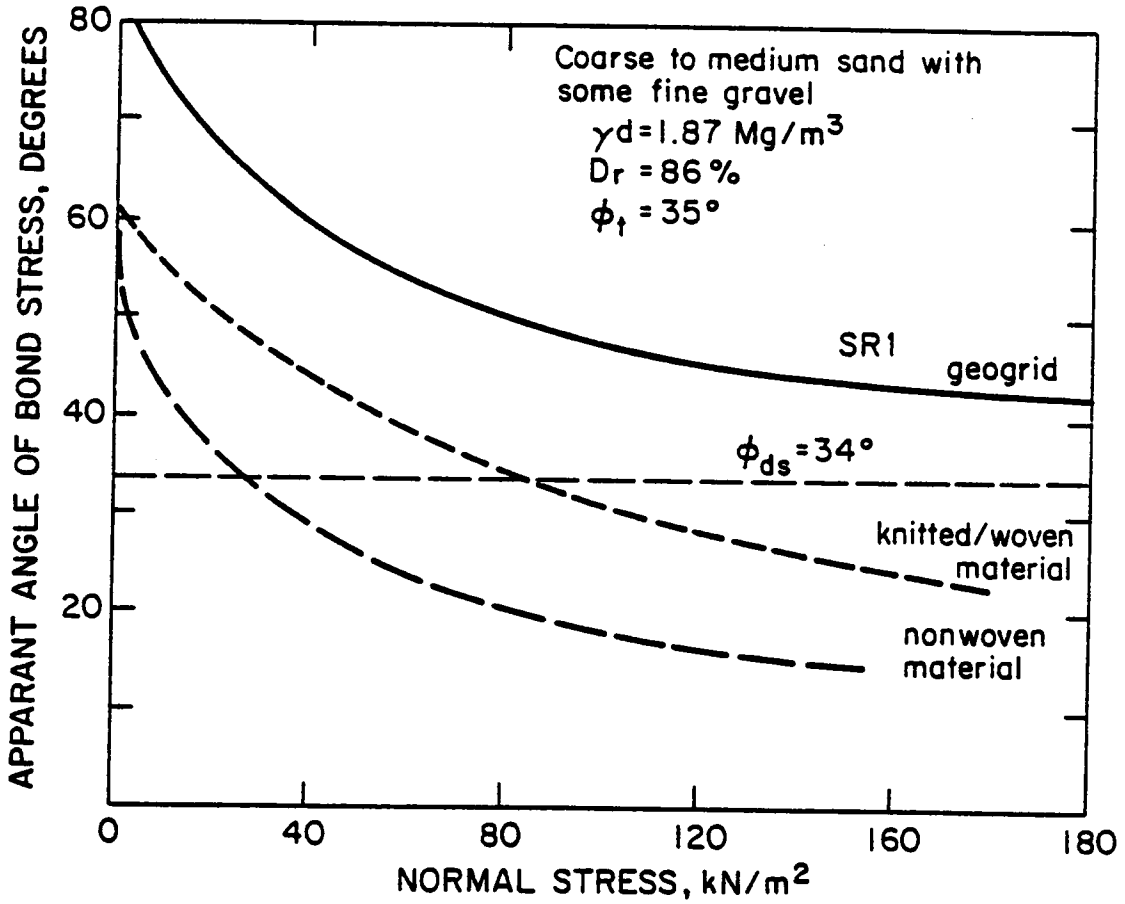

Figure 2.11 Variation of bond angle as determined in pullout tests (adapted from Ingold, 1982b).

Table 2.2. Summary of bond angle determinations δ/ϕ

Reference	Soil	D_r	ϕ	Direct Shear			Pullout		
				Nonwoven	Woven	Geogrid	Nonwoven	Woven	Geogrid
Holtz 1978	coarse, angular sand	65%	45					0.8-1.0	0.8-1.0
	medium, angular sand	65%	35						
Tumay et al., 1979	uniform, fine sand	37.8	34.5	~1.0					
		72.0	38.5	~1.0					
		91.5	41.5	~1.0					
Collios et al., 1980	rounded sand	?	39	0.9			0.85		
	rounded gravel	?	49	0.76			0.47		
	crushed gravel	?	53	0.91			0.72		
	ballast stone	?	63	0.87					
Ingold 1982a	medium to coarse sand	85%	34	0.8-0.9	0.9-1.1	0.9-1.1	0.4-1.6	0.6-1.8	1.1-2.0
Ingold 1982b	medium to coarse sand	85%	34						1.1-1.7
UC/Davis 1984	fine to coarse sand	95%	45						1.4
Jewell et al., 1984	five soils ranging from fine sand to coarse gravel					0.8-1.0			
Rowe et al., 1985	fine uniform sand	31-32	loose	1.1	1.0-1.1	0.95	1.15	1.0-1.1	0.6-0.9

results shown in Figure 2.12. The data show a directional bias, and for pullout, in the longitudinal direction, which is the direction of stress for SR2, a bond angle of $\delta = 18°$ was indicated. This is much lower than the sand friction angle of 32°. Pullout testing of SR2 geogrids conducted at the University of California, Davis (1984b) yielded bond angles of $\delta = 64°$. The differences in these results are probably attributable to the density of the sand at the time of testing. The UC/Davis tests were conducted on a medium grained sand at a relative density of about 95 percent, while the tests reported by Rowe et al. were conducted on a fine grained sand in a "loose" state.

2.2.4.3 Strain Compatibility of Reinforcement and Soil

Soil structures incorporating relatively extensible reinforcements, such as geotextiles and geogrids, are strain controlled systems (McGown et al. 1978) and hence, there must be strain compatibility between the soil and the reinforcement at all times (McGown et al. 1984). This compatibility is depicted in Figure 2.13. This figure is instructive in several ways. First, if a limit equilibrium analysis is performed using peak soil strengths, the reinforcement strength used in the analysis should correspond to the tensile force developed at a strain compatible with the development of peak soil strength. However, as the soil strains and its strength reduces from its peak value to its residual value, the reinforcement force mobilizes more force and the overall system may remain in equilibrium. A limiting condition will be reached only when tensile

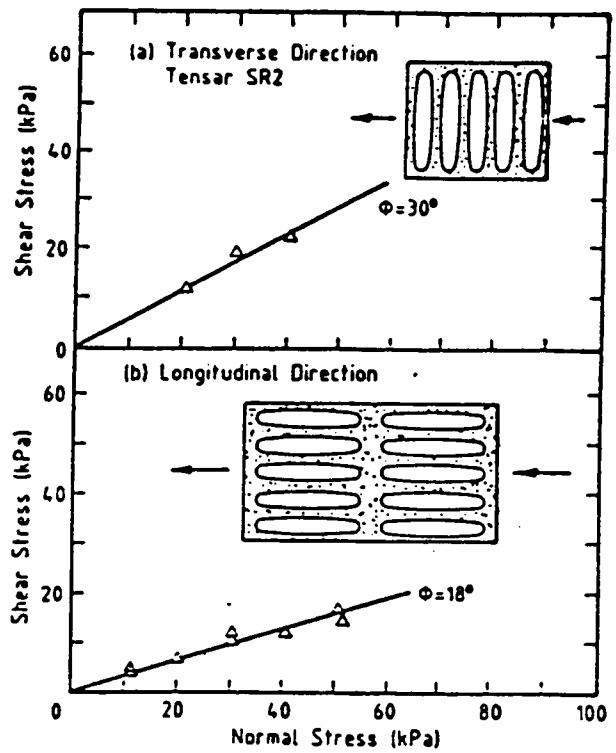

Figure 2.12 Interface strength of Tensar SR2 in pullout test (Rowe et al. 1985).

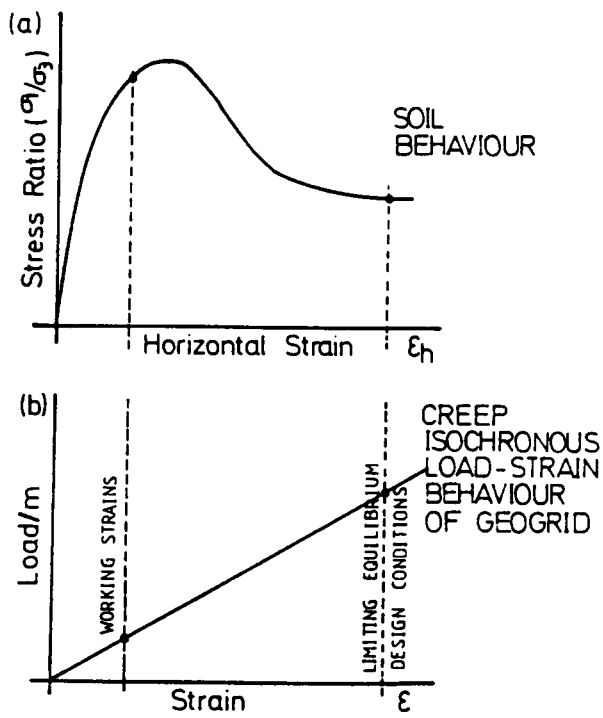

Figure 2.13 **Strain compatibility of reinforcement and soil (McGown et al. 1984).**

strains in the soil induce strains in the reinforcement which cause it to rupture. This argues for the most likely limiting condition occurring when the soil has strained sufficiently to reach residual strength or constant volume conditions. Hence, according to McGown et al. (1984), the soil strength to use in a limit equilibrium analysis of reinforced soil systems is the constant volume or residual strength.

The extension which Rowe and Soderman (1985) proposed to their BMM limit equilibrium addressed the question of strain compatibility between the soil and the reinforcement. A parametric study was performed in which the limit equilibrium and finite elements results were compared for selected embankment configurations. From the results obtained, a new parameter termed "allowable compatible strain" was coined. The allowable compatible strain is the maximum strain that would occur in a geotextile having a modulus so small that negligible load is developed in the geotextile at collapse, and it was further assumed that the strains developed in this geotextile-reinforced embankment at failure would correspond to the strains developed in a similar unreinforced embankment at failure.

The allowable compatible strain was related to a dimensionless parameter Ω where

$$\Omega = \left(\gamma_f \frac{H_c}{c_u}\right)\left(\frac{c_u}{E_u}\right)\left(\frac{D}{B}\right)_e^2 \qquad [2.13]$$

where

γ_f = unit weight of the fill.

H_c = height of the embankment at collapse.

c_u = undrained shear strength.

D = depth of soft soil beneath embankment.

E_u = undrained modulus of the soil.

B = width of the embankment.

Rowe and Soderman suggested that in a stability analysis, the force in the fabric should not exceed that developed at the allowable compatible strain (i.e., $T < \varepsilon_a E_f$ where E_f is the secant modulus for the strain range 0 to ε_a). The relationship proposed between the allowable compatible strain and the dimensionless compatiblity parameter Ω is shown in Figure 2.14.

From their study, Rowe and Soderman found that the allowable compatible strain increased to a limiting depth and then decreased. This depth was found to be D/B = 0.42 where D and B are as previously defined. They also found that below a depth of (D/B) > 0.84 a geotextile has no effect on deep-seated stability thus providing a guide to the applicability of reinforcement on deep deposits.

2.2.5 Summary of Limit Equilibrium Methods

The following conclusions can be drawn on the use of limiting equilibrium procedures to analyze the behavior of reinforced embankments on weak soils.

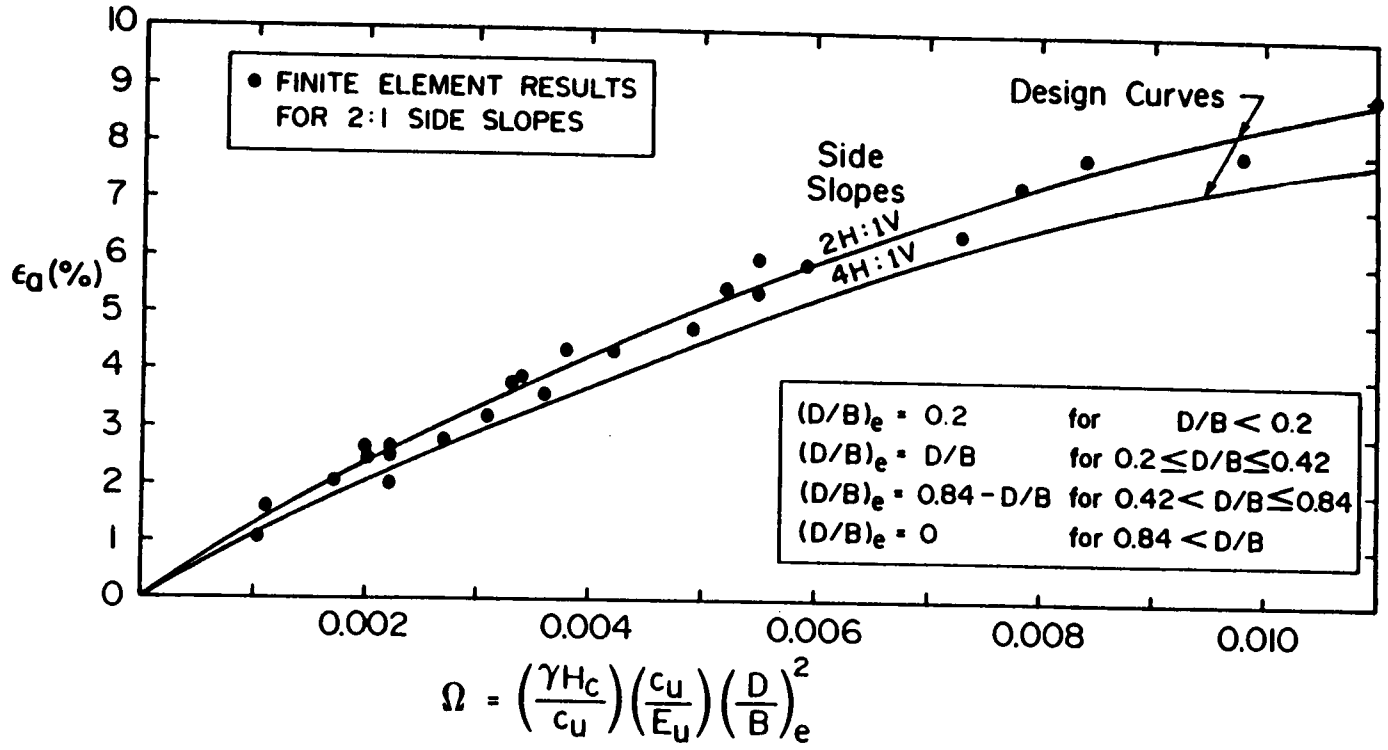

Figure 2.14 Allowable compatible strain as defined by Rowe and Soderman (1985).

1. The use of Bishop's Modified Method provides a slightly conservative approach to the design of reinforced embankments when a reasonable factor of safety is specified (i.e., minimum of 1.3 for end-of-construction).

2. The selection of the reinforcement force to use in design is an important aspect of limit equilibrium analyses and has, as yet, not been quantified definitively. The selection of the proper force to use is a function of many variables dependent upon soil and reinforcement properties and the geometry of the problem. Until further research clarifies the issues, conservative values, subject to the limitations discussed above, will need to be selected for design purposes.

3. More verification of analysis procedures by comparison to case history data is necessary before complete confidence in limit equilibrium methods can be achieved.

4. The factor of safety calculated assuming the reinforcement becomes aligned tangent to the slip surface at failure is considerably higher than that calculated assuming the reinforcement remains horizontal.

2.3 Finite Element Methods

2.3.1 General

Analyses by the finite element method have been applied to reinforced soil to obtain data on the soil-reinforcement interface, the deformation behavior under working conditions and as an aid to understanding the reinforcement mechanism. Herrmann and Al-Yassin (1978) discussed discrete and composite representations of the constituents and concluded that both approaches could be applied to reinforced soil systems with equal accuracy. The analyses have been applied to laboratory model studies of sand (McGown et al. 1981) and clay (Majes and Batteline, 1985) and to field tests (Bell et al. 1977; Boutrop and Holtz, 1983; Rowe, 1982; Rowe et al. 1984 and Rowe and Soderman, 1984). The finite element method allows consideration of construction sequence, soil nonlinearity, plastic failure, reinforcement deformation, soil-reinforcement interaction and deformation under working loads. In addition, pore pressure response may be determined depending upon the soil model chosen. While there are similarities in the finite element methods used, the procedures vary considerably with regard to the modelling of soil nonlinearity, plastic failure, reinforcement representation, reinforcement-soil interaction, large deformation behavior, and construction sequence. Table 2.3 provides a summary of the finite element methods applied to reinforced soil and reinforced embankments. To date, no method incorporates consol-

idation analysis and pore water pressures explicitly into the analysis. Several applications to reinforced embankments are discussed below.

2.3.2 Bell et al.

One of the earliest finite element analyses of reinforced embankments over soft, weak soils was that performed by Bell, Greenway and Vischer (1977). The authors analyzed a geotextile fabric-reinforced rockfill built on a 10-ft thick peat deposit in Alaska. The fill was modelled as a linear orthotropic elastic material, the reinforcing as a truss element capable of transmitting axial force only, and the peat was modelled as a homogeneous, isotropic, elastic-perfectly plastic material. The authors analyzed three cases representing embankment dead load only under conditions of no reinforcement and single layer reinforcement and the case of live loads (representing haul trucks) on the single layer reinforced embankment. The analyses showed the reinforcement to have little effect on ultimate settlements, the reinforcement stiffness to have no effect on settlements and that fabric tension increased with increasing fabric modulus.

The authors made the following main conclusions: the main function of the fabric was to prevent local bearing failures, thus holding the embankment together and causing it to act as a unit and when shear failures do not occur, and embankment settlement was essentially the same in the reinforced and unreinforced cases. It should be noted that this was one of the earliest cases of embankment reinforcement over soft soils and

Table 2.3. Finite Element Application to Reinforced Embankments

Reference	Finite Element Used	Reinforcement Model	Soil Constitutive Model	Slip Behavior Modelled?	Parameters Considered in the Study	Major Results and Comments
Bell et al. (1977)	4 node isoparametric element (NONSAP).	Bar element with axial stiffness and no flexural rigidity.	Isotropic, elastic perfectly plastic	No	Fabric stiffness	1. Compared unreinforced and reinforced cases with two geotextile stiffnesses. 2. Reinforcement had little effect on settlements. 3. Main function of reinforcement was to prevent local bearing failures.
Brown and Poulos (1978)	3 node constant strain triangles.	Axial tensile forces with zero flexural stiffness incorporated into analysis through calculated set of compatible forces to ensure compatibility conditions.	Elasto-plastic material with Mohr-Coulomb failure criterion. Davis (1968).	Yes - based on Mohr-Coulomb failure	1. Quantity of reinforcement. 2. Undrained cohesive strength.	1. Adding reinforcement increased stability of cohesive embankment by 40% on a competent foundation. 2. Comparison to Lee et at. (1973) for cohesionless material suggested that Rankine approach was incorrect.
McGown, Andrawes, Mashhour, Myles (1981)	4 node quadrilateral.	Linear structural elements.	linear elastic hyperbolic model of Duncan and Chang (1970).	Yes - by use of vertical elements	1. Horizontal and inclined reinforcement.	1. Predicted horizontal and vertical displacements agree well with measured values from model tests. Model tests not taken to failure. 2. Modeling of construction sequence is important in analyzing behavior.
Rowe, R.K. (1982)	3 node constant strain triangles.	Structural membrane with axial stiffness and no flexural rigidity.	Elasto-plastic material with Mohr-Coulomb failure criterion Davis (1968).	Yes - based on Mohr-Coulomb failure criterion	1. Large deformations. 2. Drained and undrained analyses of Pinto Pass case history.	1. Using undrained shear strength parameters with drained "elastic" parameters provides the best indication of undrained stability as well as an upper limit of deformations. 2. Increasing fabric stiffness has a very modest effect upon settlements. 3. Sufficient fabric anchorage can be mobilized without overlapping the fabric at the edge of the embankment. 4. The major role of the reinforcement is in reducing lateral spreading and in confirming the soil which reduces lateral spreading. 5. Increasing embankment stiffness tends to enhance the role of the reinforcement.

Table 2.3 (Continued)

Reference	Finite Element Used	Reinforcement Model	Soil Constitutive Model	Slip Behavior Modelled?	Parameters Considered in the Study	Major Results and Comments
Boutrap and Holtz (1983)	4 node isoparametric elements (NONSAP).	Bar elements with axial stiffness and negligible flexural rigidity.	Linearly elastic with plastic flow at failure envelope; Duncan-Prager soil model.	No	1. Drained and undrained analysis of low embankment constructed on muskeg in Southern Alaska. 2. Large displacements.	1. Fabric tension is significantly less for the drained case, suggesting that the influence of the fabric is less than for the drained case compared to the undrained. 2. Total settlements are only slightly affected by reinforcing. 3. Primary influence of reinforcing is to reduce shear stresses in the soft foundation and to reduc the vertical differential settlements at the top of the embankment.
Rowe, MacLean Soderman (1984)	3 node Constant Strain Triangle.	Structural membrane with axial stiffness and no flexural rigidity.	Elasto-plastic material with Mohr-Coulomb failure criterion Davis (1968).	Yes - based on Mohr-Coulomb failure criterion Davis (1968)	1. Shear parameters from different tests. 2. Several different geotextile stiffnesses. 3. Large deformations.	1. Strength parameters from simple shear tests provided best agreement between calculated and observed behavior. 2. Major effect of reinforcement is to reduce lateral spreading and to increase stability. 3. Reinforcement has very little effect on consolidation settlements. 4. Locating the reinforcement at the embankment-foundation interface produces the optimum performance of the reinforced embankment.
Low (1985)	4 node isoparametric element.	Bar element and mattress element, a composite soil-reinforcement element.	Hyperbolic model of Duncan-Chang (1970).	Yes, link elements based on hyperbolic relationship and Mohr-Coulomb failure criteria	1. Parametric studies of depth of foundation, reinforcement stiffness and strength of foundation.	1. Effectiveness of reinforcement depended upon mobilized forces in reinforcement. 2. Reinforcement decreased shear stresses in foundation. 3. Flatlying reinforcement more suitable than mattress. 4. Placement of reinforcement should be close to embankment-foundation interface.

the fabrics available at that time were much less stiff than those available today.

2.3.3 Brown and Poulos

Brown and Poulos (1978) used an elastic-plastic soil model (Davis, 1968) to analyze the collapse height of unreinforced and reinforced embankments on stable foundations. The reinforcement was represented as a member possessing zero flexural stiffness and as carrying axial tensile forces only. The results obtained for cohesive soils are shown in Figure 2.15 in terms a stability number $\frac{\gamma H_f}{c_u}$ and the percentage reinforcement p_r in the soil mass. (The percentage reinforcement is the ratio of the cross-sectional area of the reinforcing to the cross-sectional area of the embankment.) It can be seen that as the amount of reinforcement increases the stability number increases and hence the height to failure increases. Brown and Poulos showed that increases in stability of up to 40 percent were possible using reinforcement. Brown and Poulos also analyzed granular frictional structures. Here the results of model retaining wall tests performed by Lee et al. (1973) were analyzed with the results shown in Figure 2.16. The finite element results shown provide a better approximation to the model test results than the Rankine method proposed by Lee et al.

2.3.4 Jones and Edwards

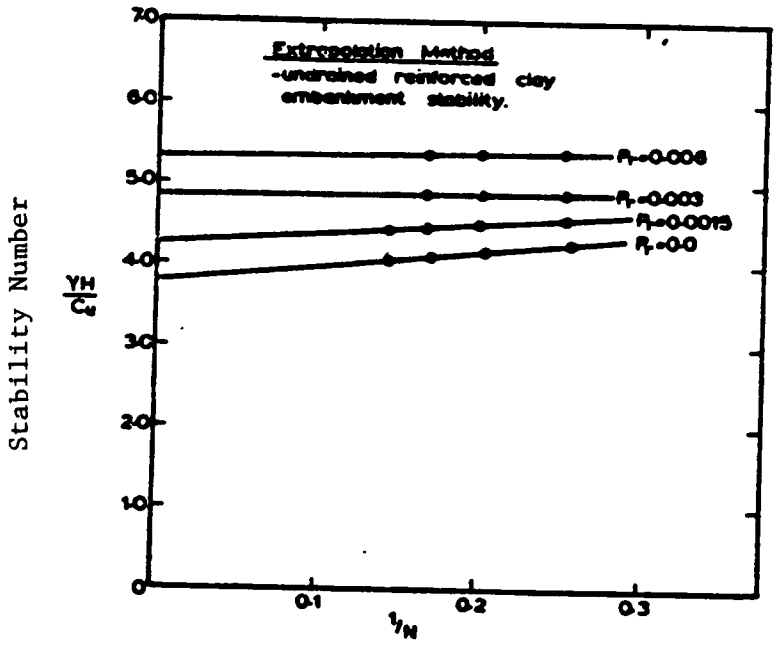

Figure 2.15 Stability number versus percentage of reinforcement in cohesive soils (Brown and Poulos, 1978).

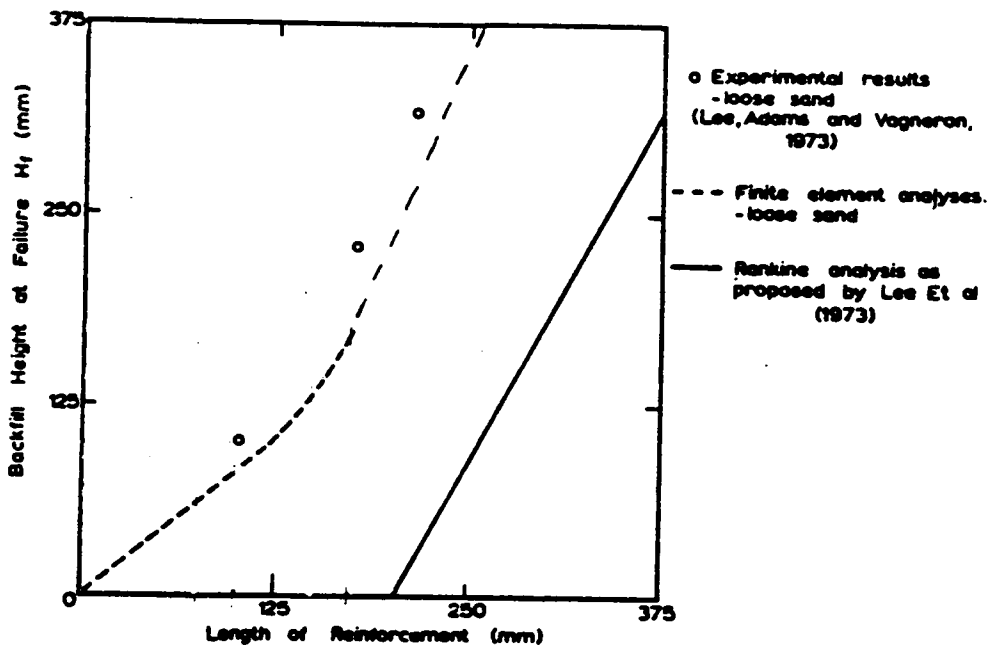

Figure 2.16 Comparison between finite element and model tests results (Brown and Poulos, 1978).

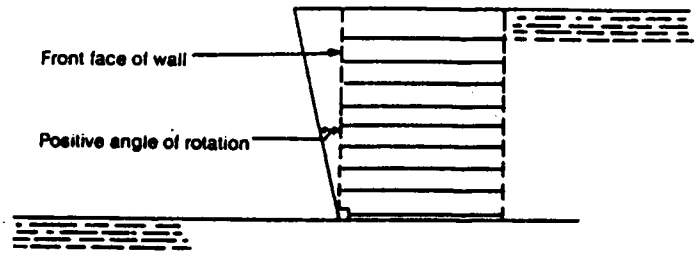

(a) **Behaviour of a stiff–stiff material system**

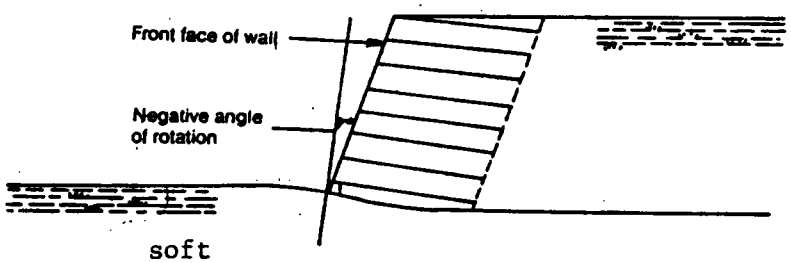

(b) **Behaviour of a stiff–stiff material system**

Figure 2.17 (a) Behavior of a stiff-stiff material system (b) Behavior of a stiff-soft material system (after Jones and Edwards, 1980)

Jones and Edwards (1980) employed a nonlinear elastic soil model to analyze reinforced earth walls over stiff and soft foundation soils. The results of parametric studies showed that a reinforced wall over a stiff foundation (i.e., a stable foundation) would tend to rotate about the toe with an active mechanism away from the fill as shown in Figure 2.17a. On the other hand, a reinforced earth structure built on a soft foundation would tend to rotate back into the fill as a rotational slip develops through the fill (Figure 2.17b). These observations show that conventional design procedures for global stability based on overturning about the toe may not be applicable to reinforced earth structures built on soft soils. The study also showed that design methods for internal stability of the reinforced soil were independent of the foundation strength and need not be altered for soft foundation conditions.

2.3.5 McGown et al.

McGown et al. (1981) used a hyperbolic soil model and bar elements representing the reinforcement to analyze laboratory model tests of geotextile reinforced sand over rubber (to simulate soft soil conditions). The analyses were limited to working conditions with no attempt to match failure conditions. The finite element results showed excellent agreement to the model tests for settlement and horizontal movements demonstrating the applicability of finite element analyses to working conditions. An interesting point from the finite element results was the need to use reinforcing properties based on in-soil tests rather than

those from unconfined tests in order to obtain reasonable agreement with the model tests. In-soil tests of the reinforcement allow rational consideration of the effect of confinement on the reinforcement-soil system.

2.3.6 Boutrop and Holtz

Boutrop and Holtz (1983) extended the work of Bell et al. (1977) by incorporating the Drucker-Prager soil model into the analysis and considering undrained and drained conditions. The results indicate that reinforcement has little effect on total settlements but does reduce differential settlements across the embankment surface. Comparison of the drained and undrained cases showed that reinforcement tension was significantly less in the drained case. The authors felt this showed that the influence of the reinforcement on embankment behavior is much less in the drained case than in the undrained case. Another interpretation may be that the reinforcement force will decrease over time as the behavior of the system changes from that of undrained to drained conditions and the drained case represents the minimum amount of reinforcement necessary to ensure acceptable long-term performance. Comparisons of stress levels in the unreinforced and reinforced cases showed that shear stress levels in the foundation were considerably reduced by the presence of the reinforcement.

2.3.7 Rowe and Colleagues

Rowe and his colleagues at the University of Western Ontario in Canada have performed extensive analysis work using the finite element method. The approach they have taken is based on a plane strain, elasto-plastic soil-structure interaction technique described by Rowe et al. (1978). The soil is assumed to be an elastic-plastic material with a Mohr-Coulomb failure criterion and a flow rule of the form proposed by Davis (1968). The reinforcement is treated as a structural membrane having axial stiffness but negligible flexural rigidity. Slip between the soil and reinforcement is assumed to occur when the shear stress between the two reaches a limiting value based on a Mohr-Coulomb criterion. A detailed description of the formulation of the method was provided by Rowe (1984).

Rowe (1982) analyzed the Pinto Pass test section (see Case Histories in Section 2.4.3) using the above analytical procedure. Due to uncertainty in the published soil and geotextile properties, a limited parametric study was performed to bracket expected properties. Both drained and undrained analyses of the test sections were performed. The undrained analyses showed relatively small settlements (0.05 m) and small fabric forces (0.4 kN/m). The drained analyses showed much larger settlements (0.5 m) and fabric forces (2.3 kN/m). An analysis in which undrained strength parameters were used with drained modulus parameters showed results of 0.6 m of settlement at the centerline and a maximum reinforcement force of 4.4 kN/m. According to Rowe, this type of analysis (mixing drained and undrained parameters) provides an indication of un-

drained stability of the embankment as well as providing an upper estimate of deformations without having to resort to a consolidation-based analysis and it provides a sufficiently accurate and conservative answer for practical purposes.

The effect of fabric stiffness on embankment behavior was studied. Increasing stiffness had little effect on settlements; even using an extremely stiff fabric reduced settlements less than ten percent from the unreinforced case. The major effect of increasing fabric stiffness was to reduce lateral displacements. This reduction in lateral spreading of the embankment results in greater confinement of the underlying soil which reduces the extent of plastic behavior in this soil. For relatively low fabric stiffness, relatively large deformations can occur prior to the fabric reaching its ultimate tensile strength and for all practical purposes, failure may be deemed to have occurred prior to rupture of the fabric. This implies that the stiffness of the fabric may be as important as the tensile capacity in stabilizing embankments on weak foundations.

The analyses also showed that sufficient fabric anchorage can be mobilized without overlapping the fabric at the embankment edge, as was concluded by Haliburton et al. (1980) from the field data. Also, consideration of the fill stiffness showed that increasing the fill stiffness enhanced the role of the fabric, thus increasing fabric stiffness has a slightly greater effect on deformations for a stiff fill compared to a loose fill.

Rowe et al. (1984) analyzed a geotextile-reinforced embankment constructed on a peat deposit using the above described techniques. Input

parameters for the peat properties were determined from direct shear tests, triaxial compression tests, uniaxial tension tests and simple shear tests. The results from these tests yielded very different values of φ' and c' as shown in Table 2.4.

The properties of the geotextile used were determined from wide strip tensile tests which provide load-elongation curves from which the tensile strength and modulus can be determined. Two types of geotextile fabric were used to reinforce the fill: Geolon 1250 which has a coarse and relatively loose weave and Permealiner M1195 which has a fine tight weave. The Geolon fabric had an intrinsic "slack" in the early stages of loading, often referred to as offset. Because of this behavior it was necessary to assign a lower modulus to this fabric during the early stages of loading in the analysis.

The effect of using different shear strength parameters was investigated by comparisons to the measured field performance of the embankment. Using strength values from field vane shear tests produced calculated settlement profiles which did not agree with the observed results. Analyses performed using remolded vane shear strengths predicted collapse to occur under fill heights of 1.5 meters, which did not occur in the field.

The strength values from triaxial tests underpredicted the settlement and lateral deformations. The best agreement between observed and calculated deformations was obtained using parameters from simple shear tests, which were very similar to parameters from direct shear tests.

Table 2.4 Comparison of ϕ' and c' of peat from various tests. (Rowe et al. 1984).

	Triaxial	Direct Shear	Uniaxial Tension	Simple Shear
ϕ'	51	26	27*	27
c' kPa	0	1.1	1.8**	3.0

* = assumed angle of friction
** = based on the assumed angle of friction

The analyses by Rowe et al. showed the viability of using finite element techniques to model reinforced embankment behavior. In addition, the following points were made by the authors: The major effect of the geotextile was to reduce lateral spreading and to increase stability. Even a high modulus geotextile will have little effect on consolidation settlements. In the design of geotextile-reinforced embankments, consideration needs to be given to both the strength and modulus of the geotextile. The modulus will usually govern the selection of a suitable reinforcement material.

2.3.8 Low and Duncan

Low and Duncan (1985) developed a composite soil-reinforcement element to model the behavior of foundation mattresses, which are composed of geogrids and granular fill. Through superposition of the stiffnesses of the reinforcement and soil, in effect, a new material is defined. An important assumption made here is that no slip of the geogrid relative to the soil in the mattress can take place. This assumption can be called into question in light of the results reported on geogrid-soil interaction in Section 2.2.4.2.

This mattress element was incorporated into a soil-structure interaction computer program (SSTIPN) which uses the Duncan-Chang hyperbolic soil model (Duncan and Chang, 1970) and has bar, beam and interface elements. Parametric studies were performed of typical geogrid mattress reinforced embankments and embankments reinforced with flat-lying re-

inforcement (represented by bar elements in the analyses). From these studies the following conclusions were reached: (1) The effectiveness of reinforcement in restraining embankment and foundation deformation depended upon the magnitude of the mobilized force at working conditions. The greater the mobilized reinforcement force, the more significant the reduction in deformation. (2) Mobilized reinforcement force increased with increasing stiffness of reinforcement and with increasing foundation depth, while it decreased with increasing foundation strength. (3) Increasing mobilized reinforcement forces decreased both shearing stresses and the extent of plastic failure in the foundation. (4) For embankments constructed on weak foundations, flat-lying reinforcement appeared to be as effective as an equivalent geogrid mattress. The flat-lying reinforcement is also much easier to construct. (5) Placement of the reinforcement closer to the embankment-foundation interface was slightly more effective in restraining deformations.

2.3.9 Summary of Finite Element Studies

From the finite element studies described above, the following conclusions can be drawn concerning the behavior of reinforced embankments over weak soils.

1. The major effect of reinforcement is to reduce lateral spreading and to increase stability. This is accomplished by reducing shear stresses and plastic flow in the soil through an increase in con-

finement pressure in the foundation soils due to the presence of the reinforcement.

2. Reinforcement has very little effect on consolidation settlements, but it does tend to reduce differential settlements at the top of the embankment.

3. Increasing reinforcement stiffness decreases the extent of plastic failure in the foundation soils.

4. The optimum location for placement of the reinforcement is at the base of the embankment.

5. Shear strength parameters from simple shear tests provided the best agreement between calculated and measured behavior.

2.4 Case History Performance

2.4.1 General

Several full-scale embankments have been constructed to demonstrate the effectiveness of reinforcing to improve the behavior of embankments on weak soils and the observed results of these trials provides much useful information on their behavior. A summary of reinforced embankment fills constructed on weak soils to failure is given in Table 2.5. From

this it can be noted that many of the fills have been built on peat or very organic clay soils.

Few of the reported case histories provide adequate details of the reinforcement properties, fill and foundation properties, measured reinforcement forces or descriptions of the analyses performed. In many cases the benefits accrued from using reinforcement were evaluated from qualitative field observations and from comparison with similar unreinforced construction. Cases that do provide detailed information are discussed below.

2.4.2 Bell et al.

A field test of a geotextile-fabric reinforced rockfill constructed over a 10-foot thick peat deposit near Petersburg, Alaska was reported by Bell et al. (1977). The peat was a fine-fibrous type eight to eleven feet thick. The shear strength, based on two-inch diameter field vane shear tests, ranged from 50 to 350 psf with an average value of 250 psf. The fabric was a nonwoven, needlepunched, spunbonded polypropylene having a tensile strength of 800 to 900 lb per foot for an elongation of 100 to 200 percent. The geotextile was instrumented with simple open/close electrical circuit strain gages which could record a fabric strain up to 50 percent. Settlement plates were installed to record the deformation of the embankment.

Test sections having no reinforcement and single and double layers of reinforcement at the base of the fill were constructed. No obvious

Table 2.5. Summary of Case History Performance Records

Reference	Foundation Soil Type and Strength	Fill Height	Reinforcement Type	Tensile Force		Instruments Used	Comments
				Reported	Possible		
Bell Greenway and Vischer 1977	Peat S_u = 50 to 350 psf. depth = 8 to 11 ft. (fine fibrous sphagnum)	Coarse sand 3-8 ft.	Nonwoven needle punched, spun bonded polypropylene geotextile. Fibretex. Tensile strength = 800 to 900 lb/ft at 100-200% elongation.	6-12 kN/m	?	Settlement plates Strain gages on fabric	1. Main function of fabric is to prevent local bearing failures 2. Reinforcement has negligible effect on settlements. 3. Other conditions being equal, the tension in the fabric depends on the modulus of the fabric, with tension increasing as modulus increases. 4. Reported 28% savings in quantity of fill material required.
Belloni and Sembenelli 1977	Peat S_u = 7kPa	1.75m reinforced	Nonwoven geotextile (Bidim u44)				1. No instruments on geotextile. 2. Reported excellent performance compared to similar embankments constructed directly on peat.
Haagdenberg 1977 Fowler 1982	Peat and very soft clays S_u = 2.5 kPa depth = 3.7-4.4m	semi-compacted sand h = 1.3m unreinforced h = 2.m reinforced	Woven geotextiles	44 kN/m	?	Piezometers settlement plates Strain wires on fabric	1. Failure by fabric rupture at fabric strain 20% 2. Several stretches of stable reinforced fill with heights up to 1.7m and T = 24 k/m.
Volman, Krekt, and Risseeuw 1977	Soft clay with peat layers. S_u = 2 to 6 kPa	unreinforced 3.5m reinforced 4.5m (did not fail)	Woven nylon fabric	20 kN/m	60 kN/m rupture	Fabric strain measured	1. Fabric strain of 10% reported. 2. Fabric served to prevent lateral squeezing.
Haliburton, Fowler and Cangam 1980	Alluvial soils of very soft, plastic clays and loose clayer silts depth = 12m S_u = 2.4-7.2 kPa	Sand 2.4 high 10:1 slopes	4 types Advanced Type I Polyfilter-X Nicolon 66475 Nicolon 66186	?	?	Settlement plates Casagrande piezometers	1. Used outside-inside construction technique. 2. Settlements of 0.3m-0.5m reported. 3. Excess pore pressures of 4.3m reported with no lateral splitting or rotational bearing failure. 4. The fabric at edges was unstressed.

Table 2.5. Summary of Case History Performance Records

Reference	Foundation Soil Type and Strength	Fill Height	Reinforcement Type	Tensile Force		Instruments Used	Comments
				Reported	Possible		
Barsavary et. al 1982 (Manchester Site)	Peat S_u = 7-16 kPa	1.8m Sandy silt overlaid by granular base course	Geotextiles 4 types 1 section reinforced	?	?	Settlement plates Geotextile elongations	1. Geotextiles provided good separation. 2. Elongation in fabric reduced with time after construction.
Barsavary et. al 1982	Peat 6 to 7.6m water at surface	1.5m. silty sand.	Geolon 1250	?	?	Inclinometers Piezometers	Showed that geotextiles can be effective in holding fill together but do not prevent consolidation settlements.
Rowe et. al 1984 Bloomington Road Site	S_u 6-38 kPa avg. = 18 kPa	Constructed in two stages to allow for consolidation	Permealiner 1195	?	?	Strain gage on fabric	
Brakel et. al 1982	Soft organic clay	1.75m unreinforced 2.75m reinforced sand	Stabilinka	95kN/m	90-100 kN/m	Piezometers Strain gages on fabric	Reinforcing force near failure surface. Good case history for comparison to slope stability studies.
Golder and Laval University 1985	Sensitive Champlain clay S_u = 10-40 kPa	Unreinforced 4.0-5.3m Reinforced flatlying grid 6.2m mattress 4.7m	Tensar SR2 Geogrid	25 kN/m	70 kN/m	Piezometers Settlement plates Strain gages and load cells on geogrid. Inclinometers	See Chapter VI

bearing capacity failures took place in the fabric-reinforced sections. Fabric strains of around 50 percent were measured after loading. The depth of rockfill necessary to construct a useable haul road was the serviceability criterion. On this basis, an unreinforced section required rock depths of five to eight feet while the reinforced sections required three to six feet of fill.

2.4.3 Pinto Pass, Mobile, Alabama

An 800-ft-long sand embankment test section was constructed at Mobile, Alabama, to verify that a geotextile could be used as a tensile reinforcement to construct an embankment over very weak cohesive soil (Haliburton et al. 1980). Subsurface conditions are shown in Figure 2.18 and consisted of very soft, highly plastic clays and loose clayey fine sands and silts 40 feet thick overlying dense clean sands. The undrained shear strength of the cohesive materials was 50 to 150 psf, with Standard Penetration Test N-values of 0 to 5.

A sand fill embankment, 8 ft high, was constructed on a geotextile fabric placed on the ground surface. The fill was a relatively clean, poorly graded fine sand. The sequence of construction shown in Figure 2.19 was developed to balance forces on the soft foundation, and to provide proper anchorage of the fabric along the toes of the embankment prior to placement of fill along the centerline. The embankment was constructed with very gentle side slopes to allow the embankment to be raised gradu-

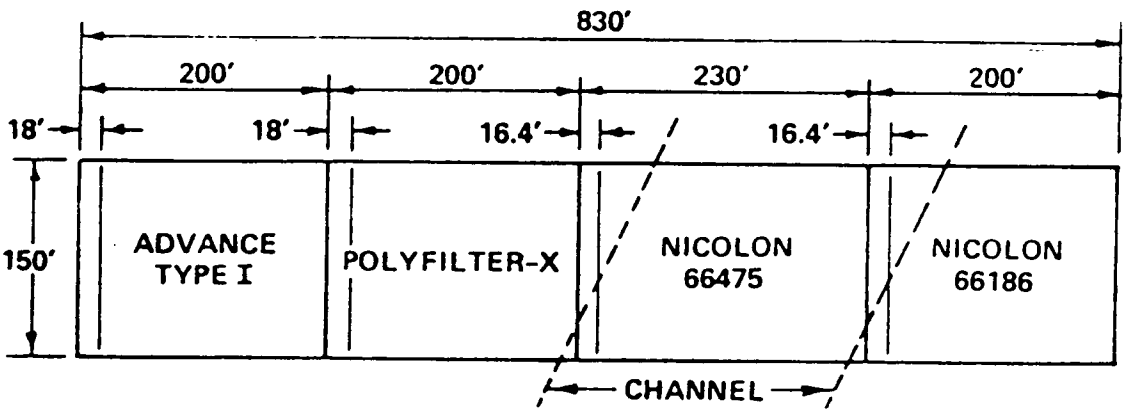

A. PLAN VIEW OF EMBANKMENT TEST SECTION

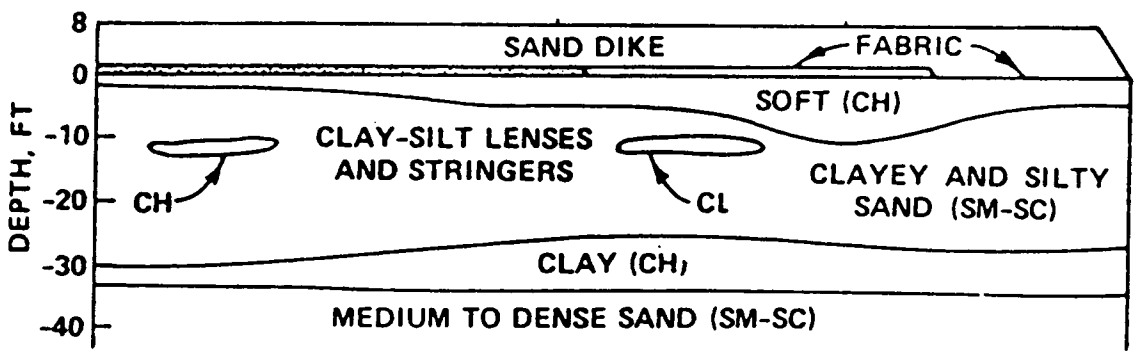

B. TYPICAL SOIL PROFILE PINTO PASS, ALABAMA

Figure 2.18 **Subsurface conditions at Pinto Pass.**

ally over the next 20 years. Four geotextiles were used for the tensile reinforcement along the locations shown in Figure 5.18.

Instrumentation consisted of five settlement plates and eight Casagrande piezometers installed at each 100-ft station along the embankment. The settlement plate risers were used to measure settlement and horizontal displacement during and after construction.

The test section was finished to design width and height without lateral splitting or rotational foundation bearing failure, despite excess pore pressures in the foundation soils rising six feet above the top of the embankment. Based on measurements made on the settlement plate risers, the lateral spreading of the embankment was minimal except near the old channel. At this location, 3.8 ft of lateral spreading developed over a width of 90 feet.

Settlements of about one foot were recorded during construction. Consolidation settlements of one to two feet occurred during the first six months after construction during which time the excess pore pressures dissipated to less than 15 percent of their maximum values.

Based on the results of the field test program, Haliburton et al. advanced the following conclusions:

1. Use of geotechnical fabrics to provide transverse tensile reinforcement is a technically sound method of rapidly constructing embankments on foundations too soft to support the unreinforced embankment without failure.

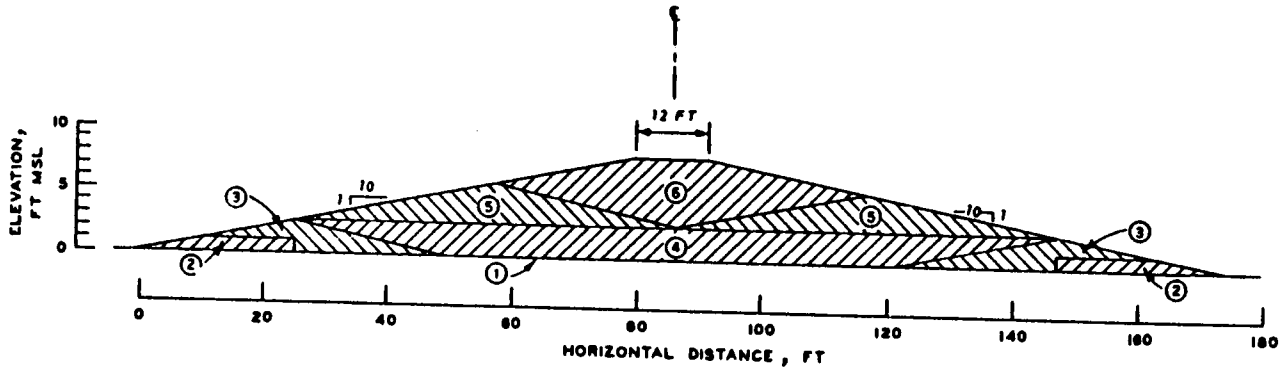

SEQUENCE OF CONSTRUCTION

① LAY FILTER CLOTH IN CONTINUOUS TRANSVERSE STRIPS, SEW STRIPS TOGETHER.

② END DUMP ACCESS ROADS AND LAP FILTER CLOTH OVER TOP.

③ CONSTRUCT OUTSIDE SECTIONS TO ANCHOR AND STRETCH FILTER CLOTH.

④ CONSTRUCT INTERIOR SECTION TO ANCHOR FILTER CLOTH.

⑤ CONSTRUCT INTERMEDIATE SECTIONS TO TENSION FILTER CLOTH IN CENTER.

⑥ CONSTRUCT FINAL CENTER SECTION.

Figure 2.19 Construction sequence used at Pinto Pass.

2. If procedures are used that provide essentially balanced loading on the foundation and that cover the outside edges of the fabric to suitable anchorage before placement of the interior embankment fill, construction of fabric-reinforced embankments by using available low-ground-pressure dozer equipment and conventional dump-truck material hauling is operationally practical.

3. Compared with conventional end-dumping displacement methods, fabric-reinforced embankment construction appears particularly cost effective. The additional construction costs of purchase and placement of fabric are more than recovered by the savings of fill required to construct the above-ground embankment cross-section.

4. Although specific situations will dictate exact fabric strength requirement, high-tensile-strength, high-deformation-modulus fabrics should prove to be the most suitable for embankment reinforcement.

5. There appears to be no particular advantage to constructing a working table before fabric placement, as long as the ground surface is reasonably level. When the mud-wave displacement method of fabric stretching is used, the longitudinal seam strength should be equal to or greater than the fill-direction tensile strength of the fabric.

Most importantly, this project demonstrated the feasibility of constructing geotextile-reinforced fills on weak soils and that tensile-resistant reinforcement can benefit embankments built on weak soils.

2.4.4 Almere, Netherlands

Two test embankments, one reinforced with a geotextile material and the other an unreinforced control section, were constructed on a soft 3.0 to 3.5 meter thick clay deposit at Almere in the Netherlands (Brakel et al. 1982). The tests were performed to assess the effect of geotextile reinforcement on the stability of embankments on weak soils. The geometry of the two sections is shown in Figure 2.20.

Brakel et al. (1982) described the soils at the site, the measured results and visual observations of the field tests, and the results of calculations on the stability of the embankments. The foundation soils at the site consist of three to three and one-half meters of soft organic clay overlying medium coarse, dense sand. The undrained shear strength of the organic clay is about 8 to 10 kPa, based on cone penetration data.

To ensure that the embankments could be brought to failure, a ditch was excavated in front of the embankments, as shown in Figure 2.20. The excavated material was used to construct a retaining bank. Both the unreinforced section and reinforced section had a length of 60 m. Stabilenka 200 polyester fabric was placed prior to construction of the clay retaining bank and extended from the toe to this bank back 25 m with an overlap of 30 cm. The fabric was instrumented with two rows of 10 strain gages placed transverse to the outer toe of the clay retaining bank. Six piezometers were installed in each test embankment to monitor pore pressures in the foundation.

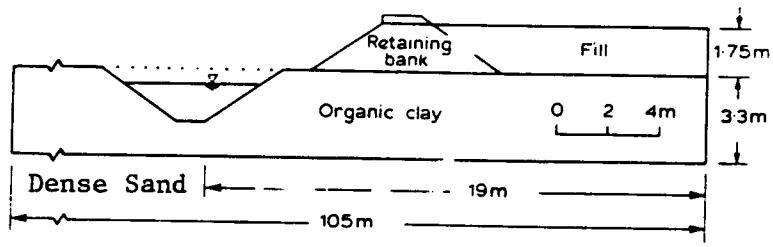

(a) Control section geometry

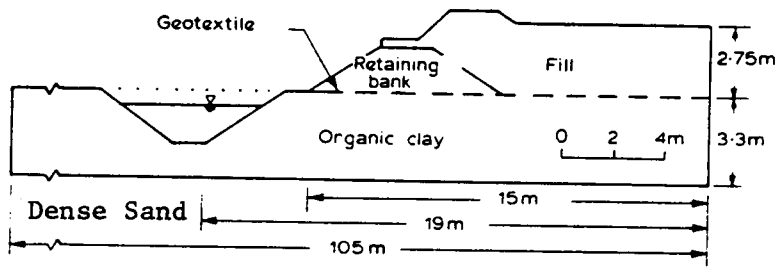

(b) Reinforced section geometry

Figure 2.20 **Test section geometry at Almere test site.**

Failure was induced by hydraulically filling sand behind the clay retaining bank. Failure of the reinforced section occurred by circular sliding at a fill height of 2.75 m. About one hour prior to the failure, a one meter displacement of the fill towards the ditch occurred. The measured reinforcement forces are shown for an instrumented section in Figure 2.21. The maximum measured force was 95 kN/m with an average value of about 80 kN/m at the time of failure. Excavation after failure revealed that the fabric had ruptured, but that anchorage on either side of the rupture location was sufficient. The unreinforced section failed at a height of 1.75 m.

This field test shows the benefit of tensile reinforcement placed at the embankment-fill interface simply on the basis of comparison of failure heights of the two test sections. However, the real benefit of this case history is in its use as a calibration tool for limit equilibrium procedures. Brakel et al. (1982) performed circular arc calculations (assumed to be the "Swedish circle" method) for an reinforced embankment height of 3.5 m assuming tangential orientation of the reinforcement at failure and obtained the results shown in Figure 2.22. Other limit equilibrium analyses of this project have been carried out by Rowe and Soderman (1984) and Low and Duncan (1985). In both of these studies an extended Bishop's Modified Method was used which allowed consideration of both horizontal and tangential orientation of the reinforcement. Identical results were obtained from these two studies as shown in Figure 2.22 and show excellent agreement to the observed results. It can be seen that assuming tangential and horizontal orientations results in calculated factors of

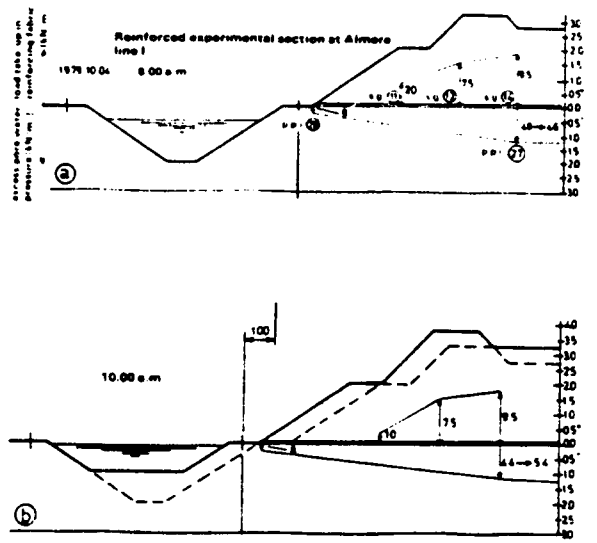

Figure 2.21 Measured reinforcement forces at Almere (Brakel et al. 1982).

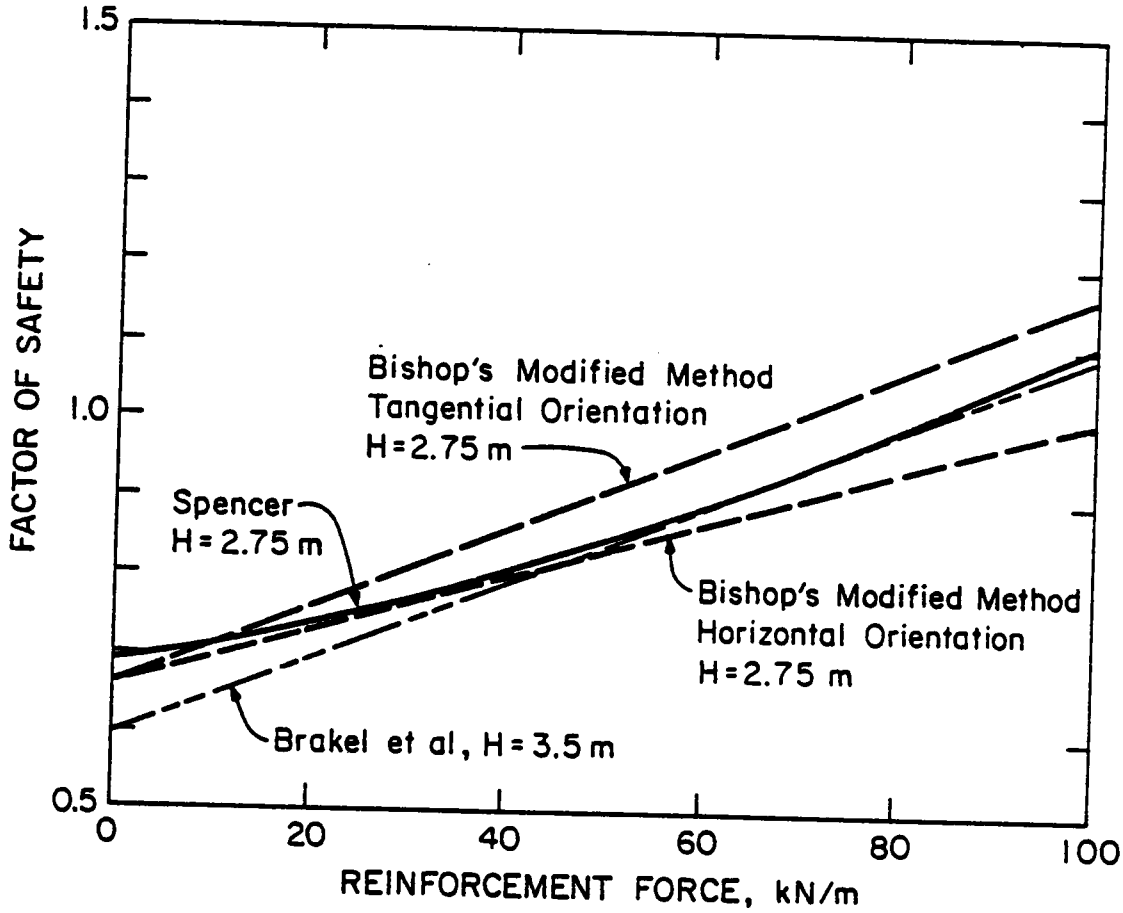

Figure 2.22 **Limit equilibrium results for Almere case history.**

safety which form a band around the the true factor of safety of "1" at failure. For comparison purposes, the factor of safety was also determined by using Spencer's method (Spencer, 1968), extended to account for reinforcing in the manner outlined in Section 2.2.3. These results are also shown in Figure 2.22. It can also be seen that using Spencer's procedure with horizontal orientation of the reinforcement yields results in near perfect agreement with the measured results. These results are nearly half-way between the BMM results shown. The results of these limit equilibrium analyses are encouraging when consideration is given to the accuracy with which the in situ shear strength of soft clay can be measured.

2.4.5 Bloomington Road, Ottawa, Canada

Rowe et al. (1984) described the design, instrumentation and field performance of a 1 to 1.5 meter high geotextile-reinforced embankment constructed on peat. The site was designated as Bloomington Road and is located near Aurora, Ontario, Canada. Foundation conditions at the site are shown in Figure 2.23. It can be seen that the depth of the peat deposits varies considerably along the centerline. The upper one meter of the peat deposit was classified as amorphous, containing wood, fine fibers held in a woody, coarse, fibrous framework while the the underlying peat was a nonwoody, fine, fibrous peat. The peat was underlain by silty sand and sand.

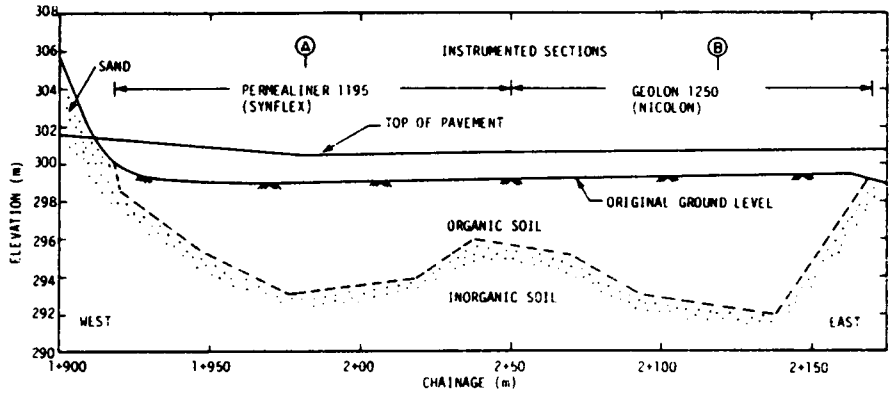

Centre line profile at Bloomington Road.

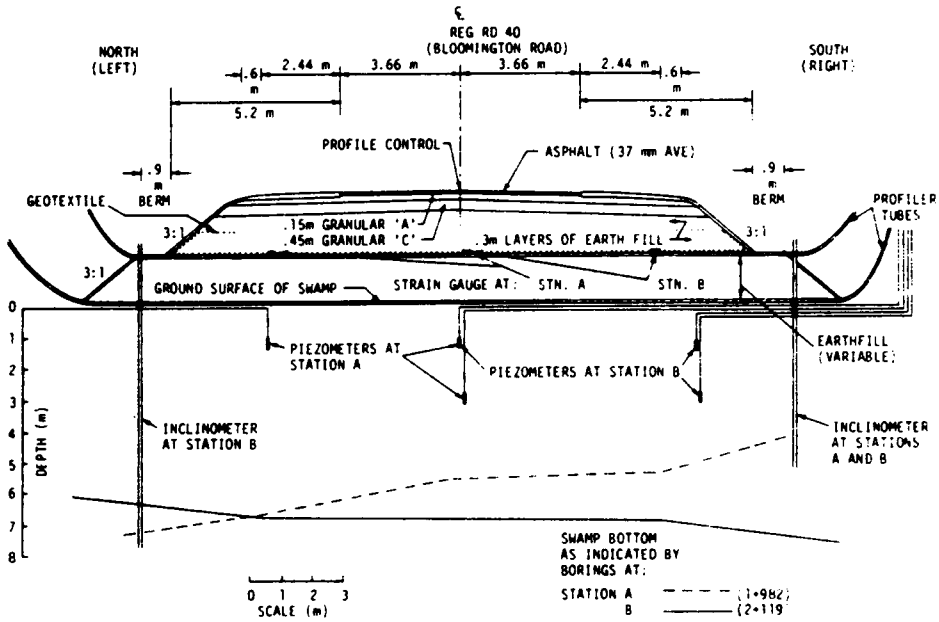

Design profile and instrumentation at stations A and B.

Figure 2.23 Site conditions at Bloomington Road.

A geotextile-reinforced embankment was selected after conventional construction methods were rejected due to either cost or construction difficulty. The geotextile was selected primarily on the basis of a circular arc stability analysis and the following assumptions: (a) The geotextile was placed with the stronger direction transverse to the fill alignment, (b) The tensile forces required to maintain stability can be mobilized at relatively small strains and (c) The tensile force in the fabric will act tangentially to the failure arc. To increase the factor of safety to 1.3, tensile forces of 20 and 39 kN/m were calculated to be needed at Stations A and B, respectively. The requirement that the stabilizing force be developed at relatively small strains implied that the geotextile reinforcement should have a high strength under relatively small elongation and this governed the selection of the geotextiles used. At Station A, a calandered polypropylene monofilament with plane weave was used. At Station B, a plane weave, twisted, polyethylene, slit film was used. Based on stability calculations, the force required to maintain a factor of safety of 1.3 against rotational failure represented approximately 0.5 and 0.3 of the estimated ultimate strength of the geotextiles at Stations A and B, respectively.

Instrumentation consisted of piezometers, hydraulic and electric gages to measure fabric elongation, inclinometers and settlement plates. The location of some of the instrumentation is shown in Figure 2.23.

Construction took place in stages. Due to swampy conditions at the site, a working platform varying in thickness from 0.3 to 1.0 m was constructed prior to placement of the geotextile. Lift thicknesses of 0.3

m were used with the geotextile folded back three meters over the first lift to provide anchorage. The outside-inside construction sequence advocated by Haliburton was used.

During stage I construction, 1.37 m of fill was added at the centerline. Immediate settlements were about 50 percent of the total height of fill added and settlements increased to 75 percent of original fill height prior to stage II construction. Dissipation of excess pore pressure occurred within 60 days of construction.

The progress of settlement with fill height at Stations A and B is shown in Figures 2.24 and 2.25. Significant immediate settlements occurred (50 percent of original fill height at Station A and 90 percent of original fill height at Station B) with stage I loading. Consolidation settlements prior to stage II increased the settlement to 95 percent of original fill height at Station A and at Station B the fill became almost completely submerged.

Stage II construction resulted in significant additional settlement at both stations. At Station A 2.5 m of additional fill yielded on 0.8 m of net fill height at the end of six months of consolidation following construction. Geotextile strains as high as 21 percent were measured in the transverse direction and eight percent parallel to the axis.

Most of the settlement during stage I was attributed to compression of the underlying peat and the geotextile had negligible effect. However, lateral movements and "mud waves" observed during stage II suggested that a large component of stage II settlement was due to shear deformation which resulted in the development of significant fabric strains.

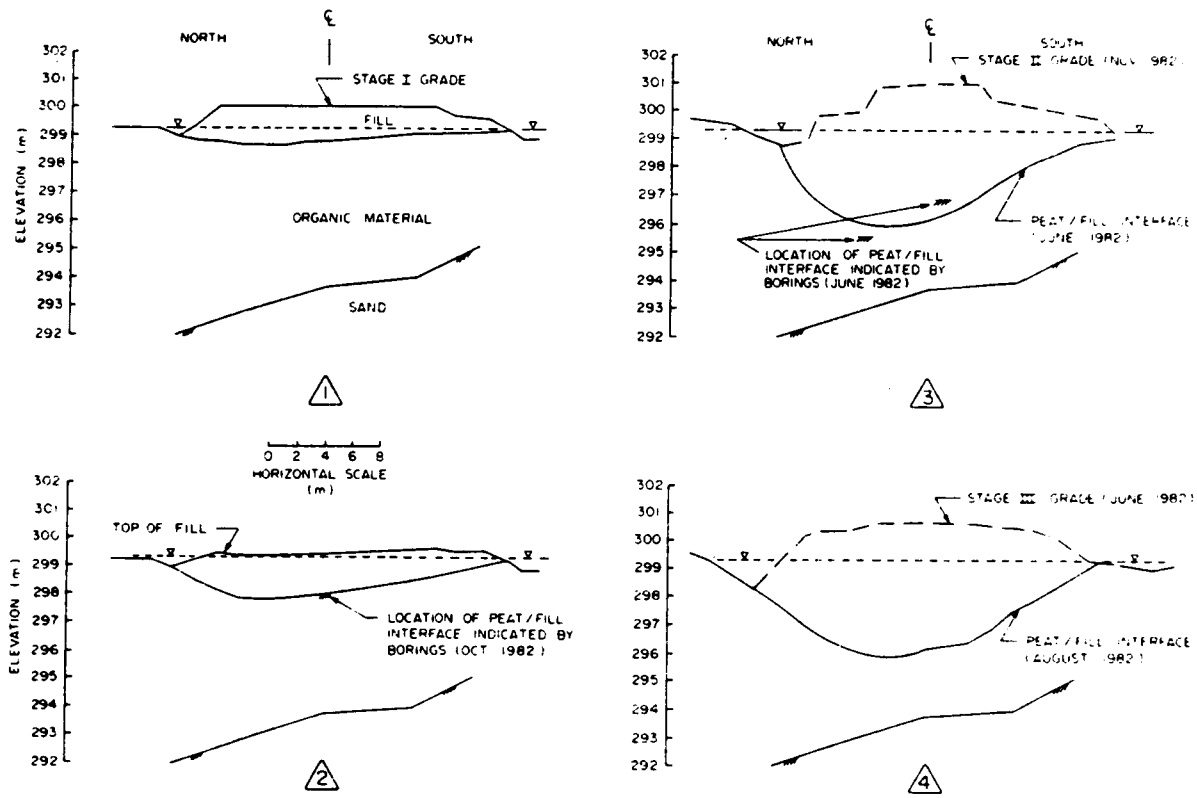

Cross sections at station A: chainage 1+982.

Figure 2.24 **Settlement at Station A.**

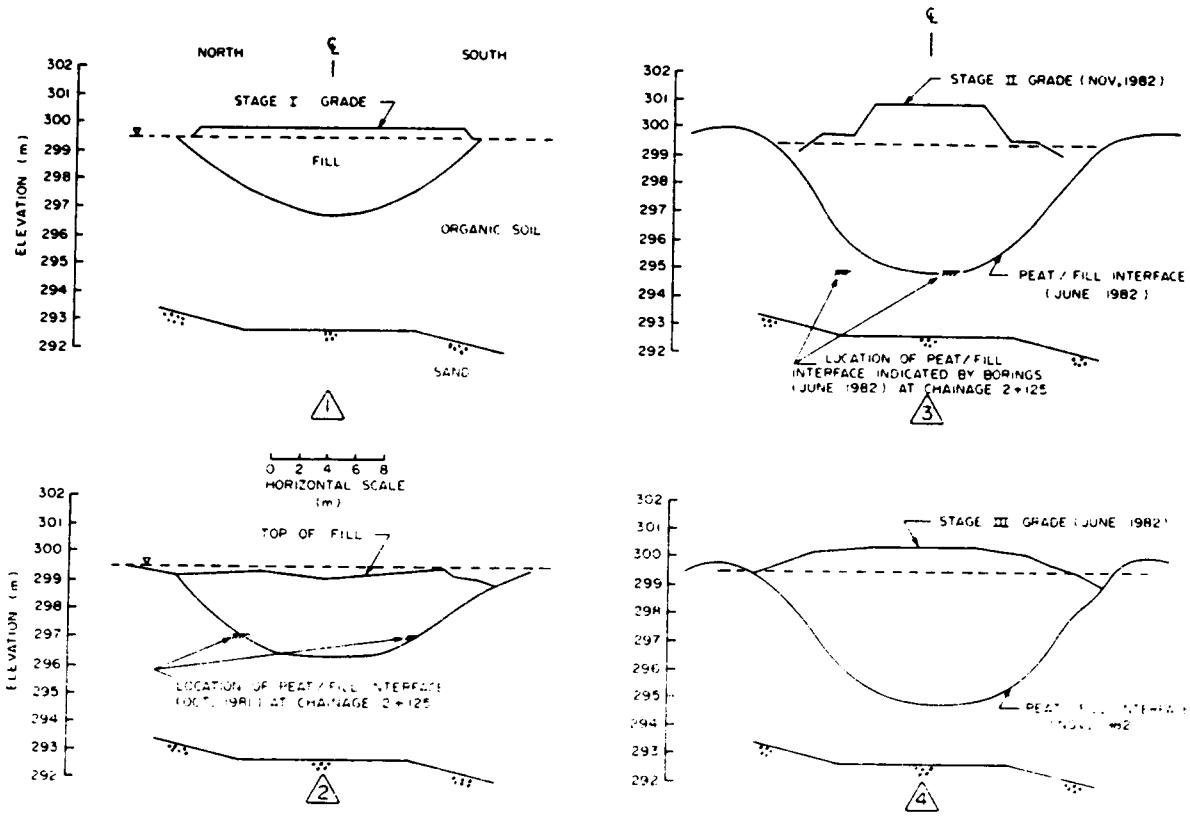

Cross sections at station B: chainage 2+119.

Figure 2.25 **Settlement at Station B.**

Stage III construction consisted of removing fill, placement of an asphalt road surface and shaping of the shoulders and side slopes. Additional settlements of 0.1 and 0.2 m were measured stations A and B in the months following construction. Following completion of the road, differential settlements in the transverse direction were minor while significant differential settlement occurred in the longitudinal direction.

Based on the observed performance of these geotextile reinforced fills Rowe et al made the following observations:

1. Large settlements were observed at both instrumented sections with a maximum fill thickness of 5.7m resulting in a corresponding settlement of 4.7m.

2. Large lateral movements on the order of one to two meters occurred.

3. The geotextile at the edge of the embankment appeared to be unstressed and hence folding back of the fabric was unnecessary.

4. When settlement was due primarily to compression of the peat, geotextile strains were small despite large settlements.

5. When large shear deformations were apparent, large fabric strains and forces developed.

6. Longitudinal strains in the fabric were significant.

7. The field data make it apparent that the use of a single layer of a very strong geotextile did not prevent large shear deformations.

8. In light of the performance of this embankment, simplified limit equilibrium procedures should be viewed with considerable caution when designing geotextile-reinforced embankments on peat.

2.5 Summary and Conclusions

Based on the above discussions the following conclusions can be drawn concerning the behavior of reinforced embankments over weak soils.

1. The use of Bishop's Modified Method, extended to include horizontal reinforcement forces, provides a reliable, slightly conservative procedure for evaluating the factor of safety of reinforced embankments.

2. The factor of safety calculated assuming the reinforcement becomes aligned tangent to the slip surface at failure is considerably higher than that calculated assuming the reinforcement remains horizontal.

3. Based on the analysis of the Almere Test embankment, the actual factor of safety is likely to be approximately equal to the value computed using Spencer's procedure with horizontal reinforcement, and about halfway between values calculated using Bishop's Modified Method using horizontal and tangential orientation of the reinforcement.

4. The optimum location for placement of the reinforcement is at the embankment-foundation interface.

5. Reinforcement has very little effect on consolidation settlements, but it does tend to reduce differential settlements at the top of the embankment.

6. The major effect of reinforcement is to reduce lateral spreading and to increase stability. This is accomplished by reducing shear stresses and plastic flow in the soil through an increase in confinement pressure in the embankment and foundation soils.

7. At low load levels (where the factor of safety is high), reinforcement does not significantly impact embankment behavior.

CHAPTER III

PROCEDURES FOR FINITE ELEMENT ANALYSIS

3.1 Introduction

The review in Chapter II showed the feasibility of using finite element analysis procedures for the analysis of reinforced earth structures. This chapter describes the finite element techniques used in this dissertation for the analysis reinforced soil structures, particularly reinforced embankments and foundations. The method used employs an elasto-plastic stress-strain soil model and allows consolidation effects to be modelled directly. Reinforcement is modelled using bar and membrane elements.

The program used in the analyses in this dissertation was originally developed by Chang and Duncan (1977). The program, called CON2D, was developed to model consolidation behavior of partially saturated soils. During its development the original Cambridge Cam Clay model was extended to provide for more suitable representation of the strength and stress-strain behavior of compacted clay. Further improvements to the program were made by Duncan et al. (1981). An axisymmetric version of the program was developed by D'Orazio and Duncan (1982).

This chapter will review the formulation of the soil model - the Cam Clay model, the formulation of the finite element equations, and the extensions made to the program. The program has been adapted to the

Virginia Tech IBM system, has been extensively rewritten to adopt the efficiencies of structured programming and to document the algorithms of the program, to extend the program to handle static pore water pressures, and to incorporate finite elements for the modelling of reinforcement. With these changes, the program was renamed CON2D86.

3.2 Soil Model

3.2.1 Cam Clay Model

Drucker, Gibson and Henkel (1957) were the first to suggest that soil can be modelled as an elasto-plastic material with work hardening or work softening effects. Based on these ideas and the concept of critical void ratio (Casagrande 1936), Roscoe, Schofield and Wroth (1958) developed an isotropic, strain-hardening model to predict the stress-strain behavior of remolded clays. Subsequent modifications by Roscoe and Schofield (1963), Roscoe, Schofield and Thurairajah (1963), Burland (1967) and Roscoe and Burland (1968) resulted in the model known today as the Modified Cam Clay Model.

The soil model used in CON2D86 is an extended version of the Modified Cam Clay Model. The sections below describe the model as it is implemented in CON2D86 and CONSAX86. Discussions of the original Cambridge version can be found in Schofield and Wroth (1968) and Atkinson and Bransby (1978).

The Cam Clay Model was developed for triaxial conditions and was subsequently extended to general states of stress. The relationships are formulated in terms of the stress invariants p' (the mean normal effective stress) and q (a generalized deviator stress). In terms of the stresses referred to an x, y, z coordinate system, p' and q can be expressed as follows:

$$p' = \frac{1}{3}(\sigma'_x + \sigma'_y + \sigma'_z) \qquad [3.1]$$

$$q = \sqrt{\frac{1}{2}\left[(\sigma_x - \sigma_y)^2 + (\sigma_y - \sigma_z)^2 + (\sigma_z - \sigma_x)^2 + 6\tau_{xy}^2\right]} \qquad [3.2]$$

An elasto-plastic model requires definition of a failure surface, a yield surface to differentiate elastic and plastic behavior, and a flow rule and hardening rule which relate plastic strain behavior to stress changes. These are described in the following paragraphs.

Failure Surface. In the Cambridge version, the failure surface for the Cam Clay model was a straight line through the origin. To represent soils which have a cohesion intercept, the failure surface was revised by Chang and Duncan (1977) as shown in Figure 3.1a, and is represented by the equation

$$q_f = M(p' + p_r) \qquad [3.3]$$

in which q_f = value of q at failure, or shear strength, M = strength parameter, and p_r = an intercept stress.

Additionally, the failure surface was modified to reflect the behavior of soils which exhibit a curved failure line, Figure 3.1b and those which

possess tensile strength, Figure 3.1c. Figure 3.1d shows the complete failure surface in $q - p'$ space.

Yield Surface. The yield surface in the Cambridge model is assumed to have an elliptical shape as shown in Figure 3.2. The surface is defined by the equation

$$\left(1 + \frac{\eta^2}{M^2}\right)(p' + p_r) - p_r = p'_o \qquad [3.4]$$

where $\eta = \frac{q}{(p' + p_r)}$ and p'_o is a preconsolidation pressure.

Flow Rule. The flow rule relates the plastic strain increments to the existing stress state. The plastic strain increments are assumed to occur as outward normals from the yield surface, as shown in Figure 3.2. For such conditions, the plastic potential function and the yield surface are identical and the flow rule is termed associated. The extended version is the same as the original version in this respect.

Hardening Law. The hardening parameter describes the magnitude of the plastic strain increments. The slope of the ellipse at the stress point determines the relative magnitude of the plastic strain increment. As shown in Figure 3.2, the plastic strain increment can be divided into a plastic volumetric strain ε_v^p and a plastic distortional strain ε_v^d (or shear strain). Thus the magnitudes of all the components of the plastic strain can be related to the value of the plastic volume strain ε_v^p which can be calculated by

$$\varepsilon_v^p = (\lambda - \kappa) \ln \frac{p'_o}{P_p} \qquad [3.4]$$

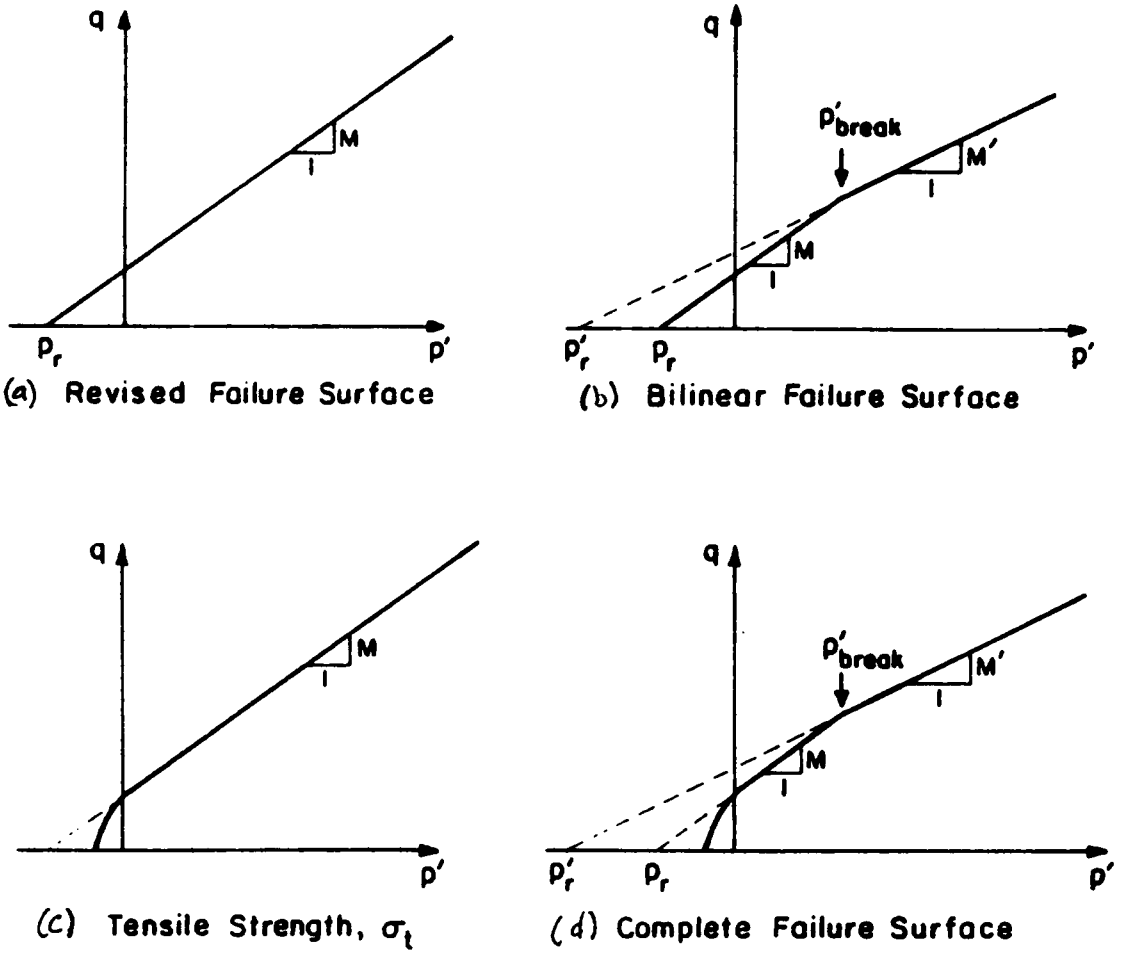

Note: Tensile failure occurs when $\sigma_3 = \sigma_t$

Figure 3.1 Failure surfaces in CON2D86 (Duncan et al. 1981).

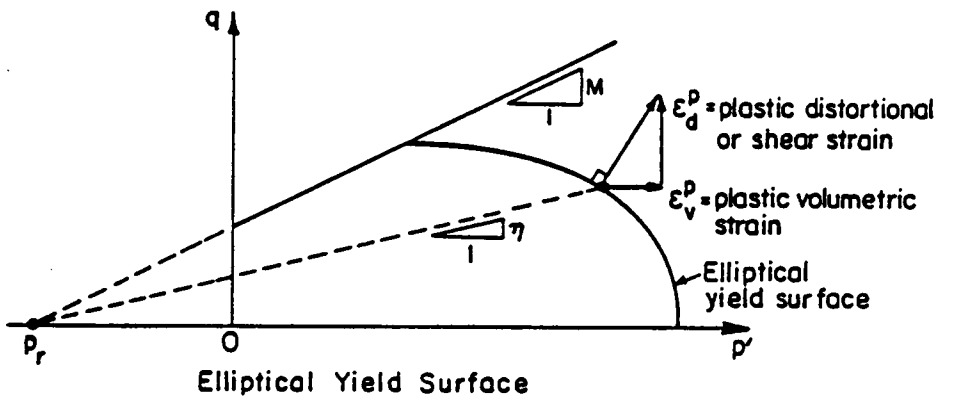

Figure 3.2 The yield surface used in finite element analyses, in q-p' space.

where λ and κ are the slopes of the virgin and rebound compression curves, as shown in Figure 3.3, and P_p is the preconsolidation pressure.

Elastic Behavior. At stress states inside of the yield surface, only elastic strain increments result from stress increments. All of the components of elastic strain are related to the stress increments through the Generalized Hooke's Law. Any two of the elastic parameters E, Young's Modulus; ν, Poisson's ratio; G, shear modulus; or B, bulk modulus, can be specified to determine the magnitude of the elastic strains. In CON2D86, the parameters used are Poisson's ratio and the bulk modulus. The bulk modulus is calculated from

$$B = \frac{(1 + e)p'}{\kappa} \qquad [3.5]$$

This provides for nonlinear stress-strain behavior because B varies with the mean pressure, p'.

3.2.2 Material Parameters

The material properties that describe a soil model should be easily determined from conventional laboratory or field tests. The Cam Clay model described above can be defined by the following six parameters.

p_r an intercept stress to represent a cohesion intercept;

M the slope of the failure line in q-p' space;

κ the slope of the rebound rebound consolidation curve;

λ the slope of the virgin isotropic consolidation curve;

ν Poisson's ratio;

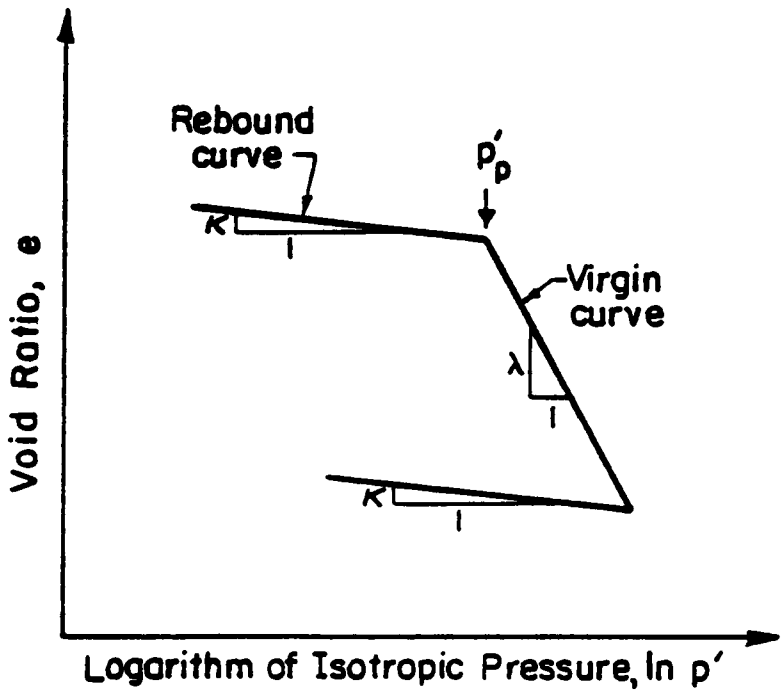

Figure 3.3 Definition of Cam Clay parameters κ and λ.

e_0 the initial void ratio.

λ , κ and e_0 can be obtained from an isotropic consolidation test as shown in Figure 3.3. The intercept stress, p_r, and the slope of the failure line, M, can be determined using the effective strength soil parameters φ' and c' in the following equations.

$$p_r = c' \cot \varphi' \qquad [3.6]$$

and

$$M = \frac{6 \sin \varphi'}{3 - \sin \varphi'} \qquad [3.7]$$

The value of Poisson's ratio may be determined from triaxial compression tests using the procedures outlined by D'Orazio and Duncan (1982). In CON2D86, the value of Poisson's ratio may vary with p' the effective mean noraml pressure.

3.2.3 Undrained Shear Strength

One of the applications of the Cam Clay Model is the prediction of the undrained shear strength of a clay because the undrained shear strength depends on the effective strength of the clay. Relationships for the variation of undrained strength S_u with effective consolidation pressure can be derived in terms of the Cam Clay parameters. One such relationship was presented by Poulos (1986):

$$\frac{S_u}{p'_o} = \frac{M}{4}[2]^{\frac{\kappa}{\lambda}}\left[\frac{p'_c}{p'_o}\right]^{(1-\frac{\kappa}{\lambda})} \qquad [3.8]$$

where S_u is the undrained shear strength, p'_o is the overburden pressure, p'_c is the preconsolidation pressure, and M, λ, and κ are as previously defined. The ratio $\frac{p'_c}{p'_o}$ in Equation 3.8 represents the overconsolidation ratio. Similar relationships for the undrained strength in terms of Cam Clay Model parameters have been presented by Atkinson and Bransby (1978) and Mayne (1980).

3.3 Consolidation Analysis

3.3.1 Finite Element Formulation of Consolidation

Finite element formulations of the consolidation problem have been presented by Sandhu and Wilson (1969), Hwang et al. (1971) and Chang and Duncan (1977). A short review of the formulation used in CON2D86 is presented here.

A solution to the problem of consolidation involves coupling the equations of equilibrium and the equations of fluid flow. Chang and Duncan (1977) have shown that the equations of equilibrium and equation of continuity can be combined and discretized into the following sets of simultaneous equations:

$$[K]\{w\} + [L]\{u\} = \{F\} + \{F_b\} \qquad [3.9]$$

and

$$-[H]\{u\} + [G]\frac{d}{dt}\{w\} - [E]\frac{d}{dt}\{u\} = \{\Gamma\} \qquad [3.10]$$

In these equations {w} and {u} are the nodal displacements and pore pressure, respectively. The integral definitions of the matrices and vectors may be found in Chang and Duncan (1977), and similar sets of equations were described by Christian (1977) and Hwang et al. (1971). The physical significance of the matrices and vectors are:

[K] soil stiffness matrix

$[G] = [L]^T$ coupling matrices between the stiffness and fluid flow equations

[H] transmissibility matrix

[E] fluid compressibility matrix

{F} vector of nodal loads

$\{F_b\}$ vector of body forces

{Γ} vector of specified fluid velocities on boundary surface.

Included in Equation 3.10 are terms relating to the flow of fluid in soil ([H]) and the compressibility of unsaturated soils ([E]). The additional soil parameters required to describe the consolidation and unsaturated behavior of the soil include the unit weight of water, the vertical and horizontal permeability of the soil, and the degree of saturation.

Because Equation 3.10 contains derivatives with respect to time, integration over time is necessary to obtain solutions. In CON2D86, a finite difference solution to the time integration is used, with a fully

explicit method specified. Combining the time integration with Equations 3.9 and 3.10 provides the matrix equation:

$$\begin{bmatrix} [K] & [L] \\ [L]^T & -[H]\theta\Delta t - [E] \end{bmatrix} \begin{Bmatrix} w \\ u \end{Bmatrix} t_1 = \begin{Bmatrix} F + F_b \\ \theta\Delta t\Gamma \end{Bmatrix} t_1 + \qquad [3.11]$$

$$\begin{Bmatrix} 0 \\ (1-\theta)\Delta t\{\Gamma\}t_o + ([H](1-\theta)\Delta t - [E])\{u\}t_o + [L]^T\{w\}t_o \end{Bmatrix}$$

where θ is a time parameter. If the solution is known at t_o, then it can be found at t_1 , and hence at t_n by forward marching.

In the original derivation of Equations 3.9 and 3.10, Chang and Duncan (1977) formulated the pore pressures in terms of excess pore pressures. At the suggestion of Chen (1984), the present version of the program has adopted the total pore pressure approach wherein static pore pressures are taken into account.

3.3.2 Stability Criterion

The stability of consolidation analyses has received considerable attention by investigators and many interpolation schemes have been proposed for the time domain. Booker and Small (1975) showed that unconditionally stable solutions result if θ in Equations 3.7 and 3.8 is greater than $\frac{1}{2}$. Despite this, finite element solutions of consolidation often exhibit oscillatory pore pressures (Sandhu et al. 1977 and Read 1984). Vermeer and Verruijt (1981) investigated the oscillation phenomena and

concluded that a lower limit on the time step, based on the coefficient of consolidation and the mesh size, could reduce the occurrence of oscillatory results. The limit proposed was $\Delta t \geq \frac{1}{6} \frac{(\Delta h)^2}{\theta c}$ where Δh is the mesh size adjacent to the draining boundary, θ is the time integration parameter and c is the coefficient of consolidation. This limit on the size of the time steps is recommended when using CON2D86.

3.4 Finite Elements Used in Program

3.4.1 Soil Elements

Isoparametric elements having a variable four to eight node configuration are used to represent the soil. These elements were developed by Bathe and Wilson (1973). These elements allow considerable flexibility in mesh layout for complicated geometries. In general, eight node elements are used where pore pressure degrees of freedom are required and four node elements where they are not. Triangular elements can be formed by superimposing nodes.

3.4.2 Reinforcing Elements

The representation of reinforcement was incorporated into CON2D86 as a simple, two-node bar element capable of sustaining axial tension or compression and having no flexural stiffness. The element equations for

such an element can be found in several standard finite element textbooks, such as Reddy (1984), and Weaver and Johnston (1984).

Analyses of reinforced foundations for three-dimensional conditions were simulated using axisymmetric analyses with the program CONSAX86 and an axisymmetric membrane element. The element is capable of transmitting radial tension or compression, but provides no flexural stiffness. The derivation of the stiffness matrix for this element is given in Appendix B.

3.5 Extensions to the Program

The incorporation of reinforcing elements and the provision for handling static pore water pressures have been discussed in previous sections. The most important modification to the program involved rewriting the code to adopt the efficiencies of structured programming.

Structured programming is a philosophy of programming that focuses on the importance of structure for the intellectual manageability and reliability of programs (Kernighan and Plauger 1974). The main concerns are the reduction of program complexity and program correctness. It was with these goals in mind that CON2D86 and CONSAX86 were extensively rewritten using structured programming. The resulting code is more efficient because dead code has been removed, and is easier to follow and understand. Many of the algorithms used to in the program are documented in the source code. This is of particular importance in program codes which are in the research realm, and are continually being modified.

Additional, more detailed documentation and a user's guide are provided in Appendices C and D.

CHAPTER IV

REINFORCED FOUNDATIONS

4.1 Introduction

A reinforced foundation is a soil foundation containing tension-resistant inclusions that increase the ultimate bearing capacity of the system. Reinforced foundations are distinguished from reinforced embankments by the fact that they are level areas designed to support external loads in addition to the weight of the soil. Two types of reinforced foundations are shown in Figure 4.1a: one involves reinforcement of cohesionless soil, and the other involves reinforcement of cohesionless soil overlying weak cohesive soil. The latter condition is the focus of the present study.

A problem of practical interest requiring use of reinforced foundations arises in the construction of oil field drilling pads in areas where soft clay and peat make up the foundation soils. The plan area of these pads is about 100 meters square, and loads from various sources such as hauling equipment, storage tanks, and drilling equipment exert bearing pressures of 15 to 150 kPa (300 to 3000 psf) on the surface (Kroshus and Varcoe 1984). Additionally, peak loads applied to the foundation by a crane raising the drill stem can be as high as 1000 kPa (21,000 psf). With undrained shear strengths in the range of 5 to 20 kPa (100 to 400 psf), these loads cannot be supported by the foundation soils without use

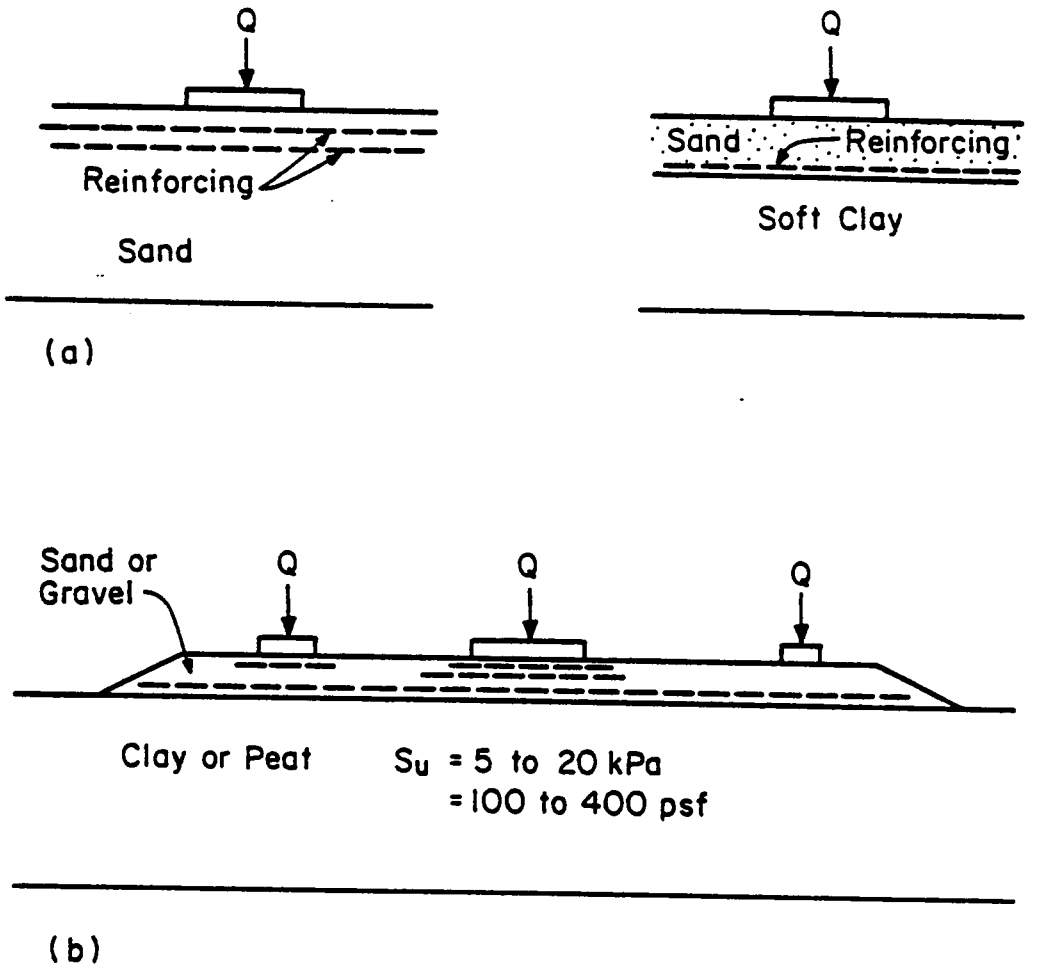

Figure 4.1 Reinforced foundations.

of a very thick pad or a reinforced pad. At present working pads are constructed from local source materials or select fill to spread the loads out over larger areas. In areas where suitable fill materials are not available such material must be imported, often from large distances. The use of reinforcement can reduce the quantity of fill needed. thereby reducing costs. The magnitude of settlement is relatively unimportant in these projects, so long as differential settlement is minimized and bearing failure does not occur. Examples of the conditions that must be considered are shown in Figure 4.1b. The imposed loads may be resisted by one or more layers of a reinforcing material. At present no rational procedures exist by which the amount of reinforcing needed can be determined.

This chapter will review previous studies of bearing capacity of sand overlying soft soils for both unreinforced and reinforced conditions. An approach for the determination of the bearing capacity of reinforced soil over soft soils is presented and compared to the results of model test studies. The results of a finite element analyses of reinforced foundations are also presented and discussed.

4.2 Previous Work on Bearing Capacity of Sand Overlying Soft Soils

4.2.1 Model Tests

Binquet and Lee (1975) were the first to show that reinforced soil technology could be applied to increase the bearing capacity of sand.

In a landmark series of laboratory model tests they showed that horizontal reinforcing strips could increase bearing capacities up to four times those of similar unreinforced granular foundations.

Binquet and Lee identified three mechanisms by which bearing capacity failure could occur: shear failure of the soil above the reinforcement, pullout of the reinforcement from the soil, and breakage of the reinforcement. These modes of failure are illustrated in Figure 4.2. It may be seen in Figure 4.2c that discontinuities of the reinforcement are shown near the edge of the footing. Binquet and Lee noted that failure of the reinforced soil occurred mainly through local or punching shear failure, in combination with general shear on one side of the footing.

The effect of the reinforcing was to increase the ultimate bearing capacity of the soil and also to increase the load-settlement stiffness for loads less than ultimate. Binquet and Lee adopted the term bearing capacity ratio (BCR) to express and compare data from reinforced and unreinforced tests where

$$BCR = \frac{q}{q_o} \qquad [4.1]$$

in which q and q_o are the average bearing pressures for the reinforced and the unreinforced soil, at any desired vertical settlement.

Binquet and Lee observed the following qualitative trends in their model tests:

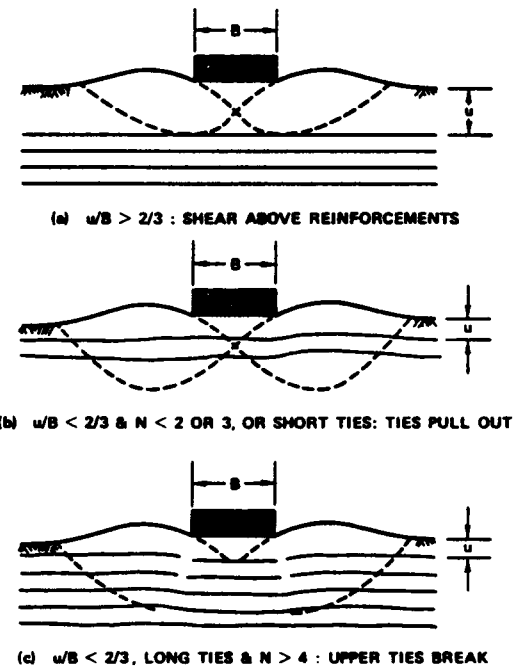

Figure 4.2 **Modes of failure identified by Binquet and Lee (1975).**

1. A minimum number of layers of reinforcing were required to obtain significant load settlement and bearing capacity improvement, with the the optimum number between four and eight layers.

2. The greatest improvement was obtained for an arrangement with the reinforcing layers beginning at a shallow depth near the base of the footing.

3. When the depth to the first layer of reinforcement was greater than 0.67 time the footing width, failure usually took place as shear above the reinforcement rendering the effect of the reinforcement small or nil.

4. In all cases where failure occurred by reinforcement breakage, the broken spots were not located near the classical slip surface, but rather in the upper layers, approximately below the edges of the footing as shown in Figure 4.2c. In these cases punching shear type failure surfaces were apparent.

The results of model test studies of reinforced cohesionless soils using various reinforcing materials have also been reported by Akinusuru and Akinbolade (1981), Fragaszy and Lawton (1984) and Guido et al. (1985a and 1985b). All of these researchers have adopted Binquet and Lee's bearing capacity ratio terminology and have shown that various reinforcing materials can increase the bearing capacity. In general, these test results have substantiated the observations made by Binquet and Lee.

Little data has been published on the bearing capacity of reinforced sands overlying weak, cohesive soils. Model test results have been reported by Milligan and Love (1984), Jarrett (1984) and University of California, Davis (1984b). In addition, Binquet and Lee (1975) performed a few tests in which a soft zone was placed beneath the reinforced sand by using foam rubber to simulate a weak clay layer. These tests have shown that reinforced sand over weak clay provides increased bearing capacity compared to similar unreinforced systems, on the order of 50 to 100 percent. In the unreinforced tests run as controls, the mode of failure was always a punching failure of the sand into the clay. In the reinforced tests the failure mode was less clearly discernible. With the exception of the tests by Binquet and Lee, the tests were performed with geogrids as the reinforcing material, and no slippage between the sand and the geogrids or pullout of the geogrids from the sand was noted by the researchers. The tests reported by Jarrett (1984) were conducted using peat as the weak foundation soil.

In the model tests reported by Milligan and Love (1984), Jarrett (1984) and University of California, Davis (1984b), where the sand was reinforced with geogrids, the reinforcing was placed near the surface of the weak clay or peat. The depth of fill was often greater than 0.67 times the footing width, and yet failure did not occur above the reinforcement as happened in the tests without a weak clay sublayer that were performed by Binquet and Lee (1975). This suggests that the failure mechanism in reinforced sand over weak clay is different than that for reinforced sand without a weak clay sublayer. Thus, the trends observed by Binquet and

Lee for a minimum number of layers and placement of reinforcing layers near the base of the footing may not hold for reinforced sand over clay. Indeed, it is expected that concentrating the reinforcement near the sand-clay interface will provide better results.

4.2.2 Analytical Techniques

4.2.2.1 Bearing Capacity of Unreinforced Cohesionless Soils Over Soft Clay

The bearing capacity of unreinforced cohesionless soil overlying soft cohesive soil has been studied by a number of investigators. For application to the present study, the cohesionless layer is considered to be relatively thin, so that the strength of the underlying clay controls the ultimate bearing capacity.

The bearing capacity for this condition has often been determined by (a) computing the capacity as if the clay did not exist, and (b) computing the capacity of a fictitious foundation (with an increased width) resting directly on the clay, and using the smaller of these two bearing capacities. When this procedure in used, the increased width of the fictitious foundation is often based on the load being distributed over a 2V:1H projection area from the base of the footing (Terzaghi and Peck 1967). The capacity of the system is controlled by the clay strength until the depth to the clay becomes very large.

From research on the design of unreinforced aggregate layers over soft soils for unpaved road systems, a clearer picture of the limitations of the projected area method has developed. In such studies, the system is subjected to a number of cycles of loading simulating loading by haul trucks. Based on experimental model tests on aggregate over soft clay, Bender and Barenburg (1978) adopted a pressure limit on the clay surface of 3.3 times cohesion, with the pressure at the top of the clay being determined from a Boussinesq stress distribution analysis. This pressure corresponds closely with πc which can be considered as the elastic bearing capacity of clay (Whitman and Hoeg 1966). Giroud and Noiray (1981), Giroud et al. (1984) and Poran (1986) also adopted this limit for the pressure exerted on the subgrade clay. The bearing capacity of the system was then calculated by spreading the surface load to the clay surface by the projected area method. The model test results of Milligan and Love (1984) and University of California, Davis (1984b) support the limit of πc as the bearing strength to use for unreinforced systems when using the projected area method.

Experimental work by Tcheng (1957) (as reported by Vesic 1973) and additional studies by Vesic (1973), as well as the model studies described in the previous section, have shown that the mode of failure for this case is punching along essentially vertical slip lines following the foundation perimeter. The procedures based on the projected area methodology do not consider this failure mechanism; instead, they consider a larger critically loaded area at the surface of the clay.

To overcome this deficiency, Meyerhof (1974) proposed the following approximate theory of the bearing capacity of a footing punching through a thin, dense sand layer into a thick, soft clay bed. At ultimate load a sand mass having an approximately truncated pyramidal shape is pushed into the clay so that, in the case of general shear failure, the friction angle φ of the sand and undrained cohesion c of the clay are mobilized in the combined failure zones shown in Figure 4.3.

Meyerhof hypothesized that the forces on the failure surface in the sand could be taken as equivalent to a passive earth pressure P_p inclined at an angle δ and acting upwards on a vertical plane through the footing edge. For a strip footing of width B and depth D, at a distance H above the clay surface, the ultimate bearing capacity was, approximately, given by

$$q_u = cN_c + 2P_p \sin \delta/B + \gamma D \qquad [4.2]$$

where N_c= bearing capacity factor = 5.14 and γ = unit weight of sand.

Meyerhof determined the passive earth pressure to be

$$P_p = 0.5\gamma H^2(1 + 2D)K_p/\cos \delta \qquad [4.3]$$

where K_p = coefficient of passive earth pressure.

The angle δ decreases from about φ near the footing edge to about zero at the clay surface. Based on trial calculations, Meyerhof found an average value of δ to be in the range of $\frac{\varphi}{2}$ to $\frac{3\varphi}{4}$ and recommended that a value of $\frac{2\varphi}{3}$ be used. In addition, it was recommended for practice to use a coefficient K_s of punching shearing resistance on the vertical plane

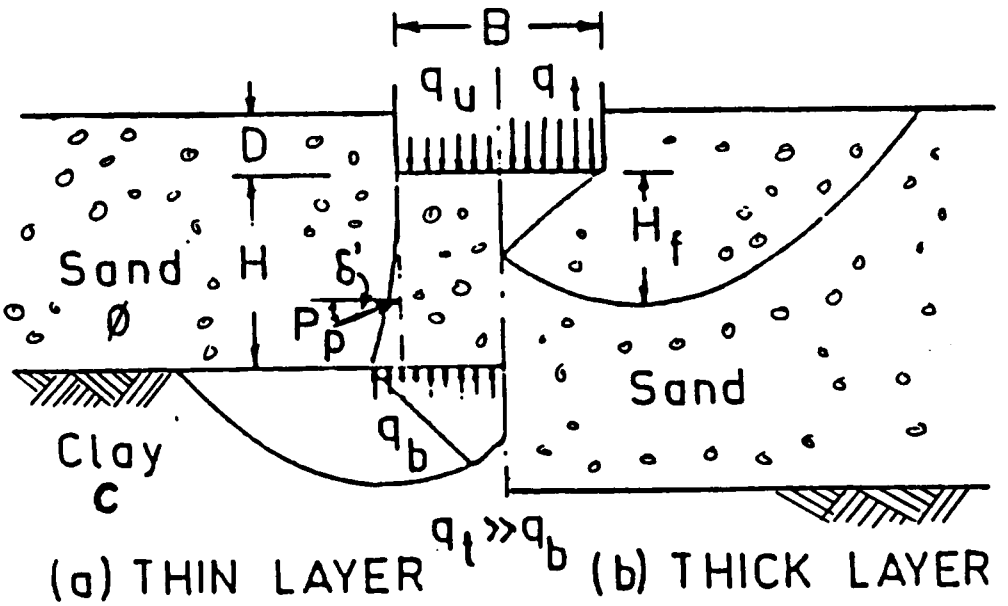

Figure 4.3 **Failure of soil below footing on dense sand layer above soft clay (Meyerhof 1974).**

through the footing edge such that, on substitution of Equation 4.3 into Equation 4.2, the bearing capacity becomes

$$q_u = cN_c + \gamma H^2\{1 + 2\frac{D}{H}\}K_s \tan \varphi/B + \gamma D \qquad [4.4]$$

where

$$K_s \tan \varphi = K_p \tan \delta \qquad [4.5]$$

and K_s is a coefficient of punching shear. A maximum bearing capacity equal to the ultimate bearing capacity of the sand was recommended as an upper limit on Equation 4.4.

The value of K_s is difficult to determine. Meyerhof presented values of K_s determined using Equation 4.5 and earth pressure coefficients K_p based on logarithmic failure surfaces as functions of φ. Values of K_s determined from limited model testing and field records were compared to values calculated from theory for $\delta = 0.6\varphi$ and found to be in good agreement.

The analysis was extended to circular and rectangular footings by determining the passive resistance P_p inclined at δ on vertical surfaces through the footing perimeter, with the increased resistance for these cases expressed through shape factors applied to Equation 4.5.

The theory as described above has been compared to bearing capacity tests on model footings and found to be in good agreement. Additional work on the determination of the coefficient of punching shear K_s was presented by Hanna and Meyerhof (1980). This work provided for considerably reduced punching shear coefficients when the undrained strength

of the cohesive layer was less than 10 kPa (200 psf). In addition, an extensive set of charts for the determination of K_s was presented. Kraft and Helfrich (1983) compared this theory to the results of 27 full-scale and model bearing capacity tests and found very good agreement between measured and predicted bearing capacity. Kraft and Helfrich concluded that the theory was of such merit as to recommend discontinuing the use of the 2:1 pressure method for calculating bearing capacities for sands overlying soft clay. Additional support for Meyerhof's theory is presented in Figure 4.4, where the measured and calculated bearing capacity of unreinforced model tests from Milligan and Love (1984) and University of California, Davis (1984b) are compared. It can be seen that quite good agreement is obtained. The data which do not show a particularly good fit are from tests on very weak subsoils (S_u less than 10 kPa), and for these soils the reductions in K_s proposed by Hanna and Meyerhof (1980) may be too severe.

4.2.2.2 Bearing Capacity of Reinforced Cohesionless Soils Over Soft Clay

Because the reinforcement of sands over weak clays is a relatively new development in geotechnical engineering, the literature devoted to bearing capacity analysis is scant. The papers of Bender and Barenburg (1978), Giroud and Noiray (1981), Giroud et al. (1984), Milligan and Love (1984) and Poran (1986) form the groundwork of the literature devoted to this subject.

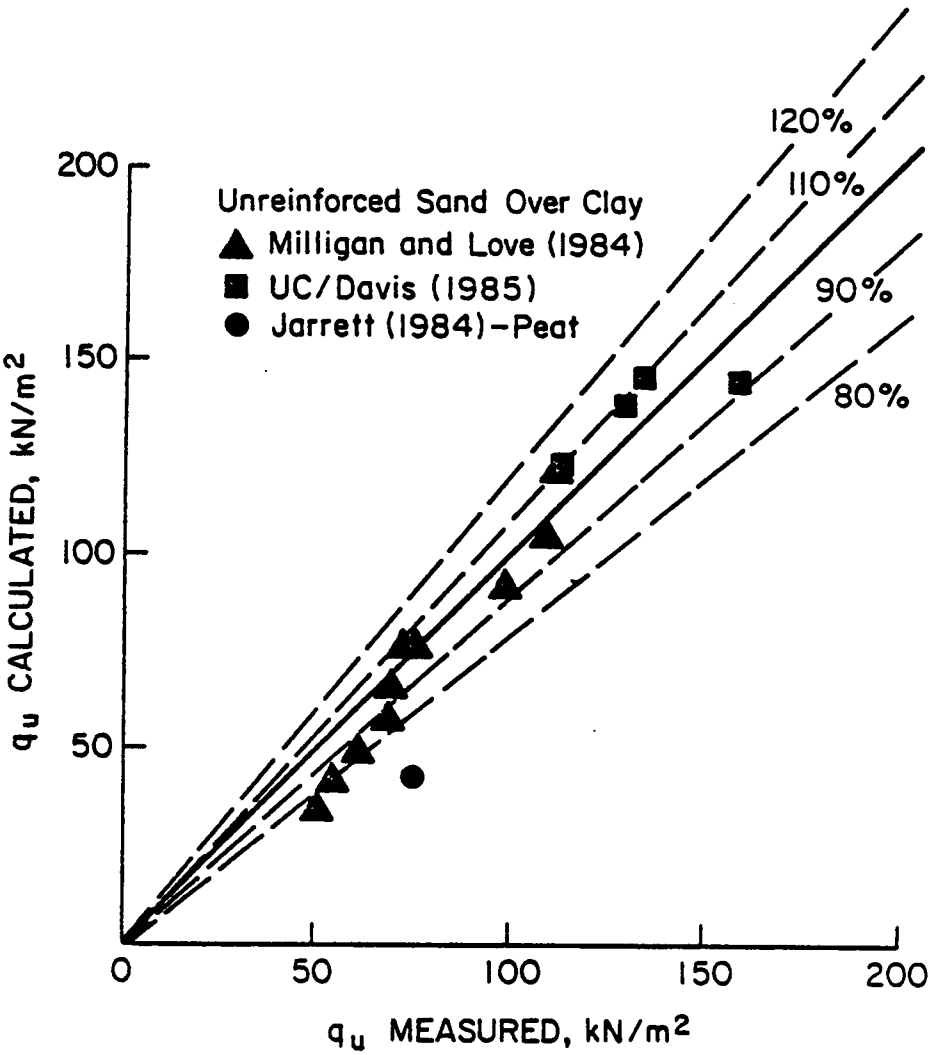

Figure 4.4 Measured bearing capacities versus calculated values using Hanna and Meyerhof (1980) procedure.

From these works, the major effects of reinforcement for improving bearing capacity appear to be:

1. Increased confinement of the cohesionless layer (Bender and Barenburg 1978) and of the subgrade material (Giroud et al. 1984), providing enhanced bearing capacity of both of these materials.

2. Alteration of the failure mechanism in the soft soils by distributing stresses more evenly over the soft soil (Bender and Barenburg 1978 and Giroud et al. 1984).

3. A tensioned membrane effect which results in a reduction of the pressure applied to the subgrade soil (Giroud and Noiray 1981).

In addition, the presence of a geotextile or geogrid at the sand-clay interface reduces intermixing of the sand and clay, which can have detrimental effects on the performance of both materials.

Bender and Barenburg (1978), Giroud and Noiray (1981), Giroud et al. (1984) and Poran (1986) have all assumed that the effective confinement induced by the reinforcement increases the bearing capacity of the clay from the value of πc applicable to brittle materials (see previous section) to the value of $(2 + \pi)c$ applicable to ductile materials. Experimental evidence for this was first presented by Bender and Barenburg (1978). Hence, all of the referenced studies indicate that the limiting bearing pressure on the clay subgrade under reinforced cohesionless layers can be taken as $(2 + \pi)c$. The bearing capacity of a reinforced system

can then be determined using procedures for calculating the load distributed to the clay, where the limiting pressure on the clay is $(2 + \pi)c$. All of these procedures considered a single layer of reinforcement at the base of the cohesionless layer. Giroud and Noiray (1981) and Poran (1986) made theoretical calculations of the tensioned membrane effect contribution to the bearing capacity, and determined that it was negligible.

The procedures described above have the shortcoming that they are limited to a single layer of reinforcement placed at the base of the cohesionless layer, and that no direct consideration of the strength of the reinforcement is contained in the procedures. It is therefore not possible to determine the required quantity or strength of the reinforcement by means of these procedures.

4.3 Finite Element Analyses

In contrast to reinforced embankments, the analysis of reinforced foundations using the finite element method has received little attention. The publications by Brown and Poulos (1981) and Poran (1986), appear to be the only previous work on application of the finite element method to reinforced foundations.

Brown and Poulos (1981) performed a finite element analysis of the experimental model tests performed by Binquet and Lee (1975). The details of the model used are the same as those described in Chapter 2 for the authors work on reinforced embankments (Brown and Poulos 1978). Their

analyses showed that the reinforcement had little effect on the elastic stiffness of the footings. This was in contrast to Binquet and Lee's test results which indicated an increased stiffness with increasing amounts of reinforcement. The analyses did indicate a significant increase in collapse load and smaller deformation to failure with increasing amounts of reinforcement. However, the analyses consistently underpredicted the collapse load compared to the experimental results. A comparison of plastic regions in the unreinforced and reinforced analyses showed that the presence of reinforcement spread the footing load and caused a deeper and wider mobilization of soil strength.

Poran (1986) performed two-dimensional, plane strain finite element analyses of them model tests that had been performed at the Unversity of California, Davis (1984b). In his analyses he used a bounding surface, elasto-plastic model (Dafalias and Herrmann 1982) and special reinforcing elements developed by Hermann (1984). Load-displacement curves from the finite element analyses indicated smaller loads than the model test curves. Poran attributed the differences to the three-dimensional geometry of the model tests. Poran applied a correction factor based on shape factors for two- and three-dimensional geometries to reduce the model test results to two-dimensional conditions and obtained much better agreement between calculated and experimental load-displacement curves. In analyses of model tests without that had been performed without reinforcement, the analyses indicated that failure should occur by localized punching of the sand into the clay,the same mechanism of failure as observed in the model tests. With the addition of reinforcement, the mode

of failure was less distinct in both the model tests and the analytical results. The failure area extended laterally away from the footing, engaging significantly more volume of soil in the failure compared to the unreinforced case.

In this study, additional finite element analyses of the model test performed at the University of California, Davis (1984b) were performed. The University of California, Davis model tests were performed in a wooden box 73 inches long, 68 inches wide and 48 inches high. A saturated clay sample 26 inches high was formed in the box and an eight inch thick sand layer was placed on top of the clay. The footing load was applied through a 12-inch square, 1-1/8 inch thick steel plate using a hydraulic jack system. Tensar SS1 was used as the reinforcement, and was placed in the sand two inches above the clay.

The computer programs describe in Chapter 3 were used in the analyses, and both plane strain and axisymmetric analyses were performed. The finite element analyses modeled a symmetrical half of the model test box, and used 35 elements to represent the clay and 36 elements to represent the sand. The mesh was finer near the footing and larger elements were used away from the footing. The reinforcement was modelled using the elements described in Section 3.4.2. It seems likely that the greatest uncertainties in the analyses arise from the selection of material properties for the clay, the sand and the reinforcement. Little data on the soils was contained in the University of California, Davis report. The only data available were the friction angle of the sand, cohesion values for the clay determined from unconfined compression tests, and gradation

and classification tests on the sand and clay. These data were used to estimate soil strength parameters for the finite element model following the guidelines of D'Orazio and Duncan (1982), and Section 3.4. Compressibility parameters were determined by trial, attempting to achieve the best possible match between the load-deformation curve computed in an axisymmetric unreinforced analysis and that measured in the unreinforced model tests.

The initial soil stresses and the preconsolidation pressures are also important for the finite element analyses. The preconsolidation pressure for the clay soil was estimated using the procedure described in Section 3.4. The saturated clay was assumed to have $K_o = 1$ initial stress conditions.

The initial stresses for the sand were more difficult to estimate. The only information available was that a high pressure pneumatic vibroplate compactor was used to compact the sand. Preliminary analyses using $K_o = 1$ in the sand resulted in failure under loads of 400 lbs (compared to failure loads of about 2800 lbs in the model tests) and were therefore deemed unrepresentative of the actual conditions. Next, the initial stresses were computed using the procedures for estimating compaction-induced stresses developed by Seed and Duncan (1983). The use of these compaction-induced stresses produced load-displacement curves which were extremely stiff and which greatly overpredicted the load-settlement behavior of the model tests. By trial, it was found that $K_o = 2$ stresses in the sand gave a reasonable match between the unreinforced model tests and the finite element results.

The value of stiffness for the Tensar SS1 reinforcement was determined from load-strain plots presented by Tensar (1983) and the values of measured strain reported by University of California, Davis (1984b). Average values of measured strain in the reinforcement varied from 0.8 to 1.8 percent in the model tests. A strain of two percent was selected for determining the value of modulus to input into the analyses. At two percent strain, the modulus was calculated to be 2000 lb/in in the strong direction and 1150 lb/in in the weak direction. The plane strain analyses of the axisymmetric tests were run using an average of the stiffness in the two directions. The axisymmetric analyses used an equivalent modulus in the membrane element, determined using the procedures described in Appendix B. The value of this modulus was E = 1440 lb/in.

The dashed lines in Figure 4.5 show typical load-footing displacement results from the unreinforced and the reinforced model tests. It can be seen that no footing displacement was measured until approximately 400 pounds of load were applied to the model footing. It can also be seen that the reinforced model test carries only slightly larger loads than the unreinforced model test, up to a footing displacement of approximately one inch. Above this footing displacement, the load carrying capacity of the reinforced system increased significantly. It would appear from this results that a critical amount of deformation is required to mobilize the behavior of the reinforcement.

The results of the plane strain finite element analyses of the model tests are shown in Figure 4.5 and the results of the axisymmetric analyses are shown in Figure 4.6. It may be seen that the plane strain analysis

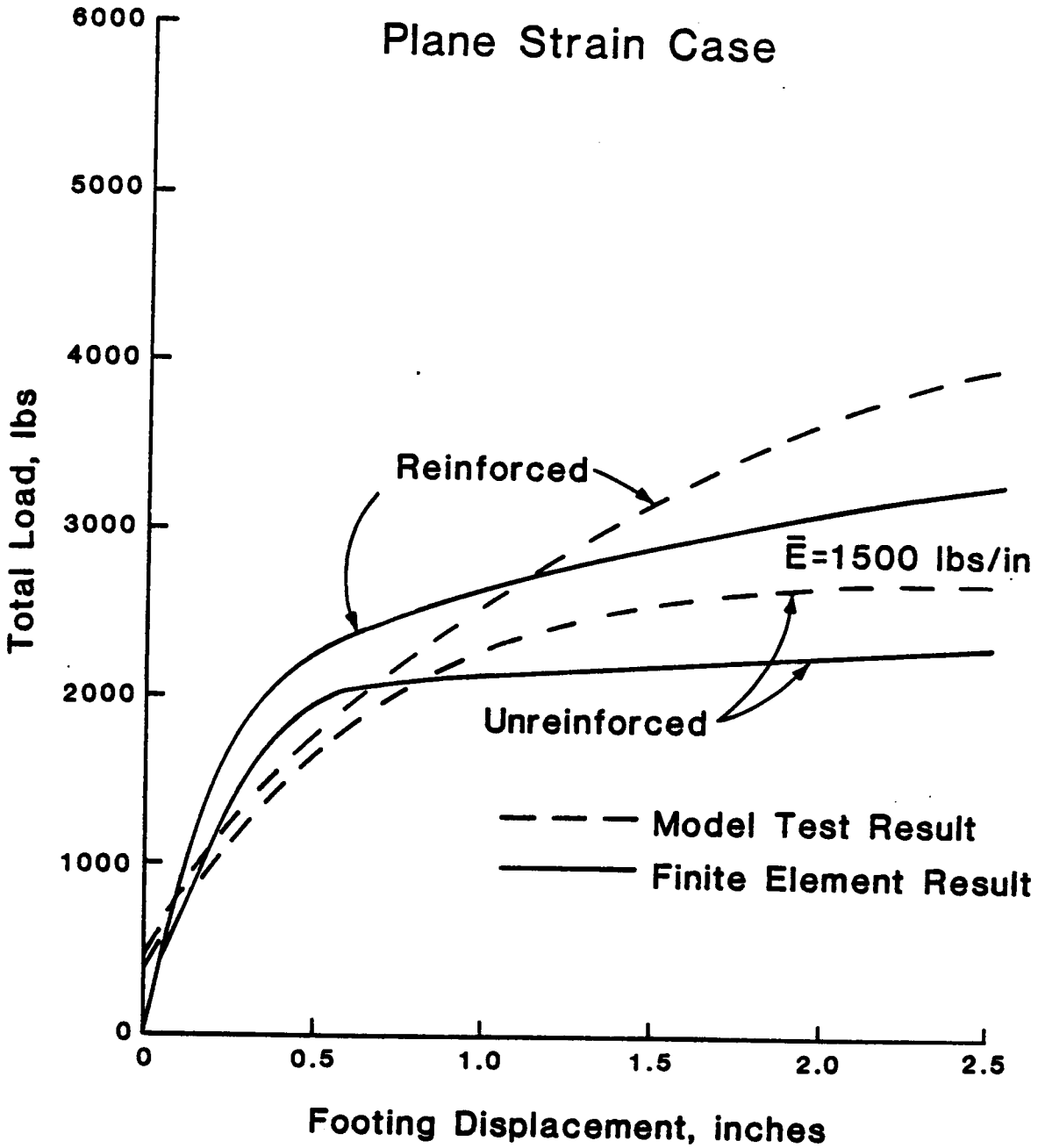

Figure 4.5 Comparison of measured and computed load-displacement curves for UC Davis model tests - plane strain case.

of the reinforced case underpredicts the ultimate load of the model test. It has been found previously by Meyerhof (1974) and others, that plane strain analyses of bearing capacity result in smaller failure loads than measured in circular plates and this result is thus as expected. The initial load-deformation behavior is modelled reasonably well considering the model test required some 400 pounds of load application before measurable movements occurred. The computed load-displacement curve is somewhat steeper than the model test curve but is in reasonable agreement.

The plane strain reinforced analyses also underpredicted the reinforced model test results. The computed results indicate that the addition of reinforcement would be expected to cause a steepening of the load-displacement response in the early part of the test, and increase the ultimate load. The differences between the computed unreinforced and reinforced behavior are comparable to the differences exhibited in the model test results, showing good qualitative agreement with the model tests.

The results of the axisymmetric finite element analyses of the model tests are shown in Figure 4.6. The model parameters used in the analyses were chosen such that the calculated collapse load and load-deformation behavior for the axisymmetric case would agree as well as possible with the model test results. It can be seen that the calculated collapse load agrees very well with the measured collapse load. However, achieving a match of the load-deformation curves was not as easy. The load-deformation curve shown in Figure 4.6 is about the best match for the unreinforced load test that could be achieved after several trials.

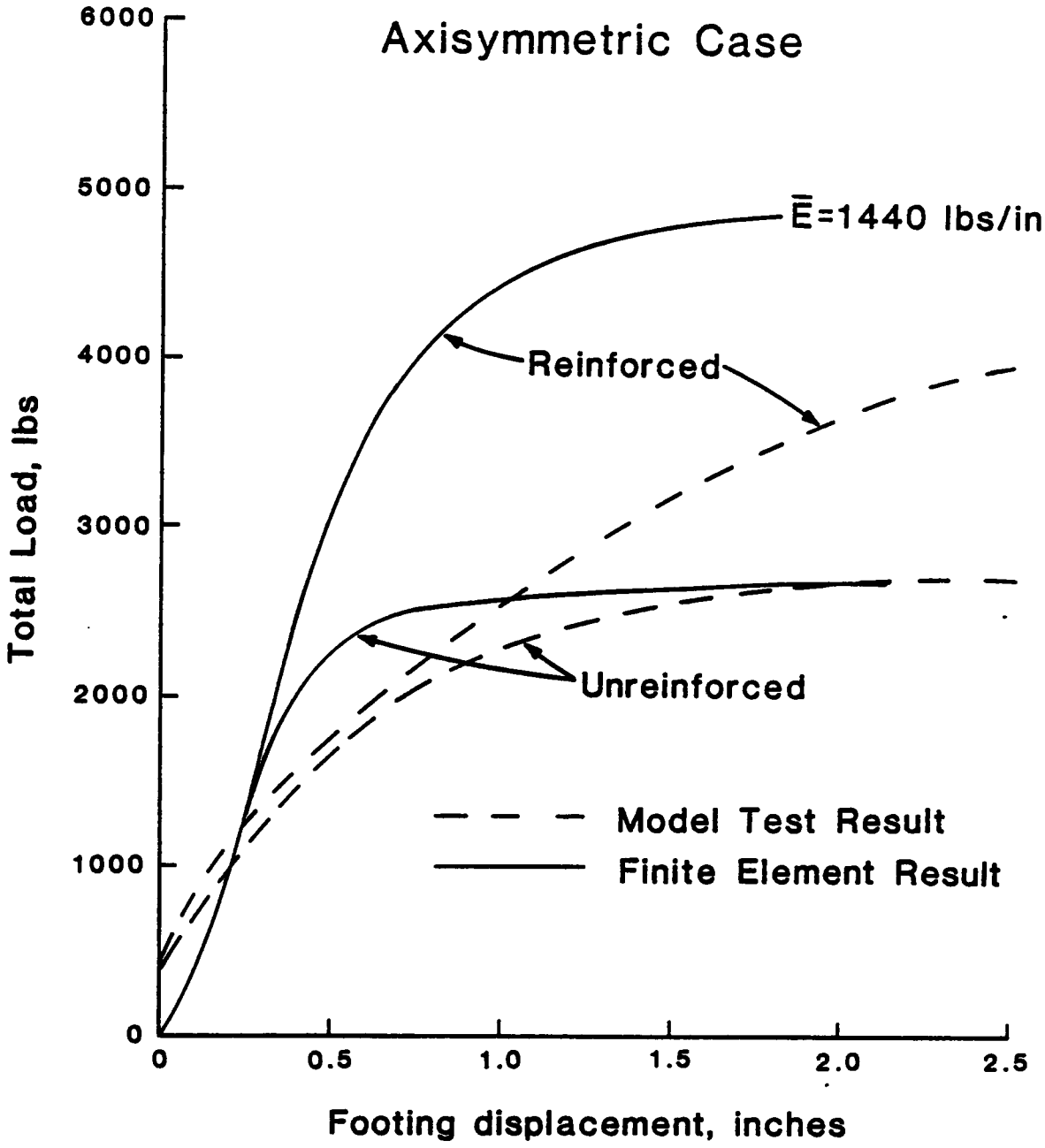

Figure 4.6 Comparison of measured and computed load-displacement curves for UC Davis model tests - axisymmetric case.

Subsequent to the initial movement, the measured load-displacement curve is somewhat flatter than the calculated curve.

The analysis of the reinforced case shows a much higher ultimate strength and a considerably stiffer load-displacement response. It can be seen that the reinforced and the unreinforced computed curves are identical up to a load of about 1500 lbs. This indicates that the reinforcement has little effect on the calculated behavior until nearly two-thirds of the unreinforced collapse load is reached. The computed results indicate that the reinforcement should greatly increase the load-carrying capacity. However, this is not in agreement with the measured results, which show a much smaller increase in load capacity at similar values of footing displacement. Additionally, the computed load-displacement response is significantly stiffer than measured response. This is likely due to the selection of soil properties, which required several assumptions, and the effect of the test box boundaries.

In addition to the load-deformation results, the following observations were made of the computed results:

1. In the unreinforced analyses, failure initiated at the bottom of the sand layer and progressively spread upward and outward through the sand. Punching failure occurred in the clay elements once the sand had failed. The punching failure occurred only in those elements directly under the footing. This mode of punching failure was consistent with the observed failure mode in the model tests.

2. In the reinforced analyses, failure began in elements above the reinforcement and did not spread to elements below the reinforcement until elements between the reinforcement and footing had failed. The zone of failed elements was much wider in both the sand and clay compared to the unreinforced analyses, and the punching mode of failure was not evident. The shear stress was reduced 20 to 40 percent at comparable stages of loading in the upper layer of clay elements.

The foregoing discussion of the computational results indicates that the finite element analyses provide reasonable qualitative agreement with measured behavior. In addition, the results are in quantitative agreement when allowance is made for the uncertainty in several of the soil properties used in the analyses. In particular, the effects of soil compressibility on reinforced soil behavior requires further investigation, and an improved understanding of initial stress conditions in soil would probably improve the analyses. The axisymmetric finite element program appears to provide a useful tool for the analysis of three-dimensional reinforced soil-foundation problems.

4.4 A Proposed Method for Bearing Capacity Analysis of Reinforced Sand Over Weak Cohesive Soils

4.4.1 Postulated Mechanisms of Failure

In the model tests reviewed in Section 4.2.1, the predominant failure mechanism observed was punching shear failure through the sands. In light of this, it is considered appropriate to develop a bearing capacity theory based on the punching shear mode of failure. In addition, an approach which incorporates the strength of the reinforcement in the procedure in a direct manner is highly desirable. Two possible deformation mechanisms are shown in Figure 4.7. The first involves punching shear whereby the footing, the sand, and the reinforcement punch into the clay in much the same manner as in the unreinforced case. For this mechanism, the additional capacity due to the reinforcement must, as an upper bound, be the tensile strength of the reinforcement.

The second mechanism involves a more general shear failure whereby the reinforcement is deformed in the manner shown in Figure 4.7b. The increase in capacity compared to the unreinforced case is considered to occur through the effects of increase in confining pressure due to the reinforcement. This occurs because, as load is added to the system, the reinforcement increases the effective confining pressure in the sand, and hence its strength.

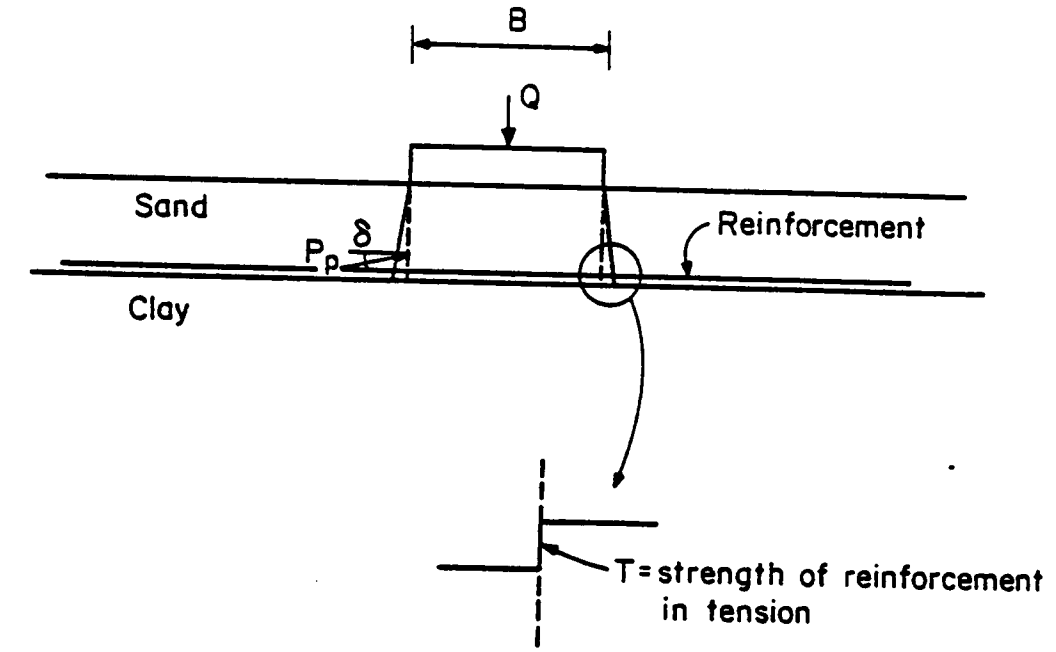

(a) Punching shear failure

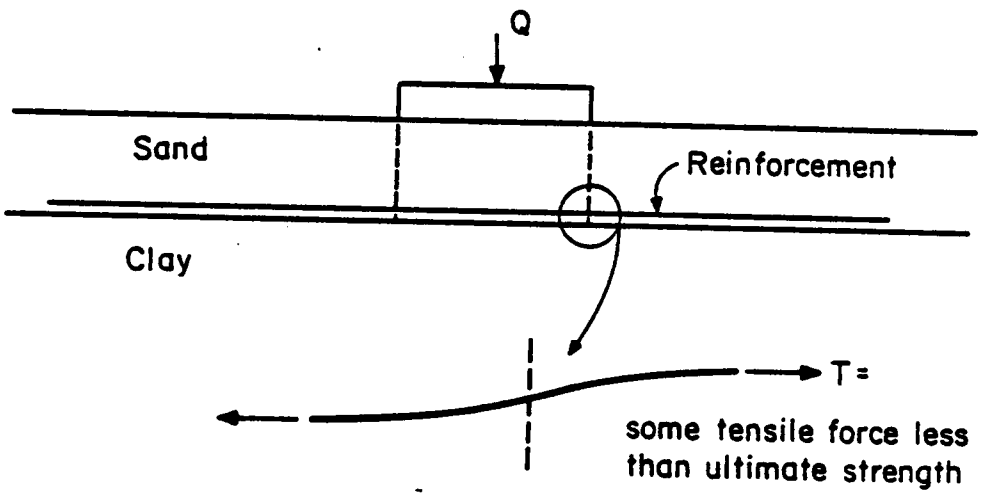

(b) General shear failure

Figure 4.7 Mechanisms of deformation for reinforced sand over clay.

4.4.2 General Shear Mechanism

In the general shear mechanism, as tensile forces are induced in the reinforcement due to the addition of load, these forces act to increase the confining pressure in the sand. This added confining pressure due to the reinforcement increases the strength of the system and may be represented by the addition of a cohesion constant to the passive earth pressure. Terzaghi (1943) showed that the passive earth pressure for cohesive soil can be written as

$$P_p = 0.5\gamma H^2 K_p + 2cH\sqrt{K_p} \qquad [4.6]$$

Combining this with Equation 4.2 results in

$$q_u = cN_c + (\gamma H^2 K_p + 4cH\sqrt{K_p})\tan\delta/B \qquad [4.7]$$

assuming a strip footing at the surface.

The results of reported studies by Schlosser and Long (1974) and by Hausmann and Lee (1976) on triaxial testing of sand reinforced with aluminum foil have shown that the increased strength due to the reinforcement can be represented as a psuedo-cohesion:

$$c_r = \frac{T}{h}\frac{\sqrt{K_p}}{2} \qquad [4.8]$$

where c_r is the psuedo-cohesion of the reinforced sand, T is the strength of the reinforcement, and h is the spacing of the reinforcement.

If Equation 4.8 is substituted into Equation 4.9, the following expression for the bearing capacity of a reinforced sand over soft clay for a strip footing at the surface is obtained:

$$q_u = cN_c + (\gamma H^2 + 4\frac{T}{h}H)K_p \tan\delta/B \qquad [4.9]$$

For a rectangular footing, the bearing capacity can be expressed by

$$q_u = (1 + 0.2\frac{B}{L})cN_c + (1 + \frac{B}{L})(\gamma H^2 + 4\frac{T}{h}H)K_p \qquad [4.10]$$

The bearing capacities for several model footings have been calculated using Equation 4.9 or 4.10, and compared to measured values, with the results shown in Table 4.1. It can be seen that the calculated results greatly overestimate the measured values of bearing capacity. This occurs because the term $\frac{2TH}{h}$ is many times larger than γH^2 for the reinforcing strengths and model geometries. Equation 4.8 was developed from triaxial tests where the reinforcement failed in tension. When embedded in the sand, horizontal layers of reinforcing may not be effective in increasing the confining pressure in the sand, up to the full strength of the reinforcement. Thus, the use of Equation 4.8 may not be the correct form by which to express the psuedo-cohesion for reinforced sand for bearing capacity analyses. A more realistic value of psuedo-cohesion may, perhaps, be based on increased confinement induced by a smaller mobilized force in the reinforcement. For a relatively strong reinforcement, this force may be much less than its ultimate strength.

Table 4.1 Measured and calculated bearing capacities for general shear.

	Measured (kN/sq.m)	nT/h (kN/sq.m)	Calculated (kN/sq.m)
Binquet and Lee	84.5	6.0	125
	114	12	167
	124	24	191
	167	48	450
UC/Davis	218	61	2890
	230	61	2890
	218	61	2477
	263	122	4528

It appears that development of a logical method for determining a suitable psuedo-cohesion for bearing capacity analyses must await additional experimental work. In this regard, the large-scale plane strain apparatus developed by Dove (1986) could provide the necessary means. In this equipment true-scale geogrids and geotextiles can be used to reinforce sand. Results from such tests would shed considerable light on the increases in strength that could be expected for the failure mechanism described here. If such testing confirmed realistic values of psuedo-cohesion, Equation 4.6 could be used for the passive earth pressure and the graphical techniques outlined by Hanna and Meyerhof (1980) could be extended to develop curves for reinforced sand over clay based on the strength of the clay and the psuedo-cohesion of the sand.

4.4.3 Punching Shear Mechanism

The mechanism envisioned is shown in Figure 4.7a. At failure the reinforcement is deformed such that the full tensile resistance of the reinforcement is mobilized to support the load. At failure the reinforcement either breaks or pulls out from the sand due to failure of the bond between the reinforcement and the sand.

The increase in bearing capacity is taken to be the strength of the reinforcement. When this added resistance is factored into Meyerhof's theory, the ultimate bearing capacity can be expressed as:

$$q_u = cN_c + \gamma H^2 K_s \tan\varphi/B + \frac{2nT}{B} \qquad [4.11]$$

for a strip footing on the surface, where T is the strength of the reinforcement per unit length, and n is the number of layers of reinforcement. The factor 2 occurs because the reinforcing provides resistance under both edges of the strip footing. This term is divided by B to obtain a unit pressure for a footing of width B.

For a rectangular footing the ultimate bearing capacity is given by

$$q_u = (1 + 0.2\frac{B}{L})cN_c + (1 + \frac{B}{L})\gamma H^2 K_s \tan\varphi/B + \frac{2nT}{B} \qquad [4.12]$$

Equation 4.12 can be used for circular footings by setting B = L. The factor on the reinforcing term remains 2 because, as shown in Figure 4.8 for a geogrid reinforcing, there are zones around a three-dimensional footing where the reinforcement does not provide effective resistance, because the reinforcing grid has very little strength or stiffness along the diagonal directions. Thus a value of 2 provides a good average of the resistance around the perimeter of a square or circular footing.

The bearing capacity for several model tests has been calculated using Equation 4.6 or 4.7, and compared to measured values, with the results shown in Figure 4.9. As mentioned in Section 4.2.1, Binquet and Lee's (1975) test were conducted using foam rubber to simulate a weak clay layer. The reinforcing in these tests was aluminum foil strips and a number of layers were used, as indicated by the small numbers next to the data points in Figure 4.9. Milligan and Love's (1984) tests were conducted using a specially made, scaled geogrid designed to simulate the behavior of Tensar SS1 at model scale. The fill was a well graded sand and varied in thickness from 50 to 100 mm. Clay strengths of 6, 10 and

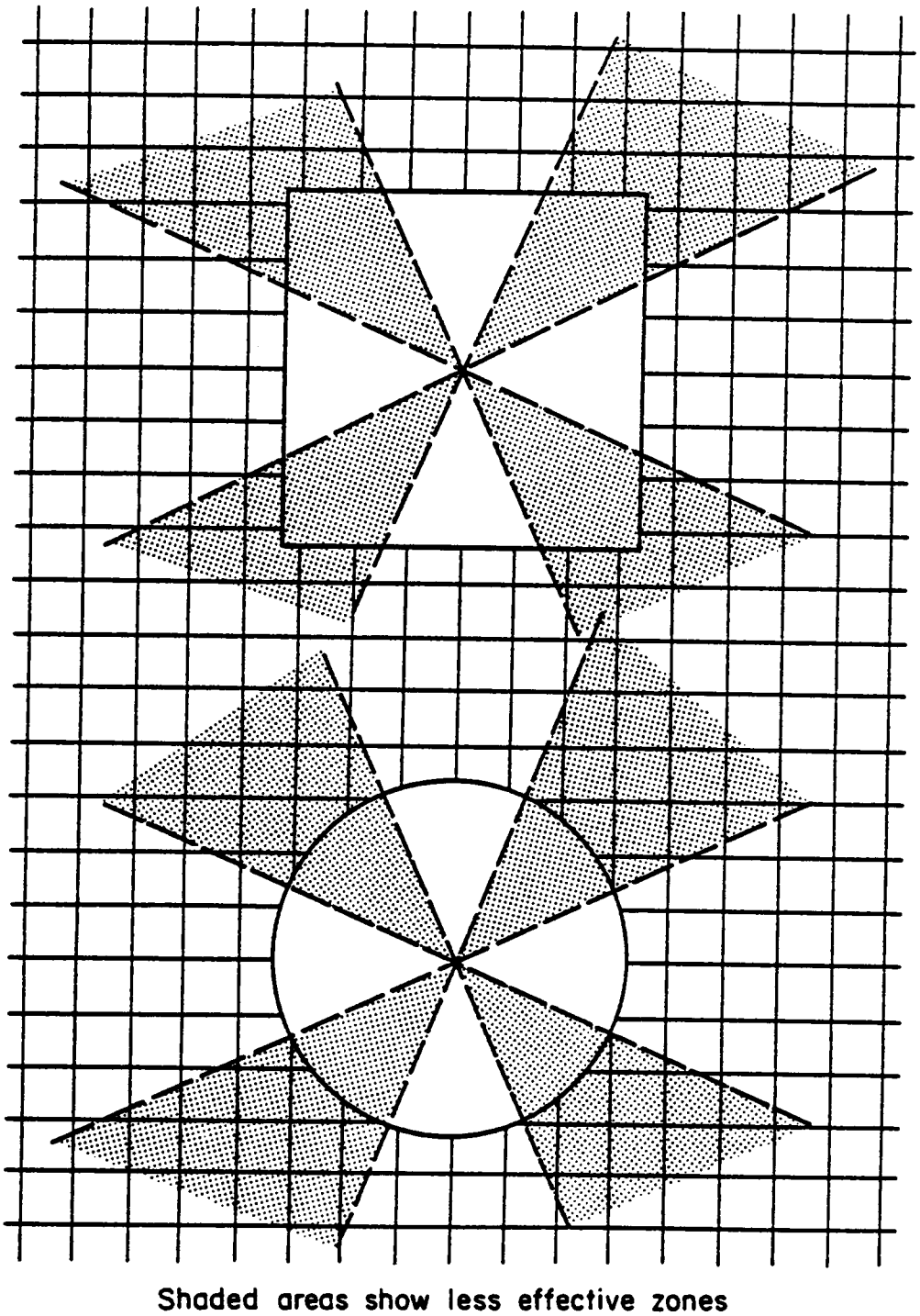

Figure 4.8 Zones around perimeter of three-dimensional footings where reinforcement is less effective.

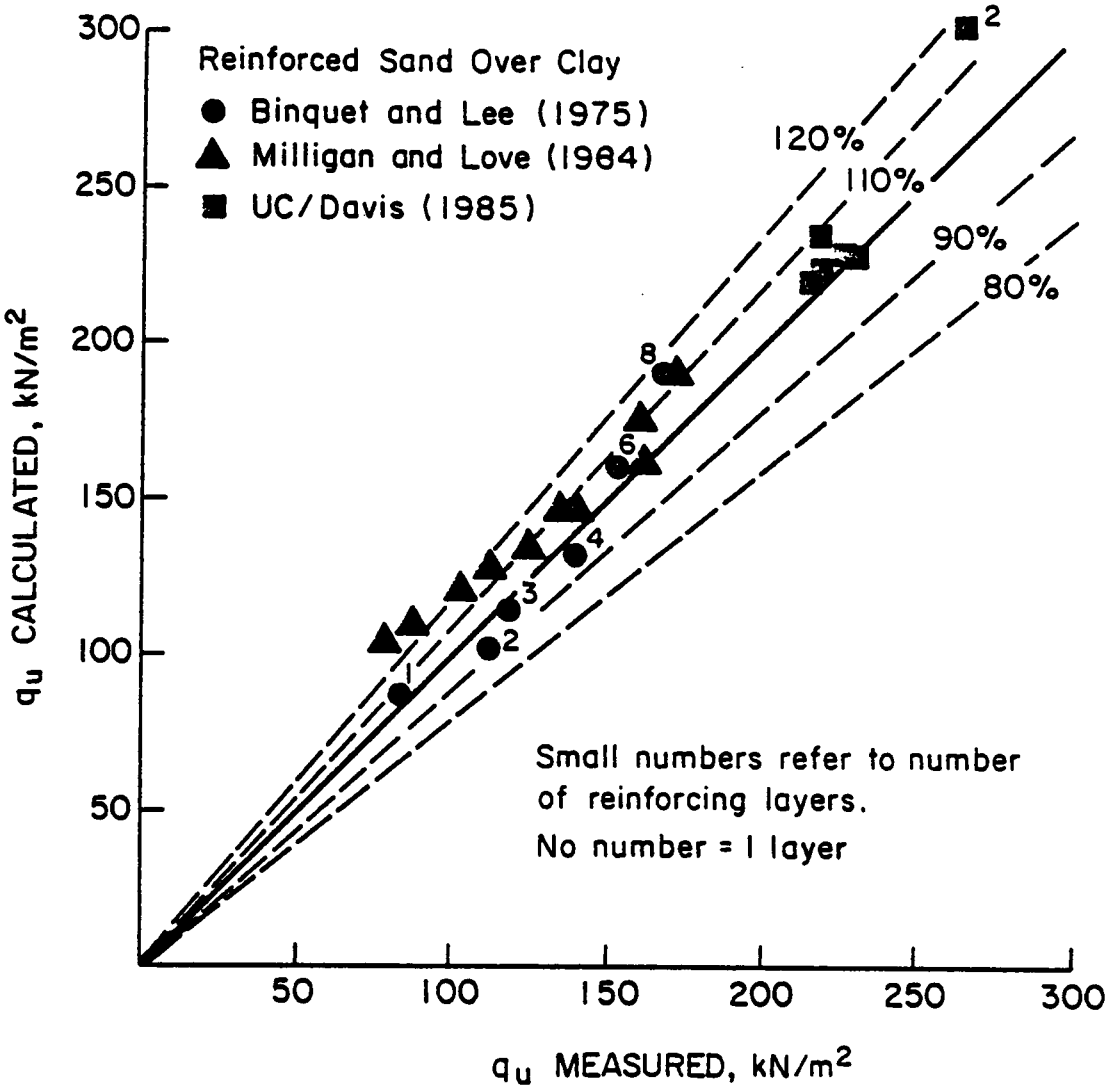

Figure 4.9 Measured bearing capacities versus calculated values for the reinforced case using Equation 4.6 or 4.7.

16 kPa were obtained by consolidating slurried kaolinite. In all their tests the geogrid was placed at the sand-clay interface. The tests by Binquet and Lee, and by Milligan and Love were conducted using strip footings. The tests conducted by University of California, Davis (1984b) used a one-foot-square plate and eight inches of sand or gravel over a soft, organic clay having an average S_u of 15 kPa (310 psf). In these tests, Tensar SS1 geogrid was placed two inches above the clay surface. In tests with two layers, the second layer was placed two inches above the first. The strength of the reinforcement used in calculating the bearing capacity was taken as the tensile rupture strength reported by the investigators. In the case of the University of California, Davis tests, the strength was considered to be the quality control value of tensile strength from Tensar literature. Because it is a biaxial geogrid, the strength of SS1 is different in the two directions. For the data shown in Figure 4.9, the tensile strength used was the minimum value in the two directions. Calculated bearing capacity values using the maximum strength were approximately 20 percent higher. A compilation of the footing width, depth of sand fill, shear strengths, reinforcement strength and number, and the measured and calculated bearing capacities is presented in Table 4.2.

Despite the apparent simplicity of the approach, quite good agreement is obtained between measured and calculated results. Although refinements may be indicated by further test results, the method appears reasonable for practical use in design. Application to one field case,

Table 4.2. Model test properties used in analyses.

	Subgrade S_u kN/m^2	Fill ϕ deg	Fill Depth mm	Footing Width mm	Fill Density kN/m^3	No. of Layers	Reinforcement Strength kN/m	q_{ult}, kN/m^2 Measured	q_{ult}, kN/m^2 Calculated
Binquet and Lee	*	35	222	76	15.1	1	1.33	84.5	87.2
						2		113.8	102.1
						3		124.1	116.9
						4		137.9	131.8
						6		154.3	161.3
						8		167.2	191.2
Milligan and Love	6	47	50	75	17.0	1	2.6	78	104
	10		50			1		112	127
	16		50			1		162	161
	6		75			1		88	110
	10		75			1		125	135
	16		75			1		160	174
	6		100			1		102	119
	10		100			1		135	146
	10		100			1		142	146
	16		100			1		170	191
UC/Davis	15		203	305	17.1	1	12.5	218	227
	15				17.0	1		230	227
	15				17.1	1		225	227
	15				17.8	1		216	219
	15				18.2	1		218	220
	15				18.7	2		263	303

* = Binquet and Lee's tests used foam rubber. Calculated value obtained by adding nT/B to unreinforced bearing capacity of same confinguration.

described below, indicates the method provides results in reasonable agreement with observed field behavior.

In a study of the performance of a Tensar SS1 reinforced haul road, Barksdale and Prendergast (1985) reported punching shear failure of reinforced and unreinforced crushed stone fills at fill thicknesses of 610 mm (24 inches). The unreinforced fill failed upon initial loading whereas the geogrid reinforced section failed on the sixth pass of a loaded C-65 Chevrolet dump truck, with the geogrid breaking under the load. The report indicated that the subgrade strength where the reinforced failure occurred was low for this site and averaged 5.5 kPa (115 psf). The bearing capacity for the reinforced section has been calculated using Equation 4.6 and a friction angle of 50° for the crushed stone fill (based on reported densities and CBR values). The bearing capacity determined was 500, 540 and 575 kPa using tensile strengths for SS1 corresponding to the minimum, average and maximum values of quality control strength of SS1, respectively. For the contact area and weights reported by Barksdale and Prendergast (1985) for the loaded C-65 dump truck, the load causing failure was about 560 kPa. This provides a single field data point in good agreement with the proposed method.

4.5 Summary

In this chapter, the problem of foundations constructed on reinforced soils overlying weak subsoils has been analyzed using the finite element method and a modified bearing capacity procedure. An axisymmetric program

for analysis of reinforced soil problems provides a capability for analyzing circular footings on reinforced soil layers. Comparison of the results of finite element analyses with experimental results from model footings on reinforced sand overlying weak clay show that good qualitative agreement can be obtained for load-displacement curves and for modes of failure. The analyses show that the reinforcement has the effect of spreading out the load over a wider area, thus reducing the shear stresses occurring in the clay, which allows larger loads to be carried by the clay before failure occurs.

A new procedure for computing the bearing capacity of reinforced sand over weak soils has been proposed. The procedure is based on a punching shear deformation mechanism. The method considers the strength and the number of layers of reinforcement in a rational way. Comparisons with several model test studies shows that the procedure provides good predictions of the ultimate bearing capacity of reinforced sand over weak soils. The method is superior to previously developed procedures in that it accounts explicitly for the reinforcement strength and the number of layers.

The above described methods provide procedures for computing the ultimate capacity of reinforced sand over weak soils, and for computing the load-deformation behavior of these systems. By using these two procedures together, reinforced foundations over weak soils can be designed with some confidence.

CHAPTER V

EVALUATION OF THE BEHAVIOR OF MOHICANVILLE DIKE NO. 2

5.1 Introduction

This chapter describes the application of the finite element techniques described in Chapter III to the analysis of Mohicanville Dike No. 2, a 28-foot high flood control dike reinforced with steel wire mesh. The scope of the study described in this chapter included an analysis of the instrumentation data collected during and shortly after construction, a finite element analysis of the dike, and comparisons of the calculated and measured results.

5.2 Background

Mohicanville Dike No. 2 is a rim dike on the Mohicanville Reservoir in Wayne County, Ohio. Constructed by the U. S. Army Corps of Engineers, the dike is 28 feet high and about 1800 feet long. Originally constructed beginning in 1936, the dike suffered a number of failures during construction, and could not be raised above 12 feet, owing to the very low strength of the peat and clay foundation at the site. Subsequent settlement reduced its height to about ten feet, and it was maintained at this height, about 18 feet below design grade, until its reconstruction in 1984 and 1985. A typical cross-section is shown in Figure 5.1 where

the foundation conditions and the bounds of the old and new embankments are delineated.

A number of alternatives for raising the dike were evaluated in the late 1970's by Law Engineering Testing Company for the Huntington District to determine the most feasible method of raising the dike to its design height (Collins et al. 1982). Because of the very low strength of the foundation soils, construction of a conventional embankment was infeasible, no matter how flat the slopes. The depth of the peat and clay was so great (about 60 feet) that excavation of the weak materials was not economically feasible. Displacement of the soft foundation soils was considered, but was rejected because of the extremely large quantities of fill required, and the uncertain quality of the resulting structure. Use of a concrete flood wall was considered but rejected because of the very poor foundation support. Eventually it was decided that the best alternative for raising the dike would be construction of a reinforced embankment.

The use of reinforcement to improve embankment stability is fairly new, and design procedures are still being developed. In the case of Mohicanville, both finite element analyses and conventional equilibrium slope stability analyses were performed. The slope stability studies were performed by Law Engineering Testing Company (Collins et al. 1982) and the finite element analyses were performed by the U.S. Army Waterways Experiment Station in conjuction with Prof. J. M. Duncan (Fowler et al. 1983). The finite element analyses were used to estimate the force in the reinforcing and the horizontal and vertical movements of the

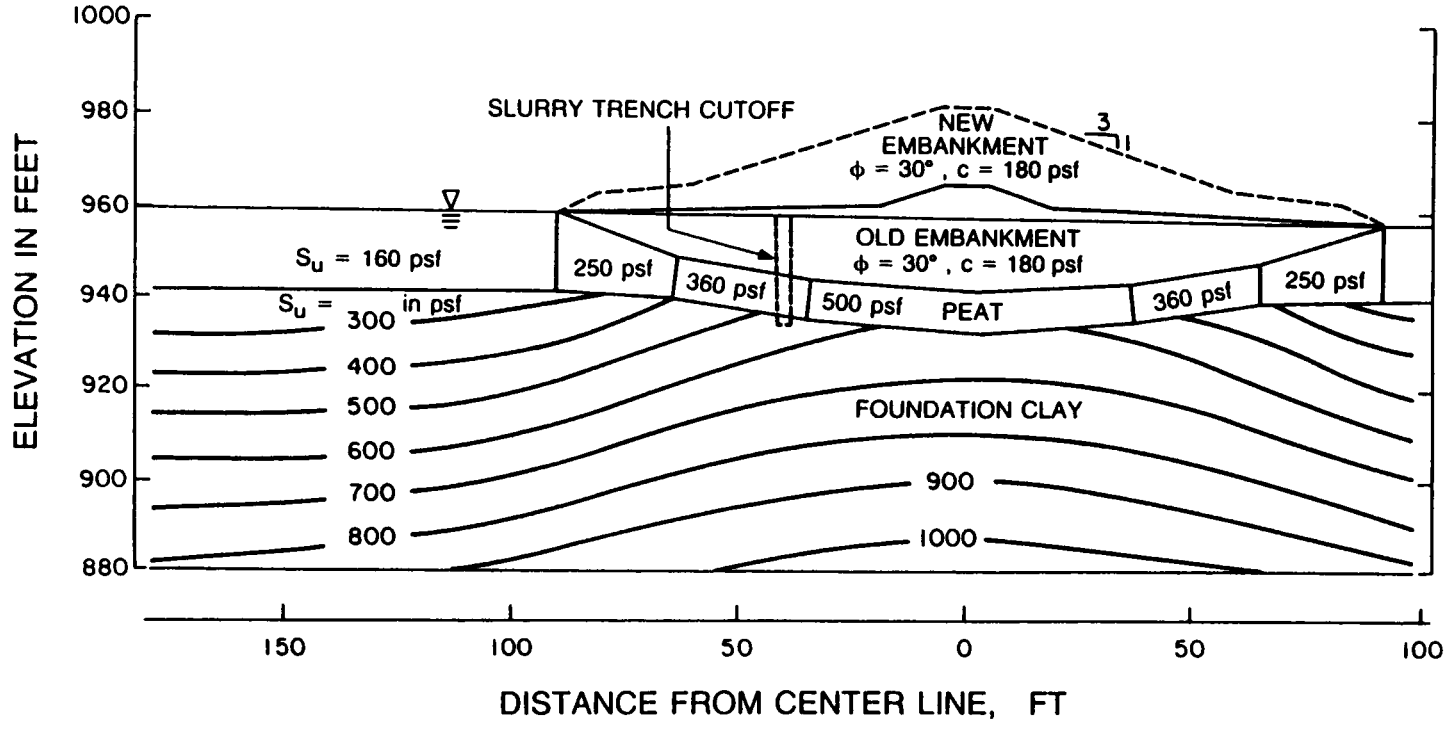

Figure 5.1 Typical cross-section of Mohicanville Dike No. 2 showing foundation conditions, old and new embankmentslimits and undrained shear strengths (after Collins et al. 1982).

embankment. The limit equilibrium analyses were used to evaluate the factor of safety with respect to shear failure through the embankment and its foundation.

Because of the unusual design concept of the embankment and the importance of the structure, a large number of instruments were installed in the embankment and the foundation to confirm that the forces in the reinforcement, the movements of the embankment, and the pore pressures in the foundation were within acceptable limits during and following construction. The information derived from these instrumentation studies has been used to monitor construction progress and assess the accuracy of the finite element analyses and stability analyses, as explained subsequently.

Following construction, a second finite element analysis was performed, the results of which are reported herein. The purpose of this new analysis was to more closely represent the actual field conditions at the instrumented sections, including the strength of the reinforcement as actually installed, and slightly different foundation and embankment strengths than had been used in the original analyses performed by WES. These changes were found to have only small effects on the calculated results.

5.3 Review of Previous Studies

Previous studies on Mohicanville Dike No. 2 have been prepared by Collins et al. (1982), Fowler et al. (1983) and Collins (1986). Collins

et al. (1982) discussed the safety evaluation undertaken of the dike, various alternatives for raising the dike, and made an analysis of the use of reinforcement for raising the dike. They also presented a large amount of data on the foundation conditions at the site, and the results of a comprehensive laboratory testing program to characterize the foundation and embankment soils. Fowler et al. (1983) performed finite element analyses and stability analyses of the proposed design, and prepared an instrumentation plan and cost estimates. Collins (1986) assembled, reviewed and analyzed the instrumentation data collected during construction of the dike.

Collins et al. (1982) proposed a procedure for determining the reinforcement required from limit equilibrium analysis of the form:

$$T = (M_O - \frac{M_r}{FS})/R \qquad [6.1]$$

where

T = required reinforcement force

FS = required factor of safety against failure

M_O = overturning moment due to embankment

M_r = resisting moment of the soil

R = radius of the critical slip circle.

Using this equation with the Law Engineering Testing Company (LETCO) slope stability program (based on a "Modified Fellinius" or "Swedish" method that satisfies moment equilibrium), the authors obtained the distribution of required reinforcement forces shown by the dashed line in Figure 5.2. Their analyses were performed for an embankment height of

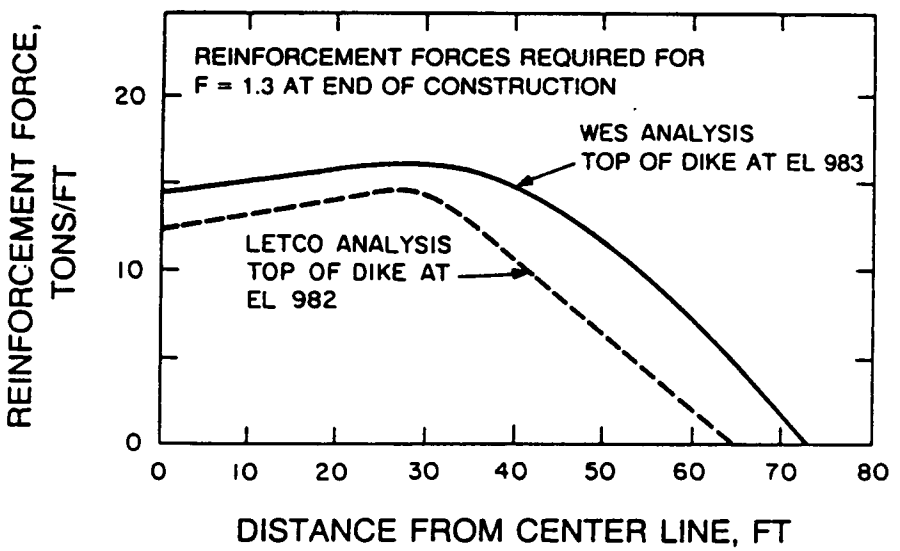

Figure 5.2 Distribution of required reinforcement force from stability analyses to provide a minimum factor of safety of 1.3 (after Collins et al. 1982 and Fowler et al. 1983).

22 feet, the design height at that time. It may be seen that these analyses showed that a reinforcing force of about 15 tons per foot would be required to raise the factor of safety to a value of 1.3 at the end of construction, as required by Corps of Engineers design standards.

A similar analysis was performed by Fowler et al. (1983) for an embankment height of 23 feet, with the results shown by the solid line in Figure 5.2. It may be seen that the results are very similar, the maximum required force being about 1 ton/ft larger for the higher embankment. Fowler et al. (1983) also examined safety with respect to bearing capacity, lateral sliding, and splitting of the embankment, using the procedures of Haliburton et al. (1982). The embankment was found to be safe with respect to these other modes of failure as well.

A finite element analysis of the dike was performed by Fowler et al. (1983) to investigate the influence of reinforcement stiffness on reinforcement force. This analysis will be referred to as the WES analysis. The 1981 version of CON2D (Duncan et al. 1981) was modified to accommodate reinforcing elements, and was used for the analyses. This program allows consideration of consolidation effects and induced pore pressures, as well as embankment deformations and reinforcement forces.

The analyses performed by WES used half sections of the embankment and boundaries as follows: top of dike at elevation 983, working surface at elevation 960, toe of dike at elevation 958 ninety feet from the centerline, general ground surface at elevation 958, rigid base at elevation 880 and no horizontal displacement at the centerline and 400 feet from the center line. The steps of the WES analysis corresponded to crest

elevations of 964, 970 and 978 during the first construction season, consolidation during the winter, completion of the dike to elevation 983 in the spring, consolidation steps corresponding to two and eleven years after the beginning of construction. The assumed cross section and loading conditions differed somewhat from the actual construction sequence, as will be described subsequently.

For analyses using CON2D, soil strength, stiffness and permeability properties are necessary. The values of these properties used in the WES analyses were obtained primarily from the LETCO report (Collins et al. 1982) and were supplemented by limited testing performed by WES. The model parameters were determined from laboratory tests following the procedures described by Duncan et al. (1981) and D'Orazio and Duncan (1982). The soil strength values used in determining the initial soil model parameters were the "design" strength values from composite envelopes wherein two-thirds of the test values exceed any design value, as is standard Corps practice. Using these initial soil parameters, the soil strength and stiffness properties were adjusted to match the laboratory stress-strain curves. These computed curves were then "softened" by reducing the soil strength and stiffness parameters such that a finite element analysis of the unreinforced dike failed in correspondence to a limit equilibrium of the unreinforced dike. In achieving these matches, the strength values were reduced considerably from the initial values. During the course of this study, computer code errors in the WES program were discovered which may have influenced the selection of the model parameters.

The reinforcement was modelled as elastic bar elements. Four values of stiffness were used in the WES analyses: zero stiffness to represent no reinforcement, 109 ton/ft to represent polyester fabrics, 625 ton/ft to represent Kelvar products, and 12000 ton/ft to represent steel mesh reinforcement.

From the analyses performed, the following conclusions were noted:

1. Lateral restraint of horizontal movement appeared to be the principal mechanism through which load is transferred to the reinforcement,

2. The stiffer the reinforcement, the greater the load it carried.

3. The force in the reinforcement, the lateral spreading of the embankment and foundation, and the pore pressures in the foundation increased during embankment construction and decreased during subsequent consolidation periods.

4. Post-construction settlement was little affected by reinforcement stiffness.

The relationship between mobilized reinforcement force and reinforcement stiffness determined from the finite element analyses is shown in Figure 5.3. Also shown are the tensile strengths for various reinforcing materials. It is clear that only the steel reinforcing possesses the necessary stiffness to achieve the working force as determined in the limit equilibrium studies.

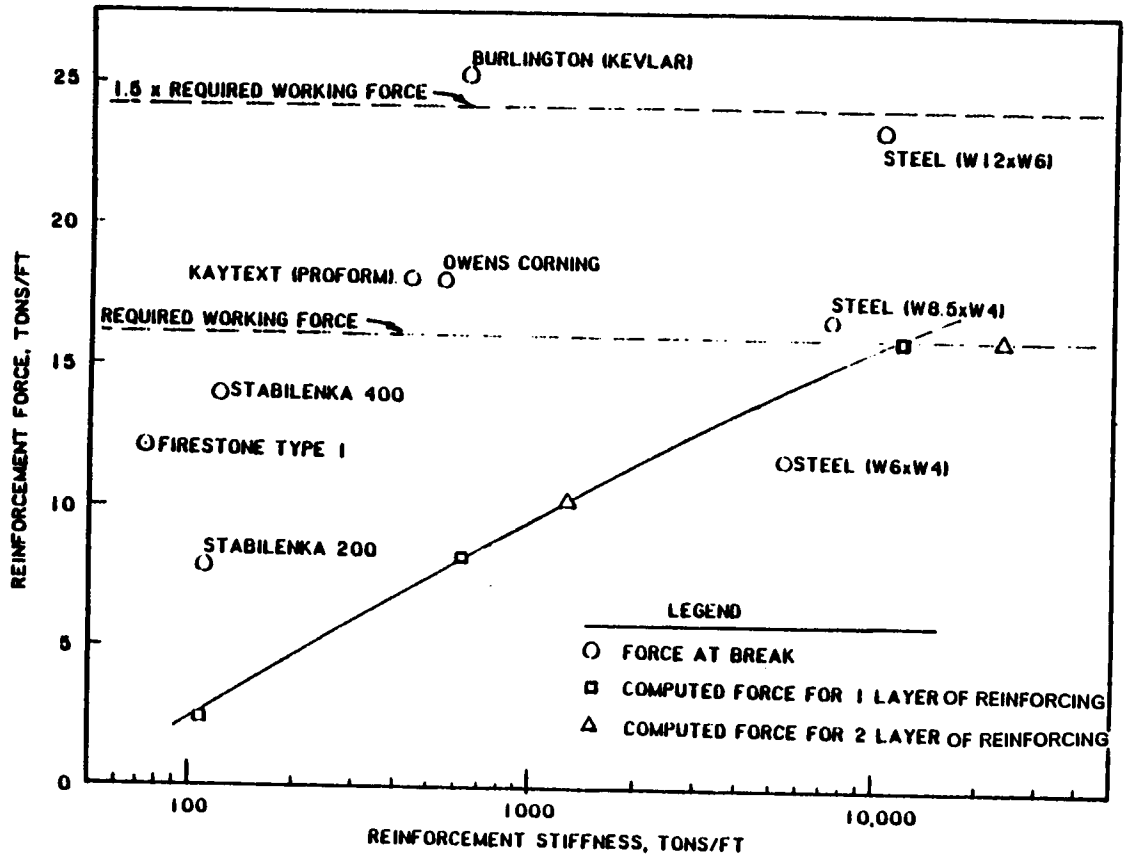

Figure 5.3 Reinforcement force and strength versus reinforcement stiffness (Fowler et al. 1983).

Collins (1986) prepared a report summarizing and analyzing the instrumentation data collected during construction of the dike. He concluded that the embankment is stable and its construction was a success. He also concluded that the finite element analyses were very valuable for choosing the reinforcement type and for estimating the reinforcement force, the pore pressures, and the deformations.

5.4 Properties of the Dike and Foundation.

The site is located on a glaciated plateau of the Killbuck Lobe of Wisconsin age glacial deposits (White, 1967). This is a moraine belt of upland glacial drift overlying bedrock with alluvium filled valley floors. The topography of the area is bedrock controlled. The glacial drift is a silty clay or "boulder clay," known as the Hayesville Till, containing a wide range of particle sizes. The upland deposits of till are from 3 to 12 feet thick. Kames and terraces are prevalent in the area, having formed along the valley walls as glacial ice melted and receded.

The alluvial deposits, located in floodplains, are often thin, and they overlie Hayesville Till deposits. The recent alluvium is generally comprised of silts and sandy silts. The floodplains contain many kettleholes formed during recession of the glaciers. These kettleholes have filled with organic matter over the years to form peat and muck bogs.

The dike is located on a peat bog, with the peat overlying soft clay, as shown in Figure 5.1. The foundation clay is very weak in the virgin

state, because the low-weight peat deposits have not caused appreciable consolidation to take place in the underlying clay.

A geotechnical investigation of the site was performed by Law Engineering Testing Company (Collins et al. 1982). This investigation provides extensive information on the foundation conditions. Soil properties of the foundation clay, peat, old embankment fill and borrow areas were assessed through field vane shear tests and laboratory triaxial, consolidation, permeability, compaction, and classification tests (Collins et al. 1982). A summary of the test results is shown in Table 5.1.

The foundation clay ranges in thickness from 10 to 60 ft and varies across the site from a silty clay to an organic clay. The shear strength of the clay where it has not been loaded by the old dike is very low, due to the low unit weight of the overlying peat deposits. Typical undrained shear strengths range from 300 to 1000 psf, as shown in Figure 5.1. Representative stress-strain characteristics of the clay as determined from triaxial compression tests are shown in Figures 5.4 and 5.5, and consolidation test results are shown in Figure 5.6.

The peat varies from fibrous near the ground surface to amorphous in the lower portions of the deposit, and ranges in thickness from 16 feet to 20 feet in the virgin state. Where it was compressed under the weight of the old embankment, the thickness of the peat had been reduced to 11 to 15 ft. Typical undrained shear strengths for the peat ranged from about 150 psf in the virgin state to about 500 psf where it had been compressed under the old embankment, as shown in Figure 5.1. Stress-

Table 5.1 **Summary of soil properties.**

Soil Property	Foundation Clay	Peat	Embankment Fill
Unified Soil Classification	CL, CH and OH	Pt	CL
Dry Unit Weight, pcf	OH: 40 to 84 CL-CH: 60 to 91	10 to 36	113 to 120
Water Content, %	OH: 37 to 67 CL-CH: 28 to 65	280 to 540	15 to 18
Liquid Limit	28 to 80	--	27 to 57
Plastic Limit	16 to 37	--	17 to 21
Plasticity Index	14 to 43	--	10 to 37
Specific Gravity	2.61 to 2.80	1.50	2.70 to 2.80
% Finer than			
#4	100	--	73 to 100
#10	100	--	60 to 95
#40	96	--	40 to 90
#200	90 to 95	--	25 to 80
2 micron	10 to 40	--	10 to 20
Undrained Shear Strength, psf	400 to 1000	200 to 500	3000 to 6000
ϕ', degrees	25 to 29	17 to 32	32
c', psf	0 to 500	200 to 400	200
Permeability, ft/yr	0.1 to 10	see Figure 5	0.1 to 1

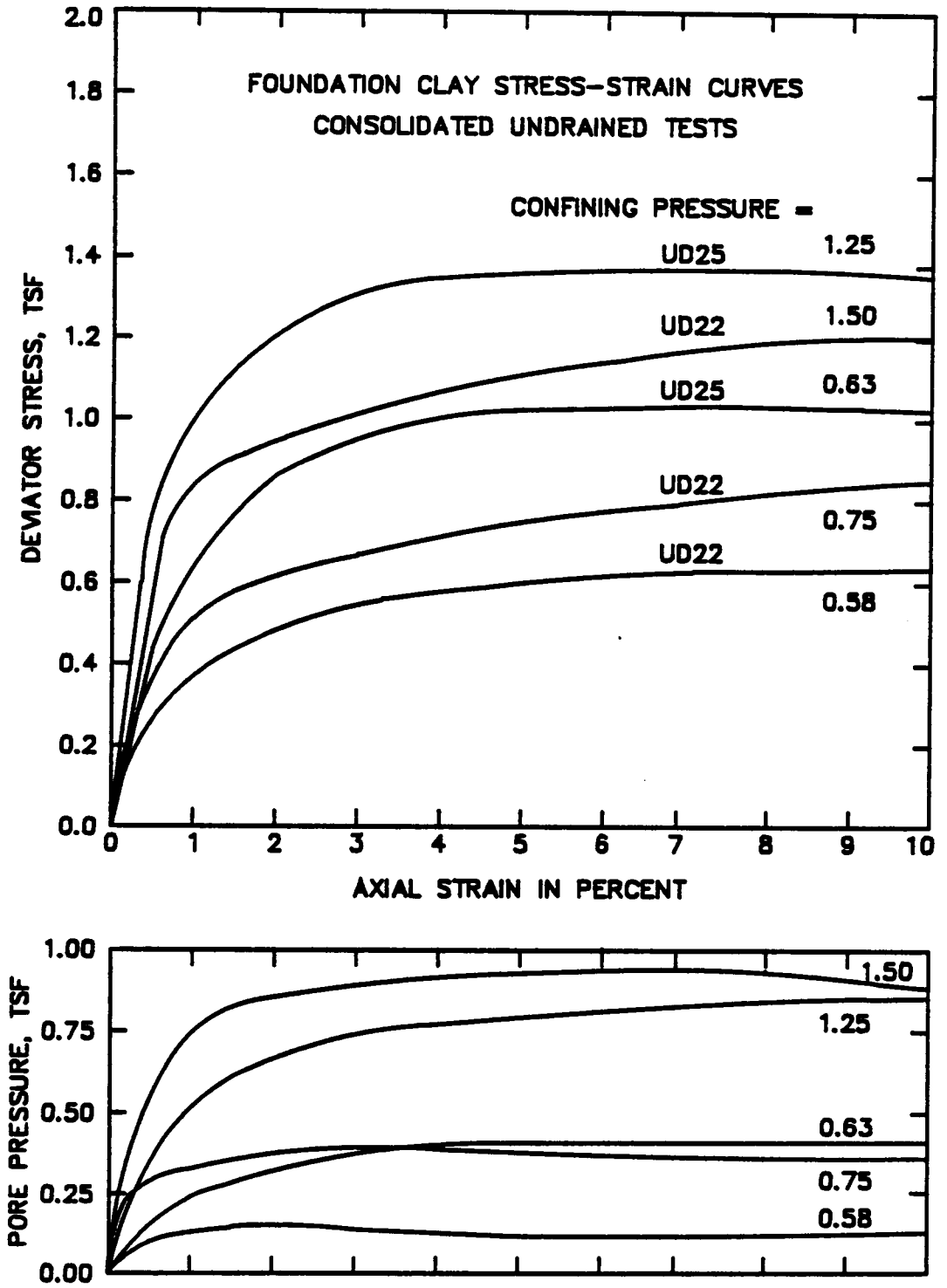

Figure 5.4 Stress-strain curves from consolidated undrained (CU) tests on the foundation clay (after Collins et al. 1982).

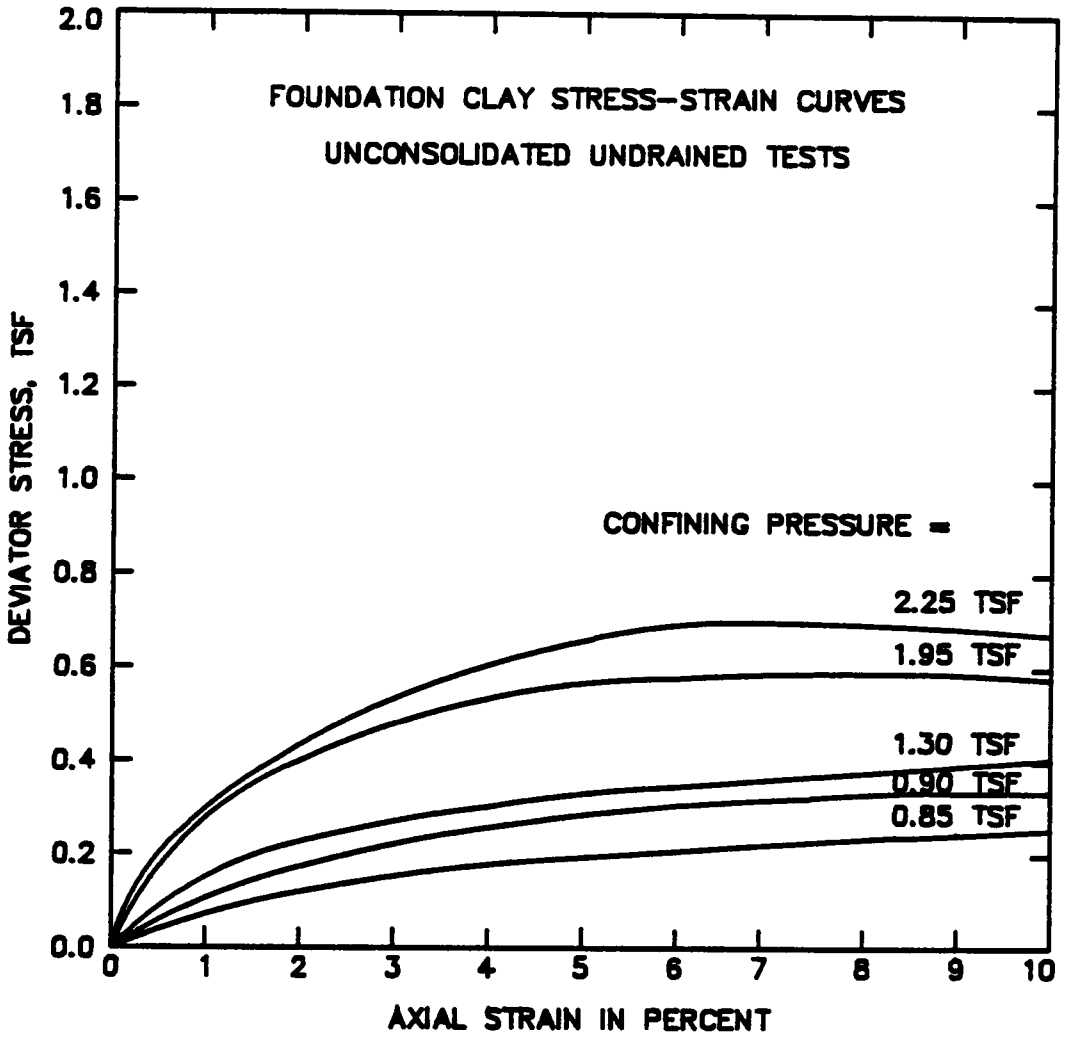

Figure 5.5 Stress-strain curves from unconsolidated undrained (UU) tests on the foundation clay (after Collins et al. 1982).

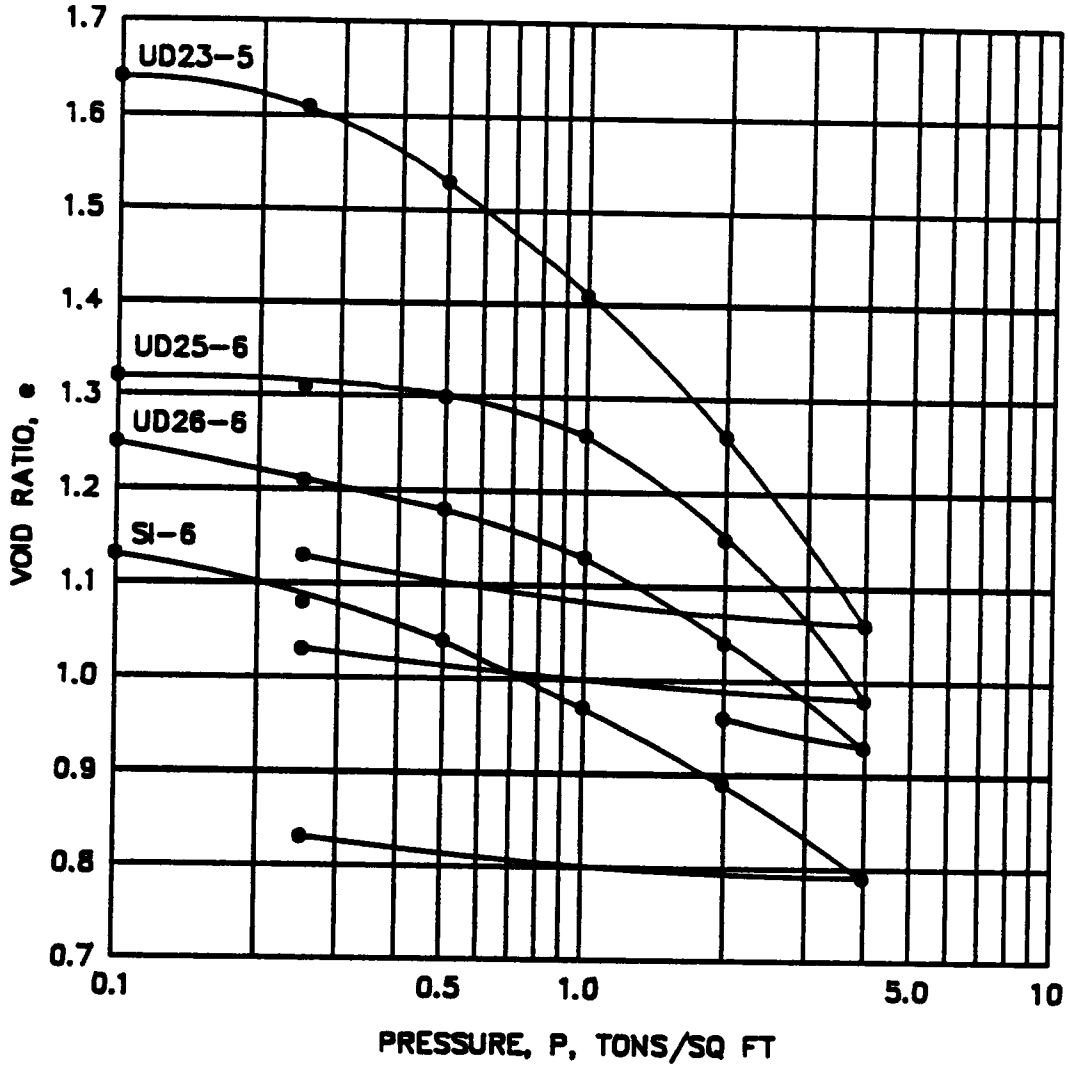

SAMPLE	USCS	LL	PL	PI	γ_d,pcf	w, %	P_o, tsf
UD23-5	CH	76	32	44	61.4	61.3	1.19
UD25-6	OH	66	33	33	70.5	48.6	1.93
UD26-6	CH	55	29	34	74.1	45.6	0.98
SI6-3	CL	37	17	20	81.3	41.0	1.42

Figure 5.6 Compression curves from one-dimensional tests on the foundation clay (Collins et al. 1982).

strain characteristics of the peat are shown in Figure 5.7, and consolidation characteristics are shown in Figure 5.8.

The permeability of the peat was assessed by performing field and laboratory permeability tests. The results are compared in Figure 5.9 with values for California peats obtained by Weber (1969). It can be seen that the variations of permeability with consolidation pressure are very similar for the California and the Mohicanville peats.

Both the old and the new embankment fill materials were derived from glacial tills in the surrounding uplands. The fill material is a gravelly sandy clay, with zones of gravelly clay. Pockets of poorly graded sand, silt, silty sand and clayey gravel are also present in the borrow pit. As it was compacted in the new embankment, the fill exhibits good shear strength characteristics, and is quite ductile at the in-place water content of zero to two percent above optimum. The strength of the old fill is somewhat lower, especially in areas where previous failures had occurred.

The stress-strain and strength characteristics of the old and new fill are shown in Figures 5.10 and 5.11. The tests on the new fill were performed by the Huntington District on block samples taken from the embankment after construction. It can be seen that the new fill exhibits higher strength and modulus than the old fill. Consolidation characteristics of the fill, determined from isotropic compression on a triaxial test specimen, are shown in Figure 5.12.

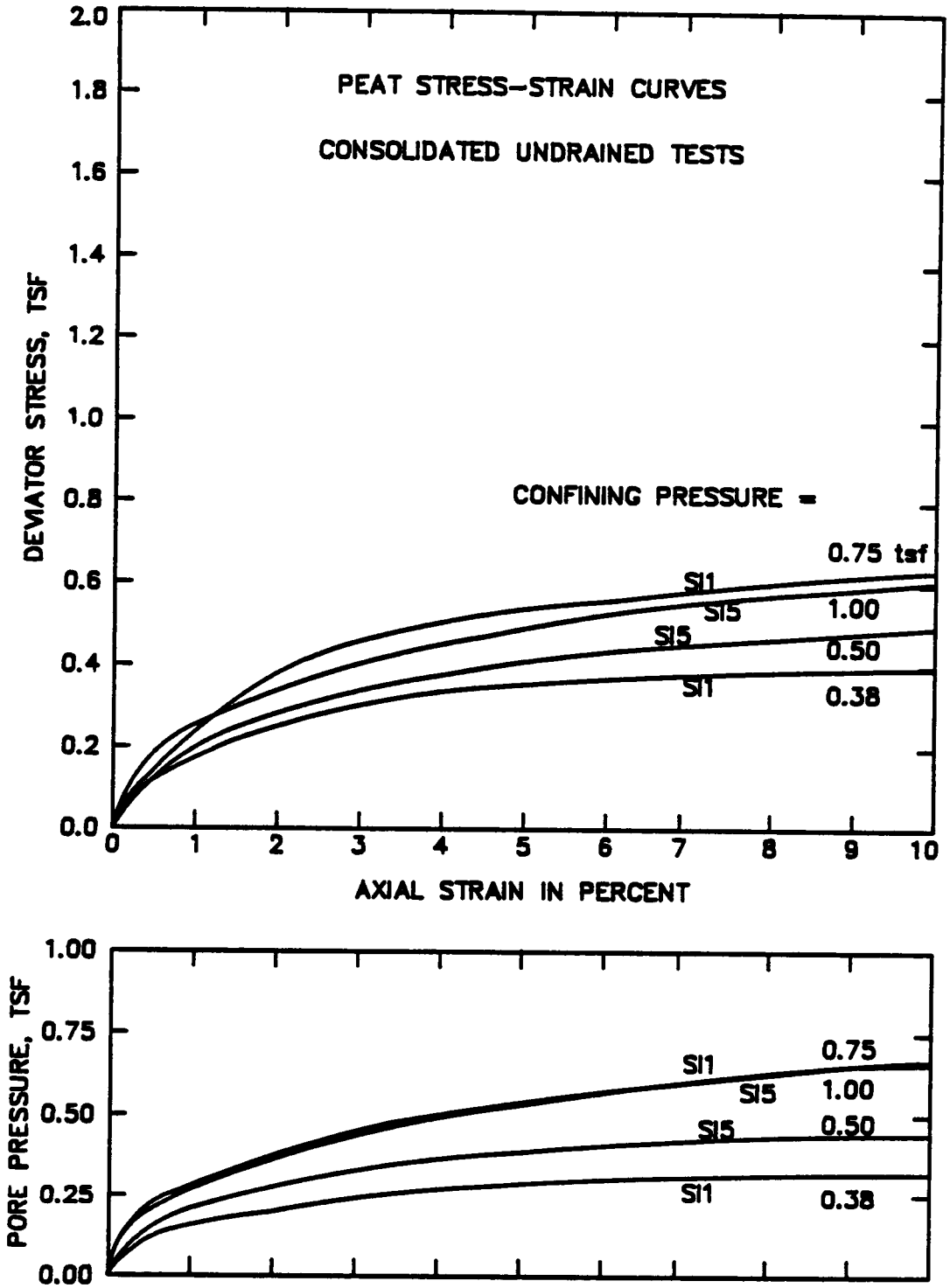

Figure 5.7 Stress-strain curves from consolidated-undrained (CU) tests on the peat (Collins et al. 1982).

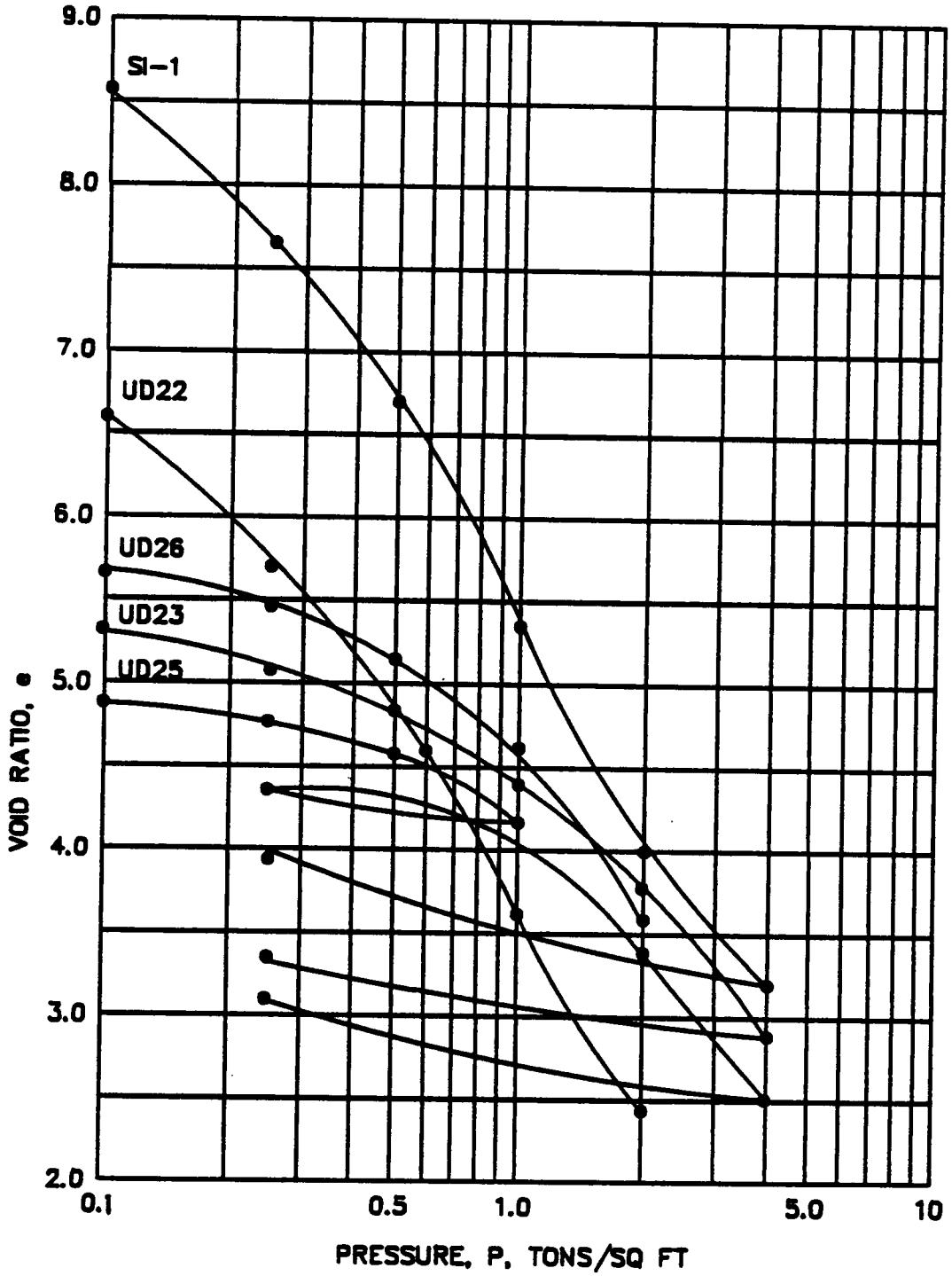

Figure 5.8 Compression curves from one-dimensional tests on the peat (Collins et al. 1982).

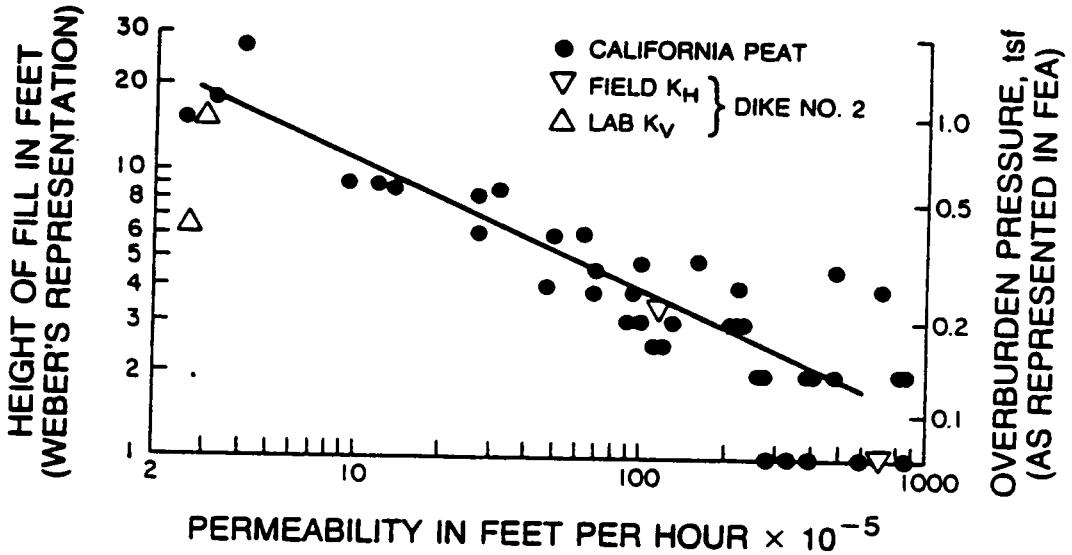

Figure 5.9 Variation of peat permeability with height of fill, adapted from Weber (1969) and Collins et al. (1982).

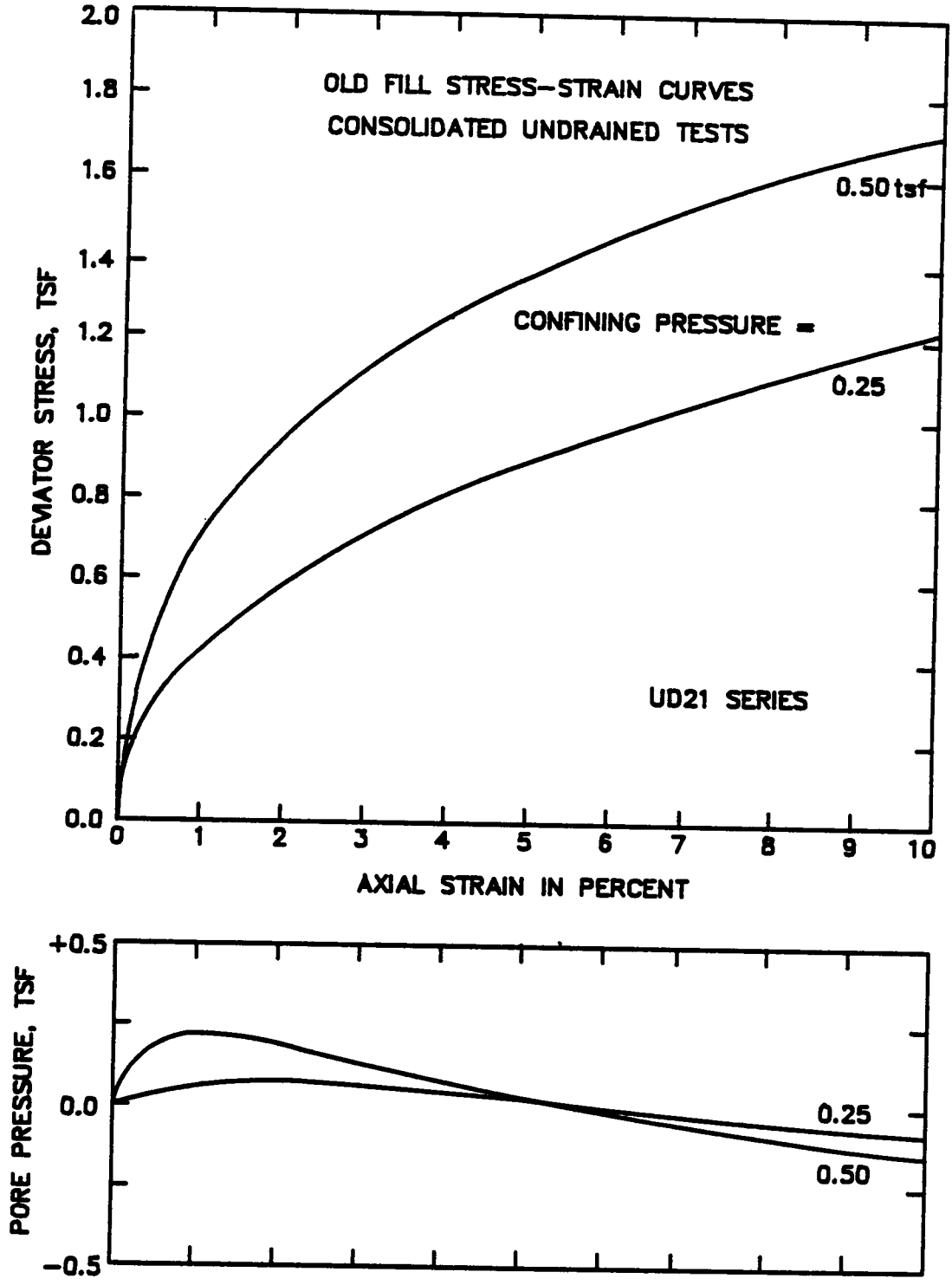

Figure 5.10 Stress-strain curves from consolidated-undrained (CU) tests on the old embankment fill (Collins et al. 1982).

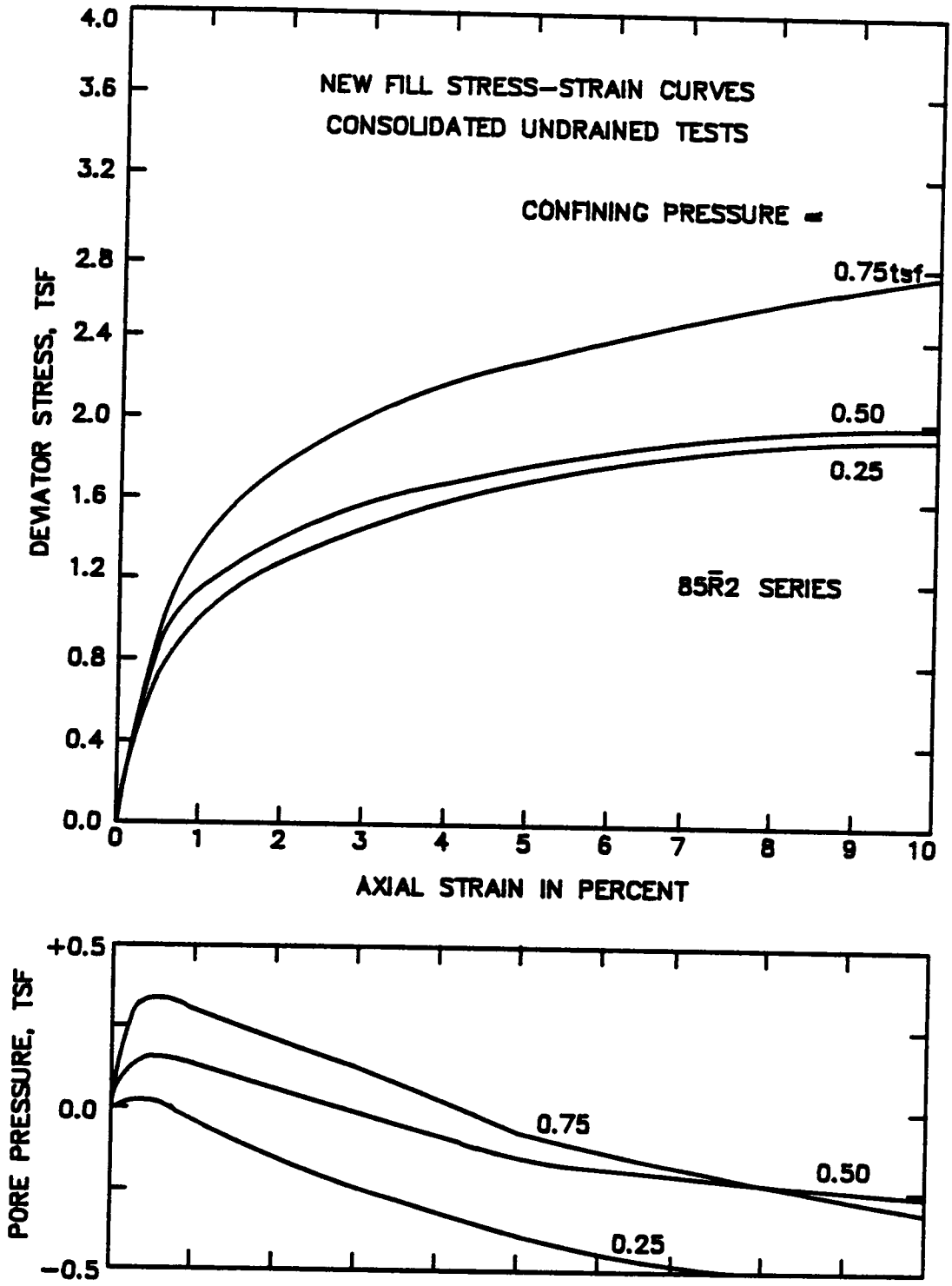

Figure 5.11 Stress-strain curves from consolidated-undrained (CU) tests on the new embankment fill.

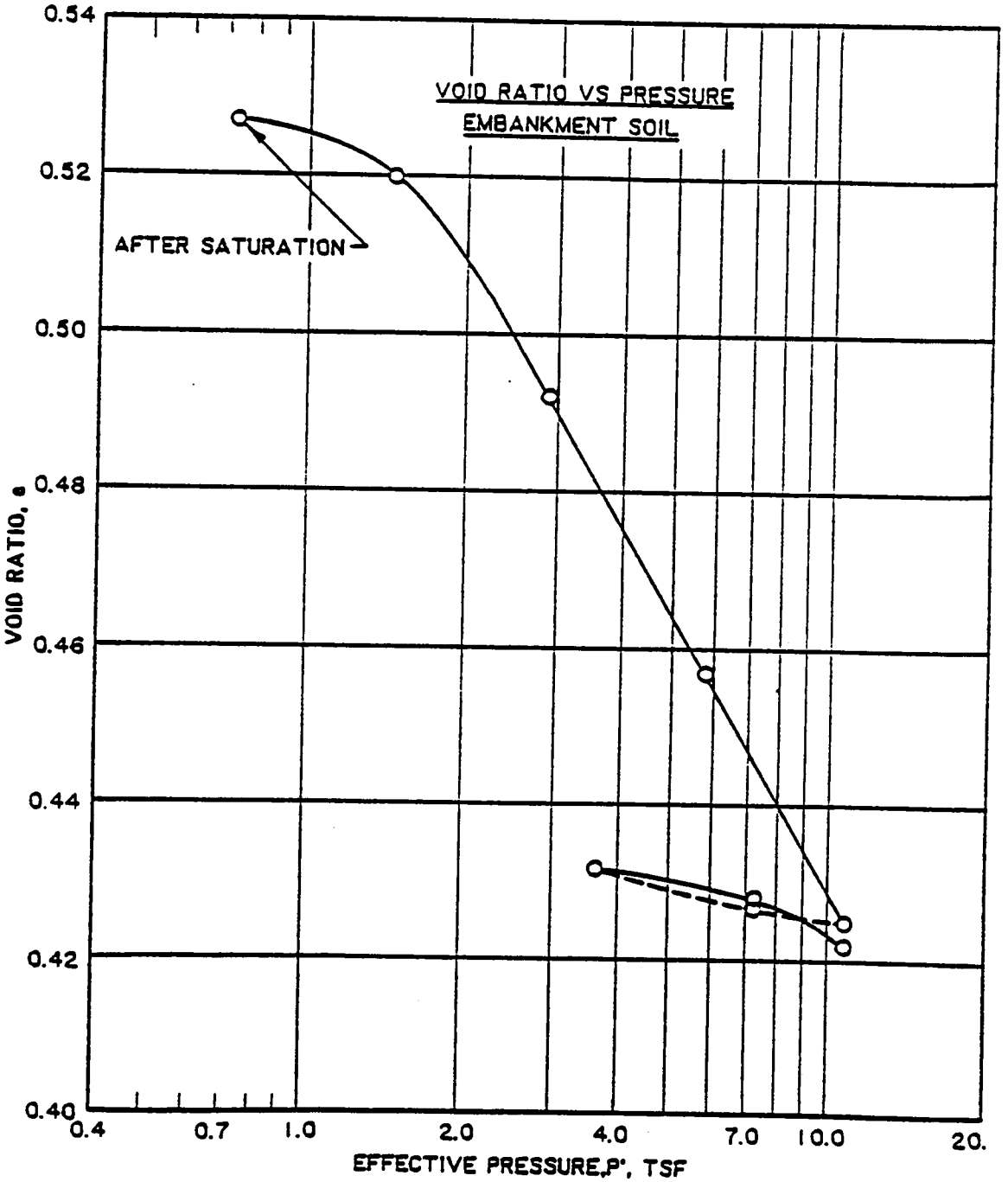

Figure 5.12 Consolidation curve of embankment fill from an isotropic compression test (Fowler et al. 1983).

5.5 Properties of the Reinforcement

The stability analyses discussed previously indicated that a reinforcing force of about 15 tons per foot of embankment would be required to raise the factor of safety to the required value of 1.3 at the end of construction. The calculated distribution of reinforcing forces across the embankment required for a factor of safety equal to 1.3 is shown in Figure 5.2. The finite element analyses performed before construction showed that a very stiff reinforcing material would be required to achieve this amount of reinforcing force under working conditions.

To meet these requirements of stiffness and strength, a specially fabricated steel mesh was used. The welded mesh consisted of #3 bars spaced two inches apart along the length of the dike, with #2 bars six inches apart parallel to the embankment axis. This mesh provides a theoretical ultimate reinforcement strength of 24 tons per foot of embankment and a stiffness of 10,440 tons per foot of embankment.

The mesh was transported to the site in eight-foot wide rolls, and was unrolled at the site using the same machine used to roll it in the fabricating plant. When unrolled, the strips of mesh were cut into two pieces, each eight feet wide and 160 feet long. These were dragged into position on the embankment using a bulldozer. The reinforcement extended 80 feet upstream and downstream from the centerline of the embankment between Stations 3+00 and 14+00.

The reinforcing mat was placed at elevation 960, approximately four feet above original ground elevation. In most areas about six to eight

feet of old fill had to be excavated to reach this elevation prior to placement of the steel mesh. In one area where exceptionally large settlements had occurred, additional fill had to be placed to raise the surface elevation to 960 before the steel mesh was placed. A second layer of reinforcing was placed at elevation 961 between Station 8+40 and Station 9+40 as an added precaution, due to the uncertain foundation conditions in this area. This was an area where extensive failure had occurred in 1936 during original construction and a localized failure occurred in 1983 during construction of the slurry trench.

5.6 Field Measurements

5.6.1 General

The dike, its foundation, and the reinforcement were instrumented along four cross-sections as shown in Figure 5.13 and detailed in Table 5.2. A total of 39 piezometers of three different types were used to measure foundation pore pressures. Thirteen inclinometers were installed to measure movements of the embankment and the foundation. Nine of these were vertical, and four were horizontal, placed just above the reinforcing mesh to determine settlements at this elevation. Twelve settlement plates were also installed to measure vertical movements near the reinforcement level, and 25 surface monuments were installed to supplement the other measurements.

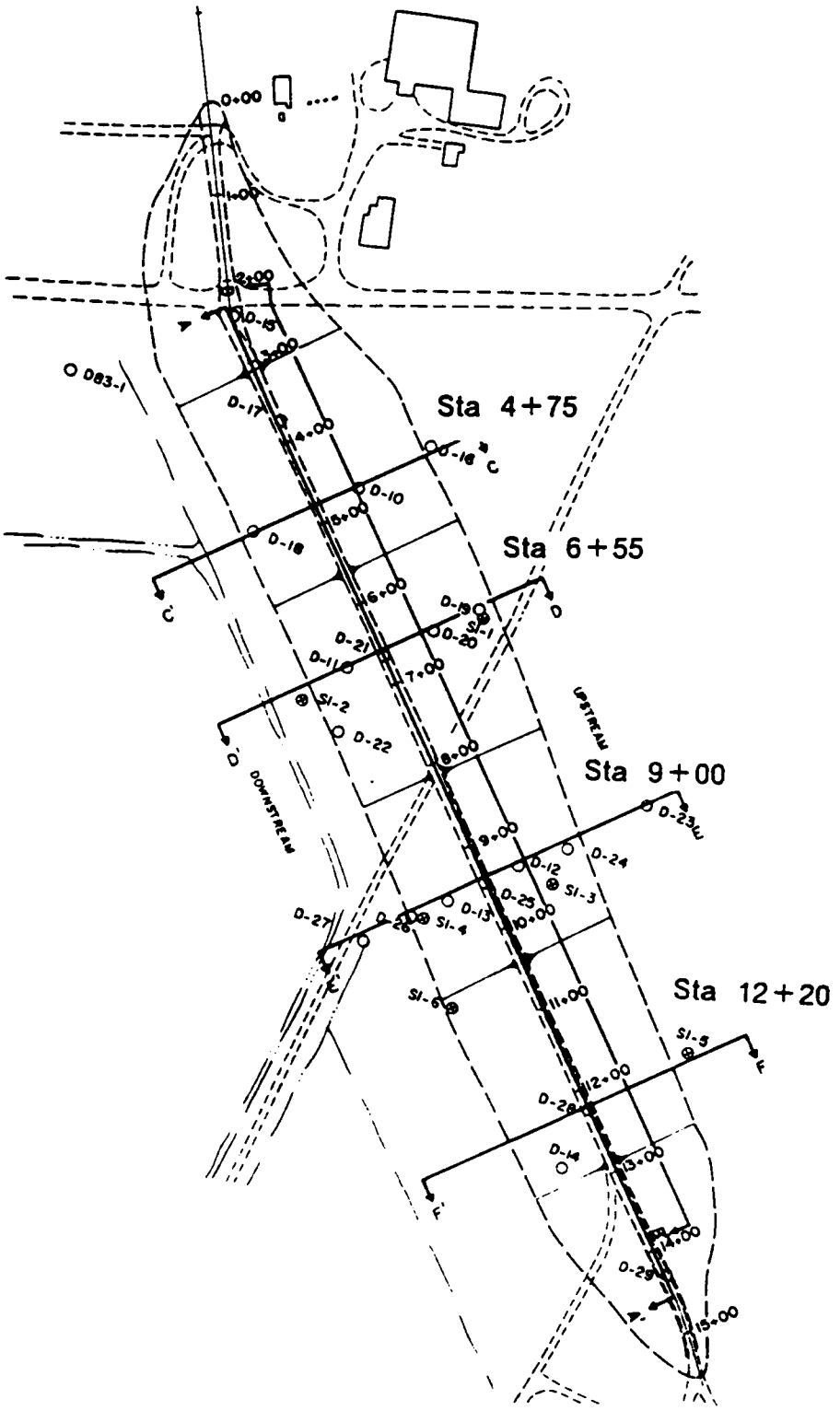

Figure 5.13. **Plan view of the dike and location of the four instrumented sections (adapted from Project Plans).**

Table 5.2 **Instrumentation at Mohicanville Dike No. 2.**

	Station						
Instrument	4+75	6+55	8+00	9+00	11+00	12+20	Total
Piezometers							
Open Tube	1	3		4		1	9
Electric	1	2		3		1	7
Pneumatic	4	8		7		4	23
							39
Inclinometers							
Vertical	1	3		3	1	1	9
Horizontal	1	1		1		1	4
Strain Gages on Steel	2	29	2	29 lower 10 upper	2	2	76
Settlements Plates	3	3		3		3	12
Surface Displacement Monuments	5	5	5	5	5		25

Strain gages on the reinforcement provided a direct means of determining the force in the steel reinforcement throughout construction. Of 76 strain gages installed on the reinforcing mesh, only two have failed to provide continuous readings, and the data appear to be very consistent and reliable.

A plan view of the project showing the dike and the location of the instrumented sections is shown in Figure 5.13. Cross-sections of the instrumented sections showing the ground surface profile and foundation conditions prior to reconstruction, are shown in Figures 5.14 through 5.17.

As may be seen from Figures 5.14 and 5.17, at Stations 4+75 and 12+20, the thickness of soft clay is about 13 feet and the thickness of peat ranges from 10 to 19 feet in the virgin state to seven to nine feet where the old embankment compressed the peat. The peat on the upstream side appears to be thicker than on the downstream. The thickness of the peat and clay is on the order of 20 to 30 feet at these sections with a firm layer at around elevation 930. Because the weak strata at these stations are thinner, higher factors of safety and smaller movements would be expected than at Stations 6+55 and 9+00, where the thickness of weak foundation materials is on the order of 60 feet.

Figures 5.15 and 5.16 show the foundation conditions at Stations 6+55 and 9+00. At these stations, the thickness of the peat is similar to that at Stations 4+75 and 12+20. At Station 9+00 a discontinuity of the peat is shown reflecting the previous shear failures that took place in the

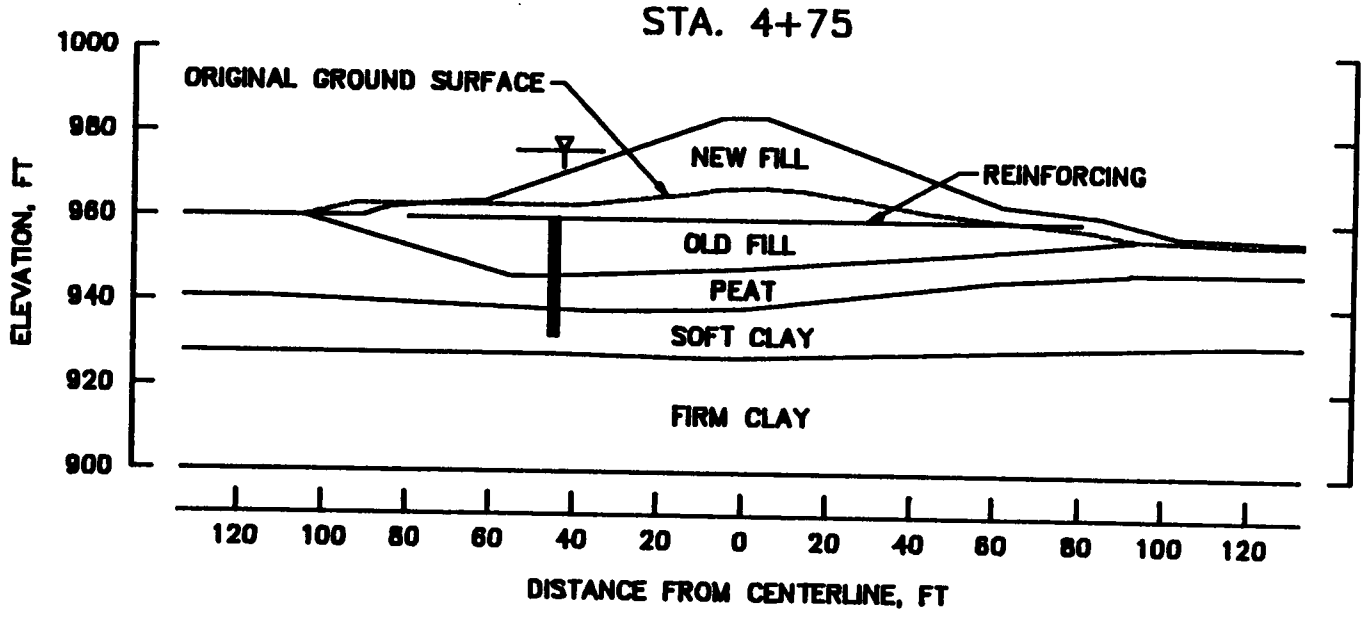

Figure 5.14 Cross section at Station 4+75.

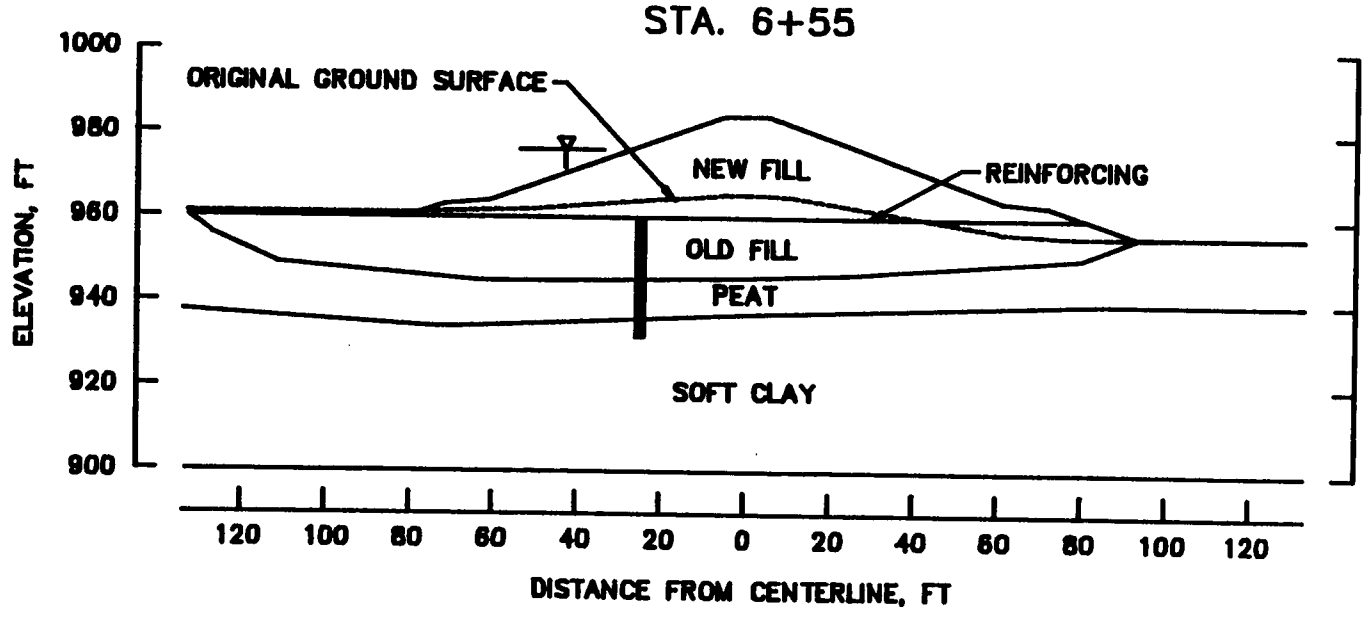

Figure 5.15 Cross section at Station 6+55.

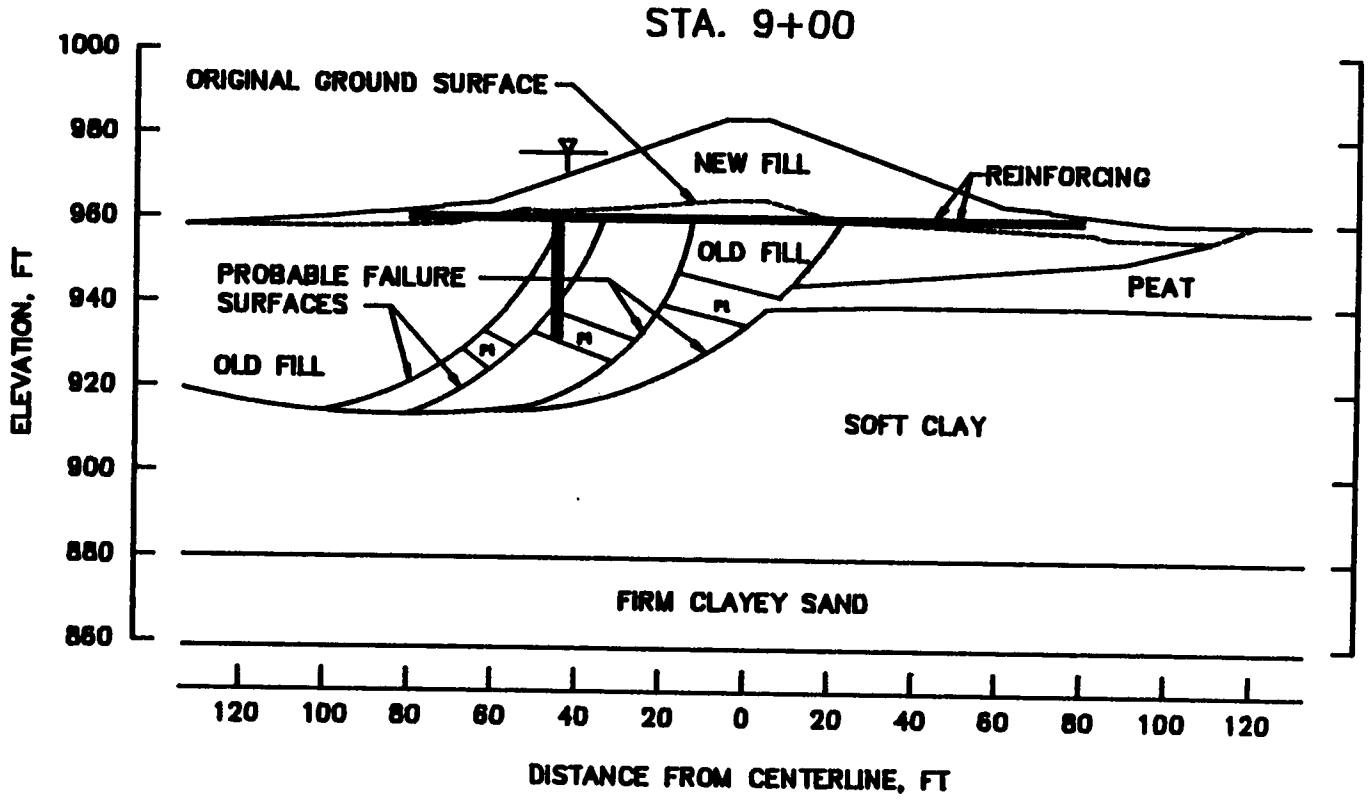

Figure 5.16 Cross section at Station 9+00.

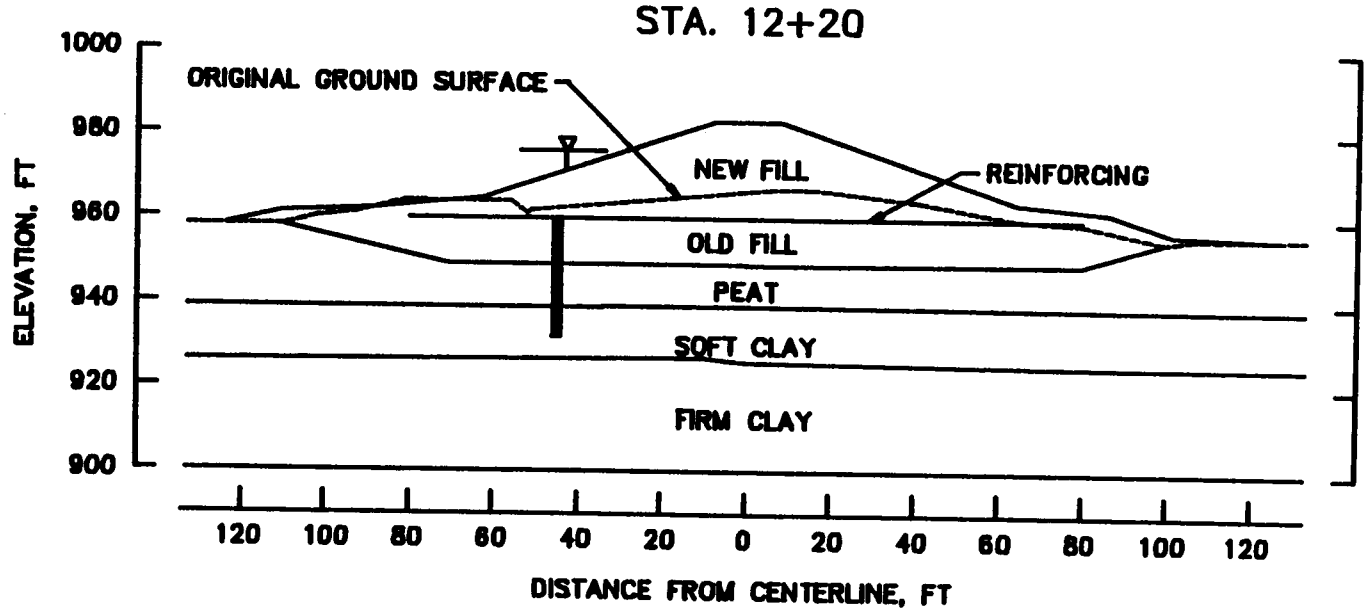

Figure 5.17 Cross section at Station 12+20.

foundation. The most prominent feature at these stations is the great thickness of soft clay, ranging from 40 to 60 feet thick beneath the peat.

5.6.2 Reinforcement Forces

Values of reinforcement force measured at the embankment centerline for the instrumented stations are shown in Figure 5.18. It may be seen that for all stations the force in the reinforcement increased as the embankment height increased. Between points A and B in Figure 5.18, which covers the period from August to November, 1984, the reinforcing force increased approximately linearly with embankment height. The highest forces in this period were recorded at Stations 6+55 and 8+00 with reinforcement forces on the order of 5.5 tons/ft. At Stations 4+75, 11+00 and 12+20, smaller forces were measured, indicating perhaps the influence of the thinner layer of soft foundation clay. The reason for the lower forces at Station 9+00 is not readily evident, as the thickness of the soft clay layer is greatest at this station. The behavior at this section may be affected by the considerable volume of old fill which displaced the peat on the upstream side of the embankment, which is shown in Figure 5.16.

In November 1984, construction was halted for the winter and was not resumed until June 5, 1985. Placement of the first three or four feet of fill on the embankment after the winter shutdown induced little additional force in the steel. It seems likely that ageing of the recently compacted embankment fill over the winter might have caused the stiffness

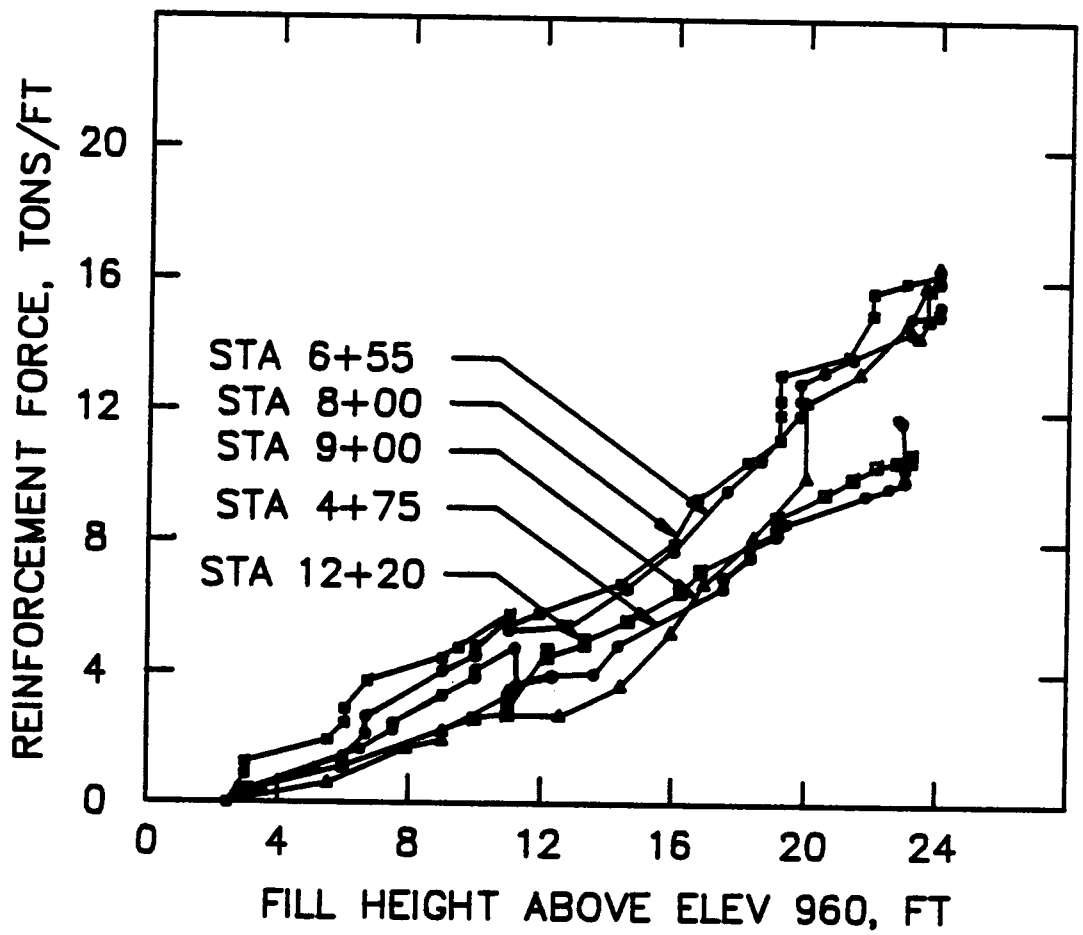

Figure 5.18 Measured reinforcement forces at the centerline of the instrumented sections.

of the fill to increase sufficiently to affect its interaction with the reinforcement and the foundation. This possibility was investigated through laboratory tests and finite element analysis and will be discussed subsequently. As further fill was placed on the embankment, above about 14 feet, the rate of increase of reinforcing force returned to that prior to the winter shutdown.

An interesting phenomenon is indicated by the data at point C in Figure 5.18. At a constant embankment height (approximately 19 to 20 feet) the reinforcement force increased by about two tons per foot over a period of nine days. The increase in force at Stations 4+75 and 12+20 was less than a half of a ton per foot, indicating the increase is most likely an effect of the thickness of the soft clay layer. This increase in force is thought to be due to undrained creep in the foundation soils, primarily the clay.

The centerline reinforcement force at all the stations initially increased after the end of construction. At Stations 8+00 and 9+00 the force began to decrease within one to two months after construction. Small increases of less than one-half of a ton per foot occurred at Stations 6+55, 11+00 and 12+20 during the period from August, 1985 to March, 1986. At Station 4+75 the force has increased nearly two tons/ft during the same period, despite a significant drop in pore pressure at this station.

Between Stations 8+40 and 9+40 two layers of reinforcement were used, spaced one foot apart vertically. This area is where the worst failures had occurred during construction of the original embankment, where a

failure of the side wall of the slurry cutoff trench occurred during its construction, and where the foundation conditions are most uncertain. A number of points of interest can be noted from the measurements of reinforcing force made in this area, which are shown in Figure 5.19: First, the lower layer of steel carries considerably greater force than the upper layer, although both have the same properties. Second, the fraction of the total reinforcement force provided by the lower layer increases with increasing embankment height. Third, after construction of the embankment was completed (Point D in Figure 5.19), the force in the lower layer of steel mesh increased slightly while the force in the upper layer decreased by about 50%. Although many factors may be involved in this complex behavior, the most important factor appears to be that the effectiveness of embankment reinforcement is improved by placing it lower within the embankment, and the lower layer of steel mesh is thus in a position to be more effective than the upper layer.

Distributions of the reinforcement forces across the embankment at Station 6+55 are shown in Figure 5.20 for various times during construction. Throughout construction the maximum force occurs at the center of the embankment, as would be expected. In the downstream portion of the embankment the variations of force with distance from the centerline are smooth and regular, indicating that the measurements probably contain little scatter. In the upstream portion of the embankment the reinforcement forces are more erratic, and are believed to be influenced by the slurry trench cutoff wall, which was located 45 feet upstream from the centerline. As the embankment height increases above 16 feet, the

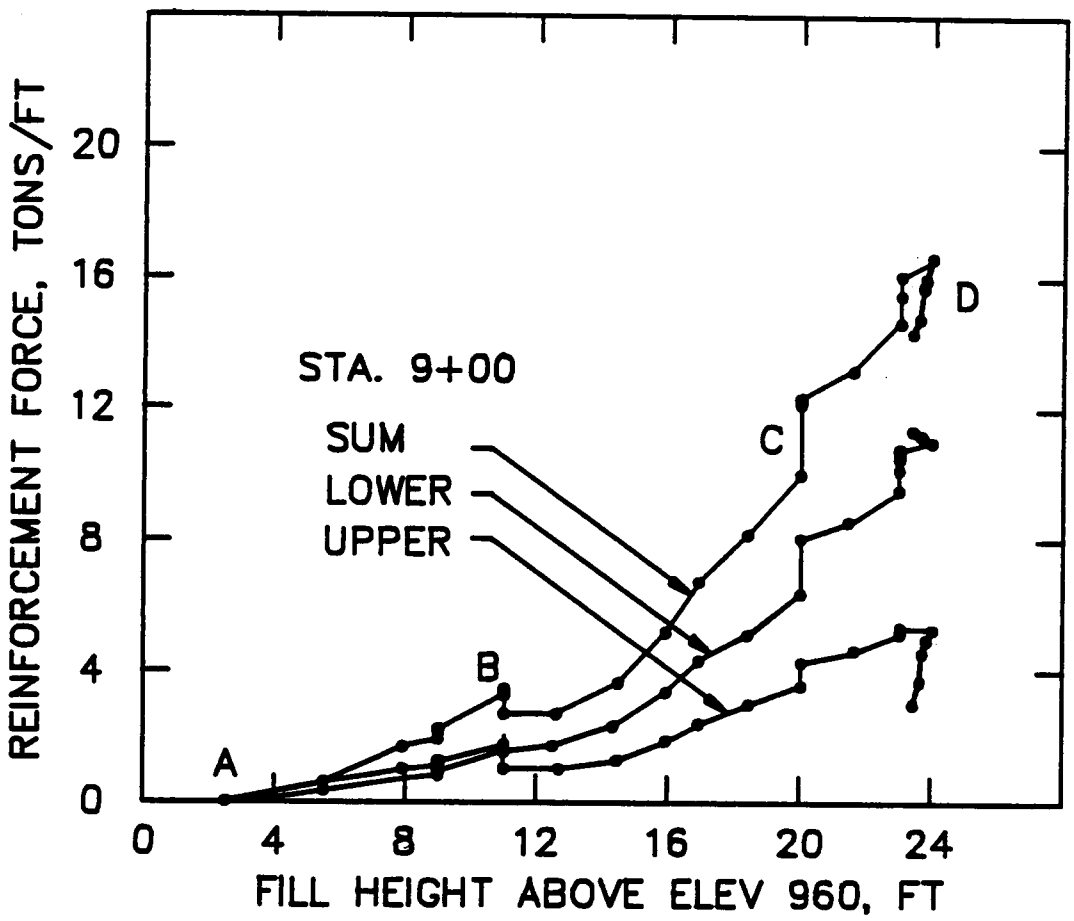

Figure 5.19 Measured reinforcement forces at the centerline of Station 9+00.

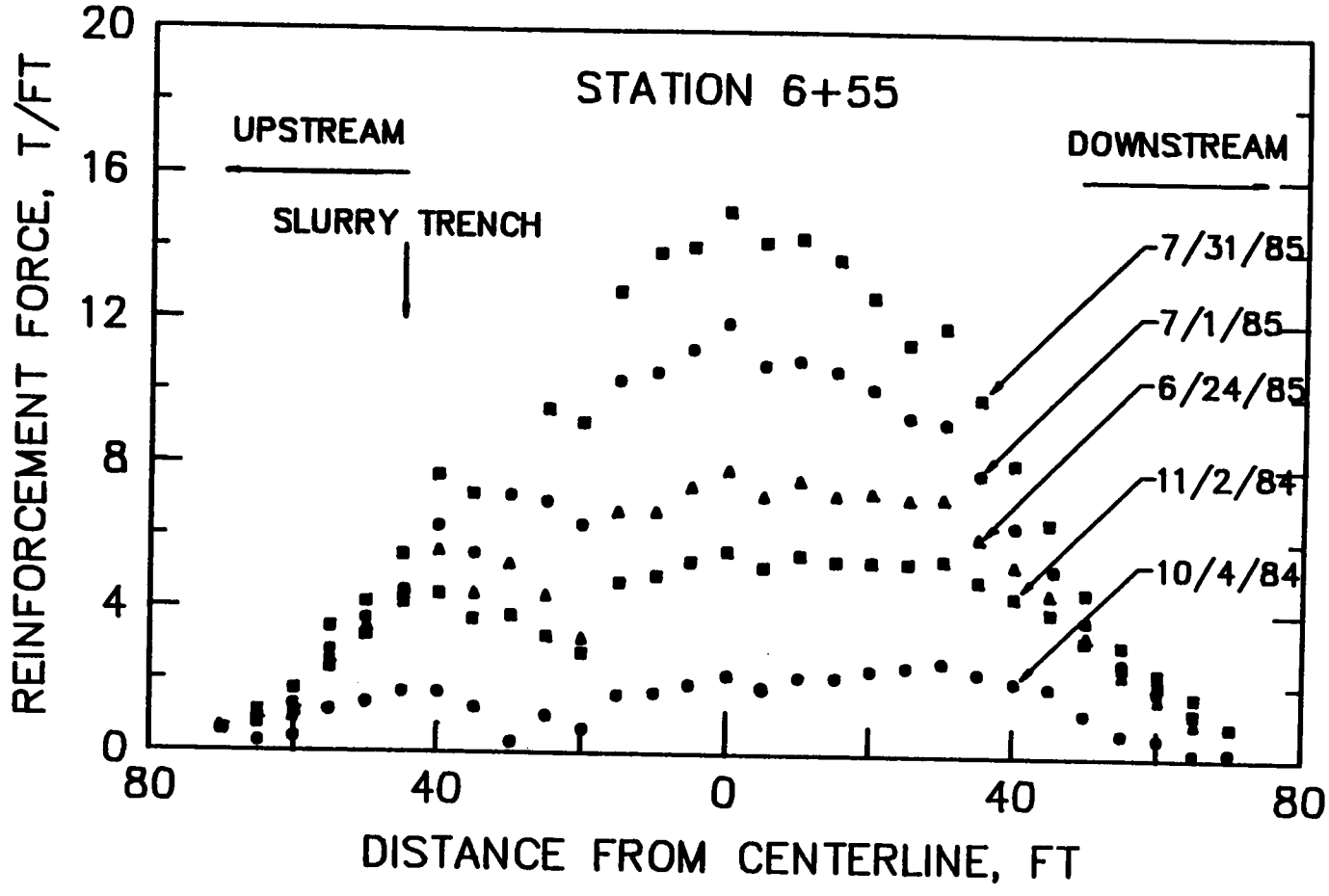

Figure 5.20 Distribution of measured reinforcement forces about the centerline at Station 6+55.

reinforcement forces continued to increase at the centerline, but did not increase much beyond about 40 ft from the centerline. Measurements of reinforcement force since the end of construction (see Table A-4 in Appendix A) show that the forces are still increasing near the centerline, although the March 1986 values show only slight increases over the December 1985 values. In the upstream portion the forces increased after end of construction and in the downstream portion the forces decreased after construction. Whether this difference is due to the presence of the slurry trench or to differences in stratigraphy is uncertain.

The distribution of reinforcement forces about the centerline at Station 9+00 also reveal some interesting tendencies. The data for Station 9+00 is tabulated in Table A-5 in Appendix A. It may be seen that while the lower steel takes the larger share of the load near the centerline as noted in Figure 5.19, near the upstream toe the upper steel takes about twice as much load as the lower steel. The trend quickly reverses itself near the slurry trench. Unfortunately, no strain gages were placed on the upper steel near the downstream toe, so it is not possible to determine if the upper steel near the downstream toe is also carrying a higher force. The data does show that the lower steel on the downstream side carries higher and more uniform forces. The variations in force in the lower steel follow the pattern noted above for Station 6+55, namely that the downstream variation is smooth and regular while the variation upstream is erratic, particularly near the slurry trench.

5.6.3 Pore Pressures

Values of pore pressure measured during and after construction are shown in Figures 5.21 through 5.27. Figure 5.21 shows pore pressure values as a function of fill height for piezometers located in the peat near the centerline of the four instrumented sections. Figure 5.22 shows a similar relationship for the foundation clay. The pore pressures in the peat at Stations 4+75 and 6+55 rise at a rate slightly greater than one foot of head per foot of fill. Because the unit weight of the embankment fill was about 136 lb/ft^3, one foot of increase in pore pressure per foot of embankment height would correspond to pore pressure ratio value of $r_u = 62.4/136 = 0.46$. The pore pressures measured in the peat at Stations 9+00 and 12+20 rise at a somewhat lower rate. The rate of rise of the crest elevation at the four instrumented stations versus time was very similar, from which it is concluded that the rate of load application for the four sections was also very similar. Thus the difference in pore pressure rise is probably due to differences in the drainage conditions and permeability of the peat at each station.

A somewhat different picture emerges when pore pressure levels in the foundation clay are considered. As shown in Figure 5.22, the pore pressures in the clay at Station 8+95 are quite high and have been high since early in construction. The pore pressures at Station 6+52 show about a 1:1 rise with embankment height but remain below the mark of piezometric head equalling embankment elevation. Collins (1986) attributed the low pore pressure in the foundation clay at this station to a faulty seal in

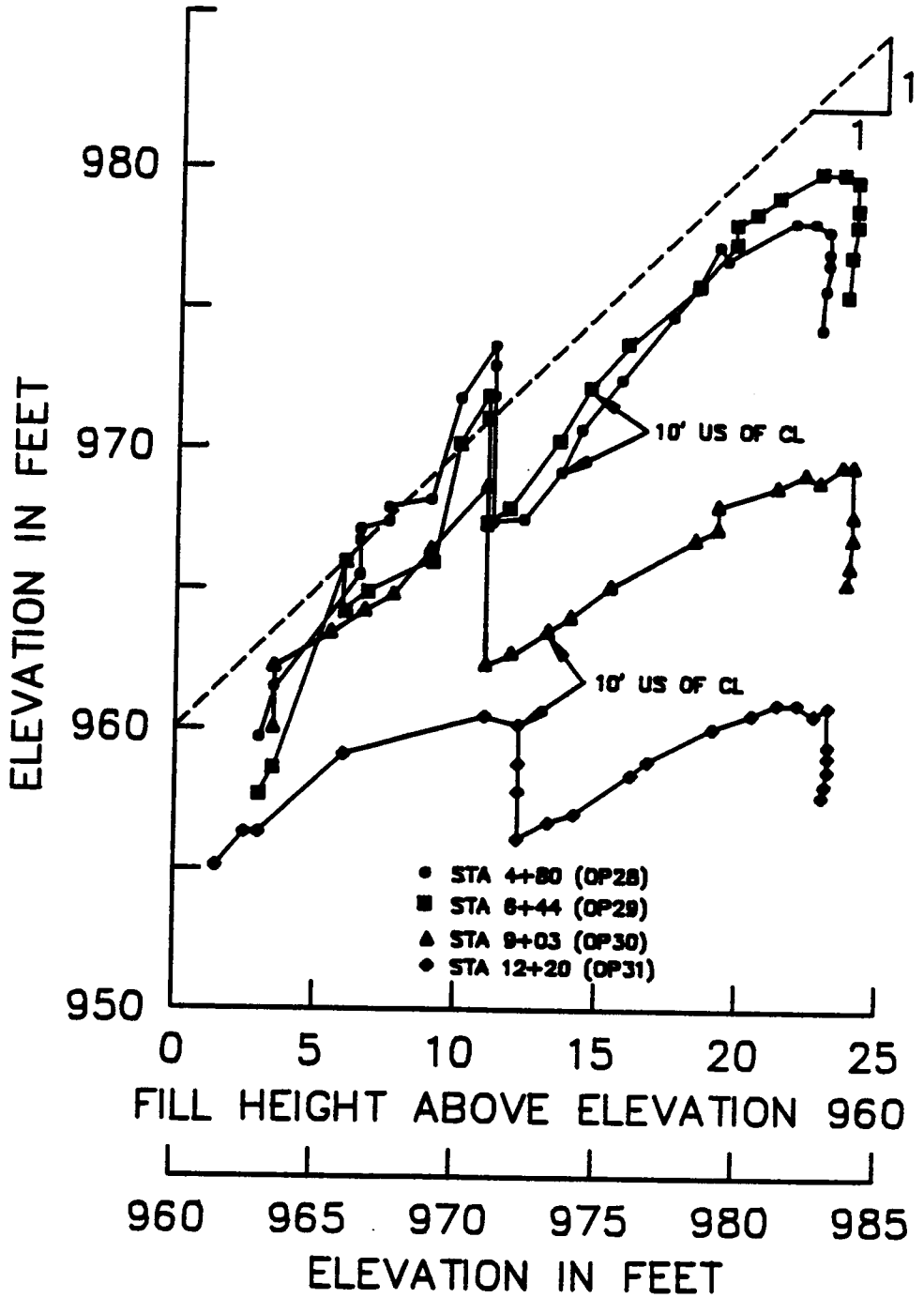

Figure 5.21 Piezometric levels in the peat versus embankment height, measured at centerline stations.

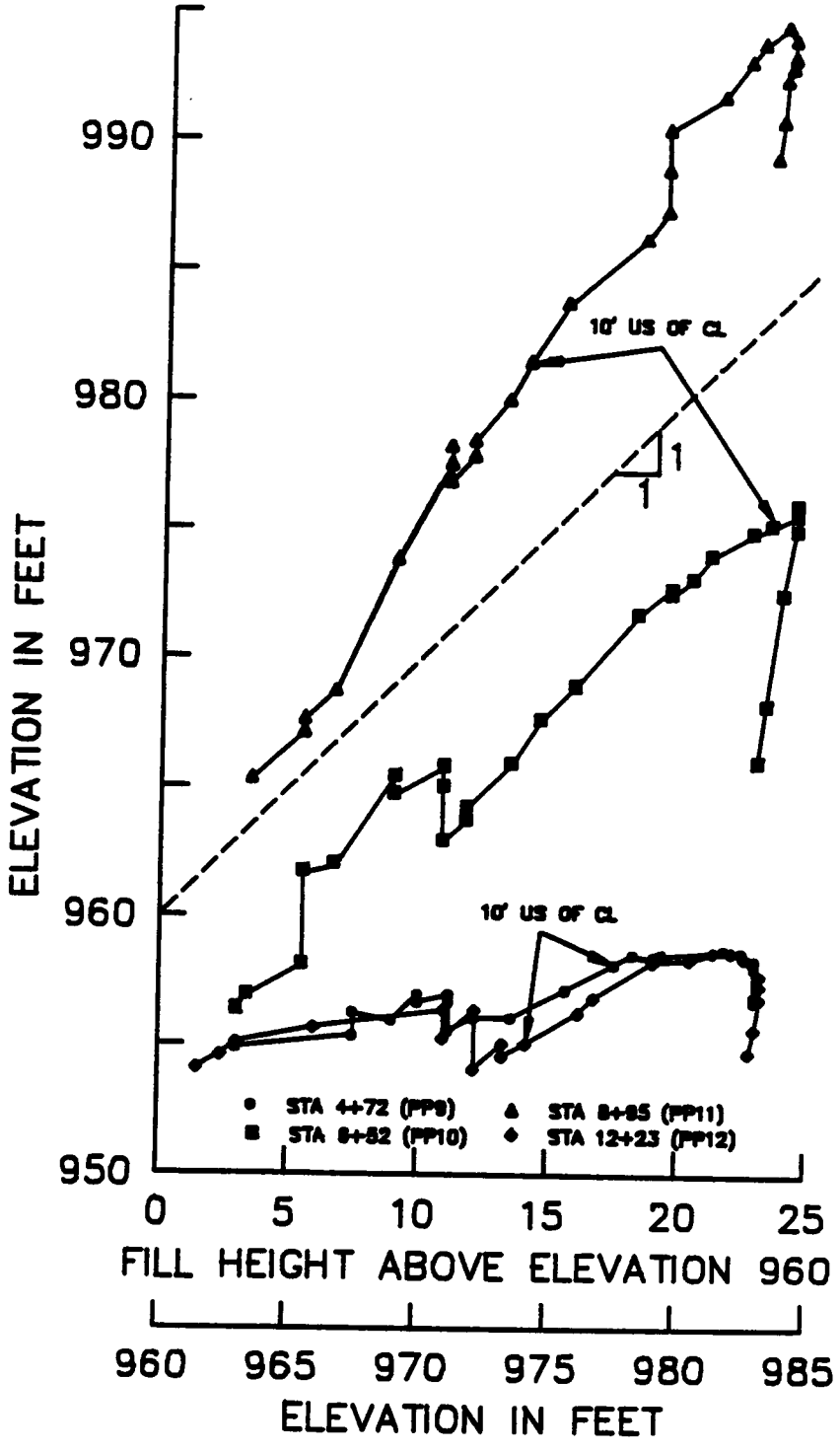

Figure 5.22 Piezometric levels in the foundation clay versus embankment height, measured at centerline stations.

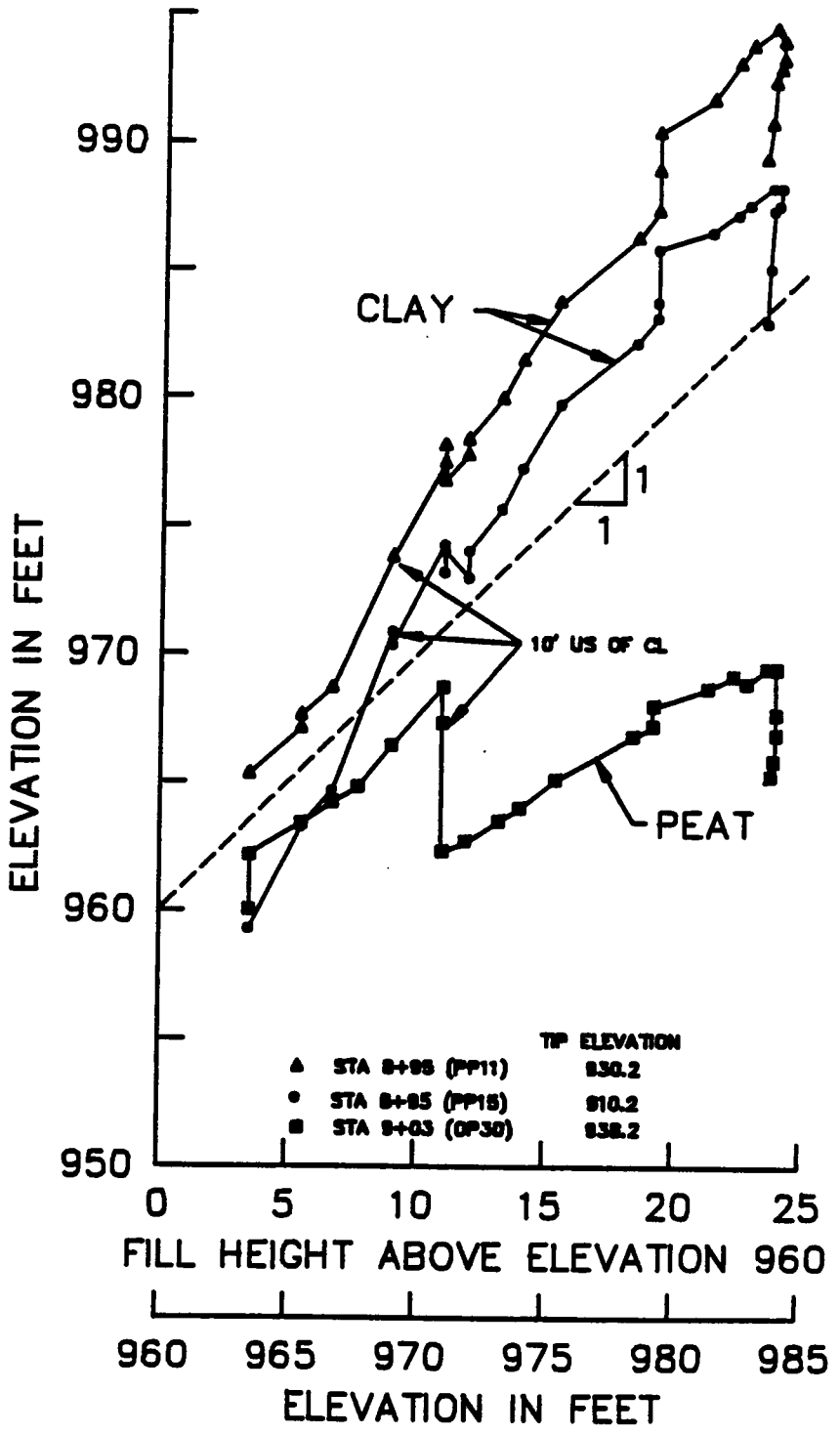

Figure 5.23 Piezometric levels in foundation clay and peat at centerline of Station 9+00.

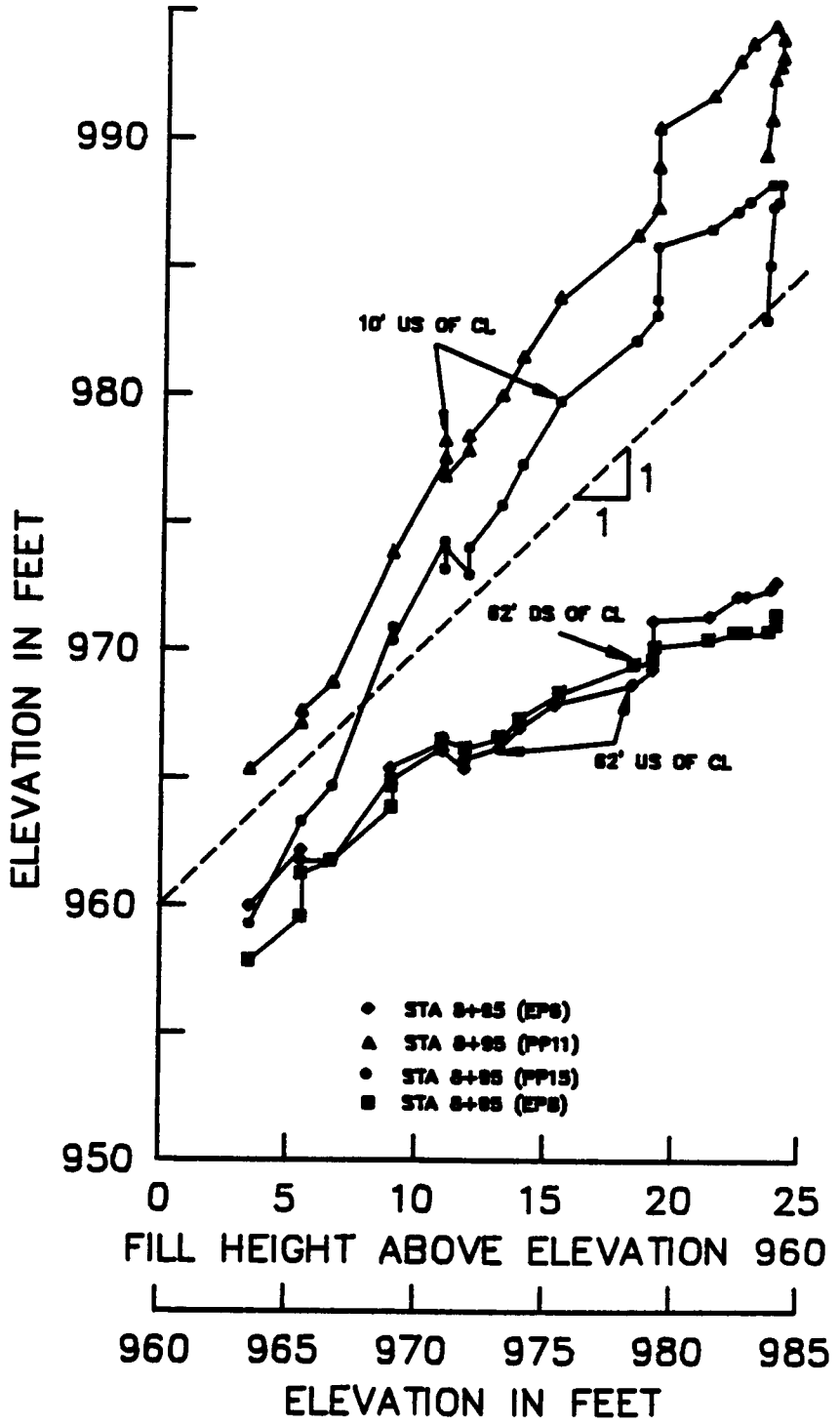

Figure 5.24 Piezometric levels in the foundation clay at Station 9+00.

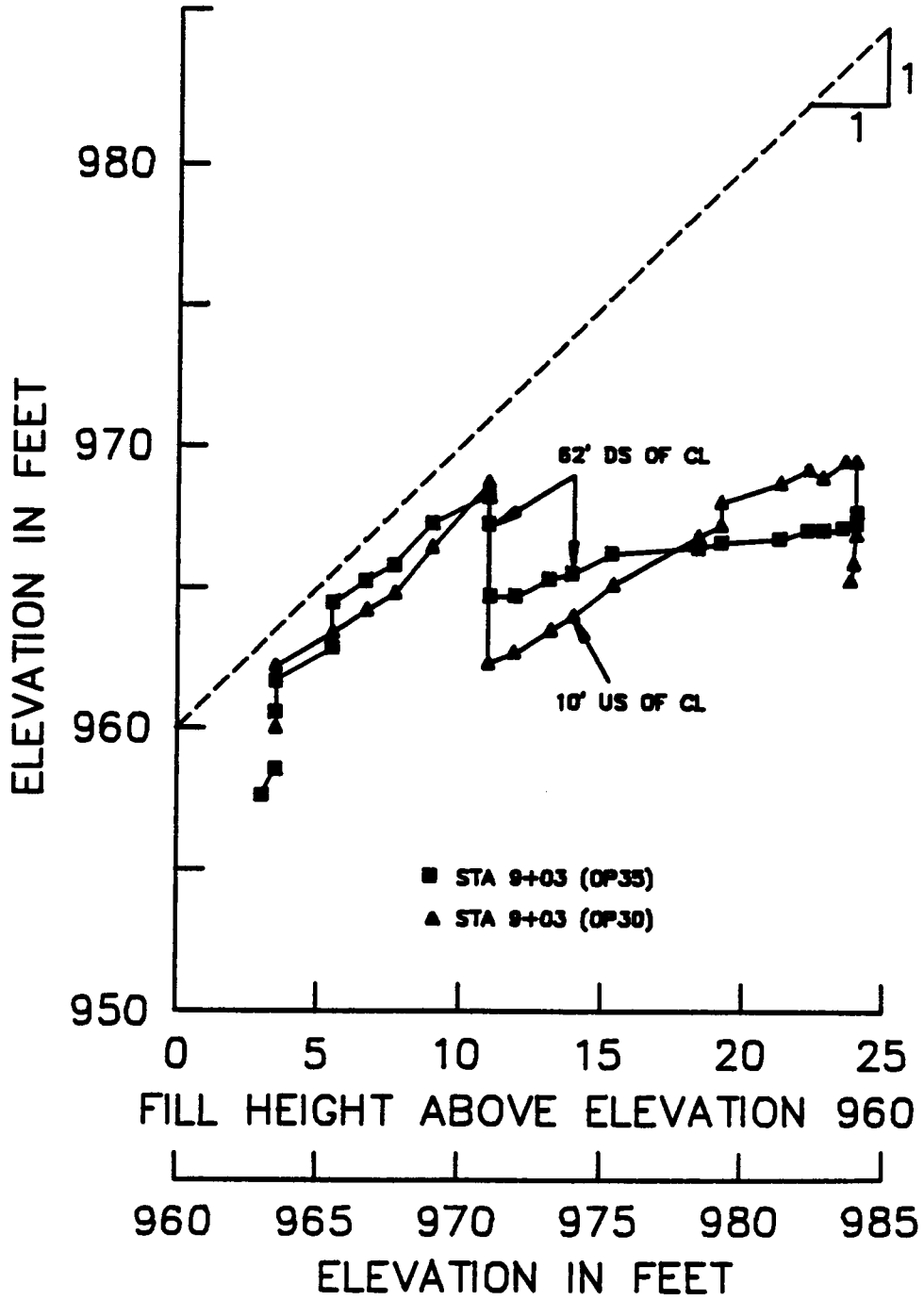

Figure 5.25 Piezometric levels in the peat at Station 9+00.

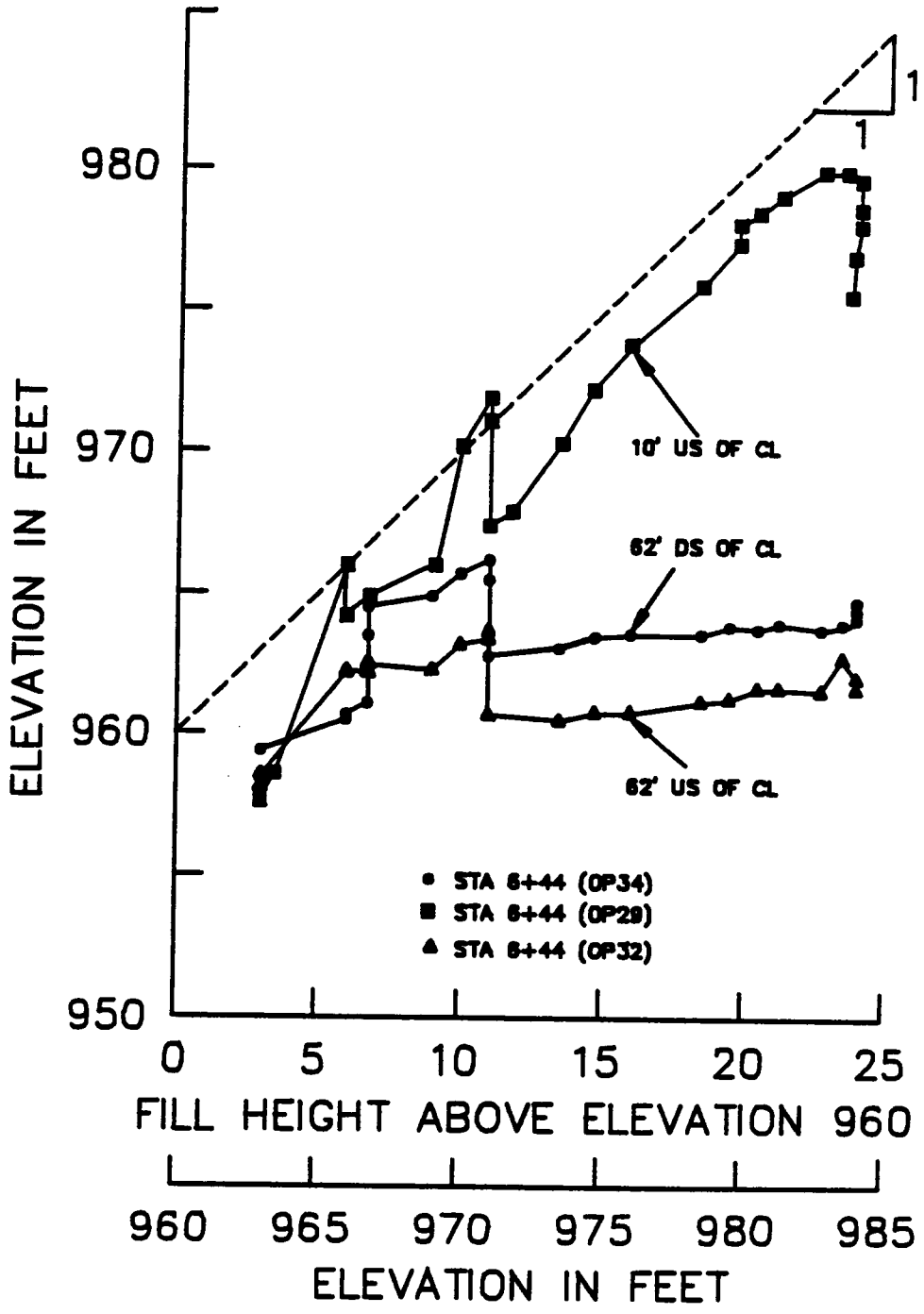

Figure 5.26 Piezometric level in the peat at Station 6+55.

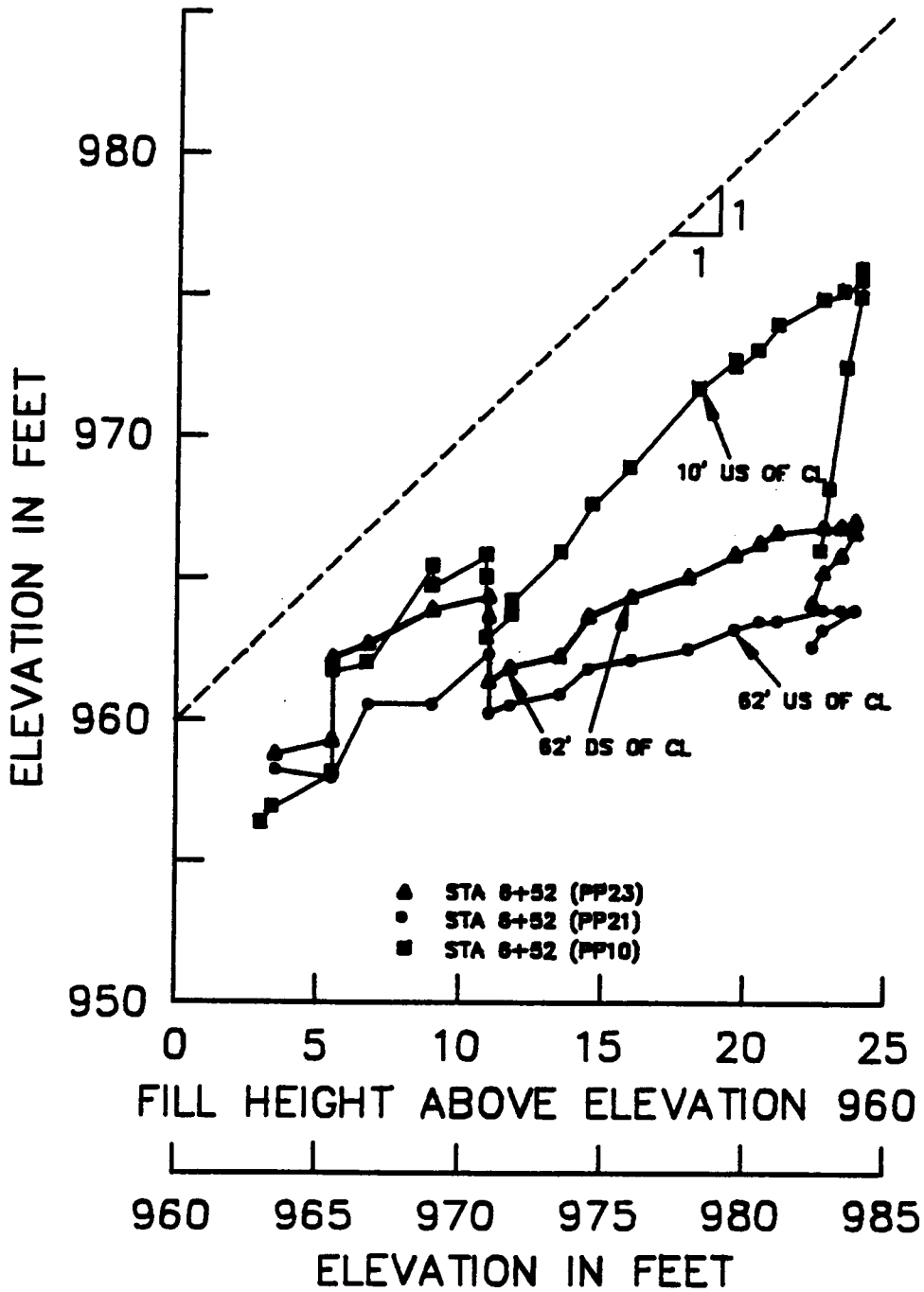

Figure 5.27 Piezometric levels in the foundation clay at Station 6+55.

the piezometer, allowing pore pressures to dissipate, and believed that the actual pore pressures probably approach those at Station 9+00. The piezometric level in the clay at Stations 4+75 and 12+29 show little response to the embankment loading.

The piezometric levels under the centerline near Station 9+00 for the peat and clay have been plotted in Figure 5.23 for ease of comparison. It may be seen that the head in the clay increased at a rate that is higher than 1:1 with embankment elevation, indicating the value of r_u is larger than 0.46. This is in contrast to the pore pressures measured in the peat which plot below the 1:1 line. A distance of only about eight feet vertically separates the tips of the two piezometers. The piezometer showing the high pore pressure levels are likely located in or near a previous failure zone in the foundation clay, as may be seen from Figure 5.16. Conditions here may be such that the prior failures have resulted in high shear stresses in the clay, such that when additional loads are imposed on the soil, corresponding higher pore pressures result. Despite these high pore pressures, the highest reinforcement forces were not measured at this station. This may be a consequence of the large volume of old fill upstream providing support to the new fill.

In Figure 5.24 the piezometric levels in the clay upstream, downstream and near the centerline are plotted versus embankment height. It may be seen that the pore pressures at the centerline are higher than at the toes, even at low fill heights when the induced loads would be of comparable magnitude. This is in contrast to the behavior in the peat shown in Figure 5.25, where at low fill heights the response at the center line

and downstream was nearly the same. Thus, much higher pore pressure response in the foundation clay at the centerline is most likely a result of the effects on the soil of the previous failures.

During the winter shutdown, piezometric levels in the peat declined considerably, while those in the foundation clay declined only slightly. In the peat, loading during the second construction season induced much more pore pressure near the centerline than at the toe, as would be expected. In the foundation clay, the pore pressure at the toes increased much more than in the peat, indicating greater load was being transferred to these areas, or slower drainage, or both. The pore pressures in the clay and peat at the centerline have been decreasing since the end-of-construction while those at the toes have increased slightly. This is believed to be due to dissipation of the pore pressures accompanied by drainage outward from the centerline to the toe areas.

Piezometric levels in the peat and clay at Station 6+55 are shown in Figures 5.26 and 5.27. It may be seen that the pore pressures near the toes in the peat increased with embankment loading through the first construction season, dissipated during the winter shutdown and then increased slightly during the second construction season. The embankment level above these piezometers was about 964 feet at the end of construction. A similar pattern exists for the piezometric levels in the foundation clay. The pore pressures in the clay during the second construction season rose more than those in the peat, which may be due to the lower permeability of the clay. The lower pore pressures experienced upstream may be due to the greater thickness of old fill upstream.

In both the peat and the clay, the increase in pore pressure is greater beneath the center of the embankment than upstream and downstream. In both the peat and the clay at Station 6+55, the response for piezometers downstream from the center is slightly greater than for piezometers the same distance upstream. In addition, at both Stations 6+55 and 9+00 the pore pressures continued to increase in the downstream peat after construction. It seems likely that this was due to the effect of the slurry trench cutoff, restricting drainage of the foundation soils. The cutoff is located 45 feet upstream from the embankment centerline, and probably restricts lateral migration of high pore pressures from the center of the embankment in the upstream direction.

5.6.4 Settlements and Horizontal Movements

Settlements measured using horizontal inclinometers located at the four instrumented station are shown in Figures 5.28 through 5.31. The measured settlements at Station 4+75 and 12+00 (Figures 5.28 and 5.31) were greatest at the centerline, with a small amount of heave occurring near the downstream toe within eight months after construction. The maximum settlements were about 0.4 feet at the embankment centerline at the end of construction (July 1985), and approximately 0.1 feet of additional settlement occurred within eight months after construction.

The settlement at Station 9+00 (Figure 5.30) was the highest recorded, with settlements of nearly one foot occurring by the end of construction and of one and one half feet by March, 1986. Rather uniform settlement

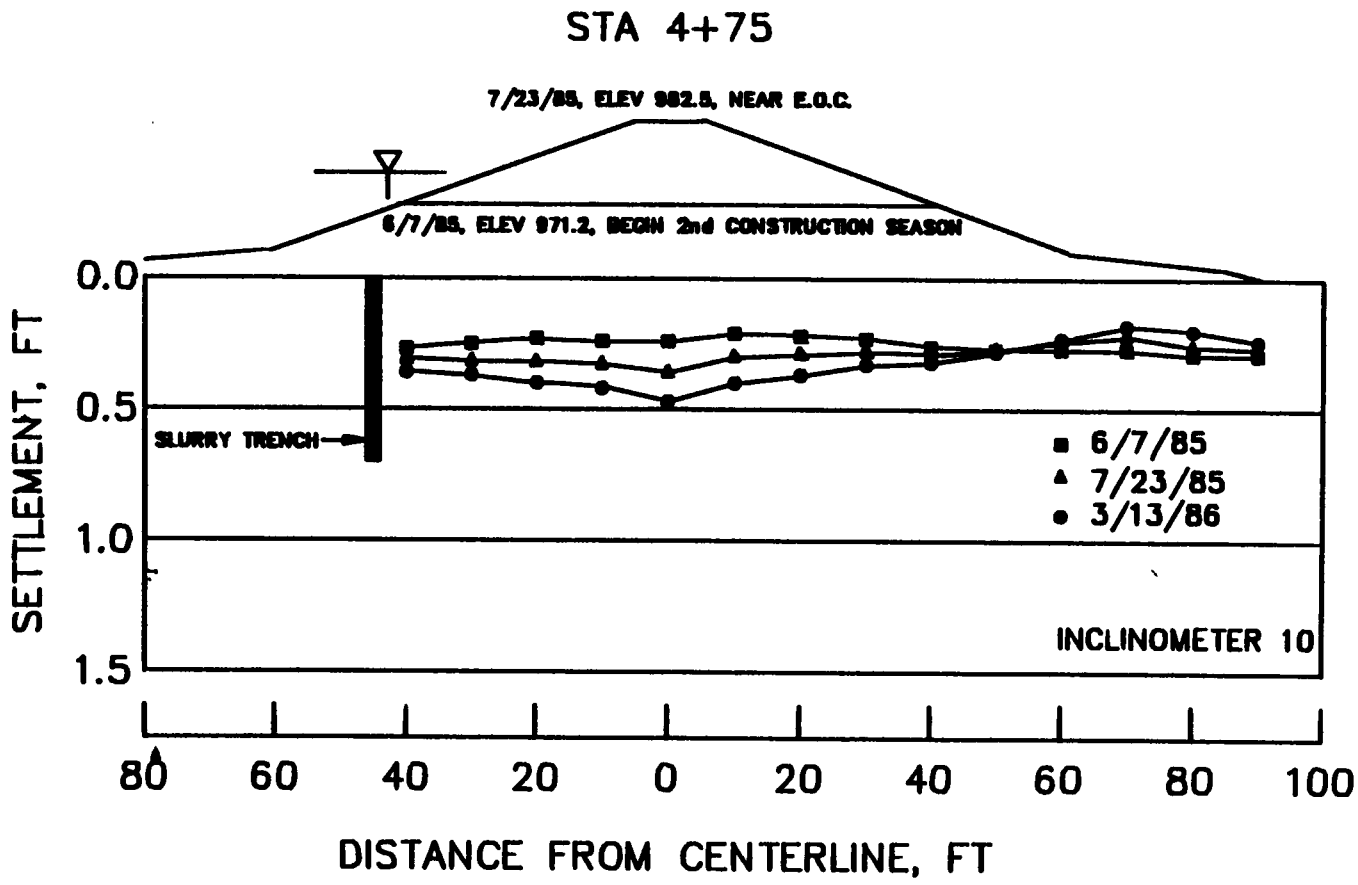

Figure 5.28 Measured settlement at Station 4+75.

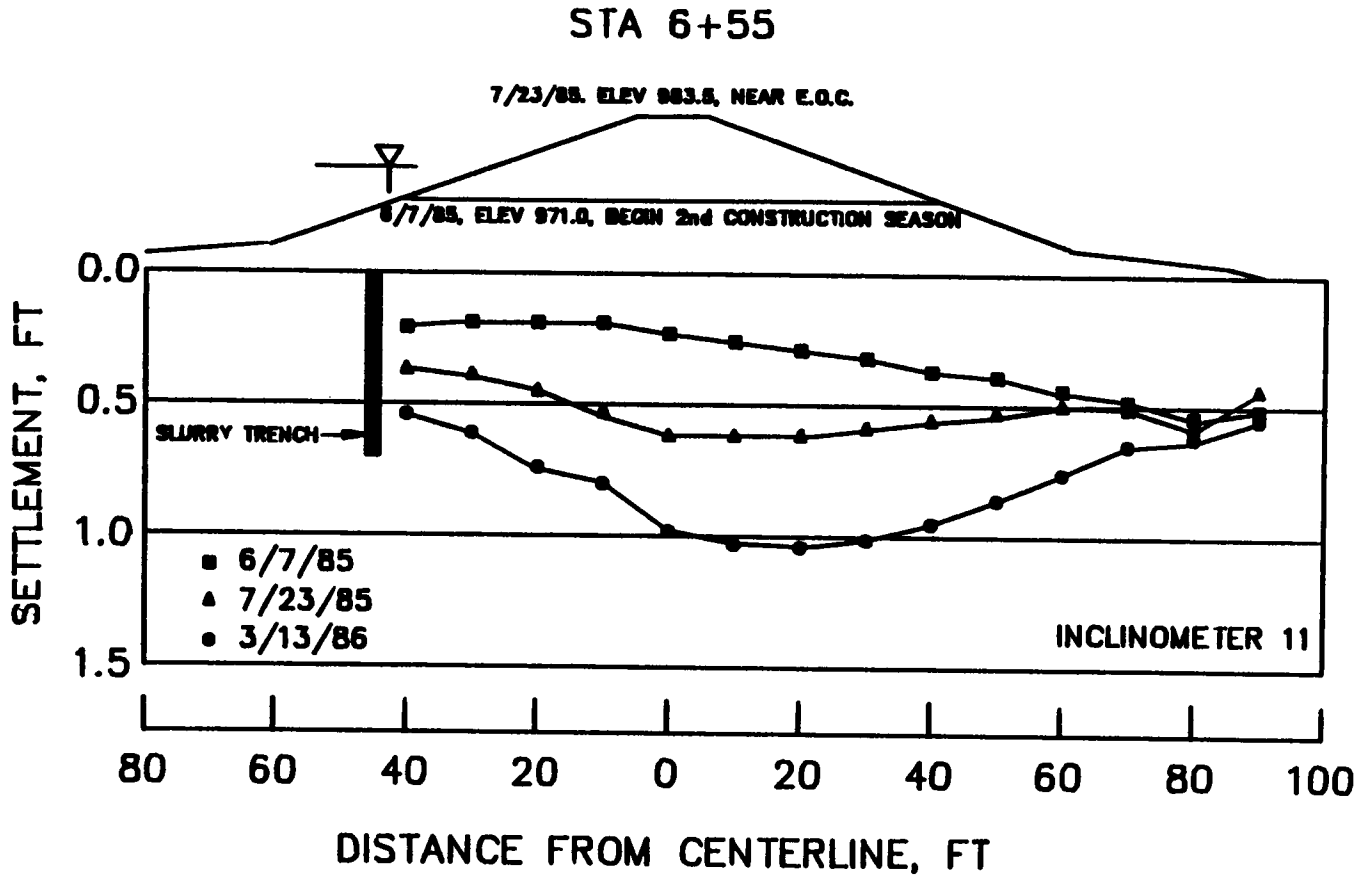

Figure 5.29 Measured settlement at Station 6+55.

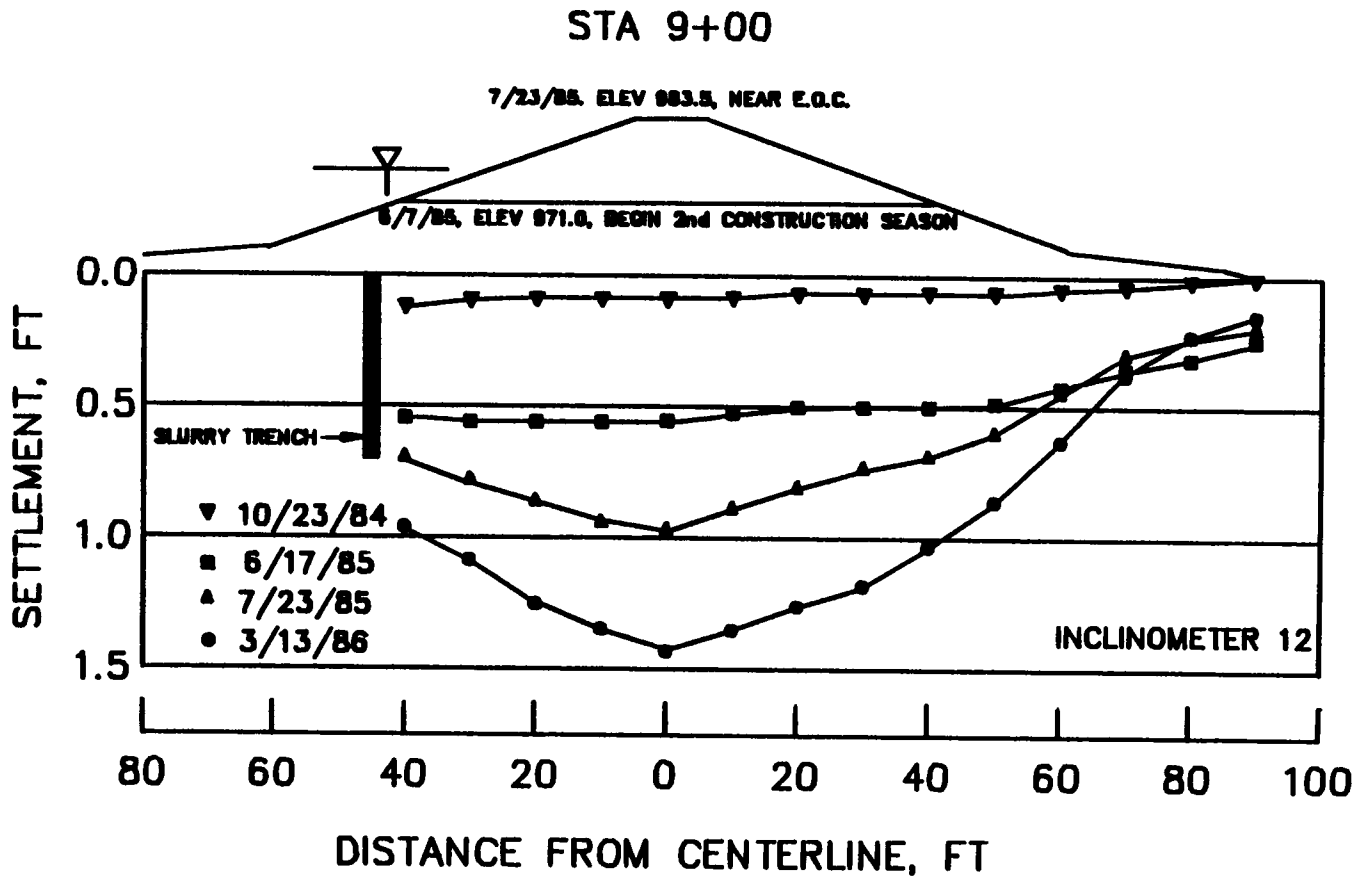

Figure 5.30 Measured settlement at Station 9+00.

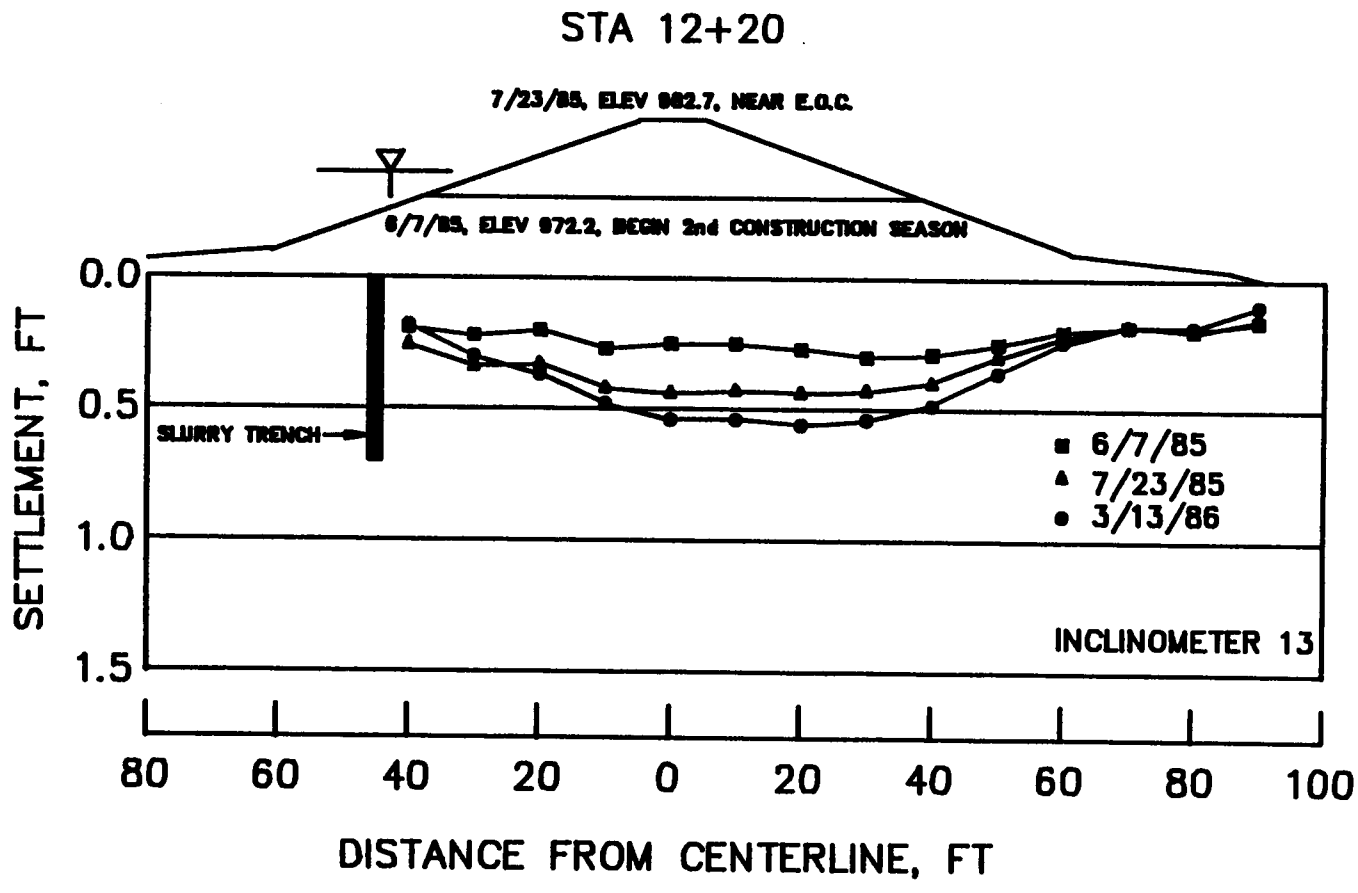

Figure 5.31 Measured settlement at Station 12+20.

occurred during the first construction season and during the winter shutdown, reflecting the uniform height of the fill during this time. As additional fill was placed, the settlement increased more at the centerline, as would be expected.

At Station 6+55 (Figure 5.29), the settlement at the beginning of the second construction season was highest at the downstream toe, where approximately one half foot of settlement had occurred. Subsequently, during the second construction season, and after the end of construction, the settlements near the center of the embankment were greater than those upstream and downstream. It seems likely that the pattern of settlements shown in Figure 5.29 is due to two separate influences, both of which tended to cause the downstream settlements to be larger than the upstream settlements. One is the influence of the old fill. The upstream portion of the old dike at this station was considerably thicker than the down stream portion. This greater fill thickness would have the effect of preconsolidating the upstream area more that the downstream area, and would lead to smaller settlements upstream (Collins, 1986). As more fill was placed and the preconsolidation effects were overcome, the settlements became more uniform.

A second influence is due to the slurry trench cutoff. It seems likely that the cutoff, by inhibiting drainage of the foundation soils in the upstream direction, effectively trapped pore pressures in the peat and clay beneath the upstream central portion of the embankment. As a result the settlements beneath the upstream portion of the embankment were smaller than those beneath the downstream portion. If this explanation

is correct, it would be expected that the settlements upstream and downstream will become more nearly equal with time.

Settlements were also measured using settlement plates and surface monuments. Data from these instruments are shown in Tables A-8 and A-9, respectively. Settlements determined from these instruments are in good agreement with the data from the inclinometers.

Horizontal movements near Stations 6+55 and 9+00, measured using vertical inclinometers, are shown in Figures 5.32 through 5.34. Movements near the toes of the embankment at Stations 6+55 are shown in Figure 5.32. It may be seen that the movements during construction were quite small, the largest measured movement being less than 0.25 feet. Both upstream and downstream, the shear deformations that give rise to most of the horizontal movements occur in the clay layer, between elevation 915 and 930. It may also be noted that the movements at the level of the reinforcement are very small, as would be expected.

Four inclinometers were installed near Station 9+00, three upstream and one downstream. The movements measured at these location are shown in Figures 5.33 and 5.34. The three inclinometers upstream indicate a pattern of decreasing horizontal movement with distance away from the centerline. The measured movements during construction are similar to those at Station 6+55, with maximum movements of about 0.25 feet. The movements at this station are small below elevation 900, indicating that the clay below this elevation is firm. The movements following construction increased substantially, nearly doubling the construction movements. The movements do not appear to be adversely affecting the

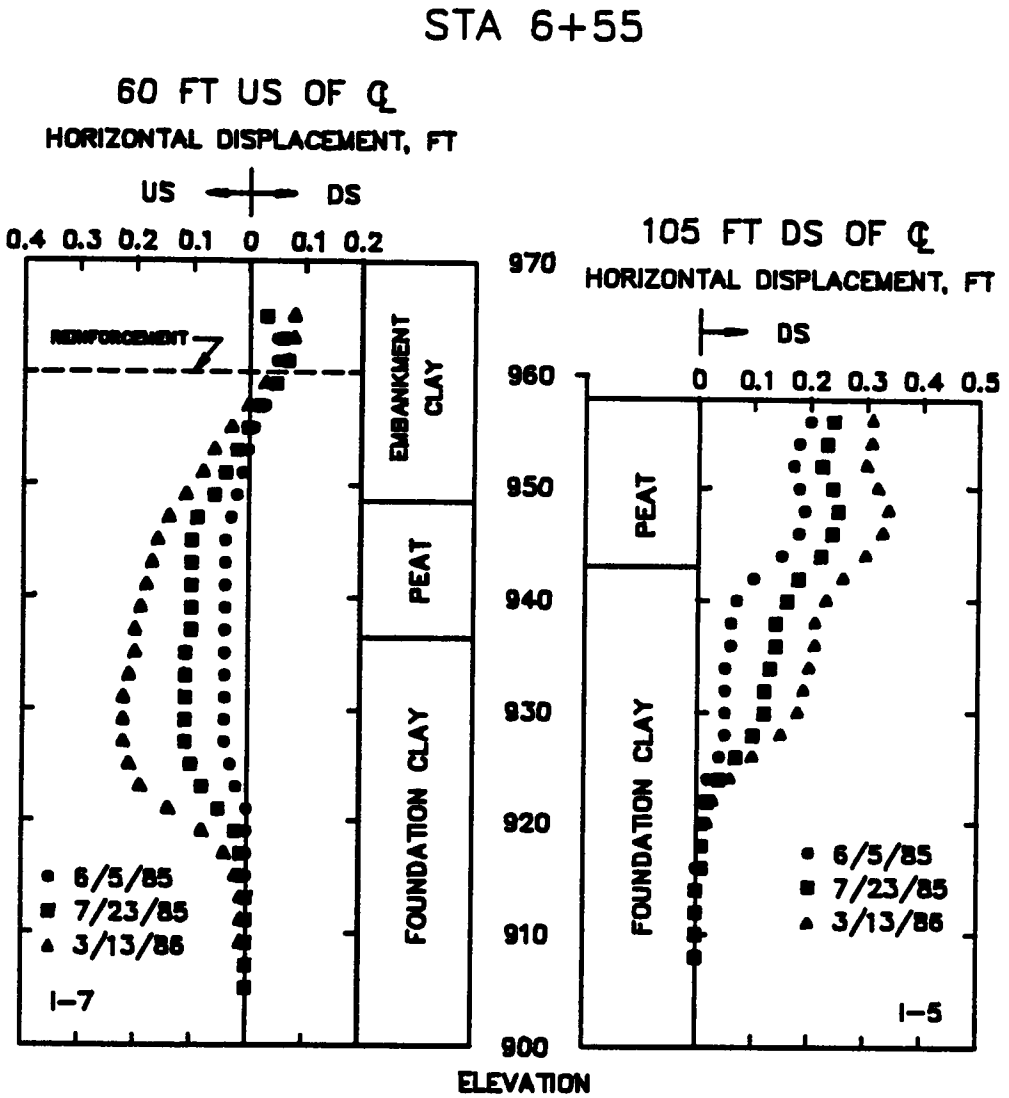

Figure 5.32 Measured horizontal movements at the toes at Station 6+55.

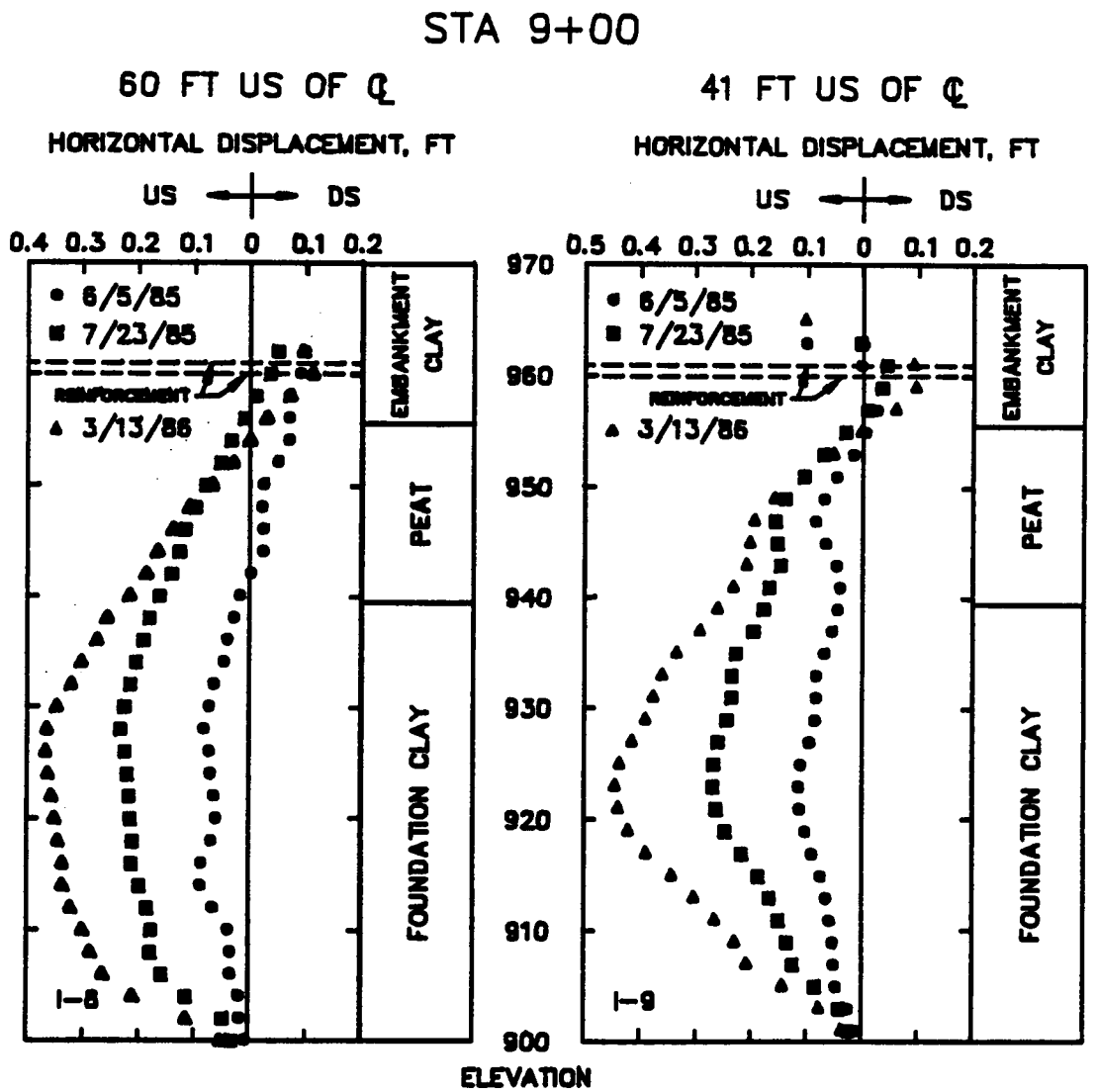

Figure 5.33 Measured horizontal movements upstream of centerline at Station 9+00.

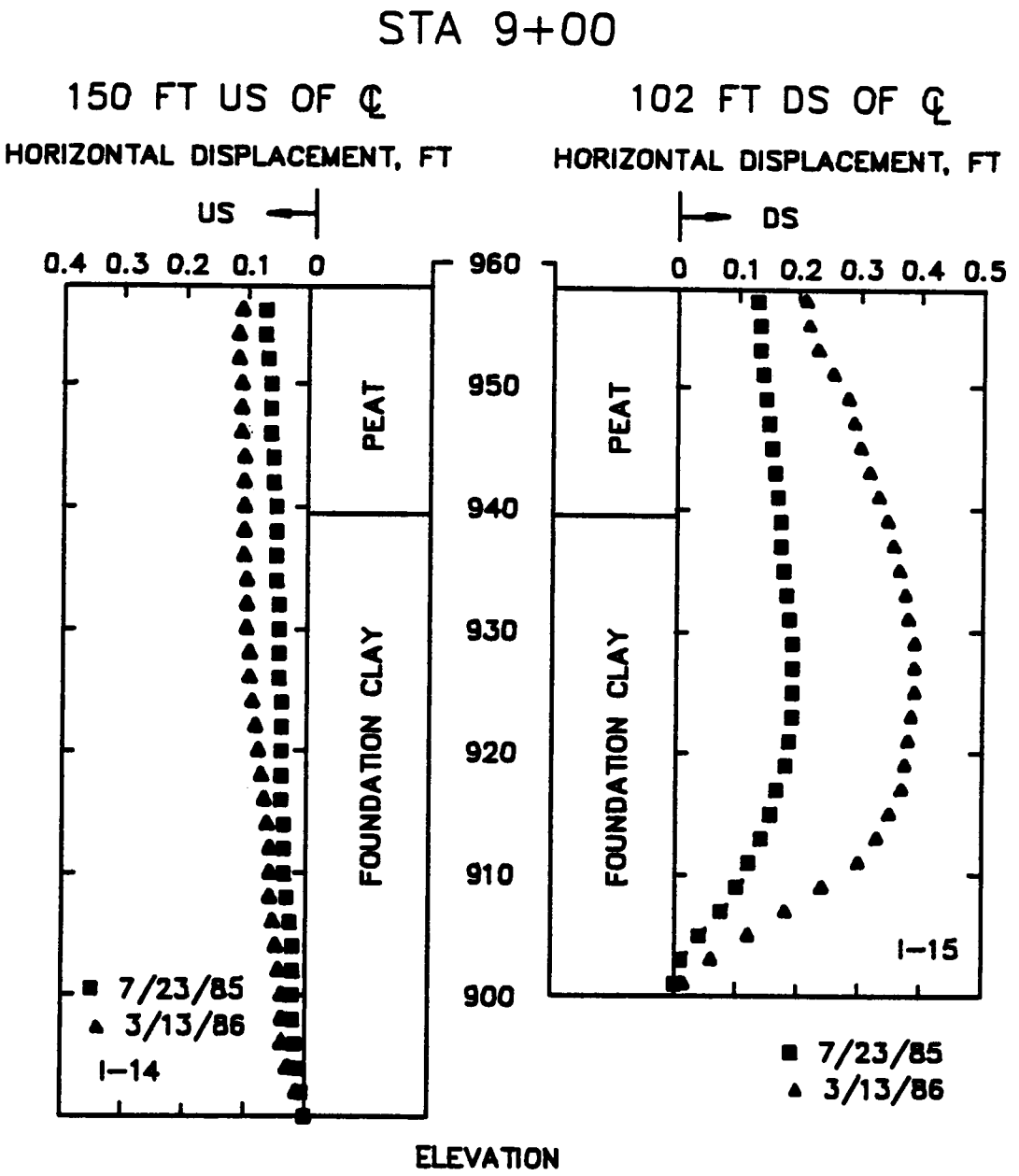

Figure 5.34 Measured horizontal movements at Station 9+00.

embankment, as the reinforcement forces at this station are decreasing. At elevation 960, the reinforcement elevation, the measured movements are consistently downstream. As noted by Collins (1986), the movements appear to indicate a downstream movement of the entire embankment.

An inclinometer located 128 ft upstream of Station 12+20 recorded movements of less than 0.01 ft at all elevations during and following construction.

5.7 Finite Element Analyses

As mentioned previously, finite element analyses were performed for design by the Waterways Experiment Station (Fowler et al. 1983), and additional analyses were performed after construction during this investigation, in connection with evaluation of the results of the instrumentation program. In both analyses the same computer program was used, although modifications to the program were made as described in Chapter III.

The degree of agreement between the actual stress-strain characteristics of the soil and those modeled by CON2D can be checked by using the parameters to calculate triaxial stress-strain curves, and comparing the computed stress-strain behavior with experimental results. The determination of the model parameters for the foundation clay, peat and embankment fill is discussed below. In selecting the parameters used in the analyses, emphasis was placed on matching the actual behavior of the soils in the small strain range, because it was known that the actual

strains would be small if they matched the measured behavior of the embankment.

Finite element analyses were performed on two of the instrumented sections. Station 6+55 was analyzed because: (1) the foundation conditions at this section were well defined and not affected by the previous failure, (2) a significant depth of soft foundation clay existed (approximately 40 feet), and (3) the reinforcing was instrumented every five feet upstream and downstream from the centerline, providing a unique opportunity to compare calculated and measured reinforcement forces. Analyses were also performed for Station 9+00 conditions to investigate the effect of the double layer of reinforcement.

The effect of ageing of the embankment clay on the reinforcement behavior was studied through a laboratory testing program to determine the effects of ageing on strength and stiffness, and through analyses performed using properties for freshly compacted and aged samples of the fill.

5.7.1 Selection of Soil Parameters

5.7.1.1 Foundation Clay

The available soil data on the foundation clay included three consolidated undrained (CU) envelopes from triaxial compression tests with pore pressure measurement, several unconsolidated-undrained (UU) tests, and one dimensional consolidation tests, as well as classification data.

A review of the test borings led to the conclusion that the foundation clay was primarily a silty clay ranging from medium to high plasticity, with occasional lenses of organic clay. Thus, the initial soil parameters were developed from tests on clays with medium to high plasticity.

The determination of the soil parameters for the model used requires consolidated drained or consolidated undrained triaxial compression tests with pore pressure measurements and consolidation test data. For the foundation clay two CU tests and four consolidation tests were available which were performed on medium to high plasticity silty clay. These data are shown in Figures 5.4 and 5.6, respectively. The parameters were determined using the procedures developed by Duncan et al. (1981) and D'Orazio and Duncan (1982).

The initial parameters determined were based on CU triaxial tests on sample UD22-7 and the consolidation test from sample SI6-3. The parameters determined from these tests are shown in Table 5.3. The degree of agreement between the actual stress-strain characteristics of the soil and those calculated using the derived parameters can be checked by using the parameters to calculate triaxial stress-strain curves, and comparing the computed stress-strain behavior with experimental results. The comparison for the soft clay foundation material shown in Figure 5.35 for confining pressures of 0.58 and 0.75 tsf, where it can be seen that the computed stress-strain behavior underpredicts the strength of the soil and overpredicted the pore pressures by a large margin. The next step was to make adjustments to the parameters to obtain better agreement.

Table 5.3 **Model parameters used in foundation clay trials.**

	φ'	C' tsf	M_T	p_r tsf	κ	λ	ν
Initial							
Sample UD22	29	0.03	1.16	0.054	0.011	0.07-0.20	0.44
			1.50	0.054	0.011	0.07-0.20	0.44
			1.16	0.20	0.011	0.07-0.20	0.44
			1.50	0.20	0.011	0.07-0.20	0.44
Sample UD25	25	0.28	0.98	0.60	0.013	0.013-0.23	0.44
Final Parameters	29	0.03	1.16	0.20	0.03	0.07-0.20	0.25

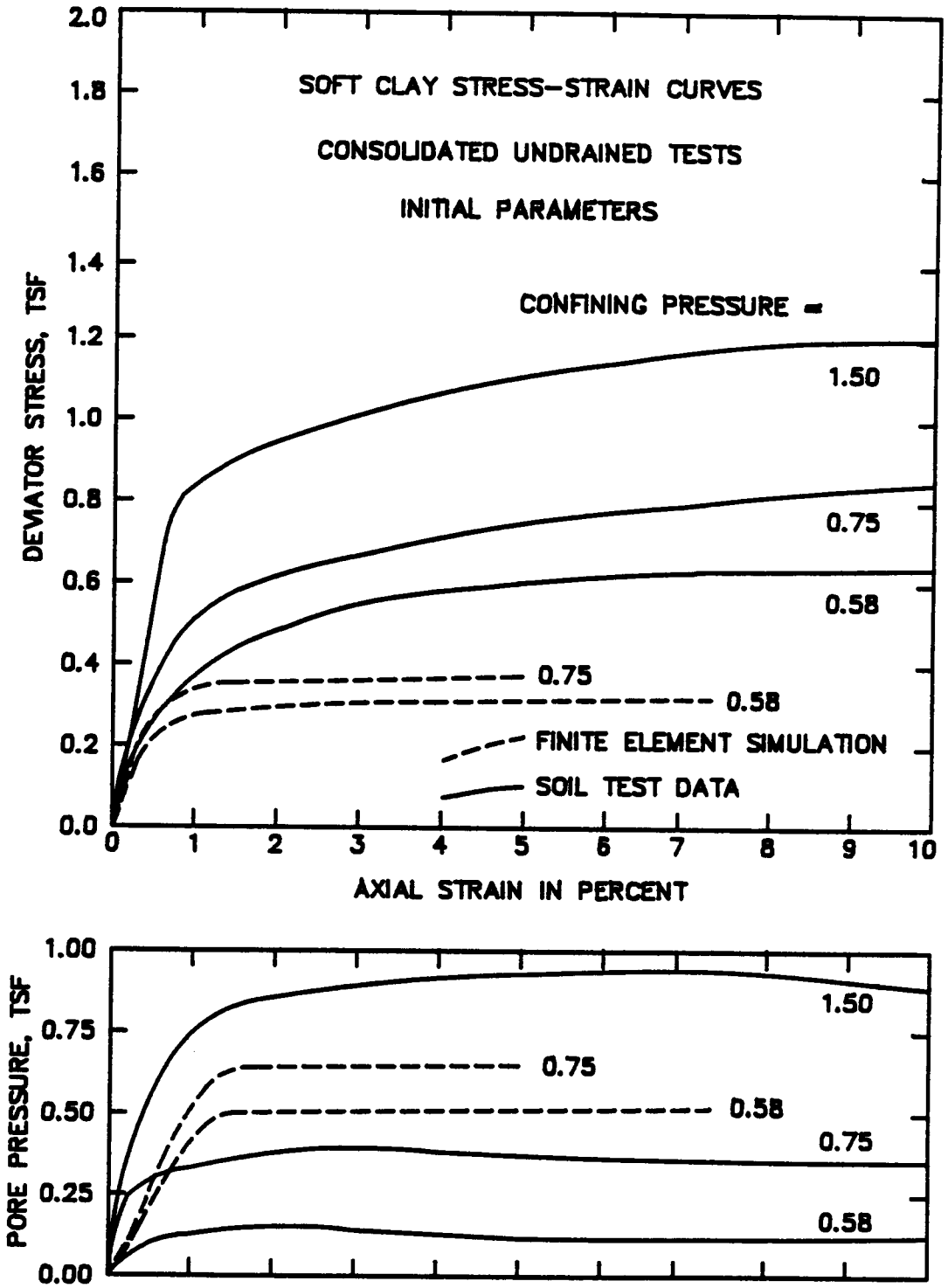

Figure 5.35 Comparison of calculated to measured stress-strain curves for foundation clay using initial parameters.

To obtain larger computed strengths, the values of M and p_r were increased. The first change involved increasing M to 1.50 from 1.16 with the results shown as curve B in Figure 5.36. Another trial, in which p_r was raised to 0.20 tsf from 0.054 tsf (keeping M = 1.16), was also performed, with almost the same effect as increasing the value of M. It may be seen that these changes raise the stress-strain curve closer to the actual data, but also increase the magnitudes of the calculated pore pressure. The effect of increasing both M and p_r to 1.50 and 0.20 tsf respectively is shown by curve C in Figure 5.36. The effect is to obtain a relatively close fit to the ultimate strength, but the calculated stress-strain curve deviates significantly from the measured curve and the pore pressure response is still overpredicted.

The severe overprediction of pore pressures was of considerable concern, and to obtain a better fit to measured pore pressures, the parameters were further adjusted. D'Orazio and Duncan (1981) studied the effect of changes in parameter values on shapes of undrained stress-strain curves and pore pressure curves with the qualitative results shown in Figure 5.37. Parts b and c of this figure show that increasing κ and ν should lower the calculated pore pressure response, but this also has the effect of greatly altering the calculated stress-strain curve. Indeed, when a change in only one of these parameters was made, large changes would occur in the shape of the stress-strain curve.

At this point, data and from additional consolidation and triaxial tests were further examined, revealing two important facts: First, the initial value of κ may have been somewhat low. Second, the test data used

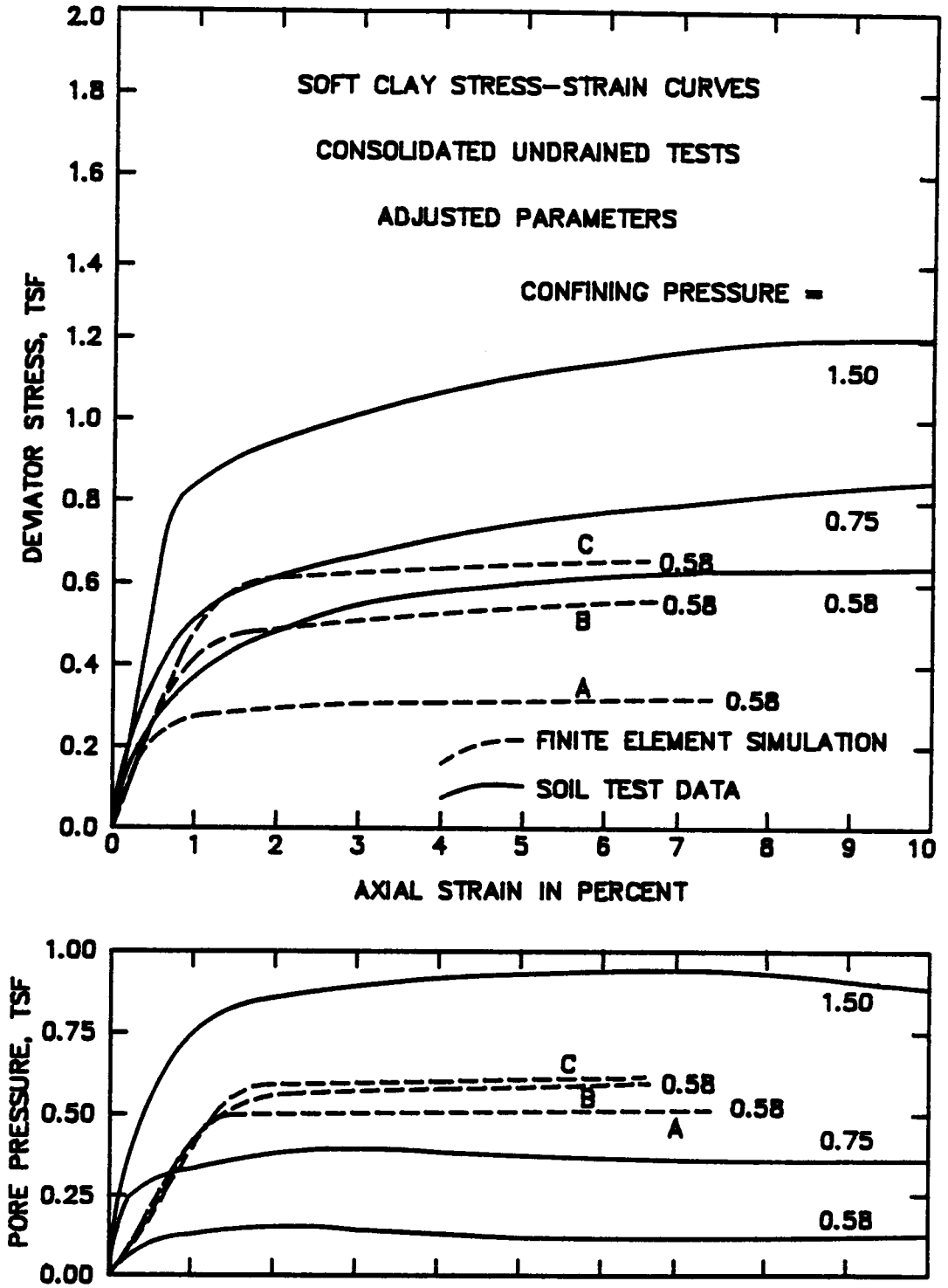

Figure 5.36 Comparison of calculated and measured stress-strain curves for foundation clay using adjusted M values.

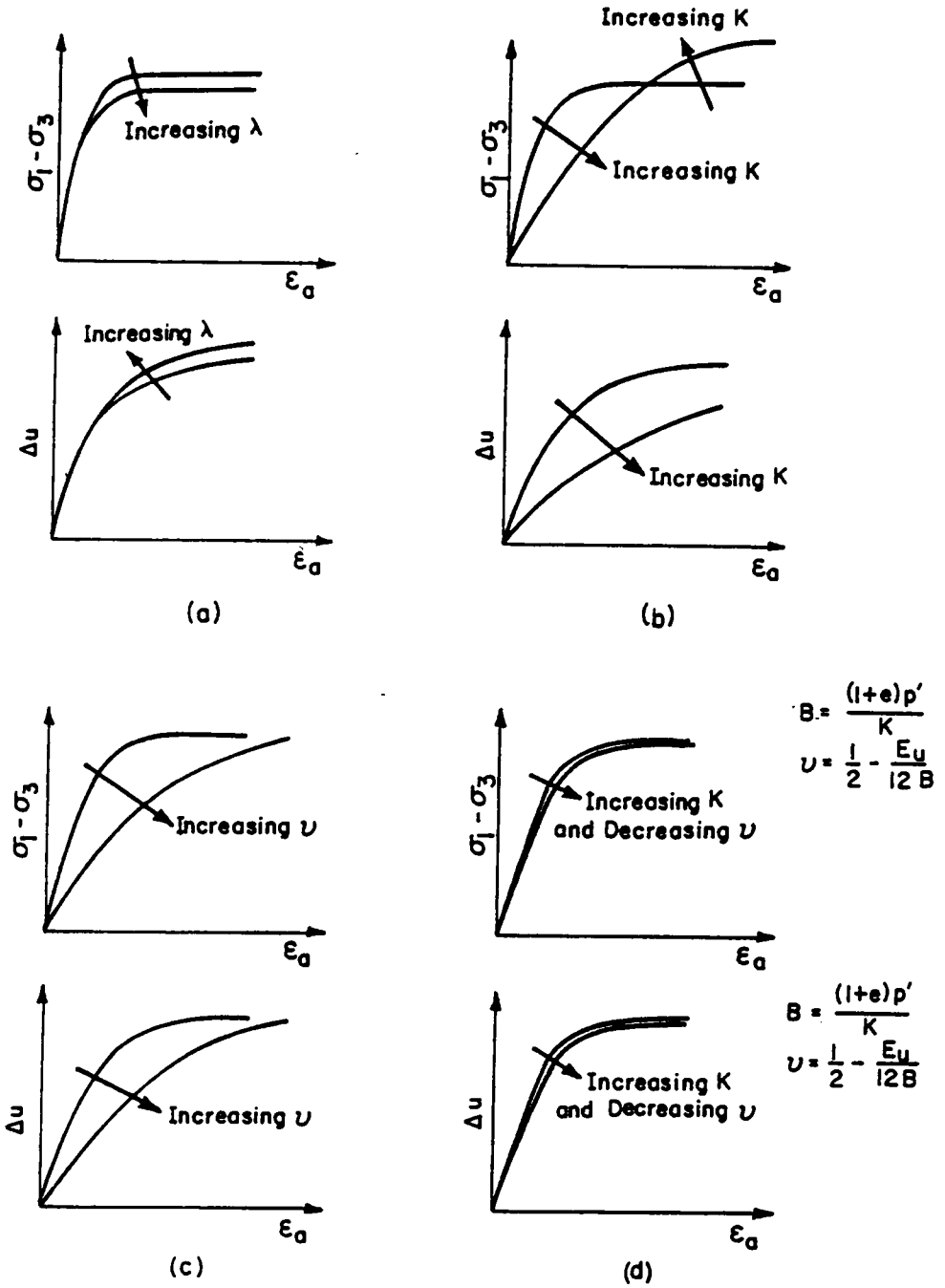

Figure 5.37 Effect of changes in soil parameters on shape of stress-strain curves (after D'Orazio and Duncan 1983).

for comparison purposes were from soil samples which were probably slightly overconsolidated. The effect of adjusting κ can be seen in Figure 5.37b; as adjustments to κ are made, either a "stiffer" or "softer" stress-strain response can be be obtained. Interpretations of additional consolidation test data showed κ to be in the range of 0.018 to 0.024, about twice as large as initially used. Also at this point, preliminary analyses of the dike were being performed and one of the things considered was the effect of Poisson's ratio on the reinforcement forces computed. It was found that using Poisson's ratio values as calculated from the test data resulted in computed reinforcement forces much greater than those measured in the field. A series of trials showed that Poisson's ratio values of 0.25 for the peat and foundation clay provided the best match to field reinforcement forces. As the value of Poisson's ratio was reduced from (0.44 to 0.25) it was necessary to raise κ to maintain the shape and slope of the stress-strain curve, similar to the effect shown in Figure 5.37d.

The two samples used for the initial comparison, Figure 5.35, were probably slightly overconsolidated. The stress paths for samples consolidated to these two confining pressures (0.58 and 0.75 tsf), shown in Figure 5.38, show shapes normally associated with overconsolidated soils. In contrast, the stress path for the sample having a confining pressure of 1.50 tsf exhibits behavior more typical of normally consolidated clays. Using the initial parameters with the higher confining pressure produces the results shown in Figure 5.39. A very good match is obtained for the stress-strain data from the test on the sample consolidated to 1.50 tsf.

As was the case previously, the pore pressure response is overpredicted by a large margin, although the match to the measured pore pressure is better at low strains.

To ascertain whether the lack of agreement between computed and actual stress-strain data was a consequence of the slightly overconsolidated nature of the soil, additional parameter determination was performed using the CU triaxial data from sample UD25-7. This sample was chosen because, as shown in Figure 5.40, the stress paths for each sample comprising the envelope show characteristic normally consolidated behavior. The derived parameters are shown in Table 5.3. Comparisons of the computed and actual test data for this case are shown in Figure 5.41. Consolidation characteristics from sample UD25-6 were used in these calculations. The stress-strain behavior is not simulated particularly well and the computed pore pressures response is overpredicted. This indicates that the overconsolidation of the soil samples in the first trial may not be the sole reason for the lack of agreement between the computed and actual curves.

Using a value of Poisson's ratio equal to 0.25, additional simulations were performed with the aim of reducing the calculated pore pressure response, while matching the initial parts of the actual stress-strain curves. No variations of the parameters were found in which the pore pressure response was changed more than 15 percent from that calculated in the initial trial.

Consideration of the stress paths followed by the samples provide an explanation. The yield surface used in the model is elliptical, as shown

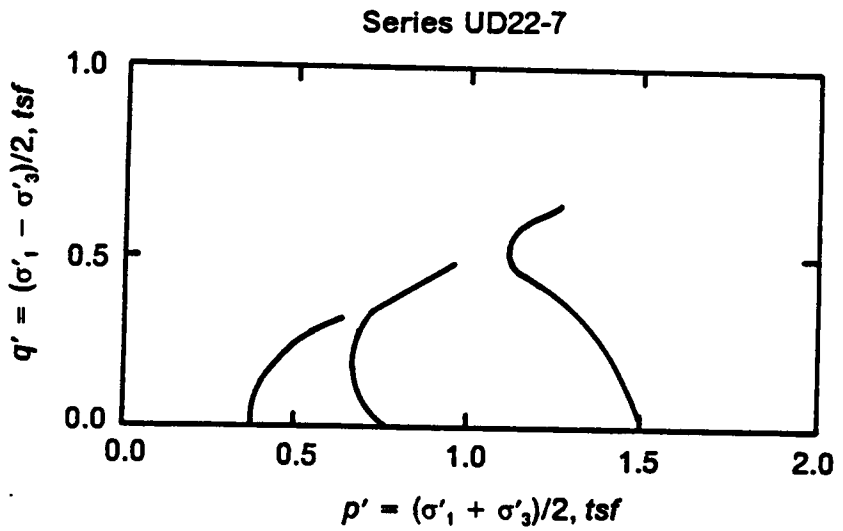

Figure 5.38 Stress paths for samples from test series UD22.

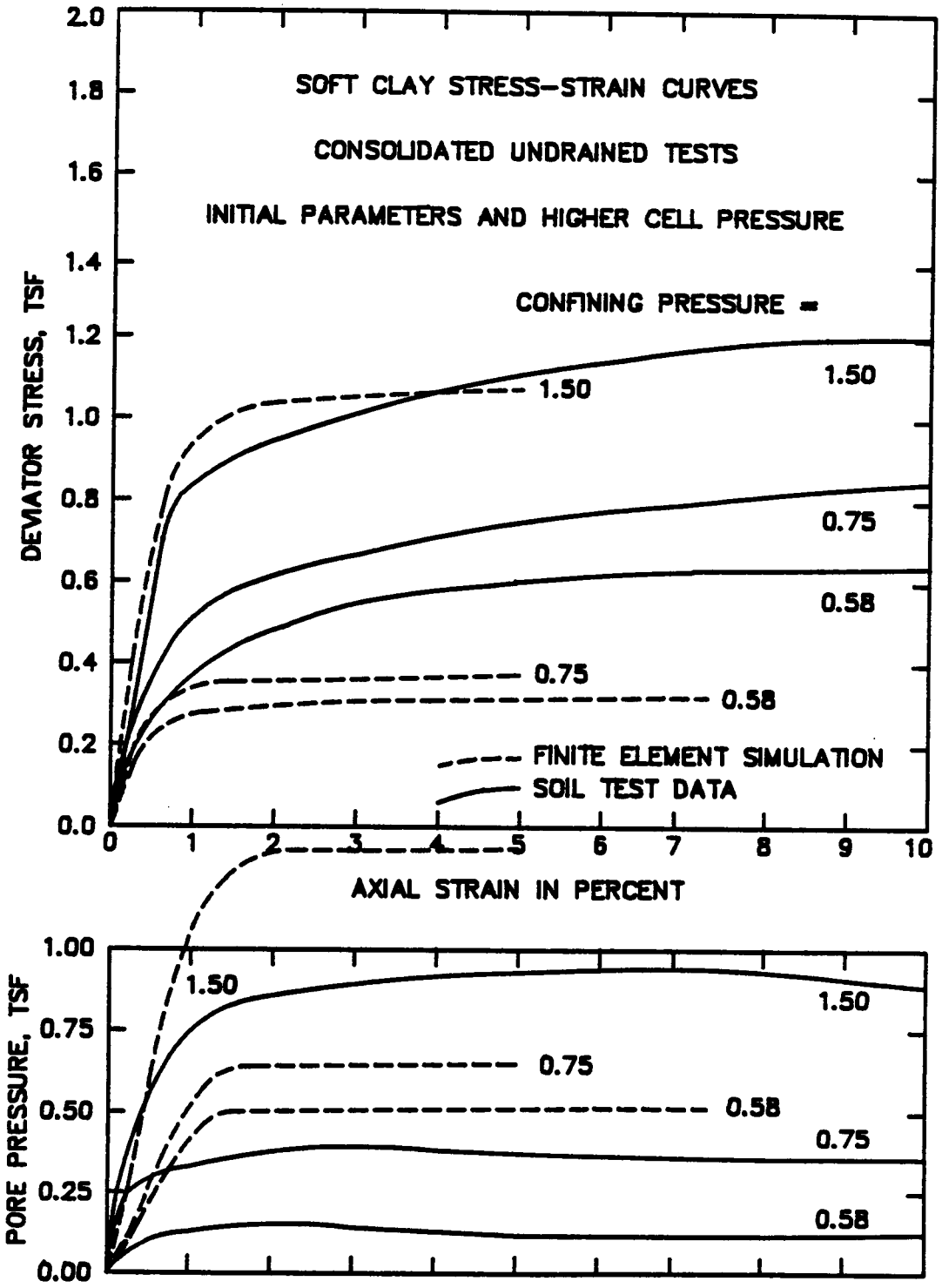

Figure 5.39 Comparison of calculated to measured stress-strain curves for foundation clay for higher cell pressure sample.

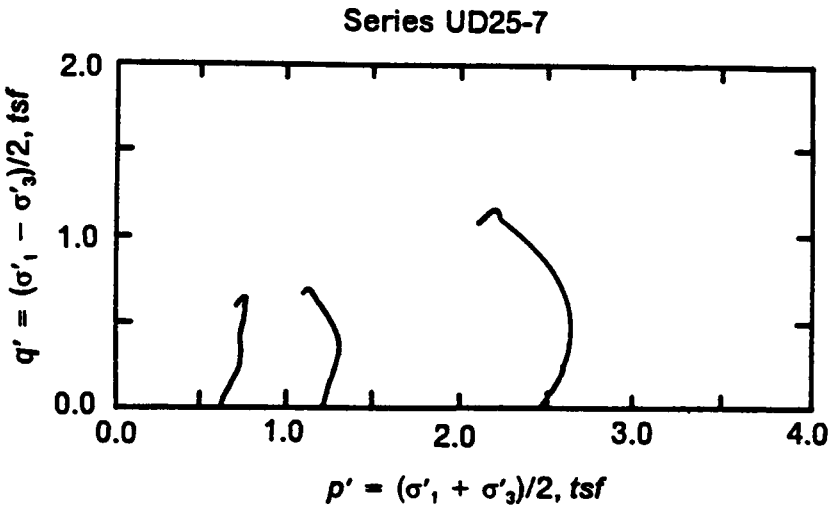

Figure 5.40 Stress paths for samples from test series UD25.

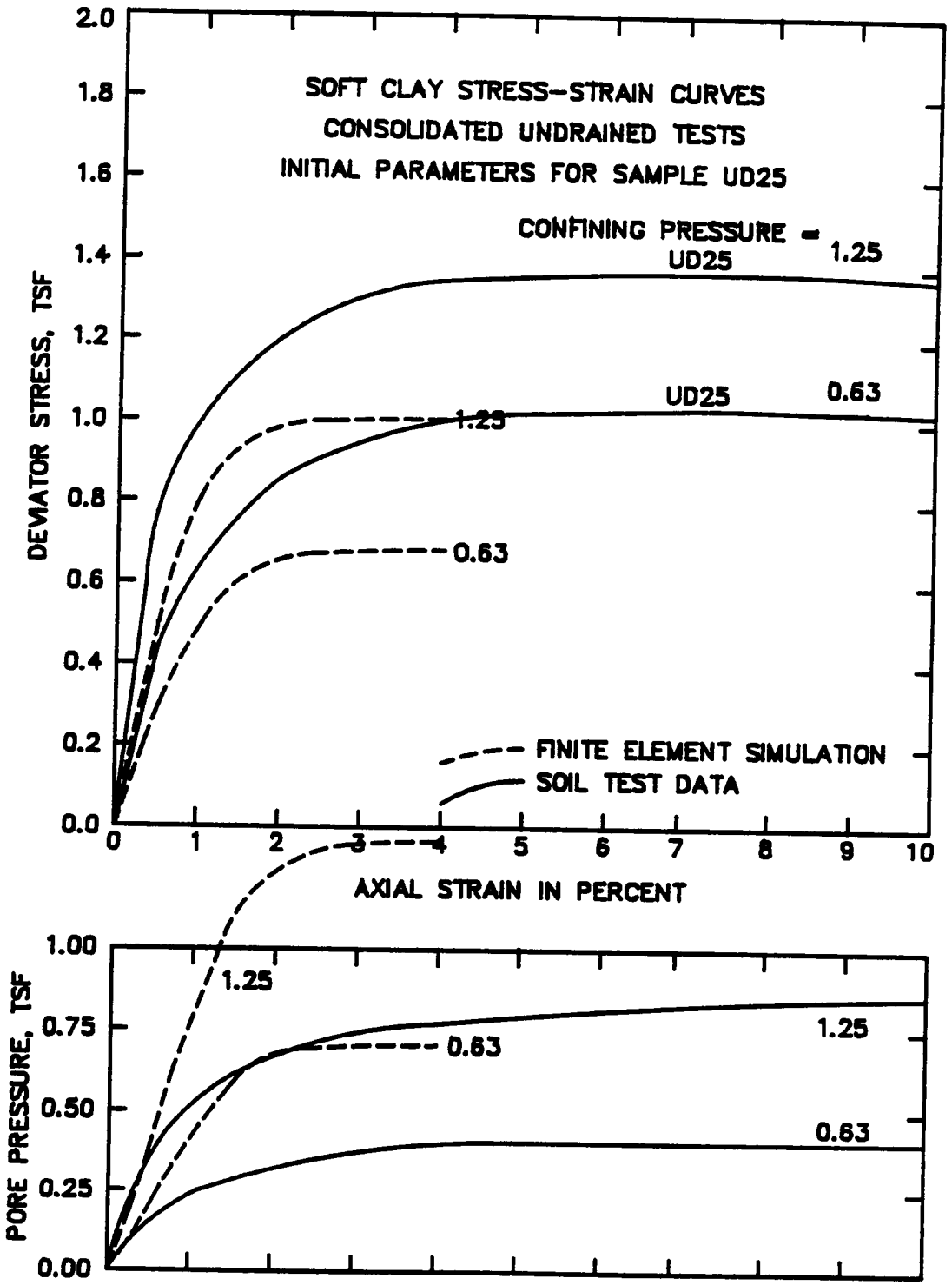

Figure 5.41 Comparison of calculated to measured stress-strain curves for foundation clay for sample UD25.

in Figure 5.42. A soil sample subjected to a confining pressure has an initial mean stress, $p' = \sigma_c$. As deviator stress is applied to the sample, the total stress path (TSP) follows curve A for triaxial conditions and curve B for plane strain conditions. The effective stress path (ESP) will follow the elliptical yield surface, the exact path to the failure surface being dependent upon the model parameters used in the calculations. The pore pressure generated will be the difference between the ESP and the TSP as shown in Figure 5.42. It is believed that the shape of the yield surface (cap) in the model leads to the large induced pore pressures and a different definition of the cap would be required to reduce the pore pressure response.

After concluding that it was not appropriate to attempt to match the triaxial pore pressures in plane strain calculations, the final parameters for the soft foundation clay were chosen based on these considerations: (1) a value of Poisson's ratio of 0.25, (2) a value of κ consistent with Poisson's ratio to reasonably match the first part of the stress-strain curves, and (3) values of M and p_r determined from strength values from sample UD22, since these values (φ' =29°, c'=0.03 tsf) are reasonably close to the "design" values of φ' = 28°, c'=0.09 tsf adopted by Collins et al. (1982) for the stability analyses. The results obtained are shown in Figure 5.43 and Table 5.3. Slightly steeper stress-strain curves than those measured for specimens from UD22 were used in consideration of the stiffer stress-strain response of samples from UD25.

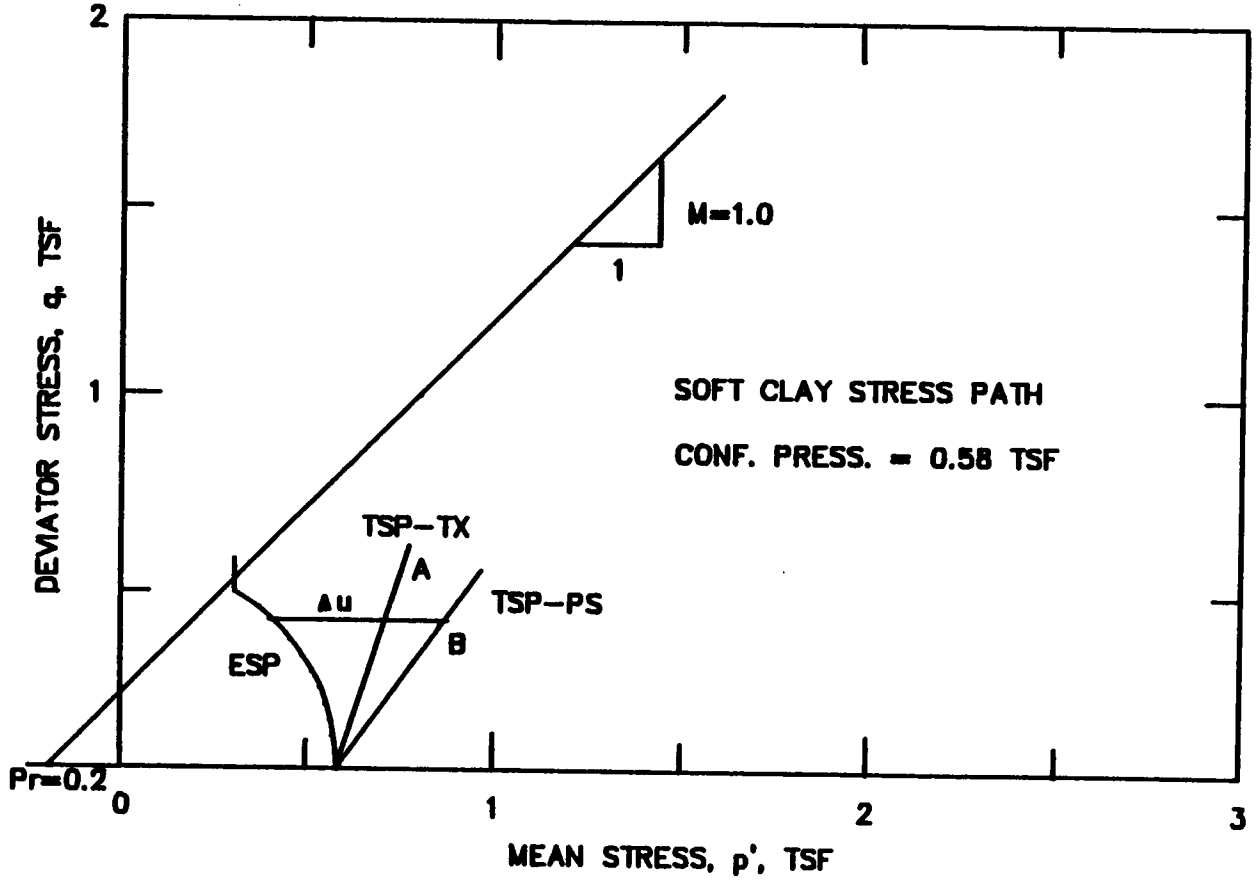

Figure 5.42 Stress paths followed in model used in analyses.

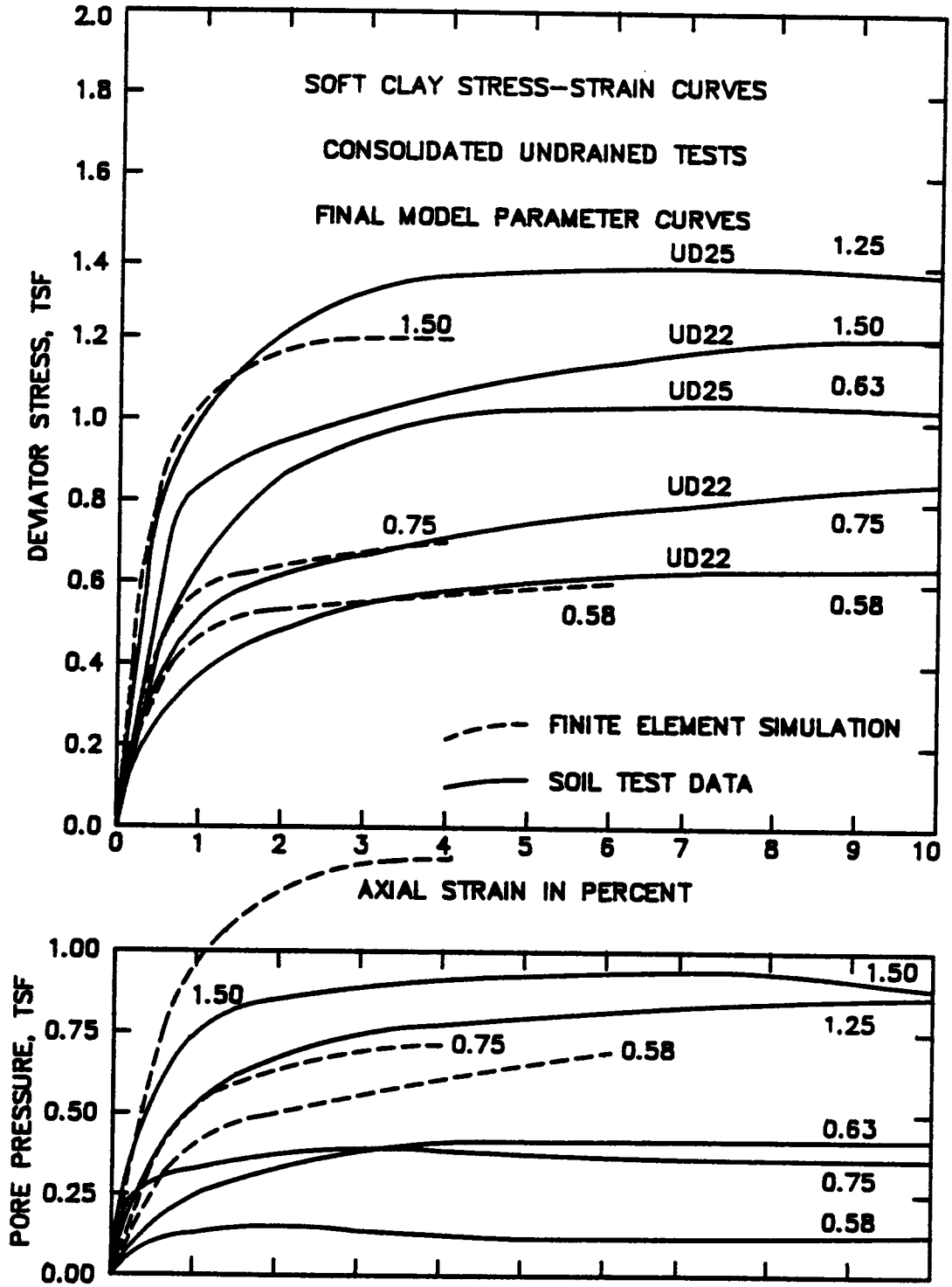

Figure 5.43 Comparison of calculated to measured stress-strain curves for foundation clay soil parameters used in analyses.

5.7.1.2 Peat

The selection of constitutive parameters for peats is difficult given their complex nature and the current state of knowledge of their behavior. The fibrous nature of peat materials gives them unique properties. The consolidation behavior of peats is much different than that of clays, and has been the subject of much recent research (Landva and La Rochelle, 1983; Dhowian and Edil, 1980; and Lefebrve et al. 1984). Secondary compression plays a significant role in the consolidation behavior of peats and thus classical one-dimensional consolidation theory is often not a good predictor of their behavior.

Data from triaxial compression tests on peats frequently show high friction angles, approaching 50° or more (Landva and La Rochelle, 1983; Edil and Dhowian, 1981; and Rowe et al. 1984). For an analysis of a geotextile reinforced embankment, Rowe et al. (1983) conducted triaxial compression, uniaxial tension, direct shear, and simple shear tests on a peat. The triaxial tests yielded values of $\varphi' = 54°$ and $c' = 0$, while the direct shear and simple shear tests gave values of $\varphi' = 27°$, $c' = 3$ kPa and $\varphi' = 26°$, $c' = 1.1$ kPa, respectively. In the finite element analyses performed using these test results, Rowe et al. found the agreement with measured embankment performance to be much better using parameters from simple shear and direct shear tests.

The permeability of peats, with their open structure, is dependent on the amount of mineral matter present in the peat, the degree of consolidation and the extent of decomposition (MacFarland, 1969). The re-

lationship of decreasing permeability with increasing consolidation pressure (load) has been discussed by Weber (1969), Lefebrve et al. (1984) and others. The relationship shown in Figure 5.9 has been adopted herein and the permeability of the peat was considered to be a function of overburden pressure corresponding to the line shown. Lefebrve et al. (1984) and Dohowian and Edil (1980) report substantial anisotropic permeability in peats, with the horizontal permeability often an order of magnitude greater than the vertical permeability.

Consolidated undrained tests on the foundation peat show much scatter. Interpretation of the data results in φ' values between 17° and 34° and c' values between 0 and 0.18 tsf. Two consolidated drained tests were performed on the peat giving φ' =11° and c'=0.14 tsf. In light of the scatter in the results, values of M=1.0 and p_r =0.15 tsf were selected, corresponding to φ' =25.4° and c'=0.07 tsf.

From the one-dimensional consolidation tests performed, values of λ ranging between 1.3 and 2.2 were determined. The smaller λ values correspond to the lower void ratios, e_0 about five, versus e_0 values of seven to nine for the higher values. A value of 1.3 was selected for the analyses. From the drained triaxial tests, values of Poisson's ratio were determined to be 0.115 and 0.23 at mean pressures of 0.40 tsf and 1.0 tsf respectively. Values of Poisson's ratio for peats in the range of 0.1 to 0.2 have been reported for peats (MacFarland, 1969 and Rowe et al. 1984). Based on preliminary analyses, a value of 0.25 was used, as in the WES analyses. Values of κ determined from the test results ranged from 0.13 to 0.26, with a value of 0.20 used in the analyses.

Comparisons of the computed and measured stress-strain and pore pressure behavior are shown in Figure 5.45. The agreement for the stress-strain curves is fair, while the agreement for the pore pressure curves is remarkably good.

5.7.1.3 Embankment Fill

Test data available for the embankment fill included four CU tests and an isotropic compression test. The CU data is summarized in Table 5.4, along with values of M and p_r calculated for each test. The four tests give very consistent values of φ' and c'. Interpretation of the isotropic compression test data shown in Figure 5.12 produced values of λ =0.052 and κ =0.0075. The data from CU test 85R-2 was used to evaluate Poisson's ratio, the resulting value being 0.30.

Using a value of M=1.29 and p_r=0.30 along with other parameters as described above, the computed stress-strain curve shown in Figure 5.45 was obtained, for a confining pressure of 0.50 tsf. The fit to the actual stress-strain data is very good for strains below three percent. The measured pore pressure response could not be simulated by the model; no attempt was made to achieve better agreement for the pore pressure data. In Figure 5.46 it may be seen (curve A) that the above parameters do not provide a good representation of the stress-strain behavior of the new fill. The curve shown as B in this figure was obtained by trial and has strength values of M=1.80 and p_r=0.30. A value of κ equal to 0.005 used to generate curve B, compared to a value of 0.0075 for curve A.

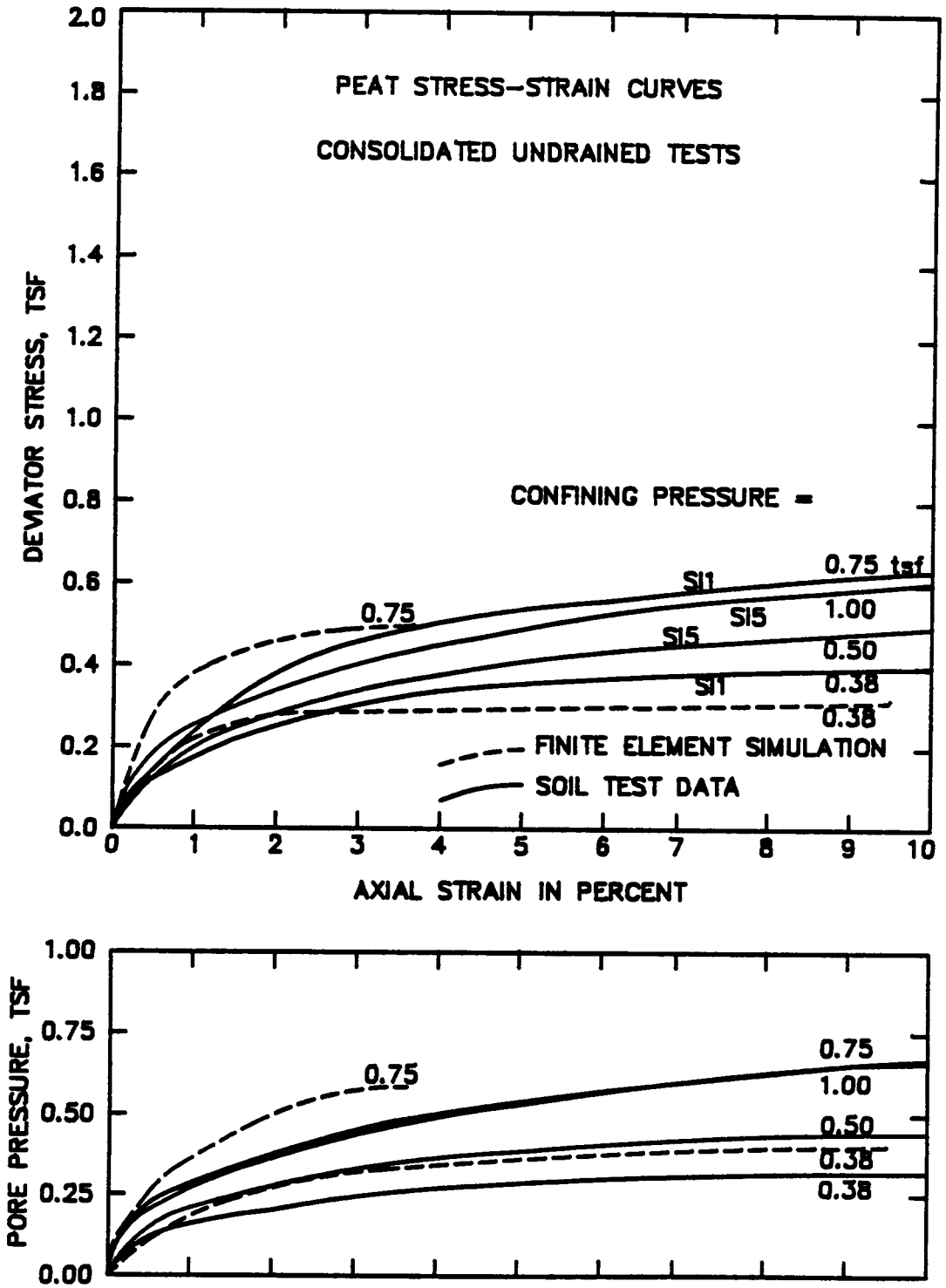

Figure 5.44 Comparison of calculted to measured stress-strain curves for peat soil parameters used in analyses.

Table 5.4 **Consolidated undrained tests on embankment fill.**

Tested by	ID	γ, pcf	w, %	LL	PI	ϕ'	c', tsf	M_γ	p_c, tsf
LETCO	UD21	114.9	15.6	27	10	32	0.09	1.29	0.14
WES	-	109.7	17.1	32	16	33	0.065	1.33	0.10
ORD	85R-1	120.2	14.3	29	16	30	0.10	1.20	0.17
ORD	85R-2	119.6	13.5	*	*	31	0.10	1.24	0.17

* - not determined

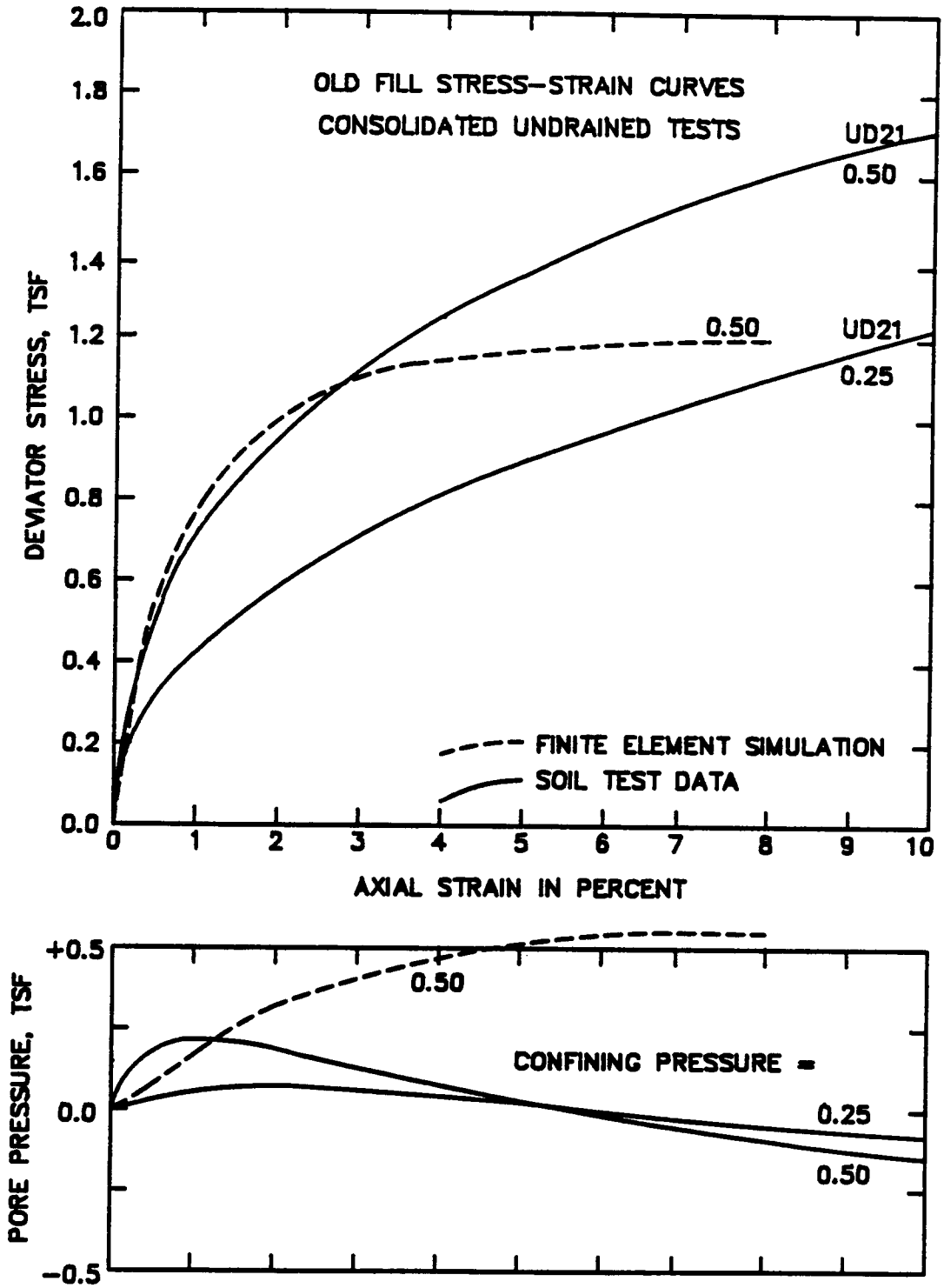

Figure 5.45 Comparison of calculated to measured stress-strain curves for old fill soil parameters used in analyses.

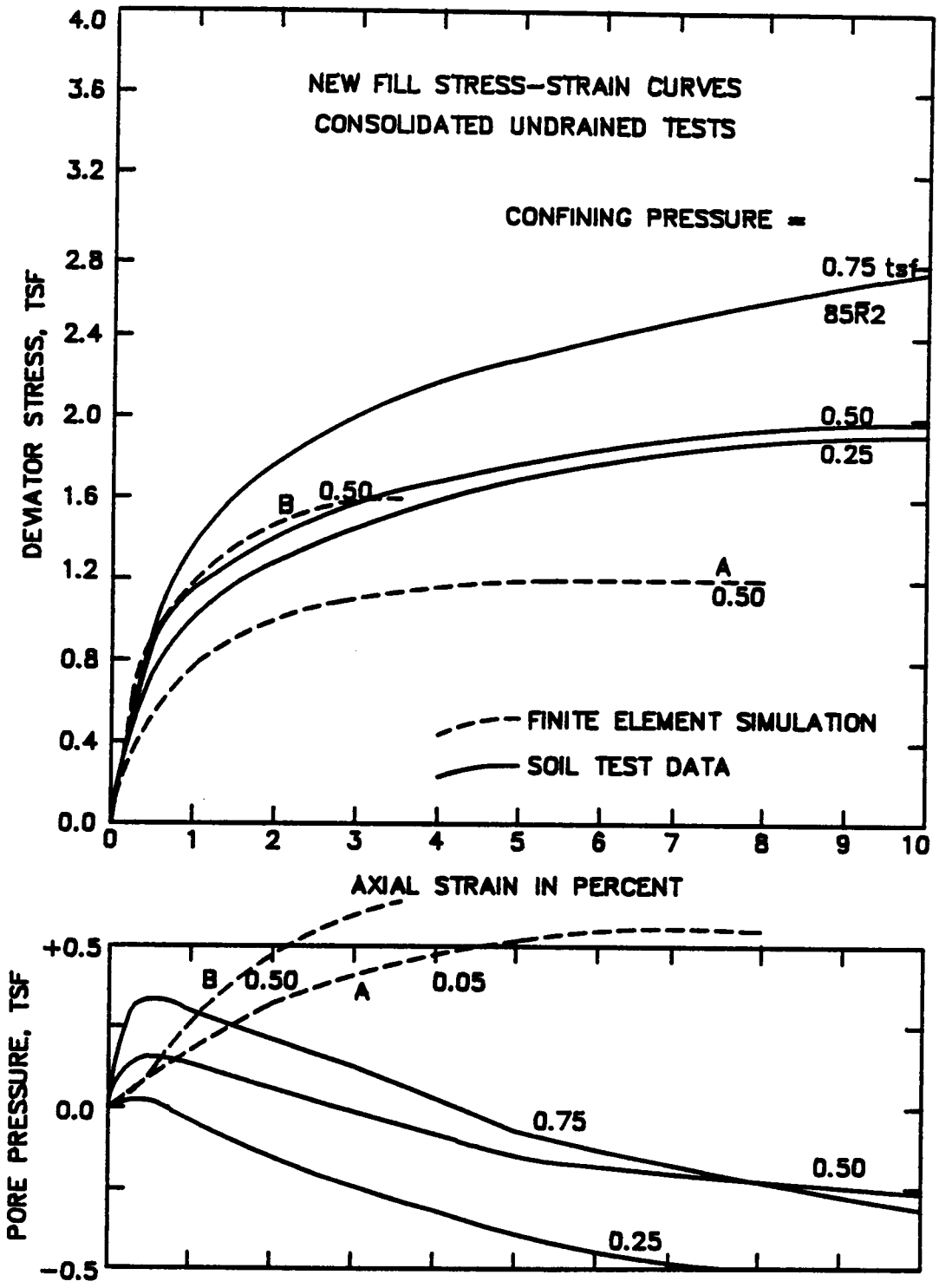

Figure 5.46 **Final stress-strain curves used for new embankment fill.**

5.7.1.4 Summary of Soil Model Parameters

The soil model parameters used in the analyses of the reinforced embankment are summarized in Table 5.5.

5.7.2 Analysis of Station 6+55

Station 6+55 is well suited for analysis because the foundation conditions are relatively well defined from the test boring program, and the 1930's failures did not impact this area. Additionally, because the soft clay is relatively deep in this location, and some of the highest reinforcement forces were measured in this area, analysis efforts were concentrated at this station. The foundation conditions shown in Figure 5.15 were reproduced in two half-section meshes representing conditions downstream and upstream of the centerline, as shown in Figures 5.47 and 5.48.

The analyses represented, as closely as possible, the actual construction sequence. Being a post-construction analysis, layer heights and dates of fill application were well known. The analyses began from an elevation of 962.5 feet to correspond to the elevation of fill when the strain gages were placed on the reinforcement. Initial stresses in the foundation were chosen to reflect overburden pressures at this time. The overburden pressures due to the old fill prior to its removal to elevation 960 feet were used as the preconsolidation stresses. Embankment construction was simulated in five construction layers and several con-

Table 5.5 Summary of soil model parameters used in analyses.

	Soft Clay	Peat	Old Fill	New Fill
M_T	1.16	1.0	1.29	1.80
p_r, tsf	0.20	0.15	0.30	0.30
κ	0.03	0.20	0.007	0.005
λ	0.07-0.20	1.3	0.04-0.05	0.04-0.05
ν	0.25	0.25	0.30	0.30

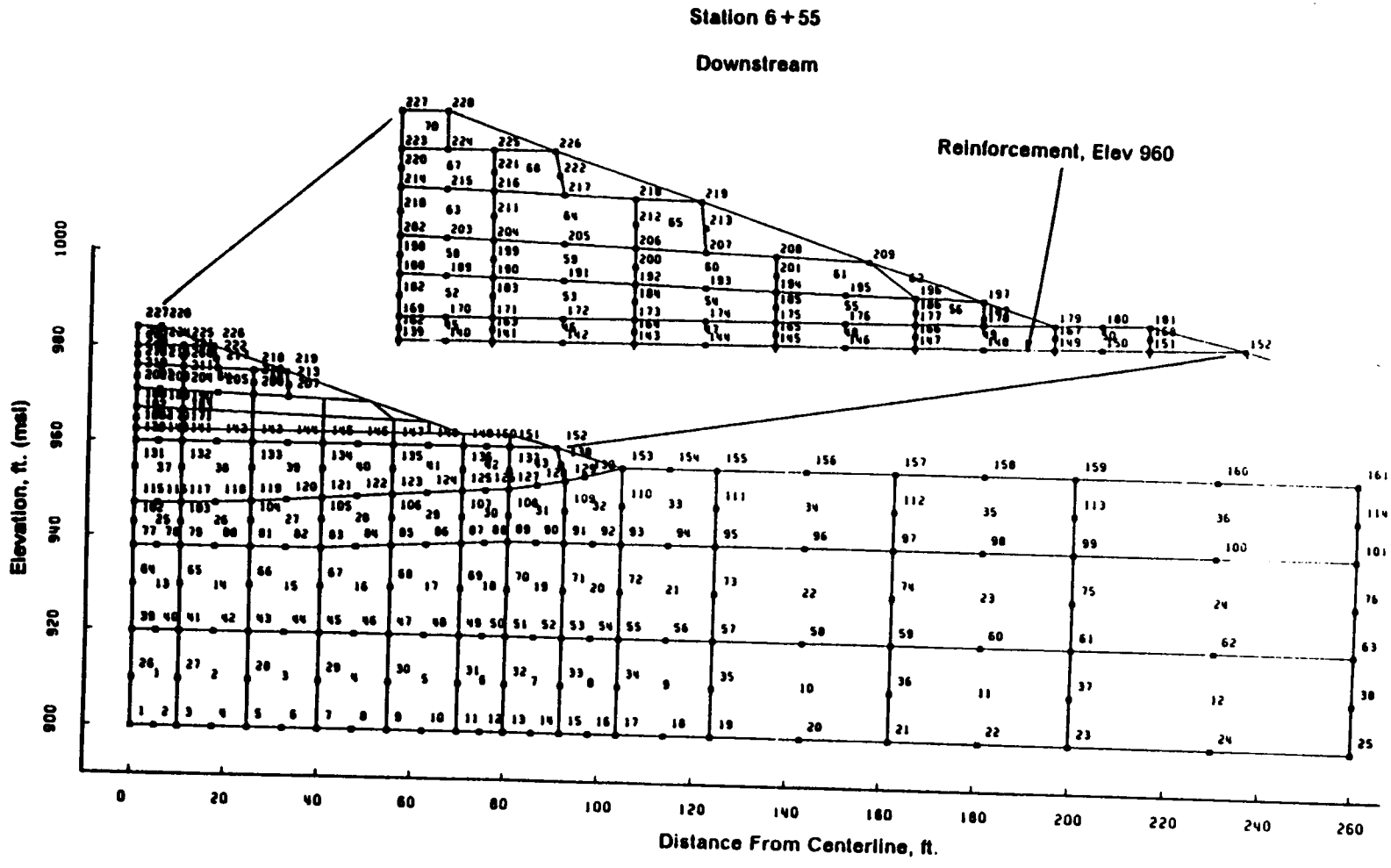

Figure 5.47 Finite element mesh used for analysis of downstream part of Station 6+55.

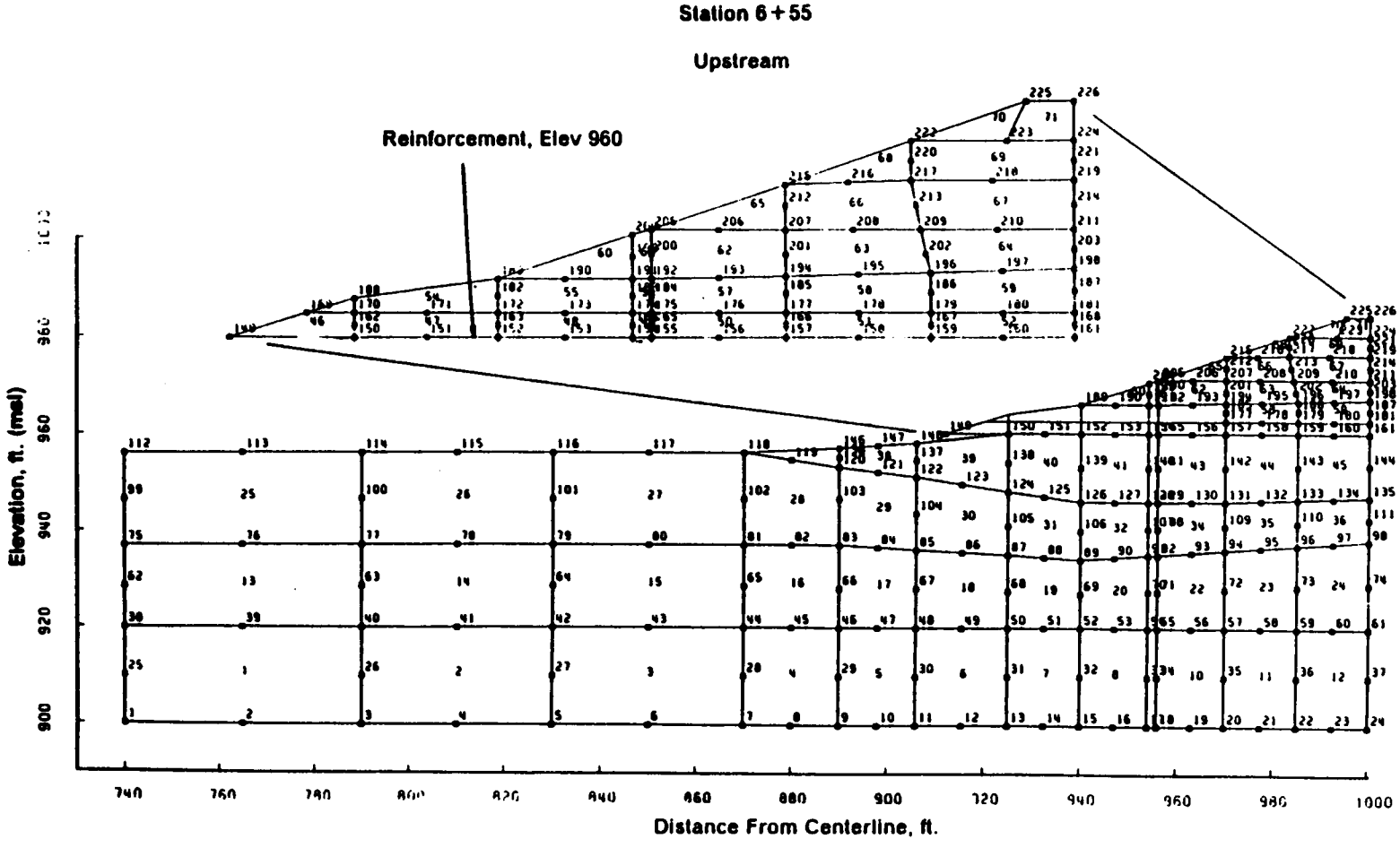

Figure 5.48 Finite element mesh used for analysis of upstream part of Station 6+55.

solidation periods. The first two layers raised the embankment height to 967.0 and 971.0 feet, over time periods corresponding to the actual time to reach these heights. A winter shutdown from November 1984 to June 1985 was simulated as a load case in which no new loads were added, but during which consolidation was allowed to occur. The final three layers were added to elevations 976.0, 980.0 and 984.0 feet. Consolidation was modelled after construction for periods of one and three years, to a total time after construction of four years.

Reinforcement forces computed at the reinforcement centerline are shown in Figure 5.49, together with the measured values from the field instrumentation. Values measured at Stations 6+55 and 8+00 are shown, because Station 8+00 experienced the highest measured values. The calculated values are in very good agreement with those measured during the first construction season. The calculated reduction in force during the winter shut down (due to consolidation of the foundation soils) is considerably greater than the amount that actually occurred. Subsequent to the winter shutdown, the calculated rate of increase in force was greater than that measured. As explained previously, it is believed that the smaller rate of increase in reinforcement force after the winter shutdown is due to an increase in stiffness of the fill that resulted from ageing during the shutdown period. This effect was represented in additional analyses to be discussed later.

One aspect of the interaction between the reinforcing and the embankment was not modeled by the analyses. It may be noted that during a pause during the second construction season, the reinforcing force in-

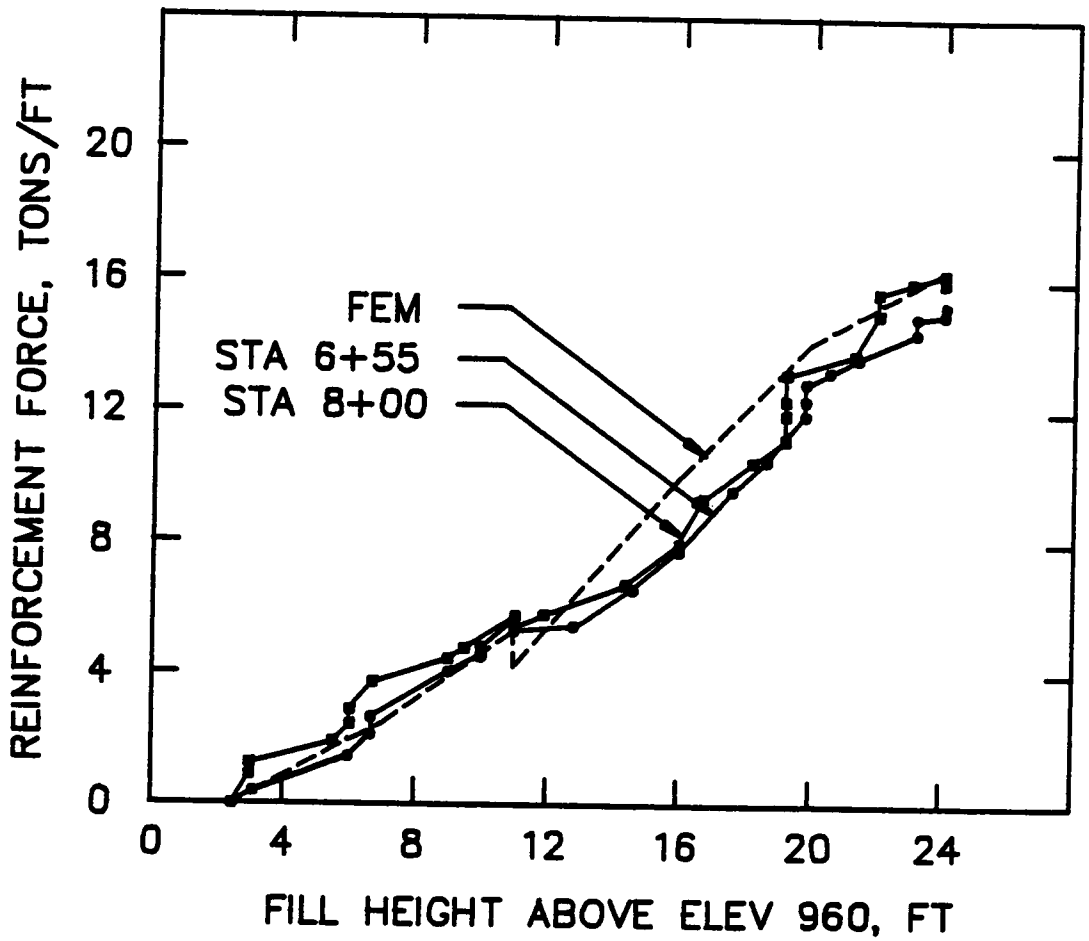

Figure 5.49 Measured versus calculated reinforcement forces at the centerline of Station 6+55.

creased. As mentioned previously, it is believed that this increase in force is due to undrained creep in the foundation peat and clay. A similar increase near the end of construction is also believed to be due to creep effects. Because the modified Cam Clay model used in the analyses does not simulate creep effects, the finite element analyses do not simulate this aspect of the actual behavior. The field data indicate that after a period of three or four weeks the effects of creep die out, and the reinforcing force begins to decrease as the foundation soils consolidate.

Calculated distributions of reinforcing force across the embankment are compared to the measured values in Figure 5.50. The calculated distributions are discontinuous at the centerline because they were calculate using two half-meshes rather than a whole mesh. It can be seen that the agreement is quite good overall, especially for the downstream half of the embankment. The behavior of the upstream half of the embankment was apparently affected to some degree by the slurry trench cutoff. Because the cutoff was represented in the analyses by only one element's width, its interaction with the foundation and the embankment, and its effect on the behavior, may not have been accurately reflected in the calculated results.

Calculated pore pressures are compared to the measured values in Figures 5.51 and 5.52. The calculated values are smaller than the measured values at the early stages, and larger than the measured values at the later stages. These differences appear to be consistent with the differences between the calculated and measured laboratory pore pressures

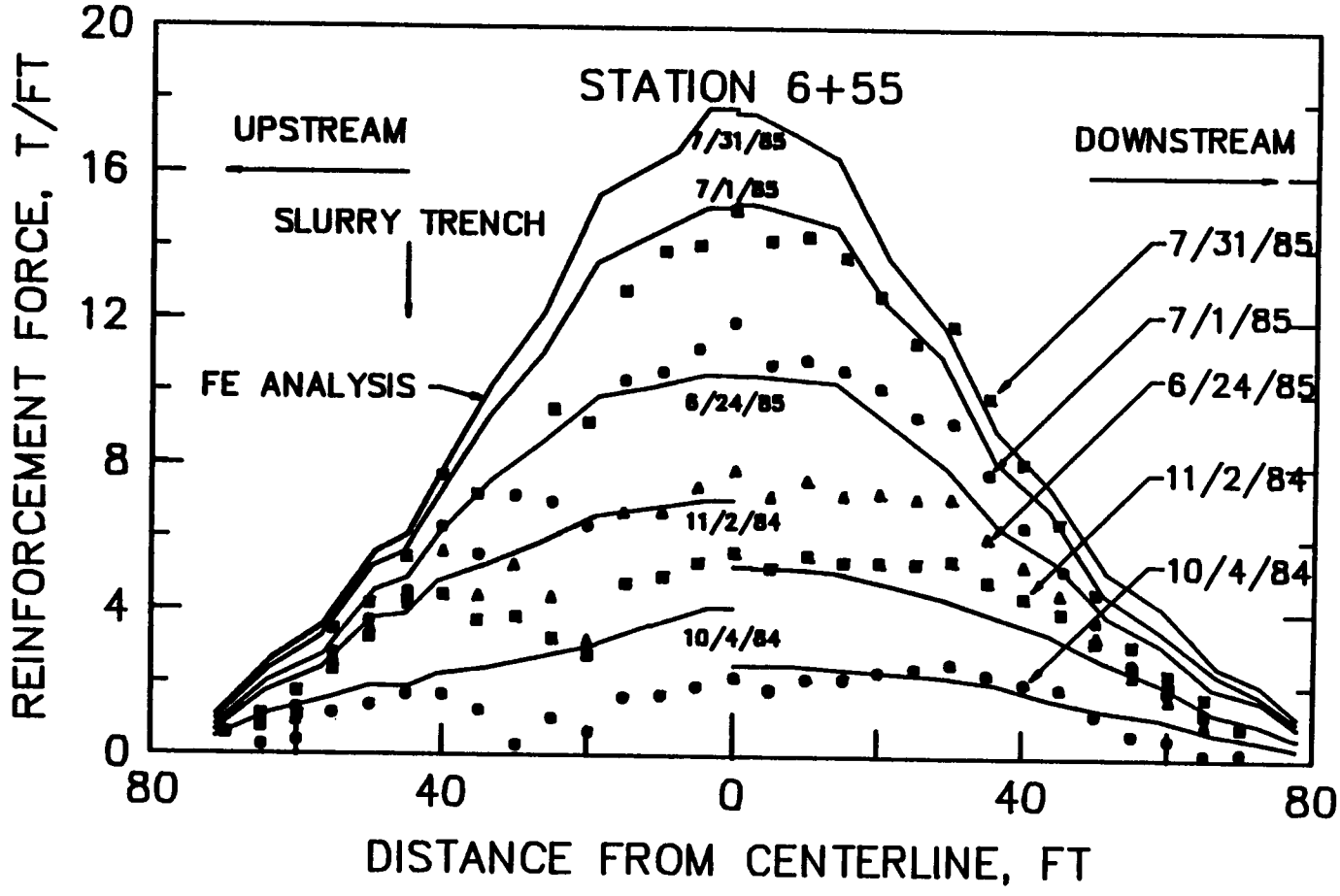

Figure 5.50 Measured versus calculated reinforcement forces distributed about the centerline at Station 6+55.

discussed previously. The calculated amounts of decrease in pore pressure during shutdown periods and after construction are in good agreement with those measured, indicating that the consolidation characteristics of the foundation soils are reasonably accurately represented in the analyses.

The calculated settlements are compared to those measured in Figure 5.53. The agreement is not good at the early stages. As noted previously, the settlements at this time were affected quite considerably by the variations in preconsolidation pressure from upstream to downstream, and this detail of the initial conditions was not represented in the finite element analyses. The settlements that occurred during the second construction season are in better agreement with the calculated values near the centerline. The settlements that occurred after construction were considerably greater than those calculated.

Calculated horizontal movements are compared to those measured near the toes of the embankment in Figure 5.54. The calculated variations of horizontal movement with depth are much more uniform than the measured values. As mentioned previously, much of the measured lateral movement was due to deformations of the soils between elevations 915 and 930, indicating existence of a soft or weak zone in this area. The fact that such a weak zone was not represented in the finite element analyses is probably responsible for the differences between the measured and the calculated horizontal movements.

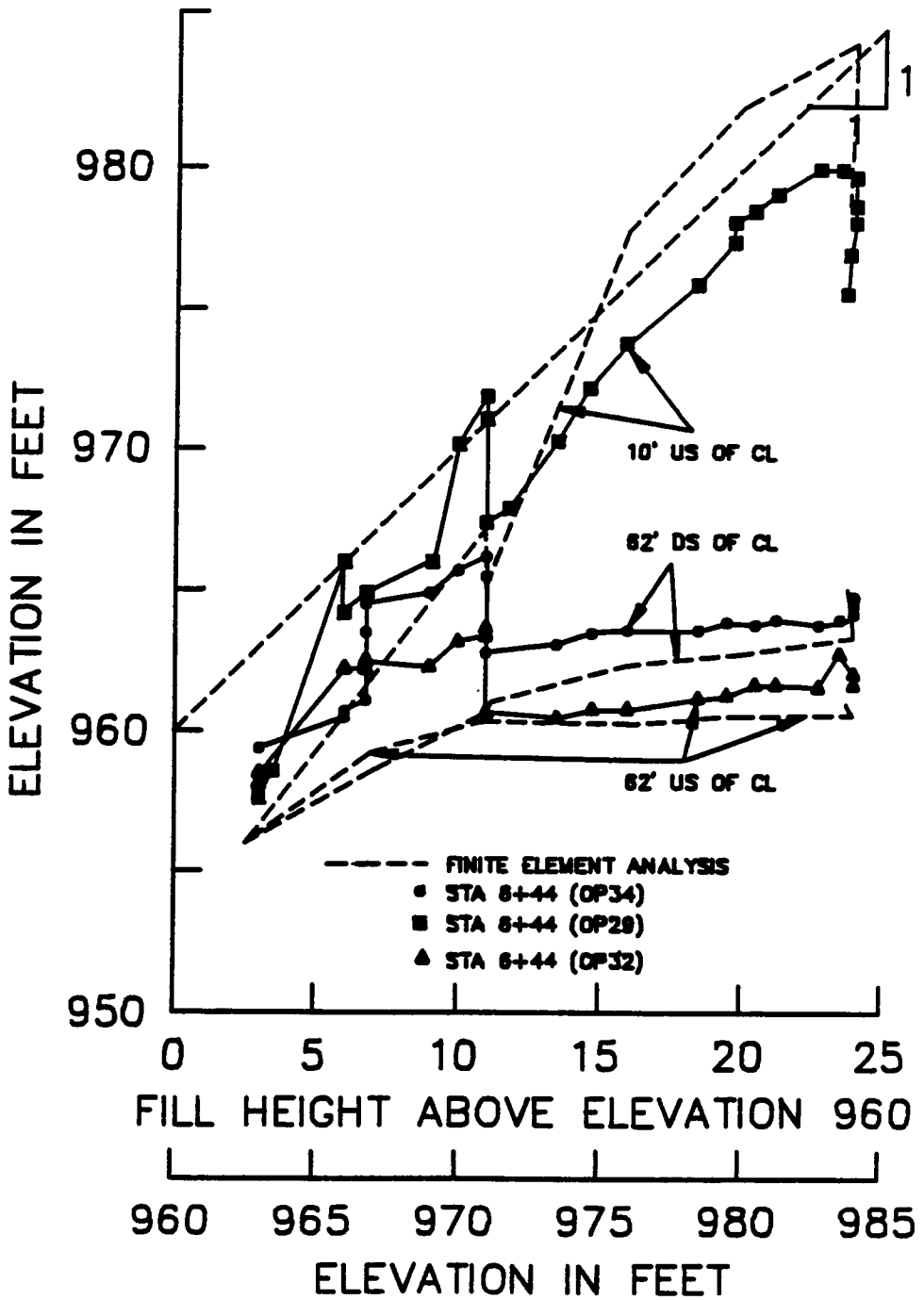

Figure 5.51 Measured versus calculated piezometric levels in the peat - Station 6+55.

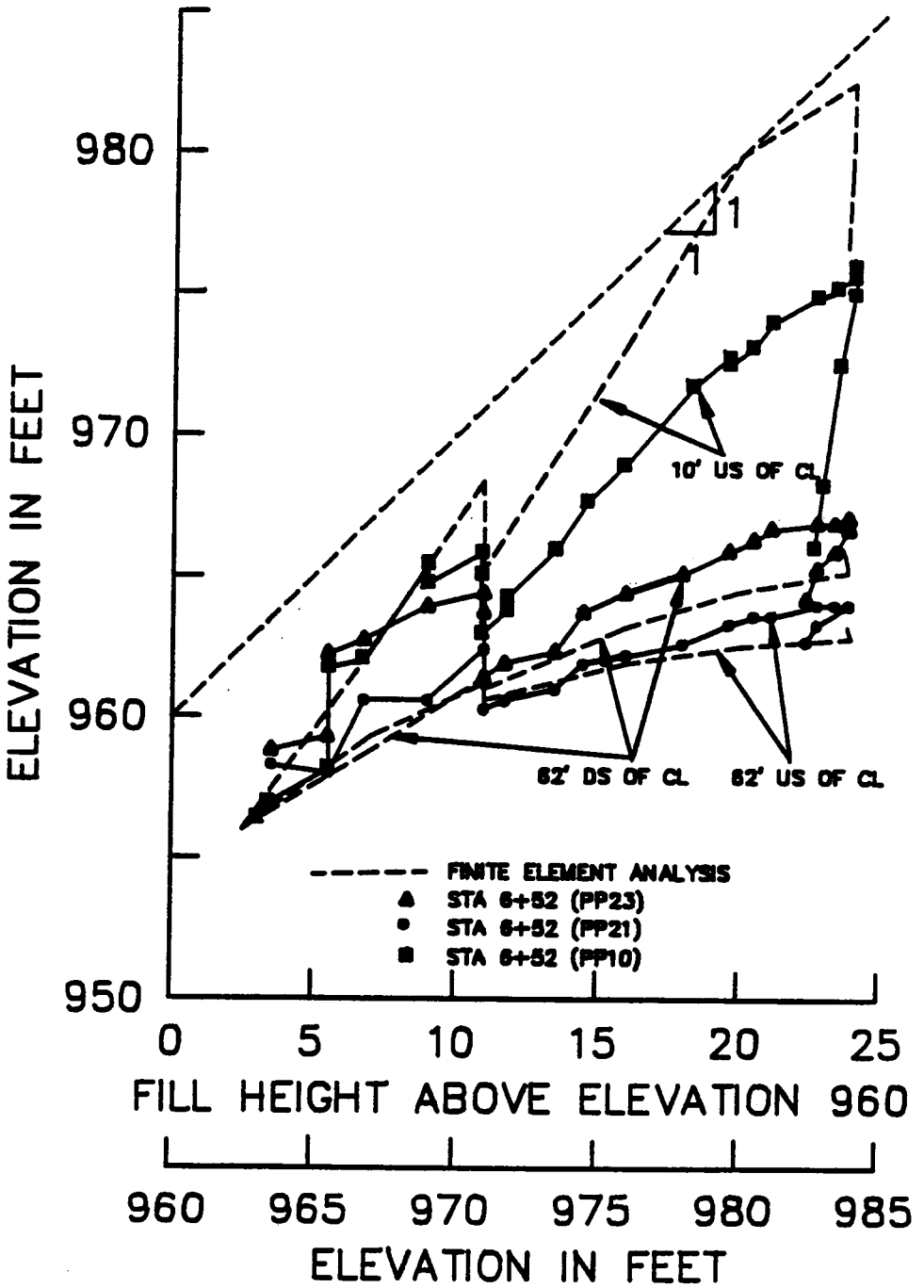

Figure 5.52 Measured versus calculated piezometric levels in the foundation clay - Station 6+55.

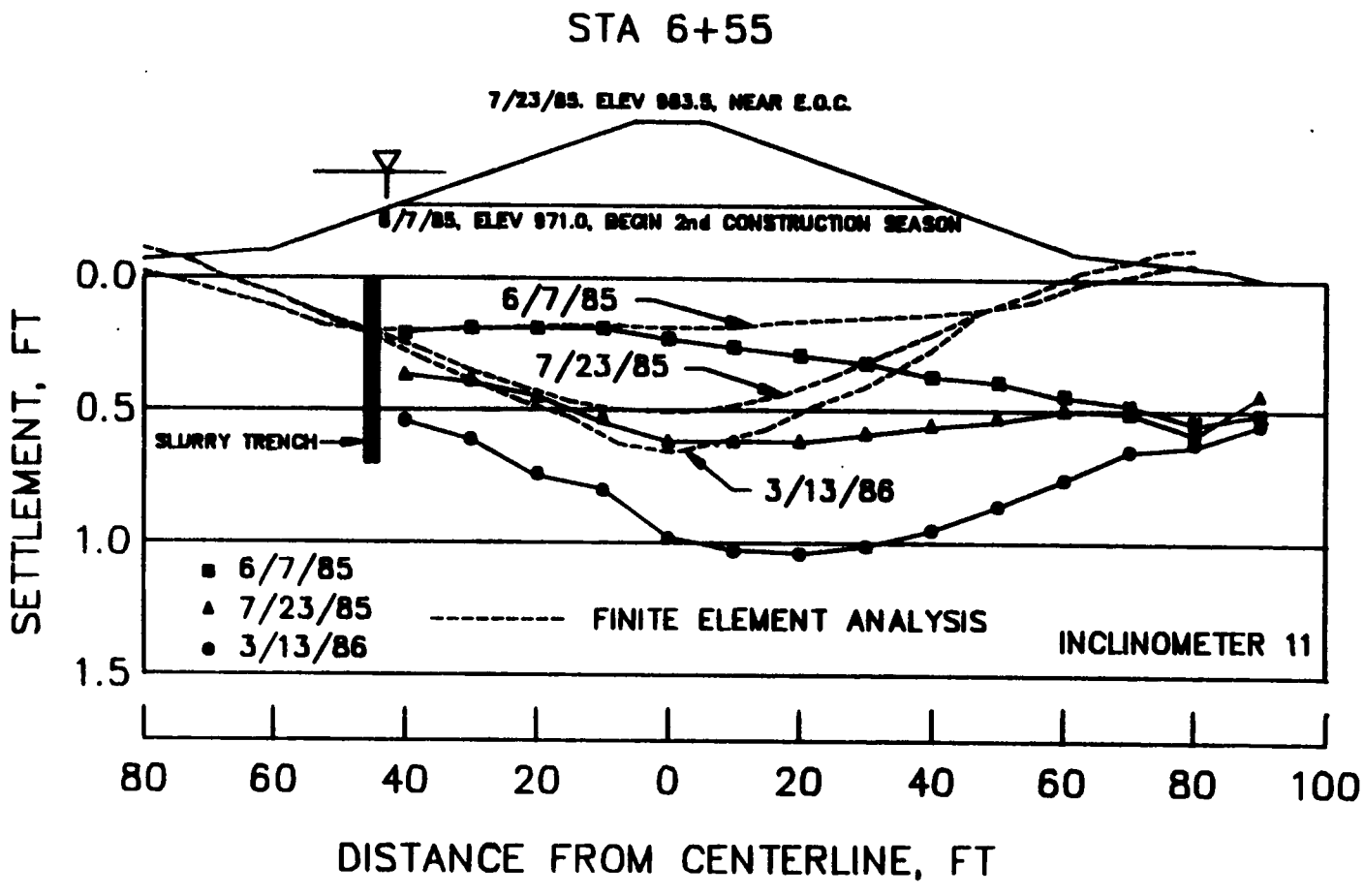

Figure 5.53 Measured versus calculated settlement - Station 6+55.

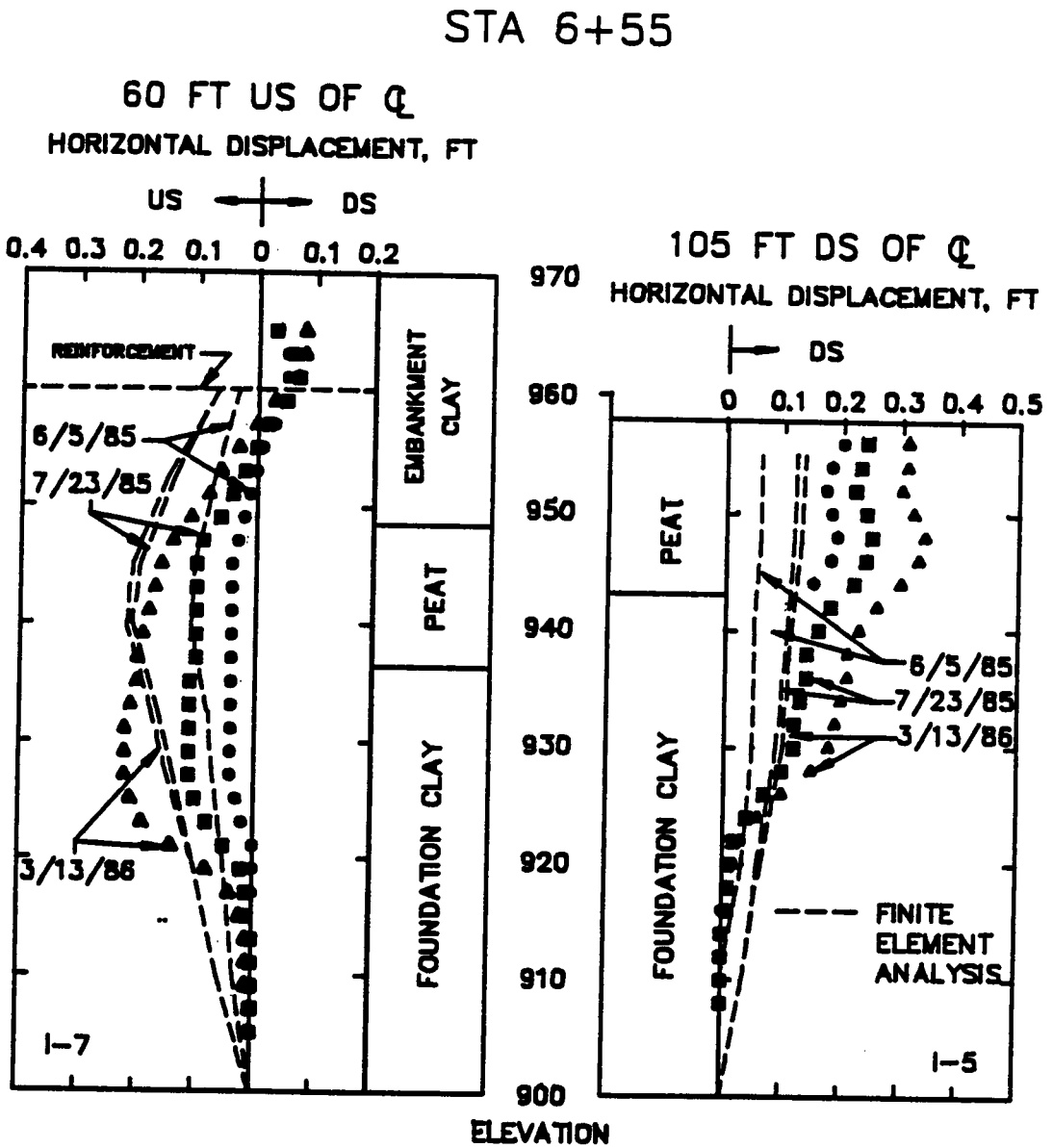

Figure 5.54 Measured versus calculated horizontal movements - Station 6+55.

5.7.3 Analyses of Station 9+00

The two layers of reinforcing placed at Station 9+00 provide an opportunity to evaluate the analytical method when applied to multilayer reinforcement. The foundation conditions at Station 9+00 are shown in Figure 5.16, and the effects of the previous failures in the upstream area are evident. No attempt to model the upstream part was made owing to its complexity. The downstream portion was analyzed using the mesh shown in Figure 5.55.

Calculated and measured reinforcement forces at the centerline are shown in Figure 5.56. Between points A and B in Figure 5.56, which covers the period from August to November, 1984, the calculated results overpredict the measured forces by a considerable amount and this trend continues between points B and C, representing the first month of the second construction season. At point C, a considerable increase in reinforcement force occurred during nine-day work shutdown in July. As mentioned previously, this is attributed to creep in the foundation soils and was not modelled in the analysis. It can be seen that the calculated and measured values agree well in two respects: One is the decrease in reinforcing force during the shutdown period (point B), and during the period following construction (point D). The second is the tendency for the upper layer of reinforcing to be less effective than the lower layer, and for the force in the upper layer to decrease at a faster rate than that in the lower layer.

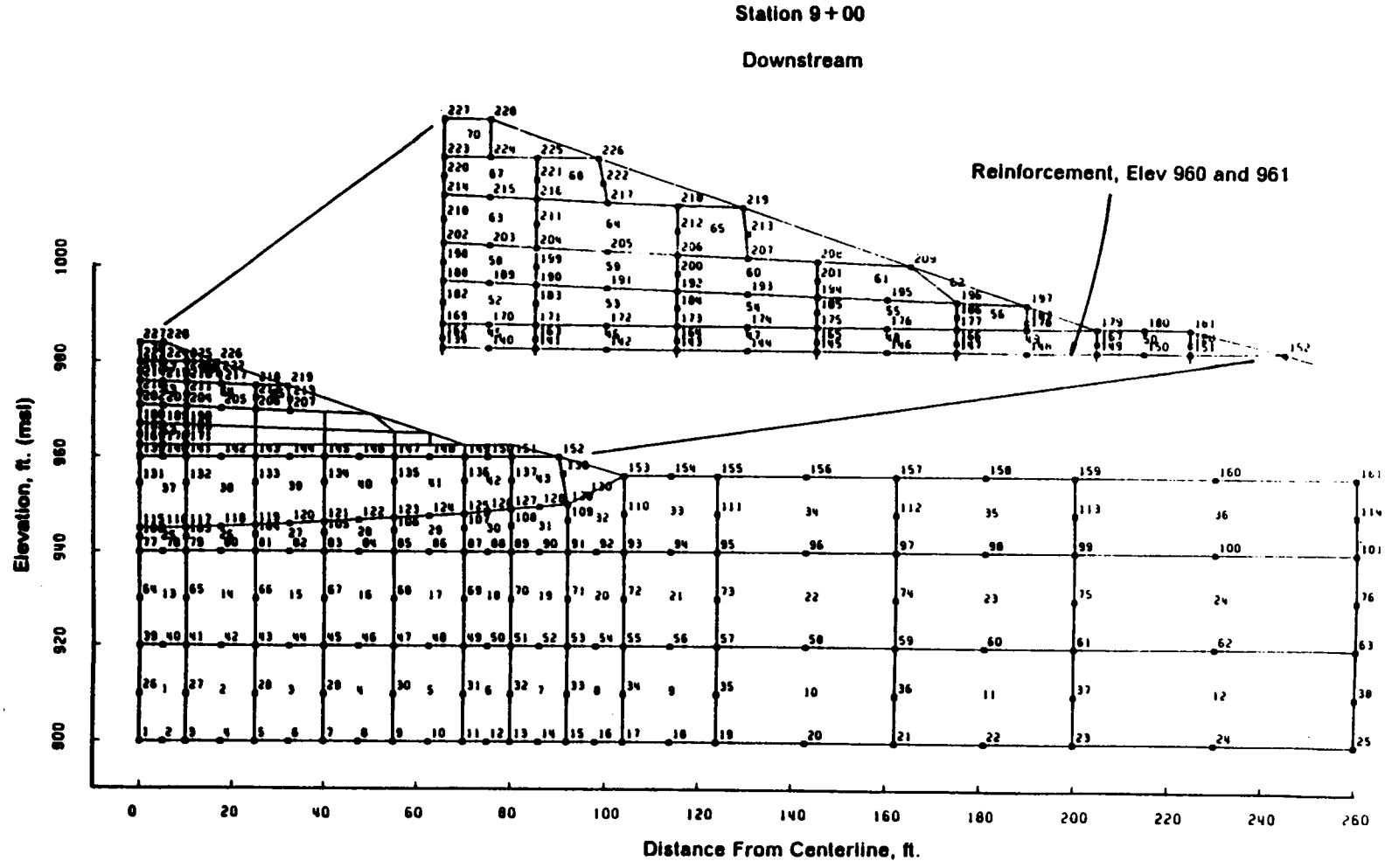

Figure 5.55 Finite element mesh used for analysis of downstream part of Station 9+00.

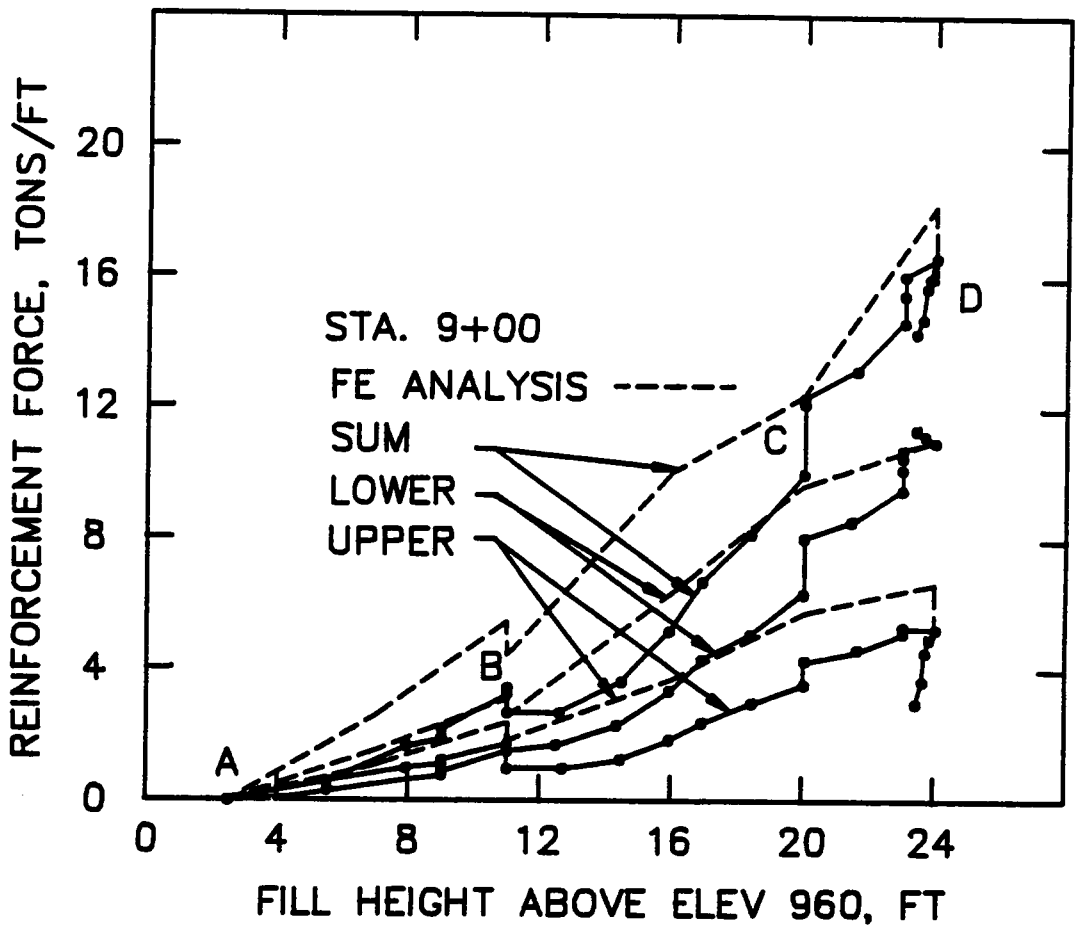

Figure 5.56 Measured versus calculated reinforcement forces at the centerline - Station 9+00.

A comparison of measured and calculted piezometric levels is shown in Figure 5.57. It can be seen that the piezometric levels in the peat are modelled reasonable well during the first construction seaon. However, the response in the peat during the second construction season is considerably overpredicted. The drainage conditions in the peat are probably quite complex given the past failures in this area and were probably not accurately depicted in the analysis despite the modification of the program to reflect the variation in peat permeability with load.

The piezometric levels in the clay were severly underpredicted by the analysis. As mentioned previously, the piezometric levels near Station 9+00 were much higher than meaured at other stations and may be a result of higher shear stresses in the clay from the past failures. Indeed, the initial piezometric level in the upper clay was some six to eight feet higher than comparable locations at other stations.

Measured and calculated settlements are shown in Figure 5.58. The calculated values are much higher than those measured. The difference may be tied to the predicted piezometric response of the peat. If the calculated piezometic level in the peat were dissipated to the measured value, more displacement in the peat would be calculated. The pattern of settlement shown appears to indicate that the analysis underpredicted the settlement due to consolidation during the winter shutdown and following the end of construction.

The horizontal movements were also underpredicted by the analysis.

The results of the analysis of Station 9+00 conditions are not as good as those for Station 6+55, but none-the-less are encouraging. Despite

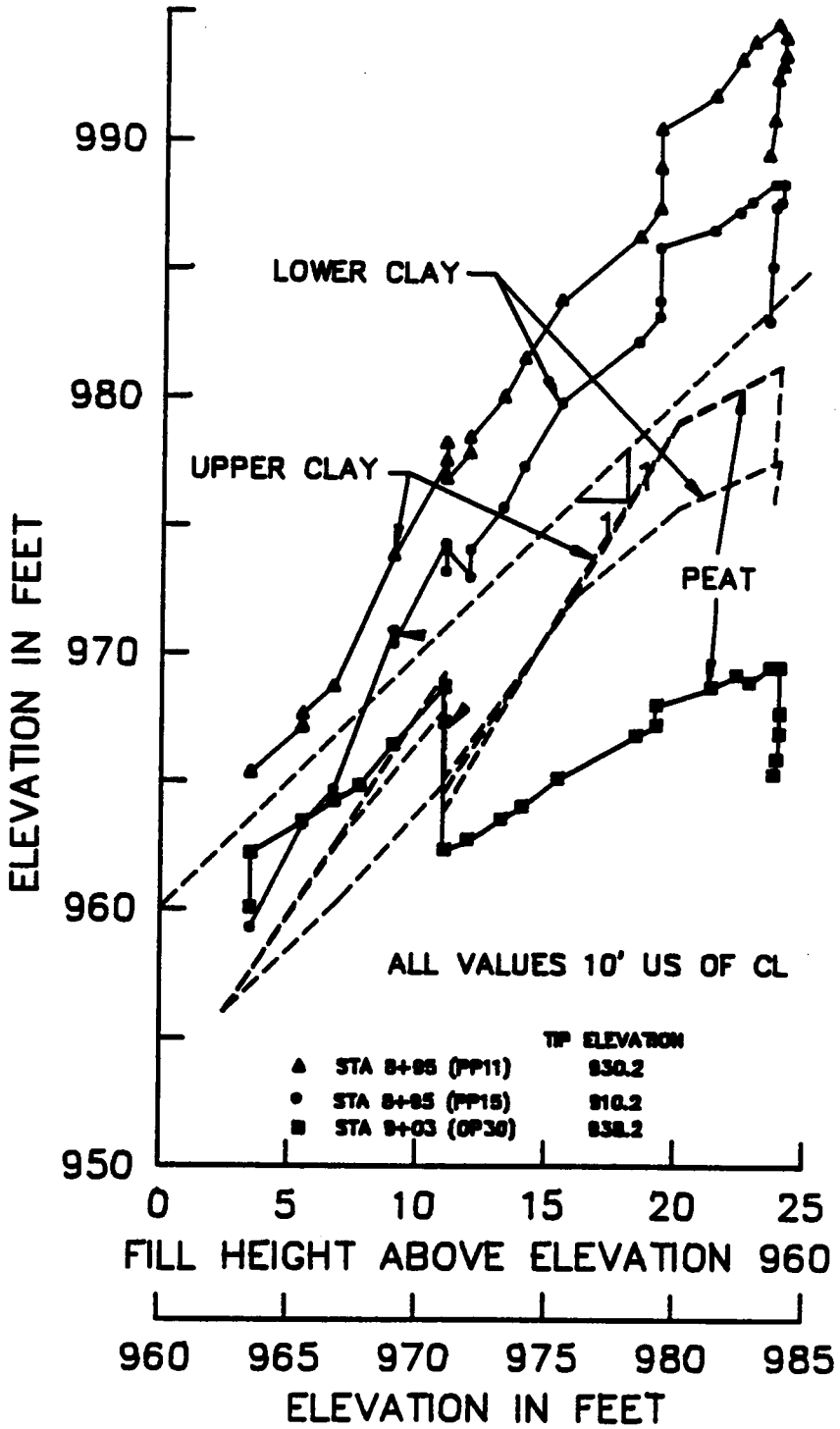

Figure 5.57 **Measured versus calculated piezometric levels - Station 9+00.**

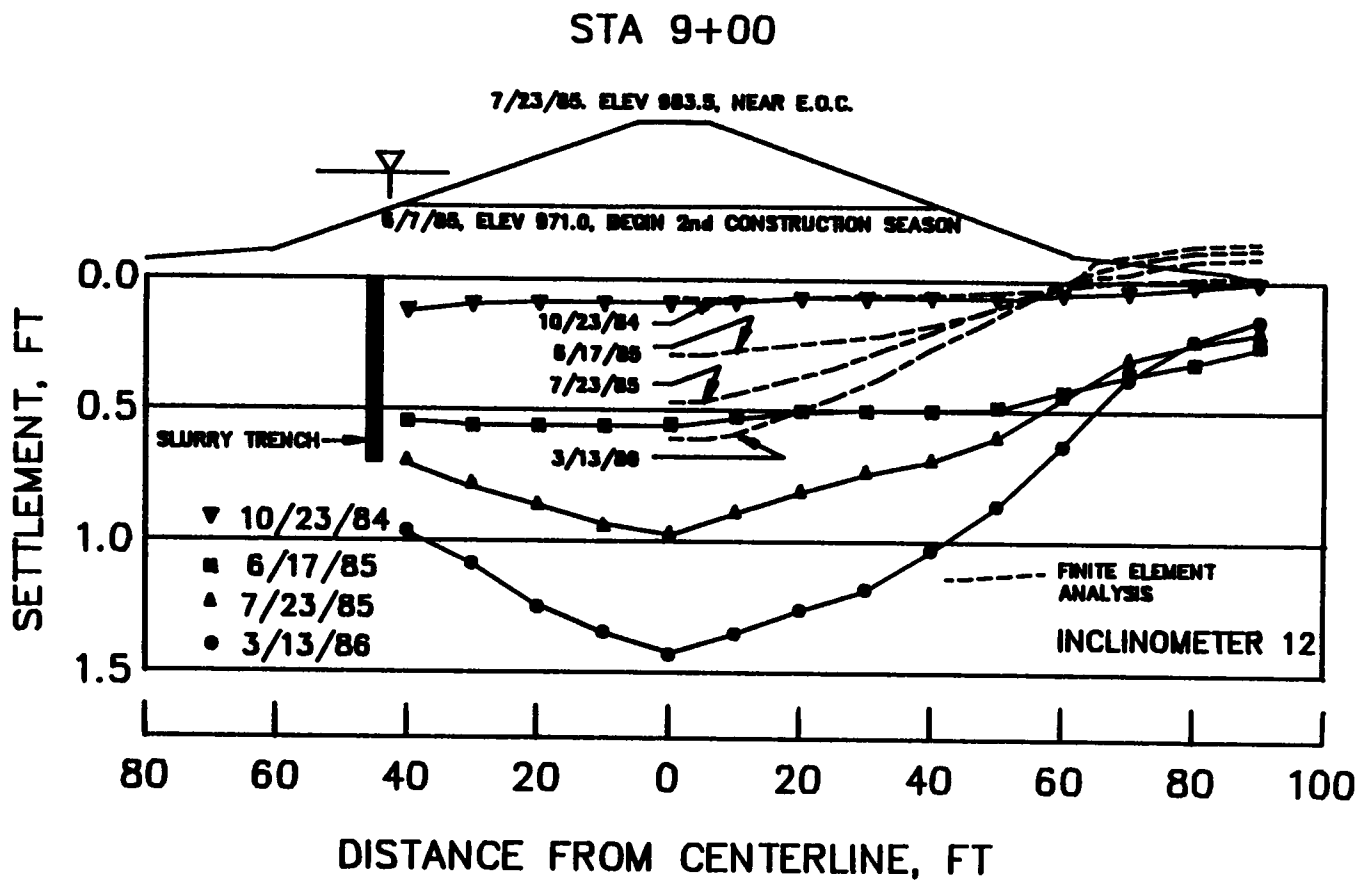

Figure 5.58 Measured versus calculated settlement at Station 9+00.

extreme simplification of complex soil conditions, the analysis reflected similar trends as the measured data. In particular, the fraction of the total reinforcement force carried by each layer was modelled well providing encouragement for the use of finite element techniques for multi-layered reinforced systems.

5.8 Study of Ageing Effects on Compacted Clay

When construction resumed in the spring of 1985, the rate of increase of load pickup in the reinforcement was smaller than it had been during the previous fall. This phenomenon was further highlighted when the finite element analysis showed that a greater rate of load increase would be expected. In attempting to explain this phenomenon, the possibility that the fill stiffened with time was hypothesized. This section will discuss the effects of ageing on the properties compacted soils, and discuss a laboratory test program conducted to measure these effects for the Mohicanville Dike No. 2 fill.

Previous studies of ageing effects on the strength and stiffness of compacted soils have been performed by Seed and Chan (1957), Trollope and Chan (1960), Seed, Mitchell and Chan (1960) and Casagrande, Hirschfeld and Poulos (1963). These studies showed that an increase in stiffness and strength of compacted clays can occur with time after compaction. The changes in behavior are often attributed to thixotropic effects, whereby property changes occur with time due to such factors as changes

in particle arrangement, changes in adsorbed water structure, and changes in distributions of ions in the fluid phase (Mitchell, 1960).

The increase in stiffness and strength that has been observed is illustrated in Figures 5.59 and 5.60. Figure 5.59 shows the increase in strength that occurred in a sample of Vicksburg silty clay which was aged for two weeks. An increase in the initial stiffness is also noted. A similar pattern may be noted for the two clays shown in Figure 5.60. Using 15 percent strain as a reference, the increase in strength for the Vicksburg silty clay shown in Figure 5.59 is 29 percent after two weeks ageing, for the Vicksburg silty clay in Figure 5.60 the strength increase is 21 percent after 37 days ageing, and for the San Francisco Bay Mud shown in Figure 5.60 the strength increase is 27 percent after seven days ageing. The increase in initial stiffness due to ageing is apparent from the stress-strain curves. A striking feature of the stress-strain curves shown is how the aged and immediate curves parallel one another above axial strains of about 2 percent.

Casagrande, Hirschfeld and Poulos (1963) conducted triaxial compression tests on samples of field compacted clay from three earth dams. The time after initial field compaction varied from three months to 20 years. The results from these tests were compared to results from tests conducted on the same material remolded and recompacted to similar density and water contents. Both strength and stiffness were compared, with the stiffness being taken as the secant modulus at 50percent (M_{50}) of the ultimate strength.

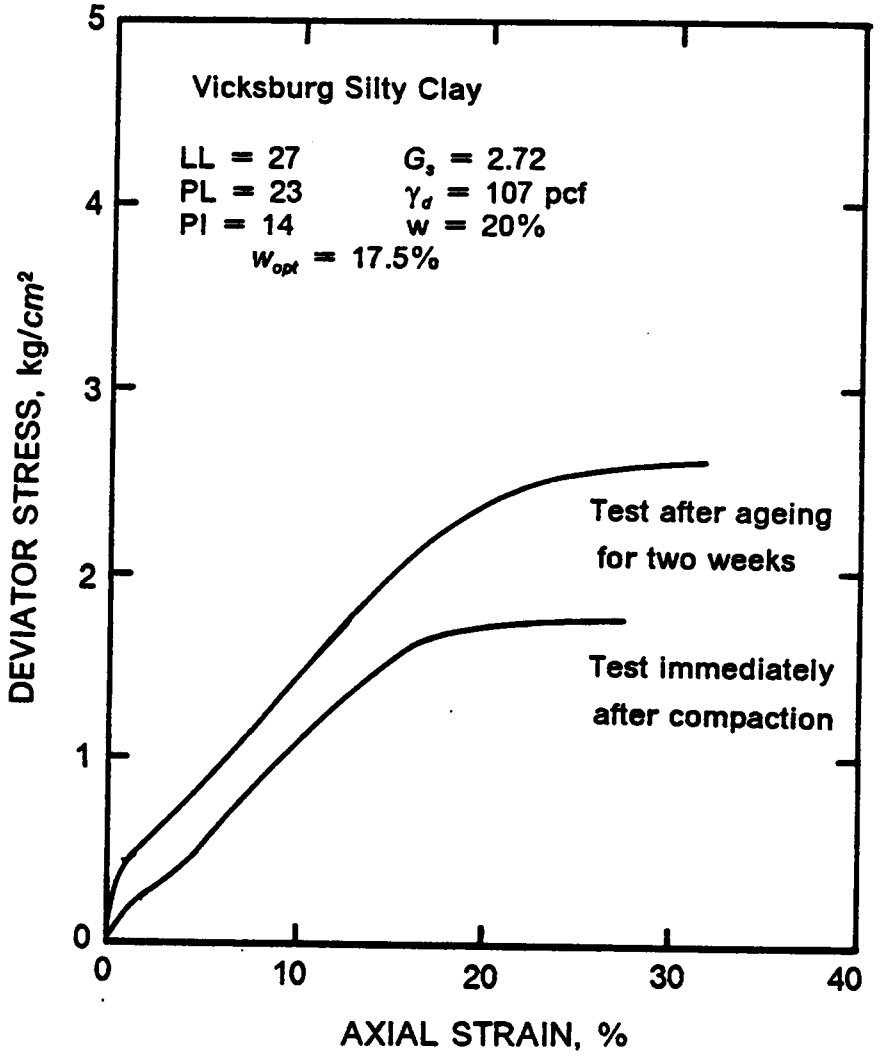

Figure 5.59 Effects of ageing on strength of Vicksburg silty clay (after Trollope and Chan, 1960).

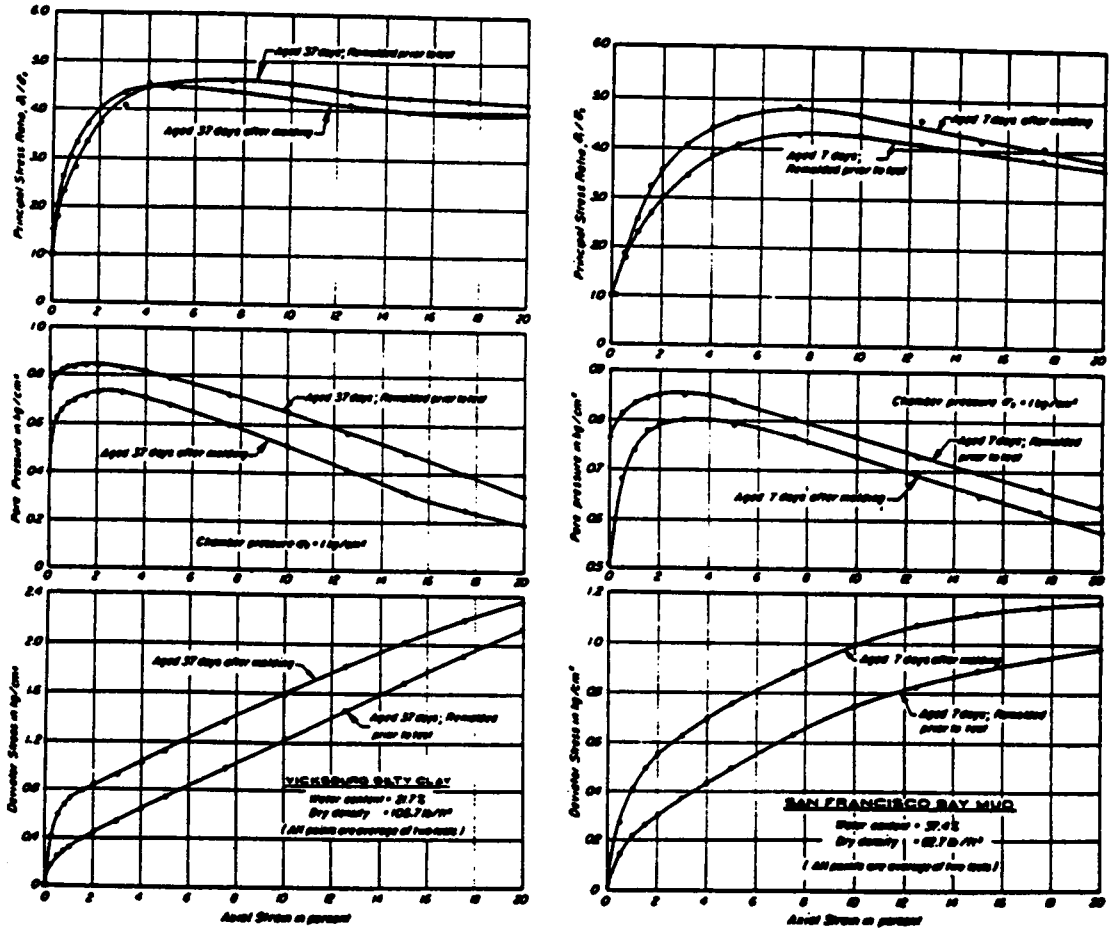

Figure 5.60 Effects of ageing on strength and pore water pressure of Vicksburg silty clay and San Francisco Bay Mud (after Seed, Mitchell and Chan, 1960).

For Canyon Dam clay, a medium plastic silty clay, undisturbed block samples were obtained three months after field compaction. Unconsolidated-undrained (UU) triaxial tests showed the undisturbed samples to have M_{50} values of about three times the M_{50} values of the lab compacted values and strengths about 30 percent greater. In consolidated-undrained (CU) tests the consolidation pressure appeared to have an effect on the ratios of M_{50}, with a ratio of three at low consolidation pressures (less than 2 kg/cm2) and a ratio nearing one as the consolidation pressure increased above 4 kg/cm2. Strengths based on the CU tests were about equal over the entire range of consolidation pressures.

For Arkabutla Dam clay, a medium plastic silty clay, undisturbed samples were tested 18 years after field compaction. Comparing these test results with those from tests on freshly compacted samples, the undisturbed and the freshly recompacted values of M_{50} and strength were about equal for UU tests. In CU tests, the strengths were nearly the same, but the values of M_{50} for the undisturbed samples were 1.1 to 1.9 times those for the freshly compacted samples.

Similar comparisons for sandy clay from the Conchas Dam, tested 20 years after field compaction, showed M_{50} values three times greater UU test on undisturbed samples than for freshly recompacted samples. In these UU tests the strengths were about the same. In CU tests practically no differences were discerned in either strength or M_{50}, values except at very low consolidation pressures where the M_{50} ratio approached a value of two.

An interesting point concerning the above tests is that all, except those on the Conchas Dam fill, were performed on soil at moisture contents at optimum or higher.

The above discussion demonstrates that the strength and stiffness of compacted soils increase with time, and that the amount of increase varies from soil to soil. The effect of ageing on the strength and stiffness properties of the fill material at Mohicanville Dike No. 2 was assessed through a laboratory investigation using unconsolidated-undrained tests on compacted samples. Based on the results of these tests, the effects of ageing were included in finite element analyses by increasing the strength and stiffness of the fill between the end of the first construction season winter shutdown and the beginning of the second. The results of these studies are described below.

5.8.1 Soil Properties

A 150 lb sample of the embankment fill material was obtained from the Huntington District Corps of Engineers. Soil classification, grain-size, water content-density relations, and unconsolidated-undrained (UU) triaxial compression tests were performed on the soil.

The material grades as a gravelly sandy clay, classified as a CL in the Unified Soil Classification System. The clay has a liquid limit of 31, a plastic limit of 17 and a plasticity index of 14, determined in accordance with American Society for Testing and Materials (ASTM) Standards D-4318 and ASTM D-2217. The specific gravity was determined to be

2.74 in accordance with ASTM D-854. The grain size distribution, determined in accordance with ASTM D-422, is shown in Figure 5.61. Also plotted in Figure 5.61 are the limits of grain size determined for the borrow materials at the site by Law Engineering Testing Company (Collins et al. 1982). The material used in this study is near the fine side of the borrow material identified at the site.

Standard compaction water content-density relations for the fill were determined in accordance with ASTM D-698 and are shown in Figure 5.62. The maximum dry density is 119.0 pcf at an optimum moisture content of 14.5 per cent. Also shown on this figure are the results of compacting the soil in a Harvard Miniature Compaction Apparatus (Wilson, 1970) at various water contents. The results plotted here are for compaction in the Harvard Miniature device using five layers and 25 tamps/layer, with a 40 lb spring. This combination of tamps and layers was used to mold the UU test specimens.

The natural moisture contest of the soil as delivered to Virginia Tech was 15.4 per cent. This moisture content is about 1 per cent above optimum. This being the case, the test specimens were molded using the soil as received after removing the material larger than the #4 sieve size (4.7 mm). Based on the results shown in Figure 5.62, it was expected that this would provide test specimens at an approximate dry density of 118.2 pcf when compacted in the Harvard Miniature apparatus. After compacting, the specimens were placed between two lucite end caps, encased in two latex membranes and sealed at each end with two O-rings. Silicon grease was

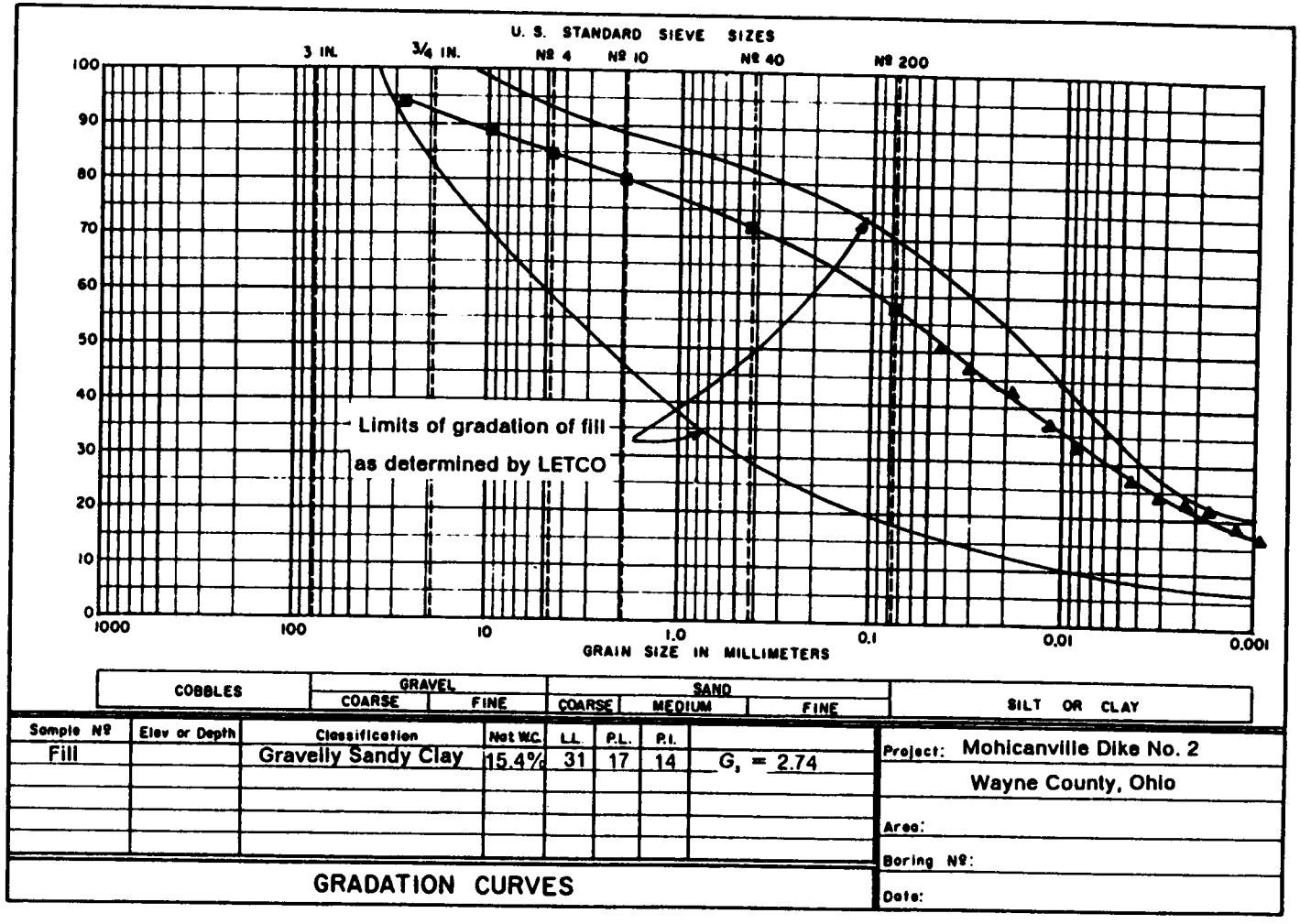

Figure 5.61 Grain size distribution of Mohicanville Dike No. 2 embankment fill tested during this study.

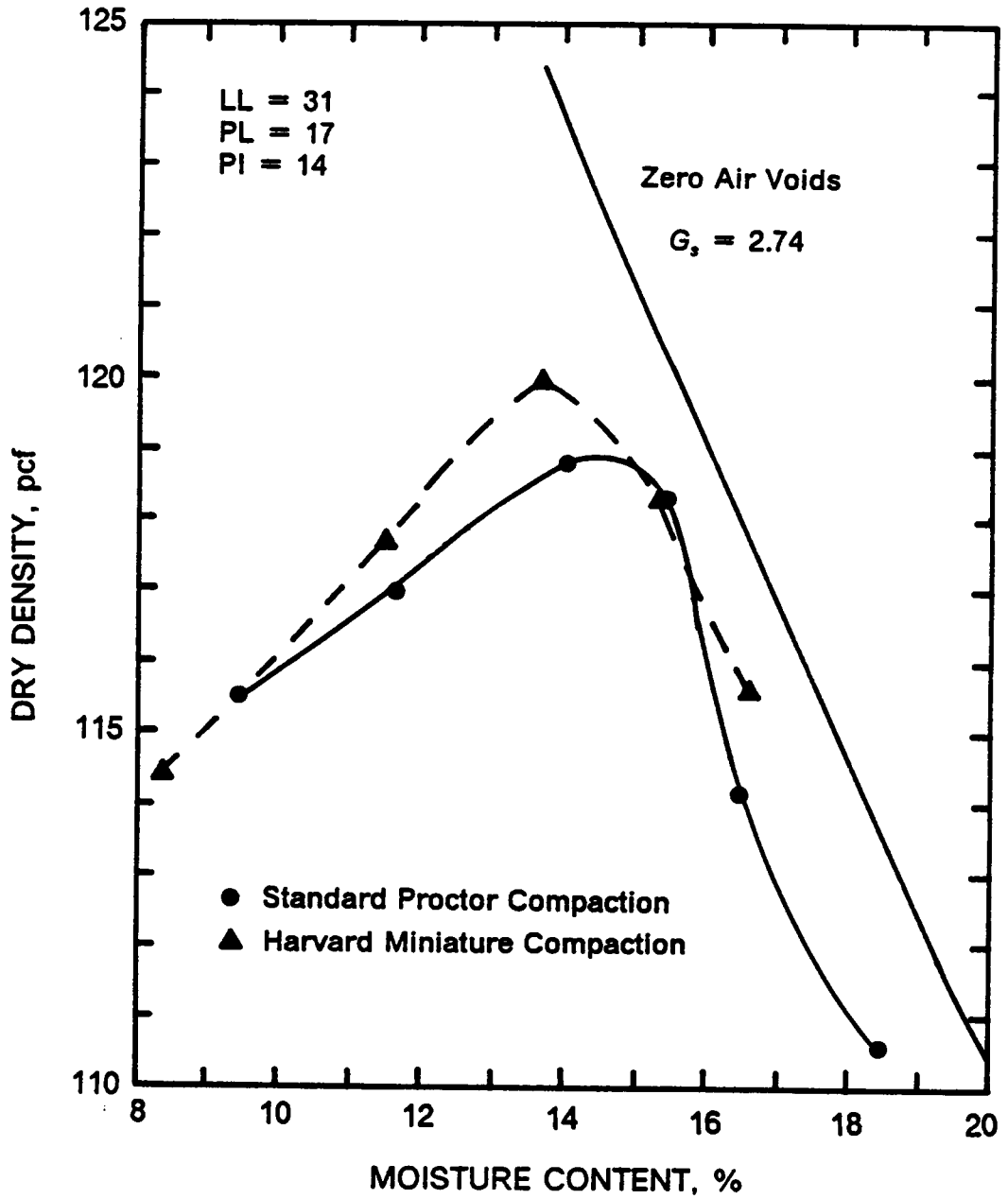

Figure 5.62 Moisture-density relations for clay tested.

placed between the membranes on test specimens which were to "age" to inhibit leakage and the samples were stored under water until tested.

The data in Table 5.6 show that the target dry density of 118.2 pcf was not met in all the specimens. These data also show that an increase in moisture content occurred as the time of storage increased. This appears to indicate that leakage of water into the soil specimens occurred despite the precautions taken. Two of the 4-week test specimens had water contests high enough to make the samples noticeably soft when removed from the water storage tank. These samples showed such low strengths in testing that the results were discarded.

The effect of ageing on fill properties was assessed by performing UU triaxial tests on soil samples immediately following compaction and on samples that were allowed to age for periods of 1, 2 and 4 weeks following compaction. The UU tests were performed in accordance with ASTM D2850. At each time four UU tests were conducted using confining pressures of 0.25, 0.50, 075 and 1.00 tsf. The stress-strain curves from these tests are shown in Figures 5.63 through 5.66. The results from two of the 4-week samples were disregarded due to an unusually high water content after testing, indicating leakage occurred during storage. The stress-strain curves exhibit behavior similar to the behavior of the Vicksburg silty clay discussed earlier: an initial stiff response followed by a relatively linear increase in strength. Table 5.7 shows the strengths interpreted from the tests based on failure at 15 percent strain. An increase in strength occurs for samples tested after 1-week of ageing. However, samples tested 2- and 4-weeks after molding, in

Table 5.6 Dry density (in pcf) and water content of UU specimans.

Confining Pressure, tsf	Series: Immediate γ	Immediate w, %	1-week γ	1-week w, %	2-week γ	2-week w, %	4-week γ	4-week w, %
0.25	117.9	15.6	118.4	15.8	116.8	15.9	113.9	19.0
0.50	118.4	15.3	117.0	15.8	117.9	15.8	116.4	16.3
0.75	118.4	15.4	116.7	16.0	117.7	15.9	114.4	18.8
1.00	118.8	15.1	117.6	15.7	117.5	15.8	116.9	16.7

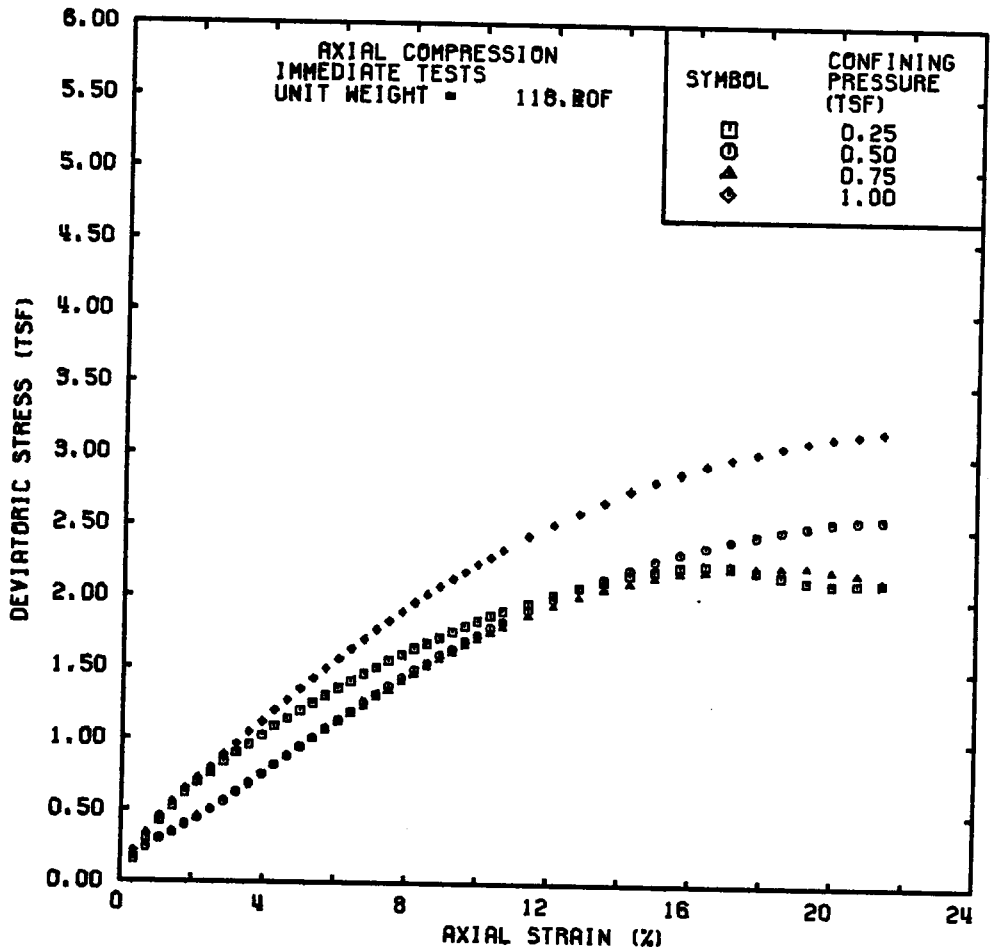

Figure 5.63 Stress-strain curves from UU tests on freshly compacted soil.

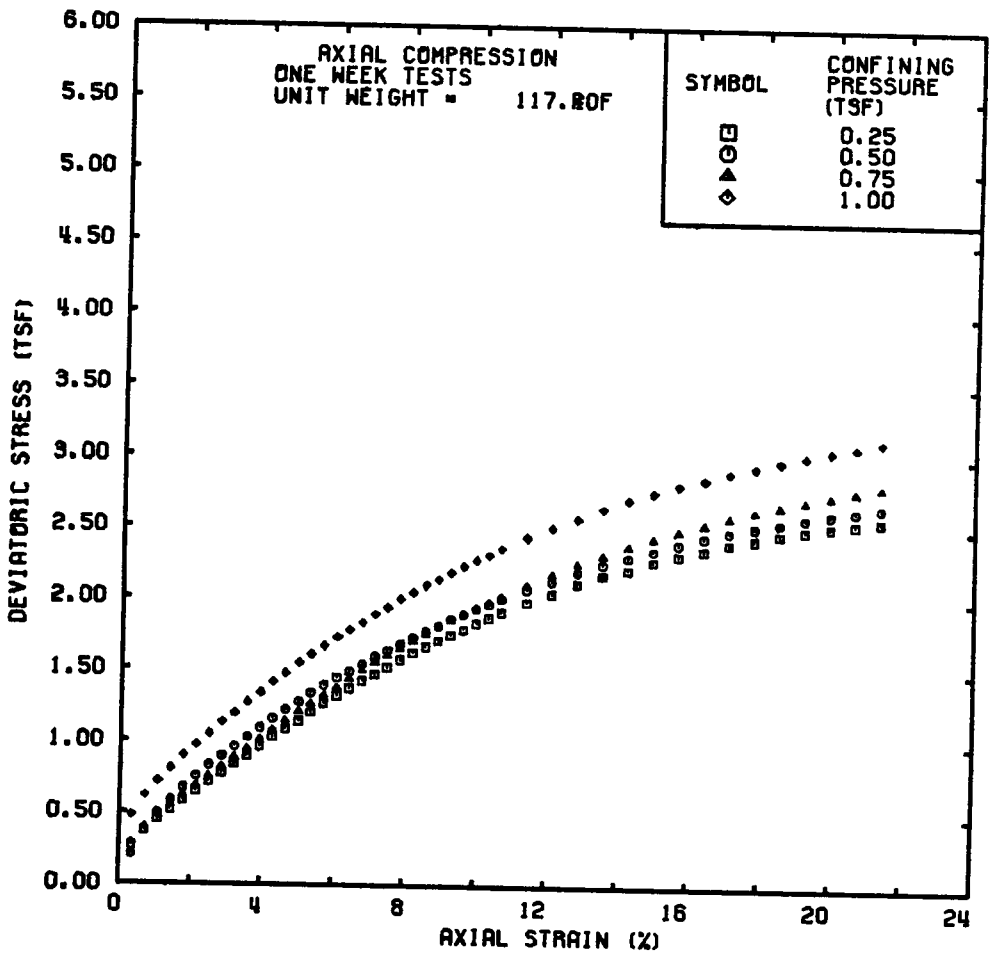

Figure 5.64 Stress-strain curves from UU tests on samples aged one week.

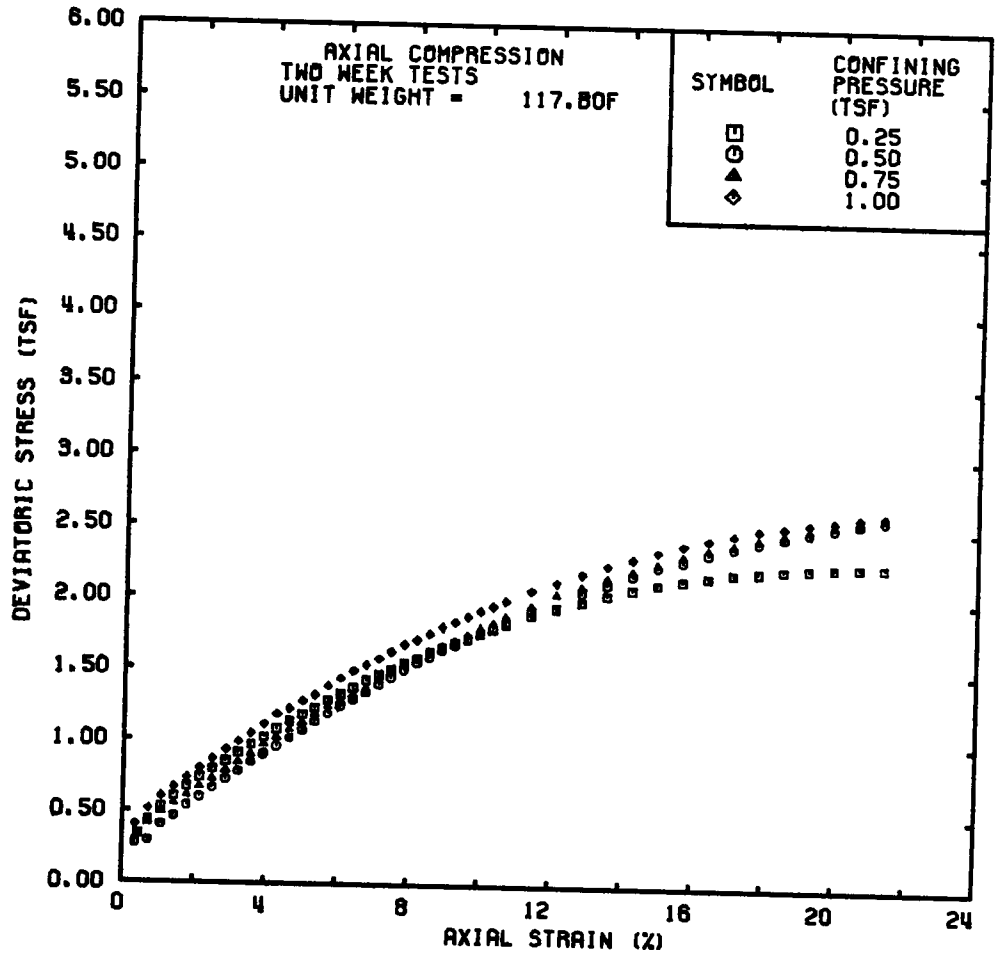

Figure 5.65 Stress-strain curves from UU tests on samples aged two weeks.

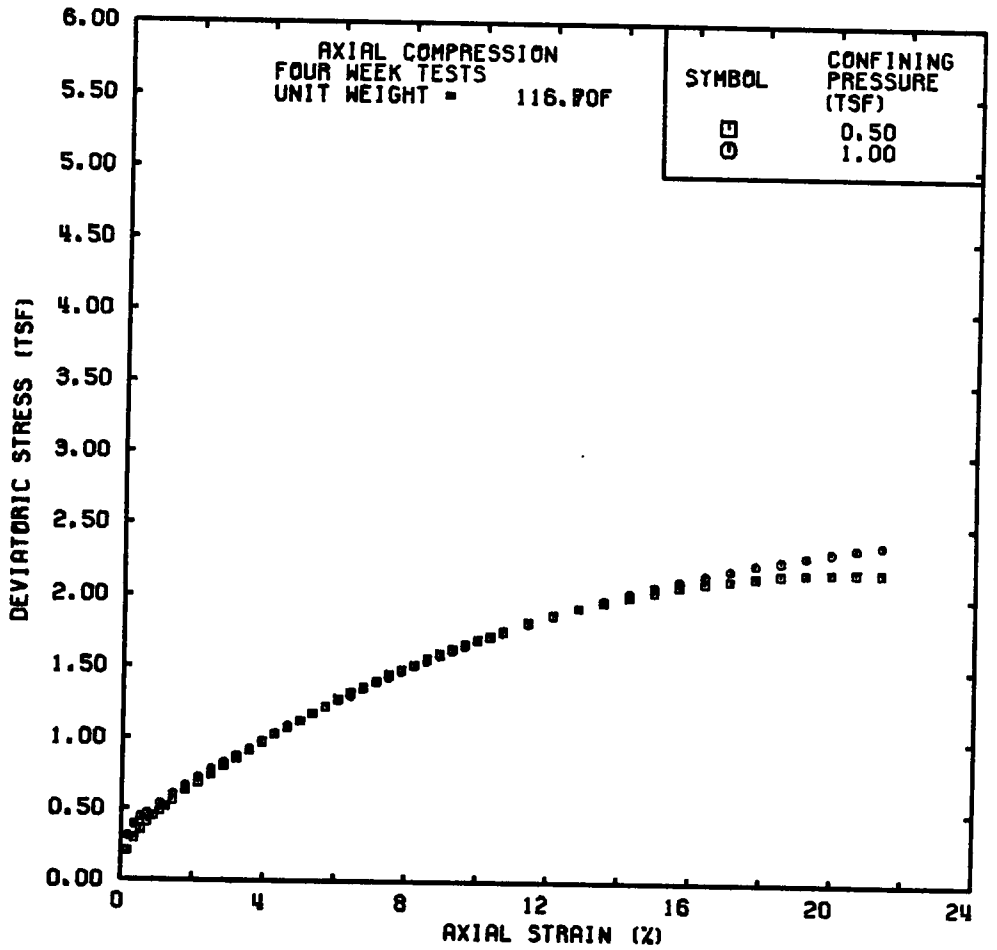

Figure 5.66 Stress-strain curves from UU tests on samples aged four weeks.

general, show slight reduction in strength. The differences in strength may be attributable to differences in molding density and water content. The data in Table 5.6 show that the samples tested immediately after molding had the highest average density of all the samples tested.

The stiffness of each sample was characterized in two ways. Table 5.8 shows the initial stiffness determined using standard hyperbolic soil model techniques (Duncan et al. 1980) and normalized by atmospheric pressure. Table 5.9 shows the secant modulus of each sample at a stress level of 0.4 tsf corresponding to an average embankment pressure at the level of the reinforcement. The trends shown in these two tables are similar to the trends of the strength data. A general increase in stiffness with time can be seen, but significant scatter in the results is evident.

Despite the scatter in the results, it is clear that some gain in strength and stiffness does occur with ageing in the clay from Mohicanville Dike No. 2. Based on the results of the laboratory tests, it was concluded that a reasonable estimate of the effects of ageing between the first and second construction season would be a ten percent increase in strength, and a 100 percent increase in modulus.

5.8.2 Finite Element Analyses

A finite element analysis to investigate the effects of ageing was performed using the mesh and profile used for previous analyses of Section 6+55. The analysis was performed by simulating the first construction

Table 5.7 Undrained shear strengths from UU tests.

Confining Pressure, tsf	Undrained Shear Strength, tsf			
	Immediate	1-week	2-week	4-week
0.25	1.08	1.14	1.00	--
0.50	1.10	1.18	1.07	1.03
0.75	1.14	1.23	1.13	--
1.00	1.41	1.40	1.18	1.05

Table 5.8 Modulus determined by hyperbolic model.

Confining Pressure, tsf	Modulus Ei/pa Immediate	1-week	2-week	4-week
0.25	1.66	1.65	1.69	--
0.50	1.37	1.78	1.46	1.89
0.75	1.25	1.46	1.47	--
1.00	1.59	1.89	1.87	1.85

Table 5.9 Secant modulus at 800 psf shear strength.

Confining Pressure, tsf	Modulus, psf Immediate	1-week	2-week	4-week
0.25	37.7	41.7	66.7	--
0.50	22.7	47.6	34.5	57.1
0.75	22.7	62.5	57.1	--
1.00	47.6	166.7	100.	133.

season and the winter shutdown as before, and increasing the stiffness and strength of the new fill at the start of the second construction season. The strength of the fill was increased by ten percent and the stiffness was increased by a factor of two as compared to the initial stiffness. The calculated centerline reinforcement force is shown as the dashed line in Figure 5.67. There was little change from the previous results indicating stiffening of the new fill had little effect on the reinforcement forces. The calculated in settlements and pore water pressures were slightly smaller than those calculated in the analyses described previously. No discernible changes in the horizontal movements were noted. During the consolidation phase of the analysis, no increases in fill strength occurred, while the strength of the peat and soft clay increased by one-half to one and one-half percent.

A second analysis was performed in which the strength and stiffness of the old fill material was raised at the beginning of the second construction season by the same ratios as the new fill. The effect of "ageing" both the old and new fill is shown on Figure 5.67 by the solid line. It can be seen that this change had the effect of reducing the reinforcement force and provides results in excellent agreement with the measured data. Ageing both fills reduced the settlement at the reinforcement level and reduced the lateral movements at the toe. However, there was little change in settlements in the peat and soft clay compared to the unstiffened analyses. In this analysis the shear stress levels in the old fill were markedly higher indicating more load being carried

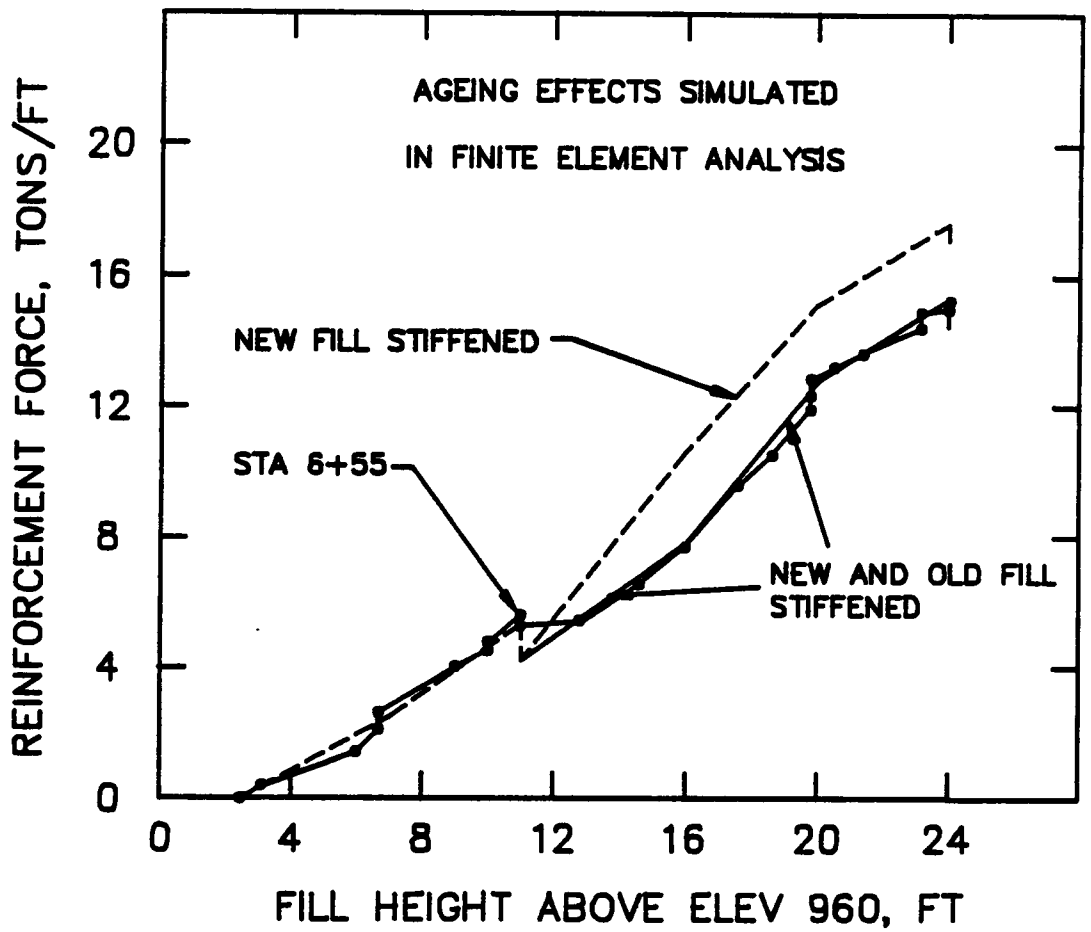

Figure 5.67 Measured versus calculated reinforcement forces at the centerline including effects of ageing on fill.

by the fill. The shear stress levels in the peat and soft clay were lower than those calculated in the unstiffened analyses.

From the analyses discussed above, it appears that ageing of the new fill did not materially affect the reinforcement forces. Further, there would seem to be little reason to suspect that ageing of the old fill resulted in the lower measured forces, because this fill had been in place some 45 years. The mechanism causing the gain in strength might be strength gain in the foundation soils due to secondary compression effects.

5.9 Summary and Conclusions

The experience gained from design, construction, instrumentation, and analysis of Mohicanville dike has provided information of considerable value with regard to the behavior of reinforced embankments on weak peat and clay foundations.

First, it has been demonstrated that it is feasible to stabilize an embankment on a weak foundation very effectively using a single layer of reinforcement near the base of the embankment. This is particularly valuable in light of the height of the embankment built at this site, some 28 feet above natural ground level. Second, it has been shown that such an embankment can be adequately designed using limit equilibrium and finite element techniques.

The instrumentation studies performed on the embankment during and following construction have provided very valuable information regarding

the accuracy of the finite element analyses and the limit equilibrium slope stability analyses used to design the embankment. Comparisons of the calculated and measured reinforcement forces indicate that the finite element analyses provide an effective means of estimating the amount of reinforcing force that would develop during construction, and the rate at which the force would decrease after construction as the foundation soils consolidate. The measured movements of the embankment have been quite small, consistent with the expected behavior of an embankment having a factor of safety equal to 1.3 at the end of construction. Thus the combination of finite element analyses to estimate reinforcing forces, and conventional limit equilibrium analyses to calculate factor of safety appears to provide an effective approach for design of reinforced embankments on weak foundations.

The study of the effects of ageing of the compacted clay fill were inconclusive. When only the strength and stiffness of the new fill was increased during the winter shutdown, the calculated results were changed very little. When the strength and stiffness of the old fill was increased as well, the results were in excellent agreement with the field measurements. That the strength of the old fill could actually have increase seems unlikely, given that it had been compacted some 45 years prior. However, it seems likely that some stiffening of the soils, perhaps the foundation as well as the embankment soils, did occur over the winter shutdown, resulting in the changed behavior over this period that was clearly evident in the measured reinforcement forces during the early stages of the construction season.

CHAPTER VI

ANALYSIS OF ST. ALBAN TEST EMBANKMENTS

6.1 Introduction

In 1984, three instrumented test embankments were constructed to failure at a site near St. Alban, Quebec, Canada, to study the effect of geogrid reinforcement on the stability of embankments on a soft sensitive clay deposit. Two of the embankments were reinforced with Tensar SR-2, a high strength, high density polyethylene geogrid having uniaxial strength characteristics. One of these embankments had the geogrid placed in a flat-lying position and the other had the geogrid placed in an upright position to form a geogrid mattress structure. A third embankment, unreinforced, was constructed as a control.

The primary objective of this chapter is to assess the suitability of various finite element techniques for the analysis of reinforced embankments on soft, sensitive clays. This was accomplished by a straight forward interpretation of the soil data, analyzing the field trials and comparing the analytical results to the observed behavior. A comprehensive report of the field trials, containing a discussion of the subsurface exploration, the embankment design, instrumentation, construction, field measurements and observations was prepared by Busbridge et al. (1985). A review of certain aspects of this report is presented here as background to the analyses performed during this study.

6.2 Soil Properties

The foundation soil at the site is a soft, sensitive and cemented clay. This clay, known locally as Champlain Clay, has been extensively studied due to its widespread distribution in eastern Canada. Among the numerous studies of these soils are those by Bozozuk (1963), Mitchell (1970), Lefebrve and La Rochelle (1974), Tavenas et al. (1974), La Rochelle et al. (1974) and others. These studies provide a substantial data base from which soil properties may be determined.

A typical soil profile at the St. Alban test site is shown in Figure 6.1. The profile consists of about 0.3 m of topsoil, a 1.5 m thick weathered clay crust, an eight meter thick layer of soft, very sensitive, cemented silty clay, and an approximately four meter thick layer of soft, sensitive clayey silt. Below a depth of about 14 m a dense, fine to medium grained sand is encountered. The results of numerous in situ vane shear and cone penetration tests at the site during various research projects have demonstrated that the clay is very uniform across the site (Busbridge et al. 1985).

The undrained shear strength of this clay increases with depth as shown in Figure 6.1. Tavenas et al. (1974) report that the value of the ratio $\frac{S_u}{\sigma'_v}$ is about 0.55, considerably higher than typical for many other clays. Effective stress parameters for this soil were reported by Tavenas et al. (1974) to be $\varphi' = 28°$ and $c' = 3.75$ kPa.

The brittle nature of these soils is shown Figure 6.2, where it may be seen that the peak strength is reached at strains of one to two per-

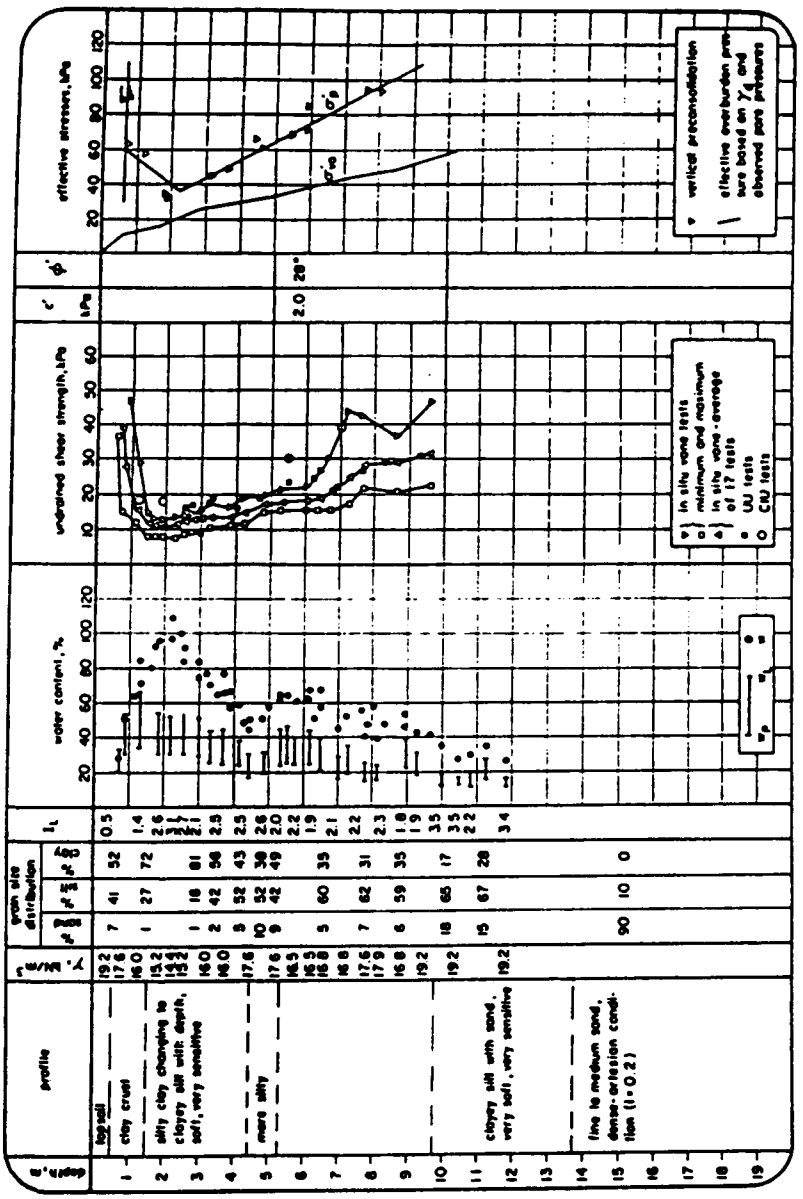

Figure 6.1 Soil profile at St. Alban site (after Pilot et al. 1982).

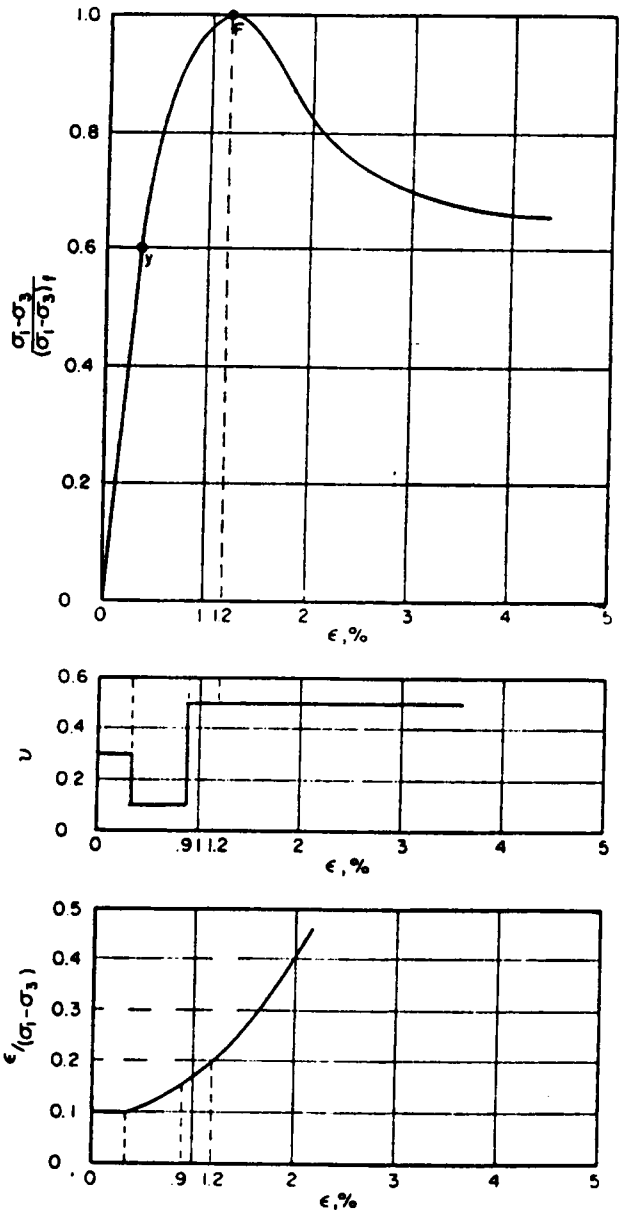

Figure 6.2 Typical consolidated undrained test results: stress-strain relationship and Poisson's ratio (Tavenas et al. 1974).

cent, and that the shearing resistance decreased rapidly beyond the peak. Tavenas et al. (1974) reported results of consolidated undrained tests in which lateral deformations were measured to obtain data on Poisson's ratio as shown in Figure 6.2. In addition, Tavenas et al. presented the results of hydraulic fracture tests from which in situ K_o values were determined.

Consolidation characteristics of this clay reported by Tavenas et al. (1974) are shown in Figure 6.3. The sharp break in the e versus log p curve is generally attributed to a structural breakdown which occurs at a critical pressure and results in a change of fabric of the clay (Quigley and Thompson, 1966). One-dimensional consolidation tests on undisturbed sensitive clays are characterized by a break at a pressure believed to correspond to the preconsolidation pressure, p_c. La Rochelle and Lefebrve (1970) report that this pressure is frequently used in practical design to determine the maximum load to be applied to the clay without resulting large settlements.

The soil used for the fill was a uniform, medium to coarse grained sand containing about ten percent fine sand and ten percent gravel, having a uniformity coefficient of 3.0 (La Rochelle et al. 1974). The sand was placed in a loose state with minimal compaction effort. The friction angle of the sand as placed was estimated to be 34° by Busbridge et al. (1985).

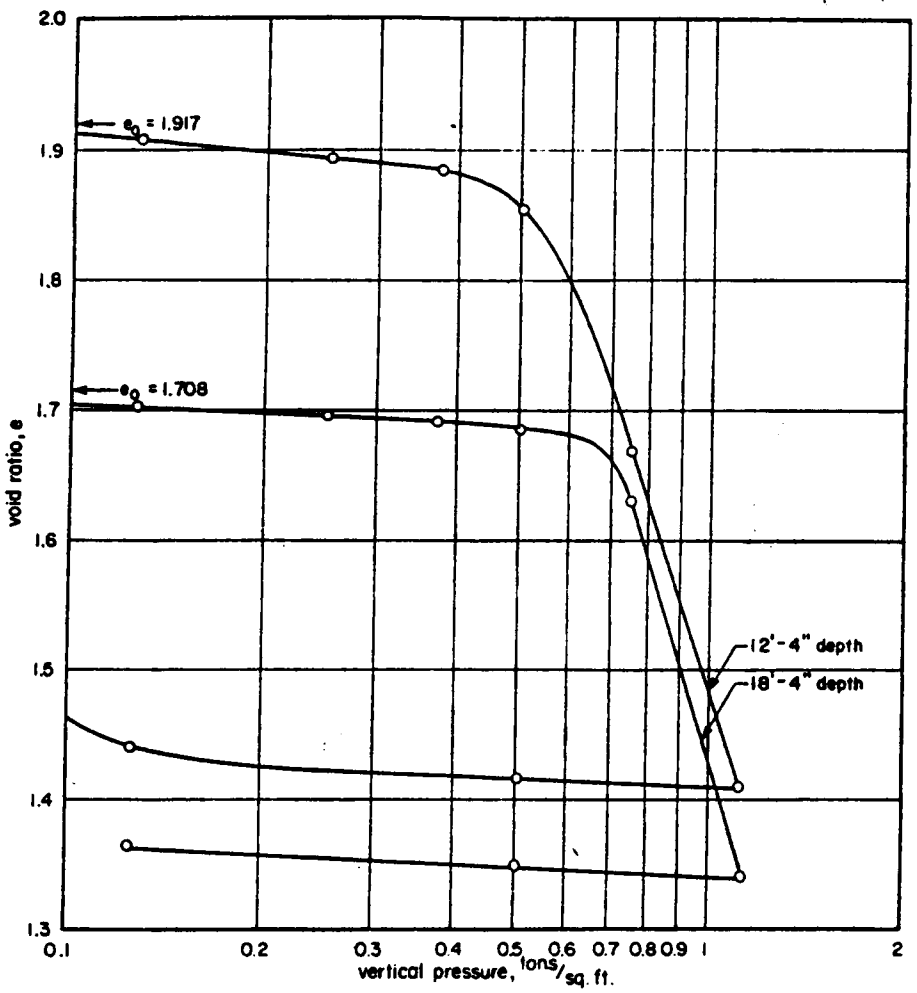

Typical e – log p curve.

Consolidation characteristics of the different strata

Stratum	Depth (ft)	$P<P_c$ C_c	$P<P_c$ c_v (cm²/s)	$P>P_c$ C_c	$P>P_c$ c_v (cm²/s)
Top soil	0–1.2	No tests, undisturbed sampling impossible			
Clay crust	1.2–5	0.020	5×10^{-3}	0.60	10^{-4}
Soft clay	5–15	0.025	2×10^{-4}	2.30	0.5×10^{-4}
	15–18	0.020	5×10^{-4}	1.20	0.5×10^{-4}
	18–32	0.020	10^{-3}	1.72	0.5×10^{-4}
Clayey silt	32–45	No tests, undisturbed sampling impossible			

Figure 6.3 Consolidation characteristics for the soft clay (after Tavenas et al. 1974).

6.3 Reinforcement Properties

The reinforcement used in the test embankments was Tensar SR2 geogrid. Tensar SR2 geogrids are molecularly oriented polymer grid structures manufactured from copolymer grade high density polyethylene. SR2 geogrids are manufactured by punching holes in a polymer sheet followed by a stretching process in one direction to align the long chain molecules. The dimensions of SR2 are shown in Figure 6.4a.

Being a polymeric material, Tensar SR2 exhibits time- and temperature-dependent characteristics. Design curves for SR2 developed by the manufacturer are shown in Figure 6.4b. The long-term design load at a performance strain of ten percent is 29 kN/m, which reflects the long term strength of the material including allowances for creep. Load-strain data from constant rate-of-strain tests are shown in Figure 6.4c. An upper load limit of 79 kN/m has been determined from tests run at a strain rate of 23 percent per minute. McGown et al. (1984) present additional information on the load-strain-time behavior of Tensar SR2 geogrids.

6.4 Instrumentation

The behavior of the three test embankments was monitored by an extensive battery of geotechnical instruments. The instruments were concentrated near the axis of the embankments and on the sides where failure was presupposed to occur (due to a stabilizing berm on the opposite side).

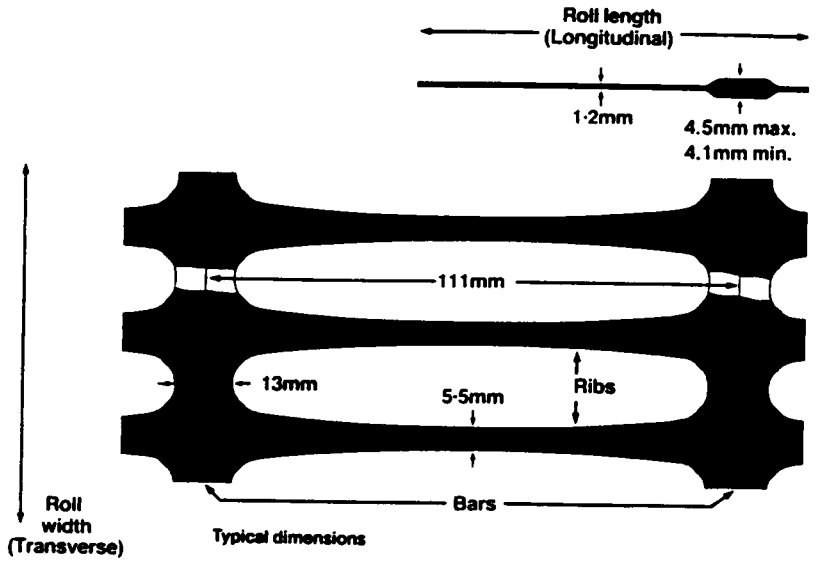

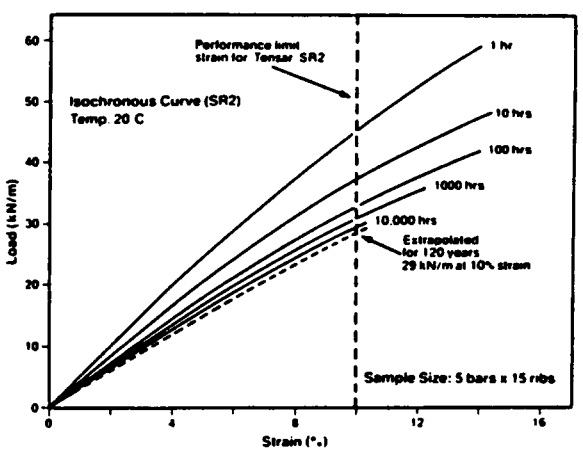

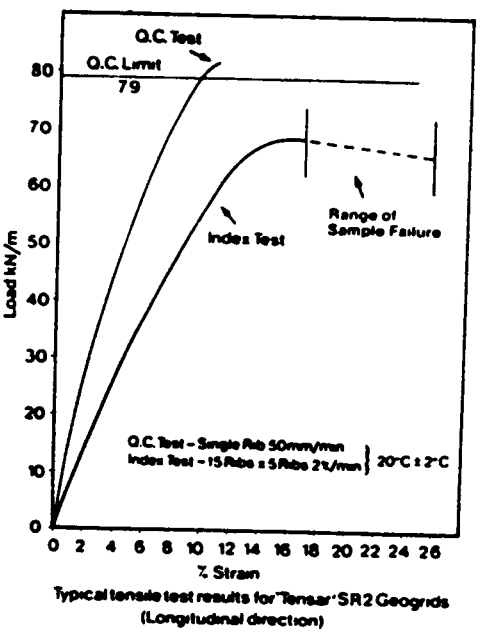

Figure 6.4 (a) Typical dimensions of Tensar SR2. (b) Isochronous load-strain curves. (c) Typical tensile test results.

The layout of instrumentation used for each embankment was similar to facilitate direct comparisons of behavior.

Pore pressures in the foundation were monitored with electrical, hydraulic and pneumatic piezometers; movements of the fill and foundation soils were monitored using settlement plates, surface displacement monuments, and horizontal and vertical inclinometers. Strains in the foundation soils were measured using electrical and magnetic extensometers. Measurements of vertical and horizontal stresses in the embankment were obtained using total pressure cells.

The behavior of the Tensar geogrid was monitored using a specially designed load cell to measure the tensile load in the geogrid with strains in the geogrid measured using Bison strain gages.

Movement between the soil and the geogrid was monitored by differential extensometers. No movement between the soil and the geogrid was recorded in the strip reinforced embankment, and these types of measurements were not made in the geocell mattress embankment.

The data provided by these instruments provides a good basis for comparing the results of analytical studies to the measured performance of the embankments. Further details of the instrumentation can be found in Busbridge et al. (1985).

6.5 Field Test Results

Construction of the three embankments took place during August to October, 1984. The strip reinforced embankment was constructed first,

followed by the control embankment and finally by the geocell mattress embankment.

Details of the construction procedures employed can be found in Busbridge et al. (1985). Each embankment was constructed in the same general manner. An initial working pad was constructed over a large plan area (30m x 70m) to a height of 1.5m, over a three- to four-day period. Following this, two lifts of 0.3m thickness were added each day on a smaller plan area until failure occurred. This sequence of fill placement provided stabilizing berms 1.5 m high on three sides of the embankment to induce failure in a preferred direction.

The failure of the strip reinforced embankment and the control embankment were sudden, occurring in 30 to 60 seconds with no prior sign of distress. The failure of the geocell mattress embankment occurred during the evening or night when the site was unattended. All three embankments failed in a rotational slip mode with the fill and foundation soil moving as a solid block. In general, the crest of the embankment moved down about 1.5 to 2.0 meters, with the toe of the embankment heaving a similar amount.

Table 6.1 summarizes the height of the fill at failure and the depth of the failure surface for the three embankments and also for an embankment constructed to failure at this site in 1972 as reported by La Rochelle et al. (1974). Also shown are the unit weights and the friction angle of the fill for each of the embankments.

Table 6.1 Height to failure of test embankments.

Embankment	Height at Failure, m	Depth of Failure Surface, m	Fill Parameters γ, kN/m3	ϕ
1972 Unreinforced	4.0	4.0	18.9	44
1984 Control	5.1	4.0-5.5	18.1	34
1984 Strip Reinforced	6.0	4.0-5.5	16.9	34
1984 Geocell Mattress	4.5	3.0-6.0	18.2	34

The behavior of the three embankments was very similar in terms of pore pressure response in the foundation, settlement, and horizontal movements.

The pore pressure response can be described in terms of the pore pressure parameter $\bar{B} = \frac{\Delta u}{\Delta \sigma_v}$ = change in pore pressure/change in total vertical stress. The $\bar{B}$ value in the soft clay was around 0.5 until the embankment heights reached about 2.8m. A rise of the incremental value of $\bar{B}$ to about 1.0 then occurred, and at a height of 4.5 to 5.0m, the $\bar{B}$ value became greater than 1.0 and approached 1.3. In a study of the 1972 embankment failure, Tavenas and Leroueil (1980) concluded that initial low values of B $\bar{B}$ were due to the effects of preconsolidation and resultant high values of the coefficient of consolidation. The onset of $\bar{B}$ = 1.0 was interpreted as the point at which the vertical effective stress σ'_v exceeded the preconsolidation pressure σ'_p and the coefficient of consolidation is reduced by a factor of 10 to 50 to approach an undrained condition. The increase in the value of $\bar{B}$ above one was interpreted as the onset of local failure in the soft clay soils.

The settlement behavior of the three embankments was nearly identical. During the first four days of construction, settlement under the centerline was between four and seven millimeters per day. On the fifth day, this rate increased to approximately 25 mm/day under the strip reinforced and the geocell mattress embankments and to 35 mm/day under the control embankment. The rate increased to 35 mm/day under the strip reinforced embankment from the sixth day until failure. The total settlements under the centerline, just prior to failure, were 240 mm, 223 mm

and 230 mm for the control, the strip reinforced and the geocell mattress embankments, respectively.

The horizontal movements measured at the toe of the fill were similar for each embankment. In general, small movements were recorded below depths of 6.5 meters. Between depths of 1.5 to 6.5 m (the soft clay zone), lateral movements on the order of 50 to 100+ mm were measured prior to failure. Movements decreased significantly with distance from the toe, averaging 60 and 20 percent of the toe movements at distances of three and eight meters from the toe.

6.6 Limit Equilibrium Analyses

6.6.1 Analyses by La Rochelle et al. and Busbridge et al.

La Rochelle et al. (1974) performed comprehensive analyses of the 1972 test embankment to develop a better understanding of the relationship between shear strength parameters derived from field and laboratory tests and the factors of safety obtained from slope stability analyses. These studies included several different assumptions concerning strength mobilized in the fill, strengths to use for the weathered crust, and strengths (laboratory or field) to use for the soft clay below the crust. Figure 6.5 shows the strength hypotheses considered in the crust and soft soils. From this work, La Rochelle et al. showed that reasonable factors of safety from stability analyses were obtained using residual strength values for the crust soil and the foundation soils. The residual strength

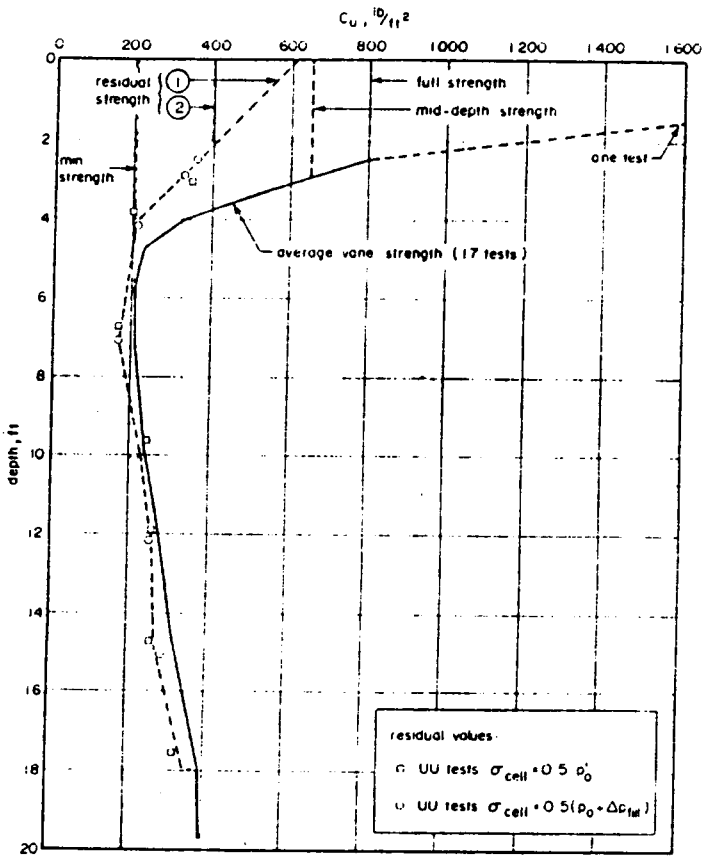

Figure 6.5 Undrained shear strength profiles of St. Alban site determined by different hypotheses (La Rochelle et al. 1974).

was defined as the undrained shear strength from CIU or UU laboratory tests at a strain of 15 percent. This concept later became known as Undrained Strength At Large Strains (USALS) (Trak et al. 1980). It is interesting to note that for material below the crust, the USALS profile corresponds closely to 0.9 times the average vane shear strength profile.

The design and back analyses performed by Busbridge et al. (1985) were based on the USALS strength profile shown in Figure 6.5. These analyses were undertaken using three slope stability computer programs. All three are based on limiting equilibrium of a circular failure surface. Two programs were for the analysis of embankments without reinforcement, one based on Bishop's Modified Method (Bishop, 1955) and the other based on the method proposed by Sarma (1973). The third program was based on a circular failure surface through the foundation with determination of moment equilibrium based upon the weight applied by the fill. This program incorporated a stabilizing moment due to a single horizontal reinforcing force at the base of the embankment. This program was calibrated for unreinforced cases by comparing factor of safety results with results from the other two programs. A description of this program was given by Milligan and La Rochelle (1984).

Preconstruction stability analyses were based on the USALS shear strength profile shown in Figure 6.5, residual strength profile 1 in the crust and fill parameters of the 1972 embankment shown in Table 6.1. With these properties, a height to failure of 4.0 m was calculated for the control embankment, which was the failure height of the 1972 test embankment. A height to failure of 5.2 m was calculated for the strip

reinforced embankment based on a reinforcement strength of 158 kN/m (two times the quality control strength to account for two layers of SR2). The quality control strength was used because rapid failure was expected.

Following the field trials an investigation of the foundation shear strength revealed that although the average vane shear strengths in the soft clay beneath the crust were nearly identical for the three test embankments, there were large differences in the vane shear strengths in the crust. Based on this finding, Busbridge et al. reanalyzed the unreinforced embankments using the various assumptions for crust strength shown in Figure 6.5. From these analyses, they concluded that the mid-depth assumption shown in Figure 6.5 was the most appropriate. Thus, the strip reinforced and geocell mattress embankment locations were analyzed using the measured vane shear strength profile (corrected to agree with USALS by applying a 0.9 correction factor) with the mid-depth assumption for the crust to obtain calculated, unreinforced heights at these locations of 4.6m and 4.0m. Further, they determined that reinforcing forces of 123 kN/m and 64 kN/m would be required to obtain the observed failure heights of 6.2 and 4.7 m. (These fill heights include an allowance for settlements which occurred during construction.) Thus Busbridge et al. (1985) attributed the difference in behavior of the test fills to differences in the strength of the crust at the three locations.

6.6.2 Analyses with STABGM

Analyses of the strip reinforced embankment were made during the course of this study using STABGM (Duncan et al. 1985), a slope stability program for analysis of reinforced embankments based on Bishop's Modified Method. This program is somewhat more general than the one used by Busbridge et al. in that horizontal layers of reinforcement may be placed at any height in the embankment, more than one layer of reinforcement may be specified, and either horizontal or tangential orientation of the reinforcement may be considered.

A limited parametric study using STABGM was made. The crust strength used was the mid-depth strength values reported by Busbridge et al. (1985) for the area where the strip reinforced embankment was located. The average vane shear strength profiles measured during the post failure investigation were about 10 to 20 percent greater than the average vane shear strength profile reported for the 1972 investigation (which are shown in Figures 6.1 and 6.5). Applying the 0.9 factor to convert average vane shear strengths to USALS strengths, results in a strength profile about the same as the 1972 average vane shear strength profile. Hence, the average vane shear strength profile from Figure 6.5 was used below the crust.

For an embankment height of 6.0 m, the factors of safety shown in Figure 6.6 were obtained for various reinforcement strengths. The factor of safety was determined for both tangential and horizontal orientation of the reinforcement at failure. It may be seen that the factor of safety

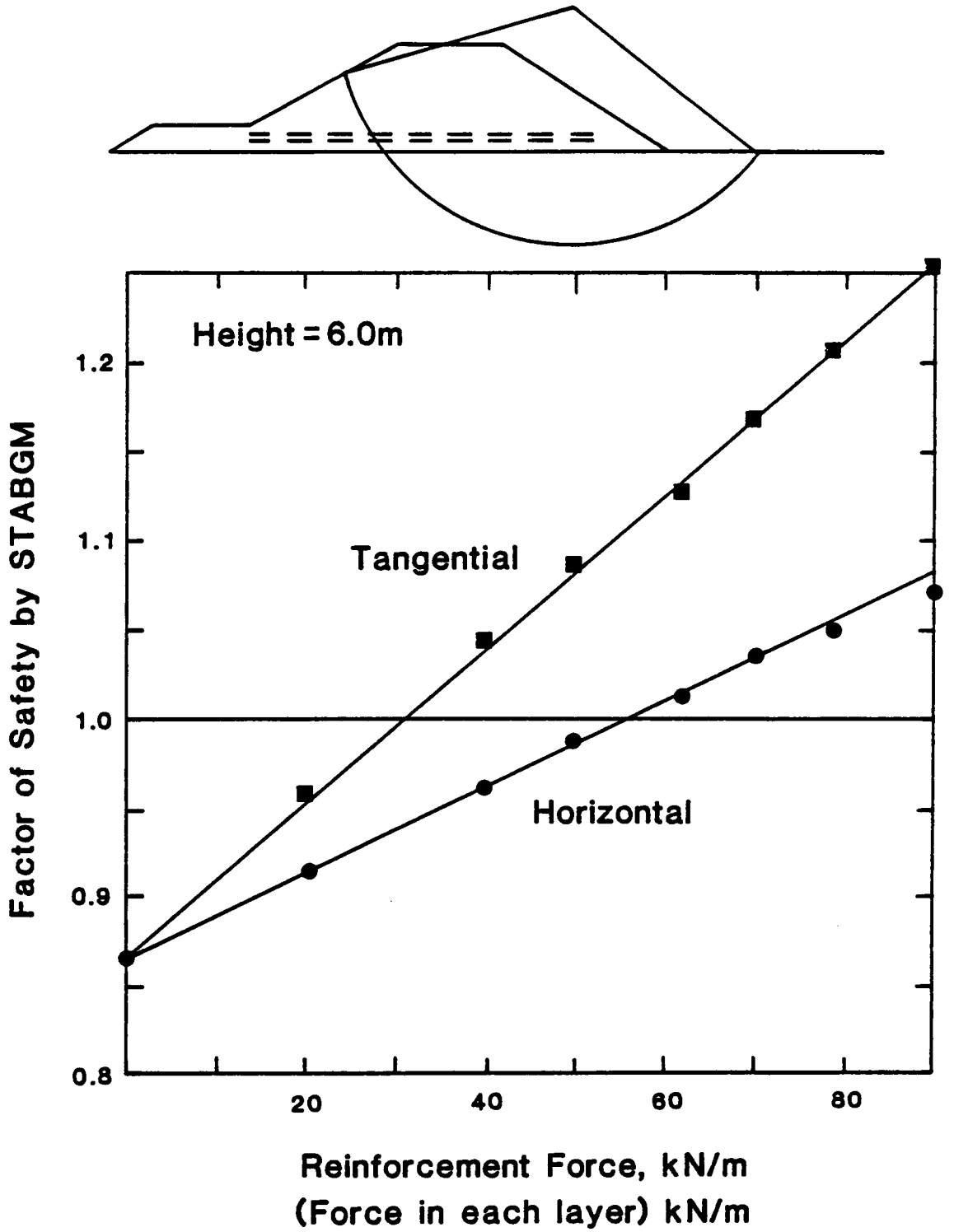

Figure 6.6 Factors of safety versus geogrid strength for strip reinforced embankment determined using STABGM.

assuming a tangential orientation is always greater the factor of safety assuming a horizontal orientation. At a factor of safety equal to unity, which is taken as the point of limiting equilibrium, the analyses show that mobilized reinforcement forces of about 56 and 30 kN/m/layer would required to maintain stability for the horizontal and tangential orientations, respectively.

A calculated failure height of 4.9 m for an unreinforced embankment based on the strength profile under the strip reinforced embankment was obtained using STABGM. This compares to the value of 4.6 m determined by Busbridge et al. (1985). Thus, the results obtained using STABGM are slightly less conservative than those obtained by Busbridge et al. (1985) for the same soil strengths.

6.7 Finite Element Analyses

6.7.1 General

The behavior of the test embankments was also analyzed using finite element techniques. Three types of finite element programs were used for the analyses conducted in this study. The strip reinforced embankment was analyzed using CON2D86, which was described in Chapter III, and SSTIPN, a soil-structure interaction program based upon the Duncan-Chang hyperbolic model (Duncan and Chang, 1970). The geocell mattress embankment was analyzed using SSTIPG, a program developed by Low and Duncan (1985), in which a special mattress element was incorporated for

particular application to Tensar geocells. Analyses of the strip reinforced and geocell mattress embankments with no reinforcement were made for comparison purposes.

The analyses simulated as closely as possible the actual construction sequence and rate. The template used in the analyses is shown in Figure 6.7 and was modified as needed to fit the various analyses. In the analyses using CON2D86, the foundation soils were represented by eight node elements in four layers. One layer each was used for the clay crust and for the clayey silt and two layers were used to represent the soft clay layer located 1.5 m to 6.5 m below the surface. In the CON2D86 analyses, eight construction layers were used, with the reinforcement placed in two layers. The first two construction layers raised the embankment height to 1.5 m, and were placed over a period of three days. The third layer was 0.5 m thick, and was placed in one day. The remaining layers were 0.8 m thick, and were placed in time increments of 1.2 days to correspond to the loading rate as constructed.

In the analyses using SSTIPN, the eight-node elements from the CON2D86 mesh were subdivided into four-node elements, and the same geometry was used. Nine construction layers were used in these analyses. Due to a constraint in SSTIPN, the reinforcement was placed after the second construction layer, but still in two layers at the proper height. SSTIPN does not model consolidation behavior or time effects and thus the analyses assumed undrained conditions in the foundation. Above the reinforcement layers, the same loading increments were used as in the CON2D86 analyses.

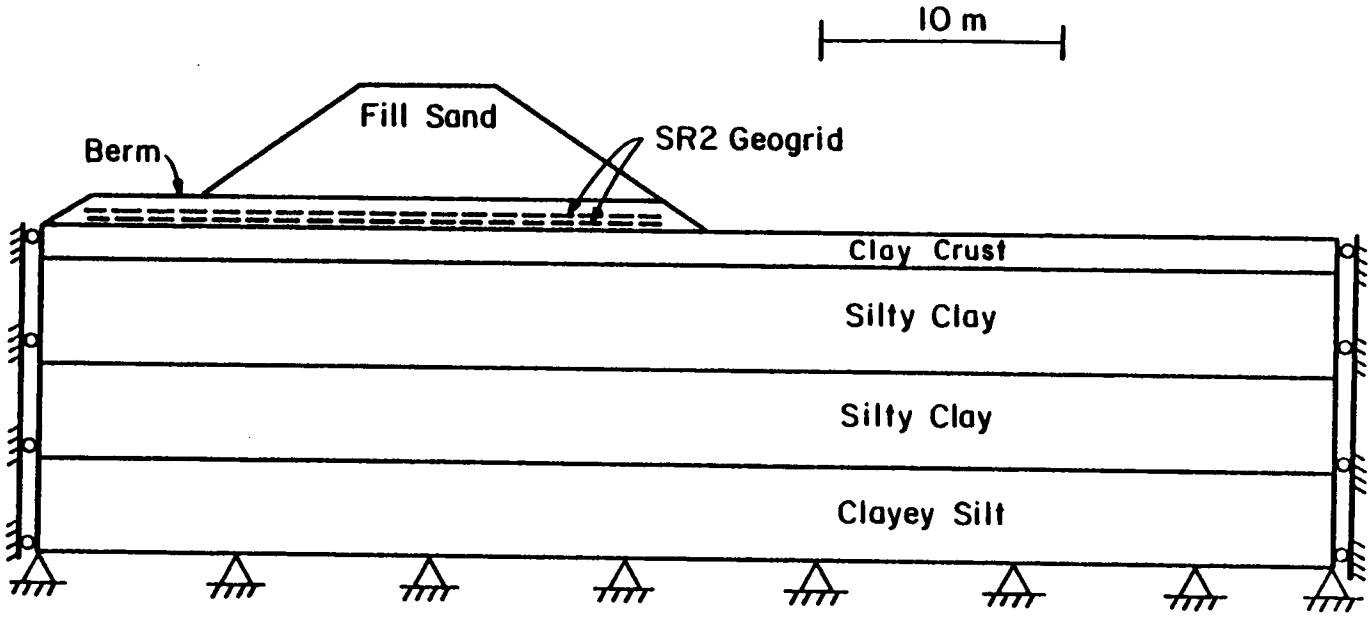

Figure 6.7 Template used for the finite element analyses.

In the analysis of the geocell mattress embankment, the geometry used was identical to that used in the SSTIPN analyses except that the first construction layer was one meter high to accommodate placement of the geocell mattress.

In the CON2D86 and SSTIPN analyses the reinforcement was modelled as a standard bar element. A stiffness of 1390 kN/m-width was used for the geogrid. This value was determined from the quality control tensile test curve for a strain of two percent, roughly the strain at failure of the soft, sensitive foundation soils.

6.7.2 Soil Parameters

6.7.2.1 Cam Clay Model

The soil parameters used in the analyses using CON2D86 are shown in Table 6.2. The foundation soil profile was divided into three zones representing the clay crust, the soft silty clay and the soft clayey silt. The parameters were determined in a straightforward manner using the data shown in Figures 6.1 to 6.3. Permeability values used were obtained from Tavenas et al. (1983) based on a laboratory and field study of the St. Alban site.

Effective stress parameters φ' and c' are shown in Figure 6.1 for the soil at a depth of five to ten meters. These parameters correspond to M = 1.11 and p_r = 3.75 kPa. For the soft clay zone from 1.5 to 5 m a value

Table 6.2 Soil parameters used in CON2D86 analyses.

Parameter	Symbol	Clayey Silt	Silty Clay	Clay Crust	Fill
Kappa	κ	0.009	0.009	0.0119	0.01
Lambda	λ	0.5-1.0	0.5-1.0	0.26	0.03
Intercept kN/sq.m	p_r	3.75	3.75	3.75	0
Slope	M	1.11	0.94	0.94	1.375
Permeability m/day	k	0.00005	0.0005	0.05	50
Initial Void Ratio	e_o	1.7	1.9	1.5	0.62
Saturation, %	S	1.0	1.0	0.9	0.2
Poisson's Ratio	υ	0.3	0.3	0.3	0.3
Unit Weight kN/cu.m	γ	19.2	16.8	18.5	16.9

of M = 0.94 was used based on the relationship between M and undrained shear strength described in Section 3.2.3.

For the Cam Clay model employed in CON2D86, the parameter P'_0 determines whether the soil is undergoing elastic or plastic behavior. Because sensitive clays develop large strains when loaded past P'_c, the determination of P'_0 for these analyses is particularly important. Two approaches to the determination of P'_0 were used. First, the value of P'_0 was determined based on the P_{CV} and P_{CH} values reported by Tavenas et al. (1974) (the P_{CV} are shown in Figure 6.1) where P_{CH} averages 0.7 times P_{CV}. A second approach was to determine P'_0 for a stress level of 0.6, the point where Tavenas et al. (1974) indicated that elastic behavior ceases in the stress-strain curve shown in Figure 6.2. The consequences of these different assumptions are discussed in the section describing the finite element results.

6.7.2.2 Hyperbolic Model

The soil parameters used in the programs SSTIPN and SSTIPG are shown in Table 6.3. These analyses were performed for the undrained case and hence undrained shear strength parameters were used for the foundation soils. The average vane shear strength profile shown in Figure 6.1 was used for the foundation soils. For the crust soils the mid-depth strength values reported by Busbridge et al. (1985) were used, in accordance with the discussion in section 6.6.1.

Table 6.3 Soil parameters used in hyperbolic soil parameter analyses.

Parameter	Symbol	Clayey Silt	Silty Clay	Clay Crust	Fill
Cohesion kN/sq.m	c	*	*	*	0
Friction Angle	ϕ	0	0	0	34
Modulus Number	K	15 x c	60-70	120	200
Modulus exponent	n	0	0	0	0.4
Failure Ratio	R	0.5	0.5	0.5	0.7
Bulk Modulus Number	Kb	0.8 x K	0.8 x K	0.8 x K	50
Bulk Modulus Exponent	m	0	0	0	0.2
Unit Weight kN/cu.m	γ	**	**	**	16.9

* = Value varied with depth according to average vane shear strength profile in Figure 6.1.

** = Value varied with depth according to data shown in Figure 6.1.

The modulus number for the foundation soils was determined from data presented by Tavenas et al. (1974). These authors presented values of E_u determined from unconfined, UU and CIU compression tests as a function of depth. The E_u values were defined as the secant moduli at a stress level of 50 percent. For the determination of K, the modulus number, it is necessary to determine values of E_i, the initial tangent modulus. E_i values were calculated from the E_u values by taking the E_u values times a factor of 1.4. The basis for this factor of 1.4 is as follows:

For $\varphi = 0$ conditions, the tangent modulus can be written (Duncan et al. 1980) as

$$E_t = E_i[1 - \frac{R_f(\sigma_1 - \sigma_3)}{2c}]^2 \qquad [6.1]$$

Also, $2c = (\sigma_1 - \sigma_3)_f$ and thus, $\frac{(\sigma_1 - \sigma_3)}{2c} = \frac{(\sigma_1 - \sigma_3)}{(\sigma_1 - \sigma_3)_f} = S$, a strength ratio. Equation 6.1 can be written as

$$E_t = E_i(1 - SR_f)^2 \qquad [6.2]$$

If the tangent modulus at a stress level of 25 percent is assumed to be parallel to the E_u modulus, the ratio of $\frac{E_t}{E_i}$ or $\frac{E_u}{E_i}$ can be determined from Equation 6.2 for known values of R_f. The failure ratio, R_f, was determined by matching hyperbolic stress-strain curves to those from unconsolidated-undrained tests reported by La Rochelle et al (1974). Based on these data, it was determined that a representative factor for initial tangent moduli based on E_u values from UU tests was 1.4. The values of E_i so calculated were used to determine the modulus number K

assuming a modulus exponent of zero. Average K values were selected for each soil layer in the analyses.

In cases where insufficient data was available to define model parameters, the guidelines provided by Duncan et al. (1980) were used to estimate parameter values. The bulk modulus values were chosen to provide a Poisson's ratio value of 0.3 in the foundation soils. Work by Tavenas et al. (1974) on the settlement of embankments at the St. Alban site showed that a value of 0.3 provided much better agreement between calculated and observed settlement than the typical undrained value of 0.49.

6.7.3 Strip Reinforced Embankment

The results of three finite element analyses using CON2D86 are compared to the measured values of settlement, horizontal movement, reinforcement force and piezometric level in Figures 6.8 through 6.11. One analysis, labelled A in the figures, used the soil strength profile based on the average vane shear strength profile shown in Figure 6.1, and P'_o values based on preconsolidation pressures P_{CH} and P_{CV} reported by Tavenas et al. (1974). A second analysis (labelled B) was based on the same shear strength profile, but used P'_o values determined to provide plastic behavior in the elements when the stress level reach 0.6. A third analysis (labelled C), which was performed to represent the unreinforced condition, had the same soil properties as the second analysis.

The data in Figure 6.8 show that analysis A predicted less settlement than was measured. The shape of the settlement curve parallels the

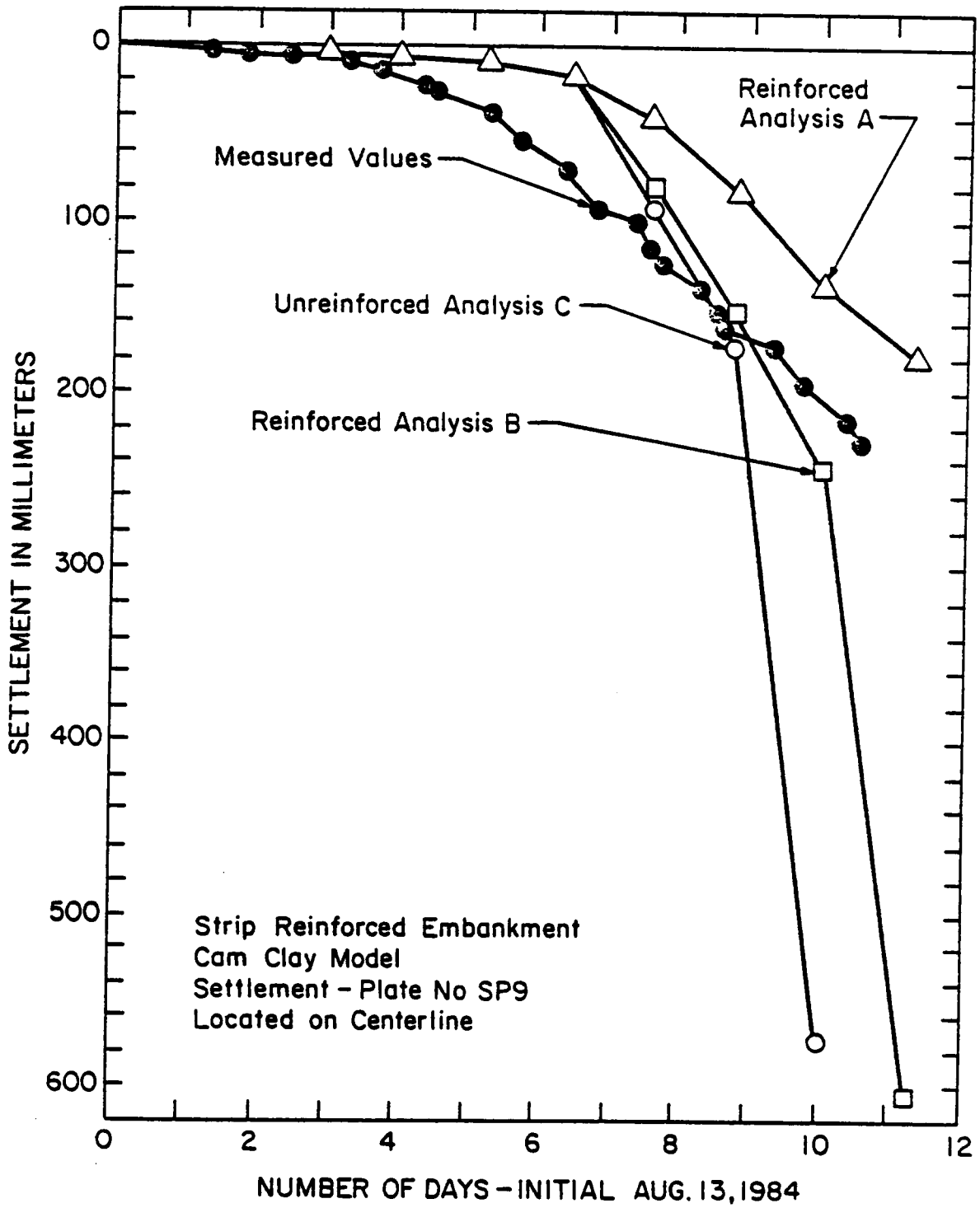

Figure 6.8 Measured settlement behavior of the strip reinforced embankment compared with calculated settlement using CON2D86.

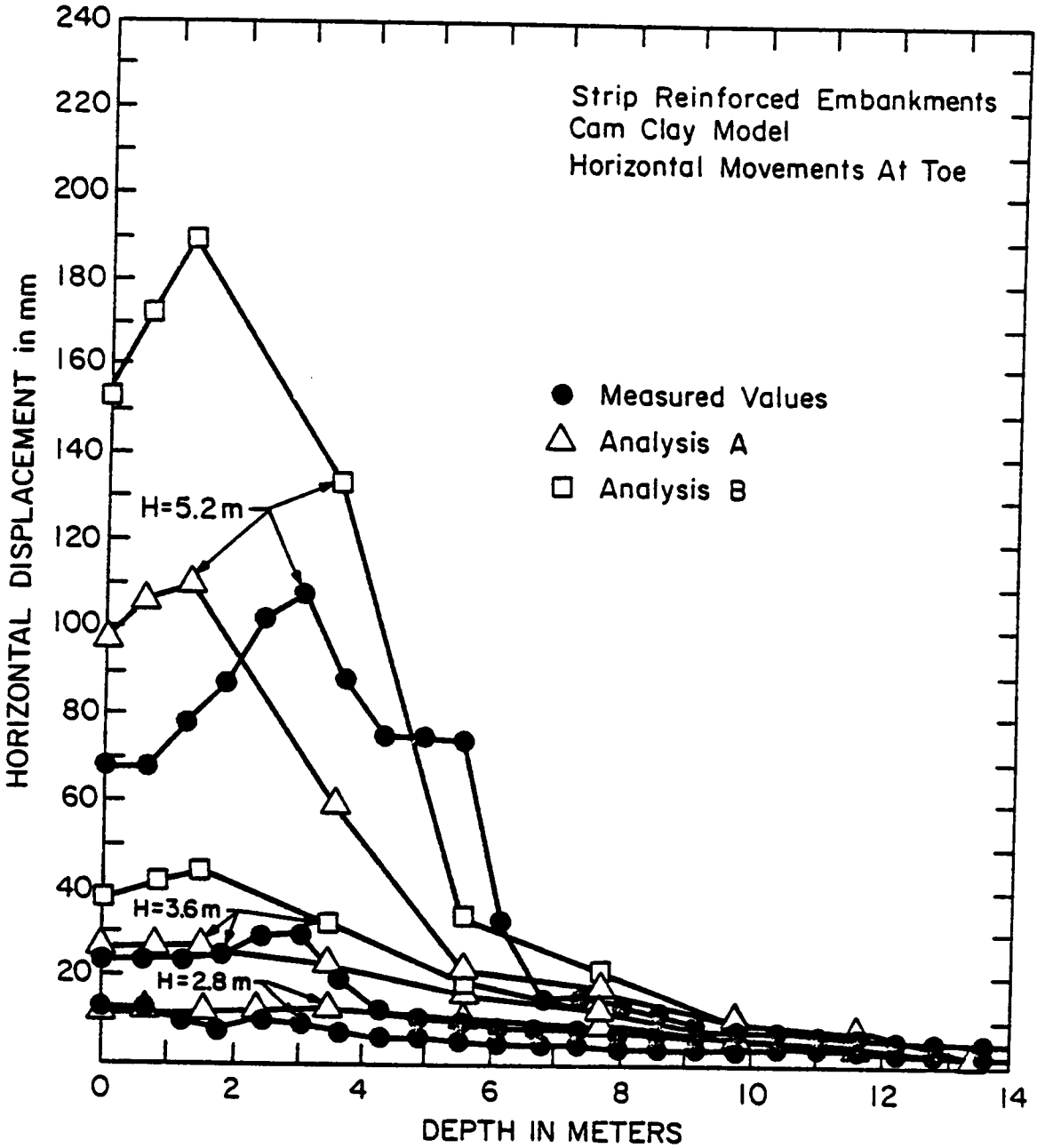

Figure 6.9 Measured horizontal movements at the toe of the strip reinforced embankment compared with calculated values usning CON2D86.

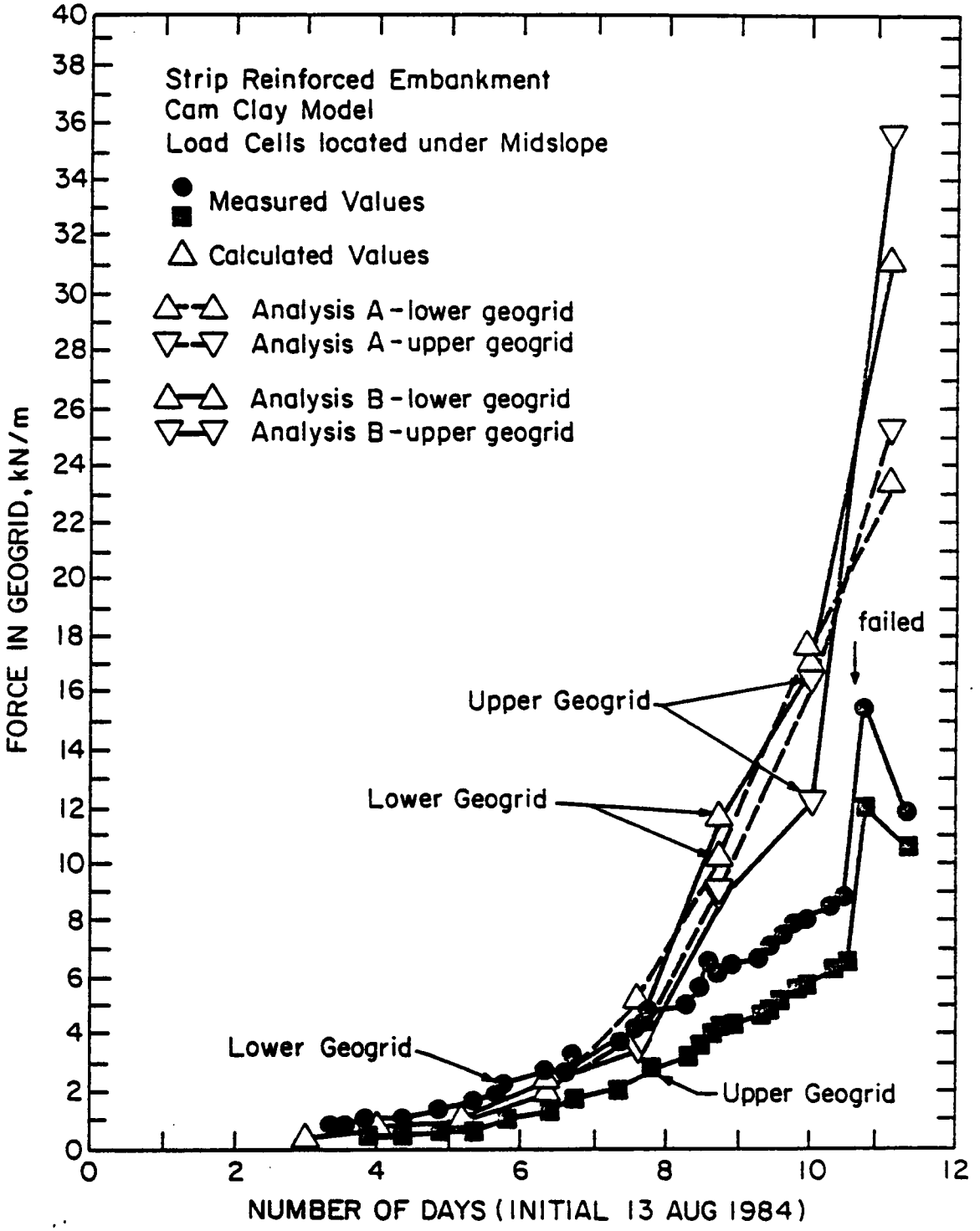

Figure 6.10 Measured geogrid forces in the strip reinforced embankment compared with calculated reinforcement forces using CON2D86.

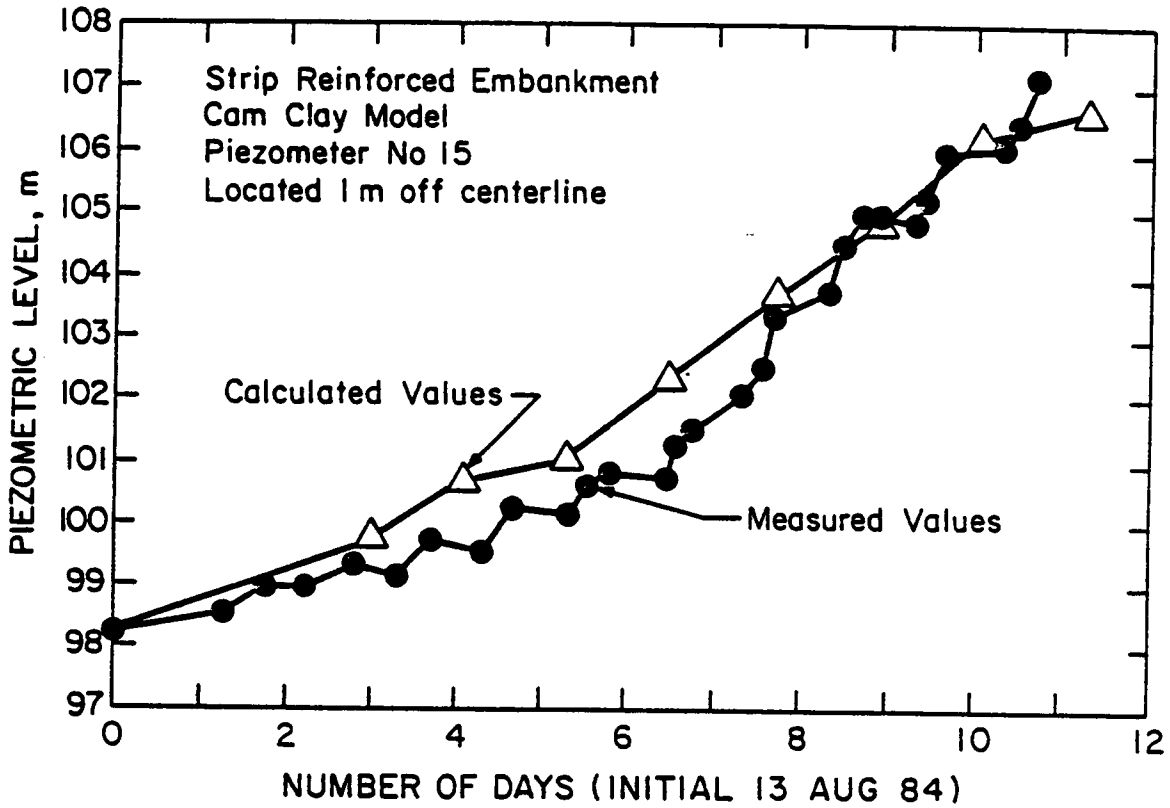

Figure 6.11 Measured piezometric levels in the foundation under the strip reinforced embankment compared with calculated values.

measured data but the downward break occurred at a much higher applied pressure in the analysis. This is believed to be attributable to using too high of values of P'_o in the analysis. An inspection of element behavior in analysis A showed foundation elements to remain in elastic behavior up to stress levels of 0.85. Considering the stress-strain data in Figure 6.3, where plastic behavior begins at a stress level of about 0.6, it was felt that the foundation elements should begin plastic behavior at a comparable stress level in the analysis. This was accomplished by reducing P'_o to cause plastic behavior to begin at a stress level of about 0.6. The consequence of this reduction is apparent in the results for analysis B shown in Figure 6.8.

It may be seen that reducing P'_o resulted in considerably more settlement in the analysis, and better agreement with the measured values. Indeed, with the reduced P'_o in analysis B, failure of the reinforced embankment occurred at a height of 6.0 m, matching the field behavior.

The settlement behavior for analysis C, representing the unreinforced condition, shows large settlements at an embankment height of 5.2 m, which may be interpreted as failure of the embankment. While soil conditions at the control embankment location were slightly different than those at the strip reinforced embankment location, this unreinforced analysis matches well with the observed behavior of the control embankment.

Calculated and measured horizontal deformations are compared in Figure 6.9. In the early stages of construction, the calculated and measured values agree quite well. In analysis A, the absolute magnitude of movement was predicted well, but the precise locations and shape of the

movement profiles differ somewhat from the measured values. In analysis B, the horizontal movements are somewhat larger than those measured. The horizontal movements occurring in the unreinforced analysis were on the order of one meter (five to six times larger than those calculated in analysis B), when the embankment was one meter lower, and are, therefore, too large to be shown in Figure 6.9.

The reinforcement loads measured in two load cells located under the midslope of the embankment are shown in Figure 6.10. The measured forces, which are relatively small, increase as the embankment height increases. At failure, forces of 15.4 and 11.8 kN/m were measured in the lower and upper layers, respectively. It seems likely that the location of the load cells was not appropriate for detecting the maximum force in the reinforcement. The failure surface formed near the axis of the embankment, and the location of greatest stress in the reinforcement would have been close to the centerline. The calculated forces shown in Figure 6.10 correspond to the location of the load cells in the embankment. The calculated forces agree relatively well with measured values in the early stages of construction. When the embankment height increased above four meters, the calculated forces increased significantly, reaching values of about 25 kN/m for analysis A and of about 35 kN/m for analysis B at an embankment height of 6.0 m. In the analyses, the highest reinforcement forces, under the centerline, were about 29 kN/m/layer for analysis A and about 69 kN/m/layer for analysis B. The value of force in analysis B is very close to the strength which could be mobilized in a rapidly loaded sample of Tensar SR2, as may be deduced from Figure 6.4. It seems likely

that a value of force in the range of 65 to 70 kN/m was mobilized in the geogrid at failure, and this load lead to rupture of the geogrid.

The measured and calculated piezometric levels for a piezometer located one meter off of the centerline are shown in Figure 6.11. It may be seen that the calculated and measured values are in very good agreement. Only one calculated curve is shown as the calculated piezometric levels in all three analyses were within 0.2 m of each other. The agreement between calculated and measured values at other locations was similar.

The results of analyses using SSTIPN and the hyperbolic soil model are shown in Figures 6.12, 6.13 and 6.14. From Figure 6.12 it can be seen that the calculated settlement behavior models the measured values very well throughout the analysis. No distinct failure was observed in the analytical results, although numerous elements in the foundation under the embankment and beyond the toe were overstressed. There was very little difference in the settlements calculated in the reinforced and the unreinforced analyses.

Calculated and measured horizontal deformations at the embankment toe are shown in Figure 6.13. The calculated movements at an embankment height of 2.8 m are in quite good agreement with the measured values. However, it cam be seen that at a height of 3.6 m, the calculated values overpredict the horizontal movement, and this trend continues to an embankment height of 5.2 m. The movements which occurred in the analyses at an embankment height of 6.0 m are also shown in Figure 6.13. These

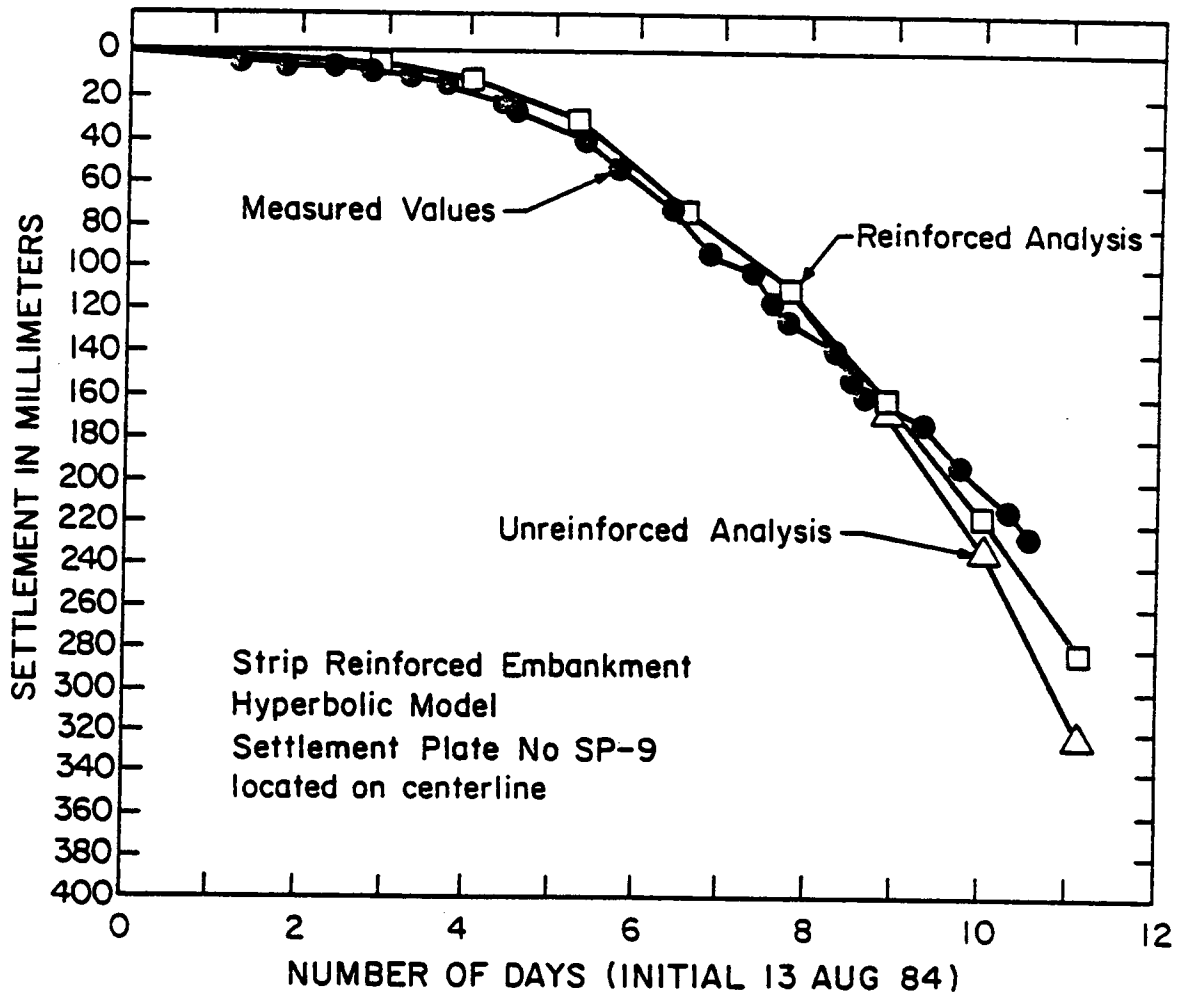

Figure 6.12 Measured settlement behavior of the strip reinforced embankment compared with calculated settlement using SSTIPN.

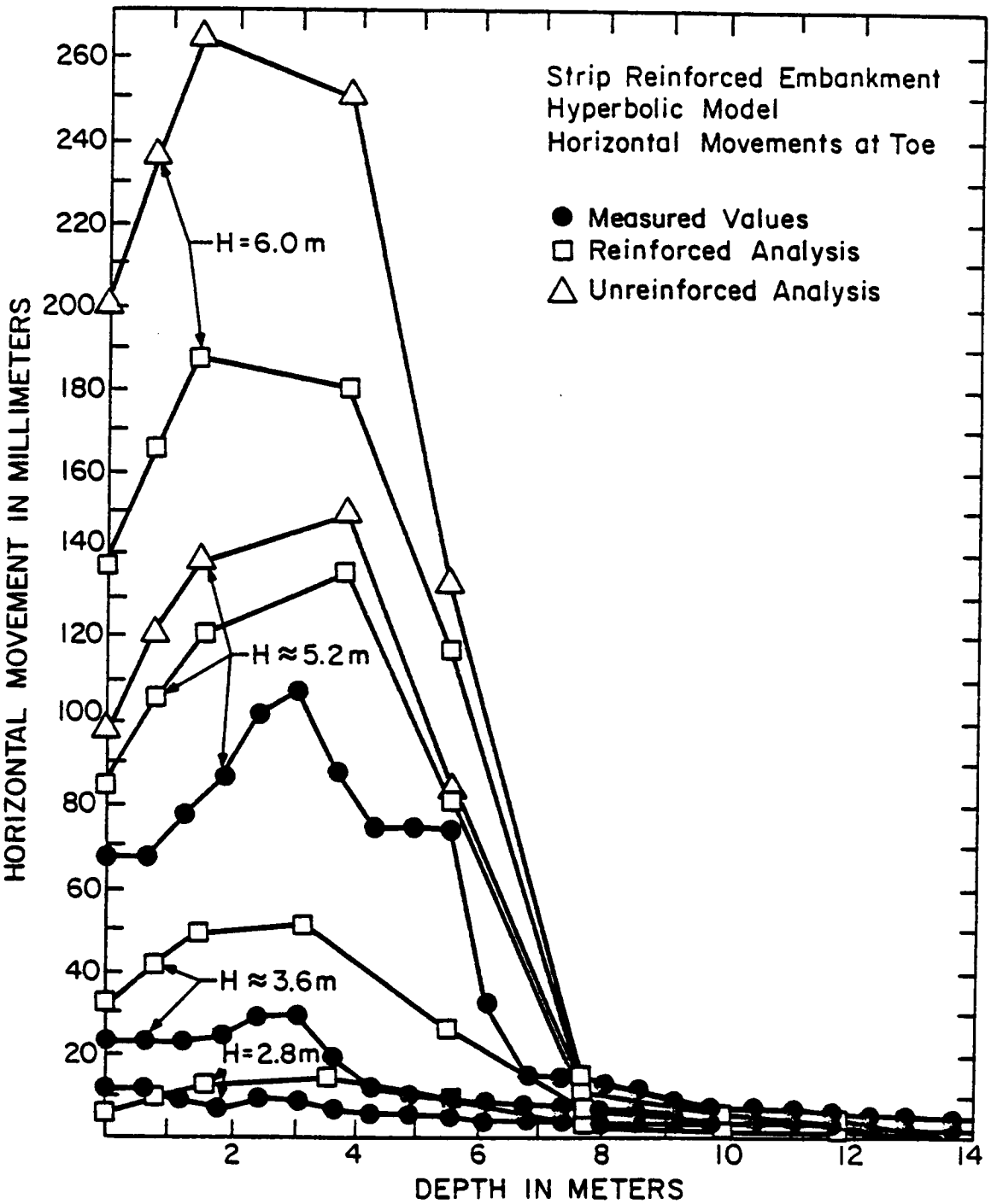

Figure 6.13 Measured horizontal movements at the toe of the strip reinforced embankment compared with calculated values using SSTIPN.

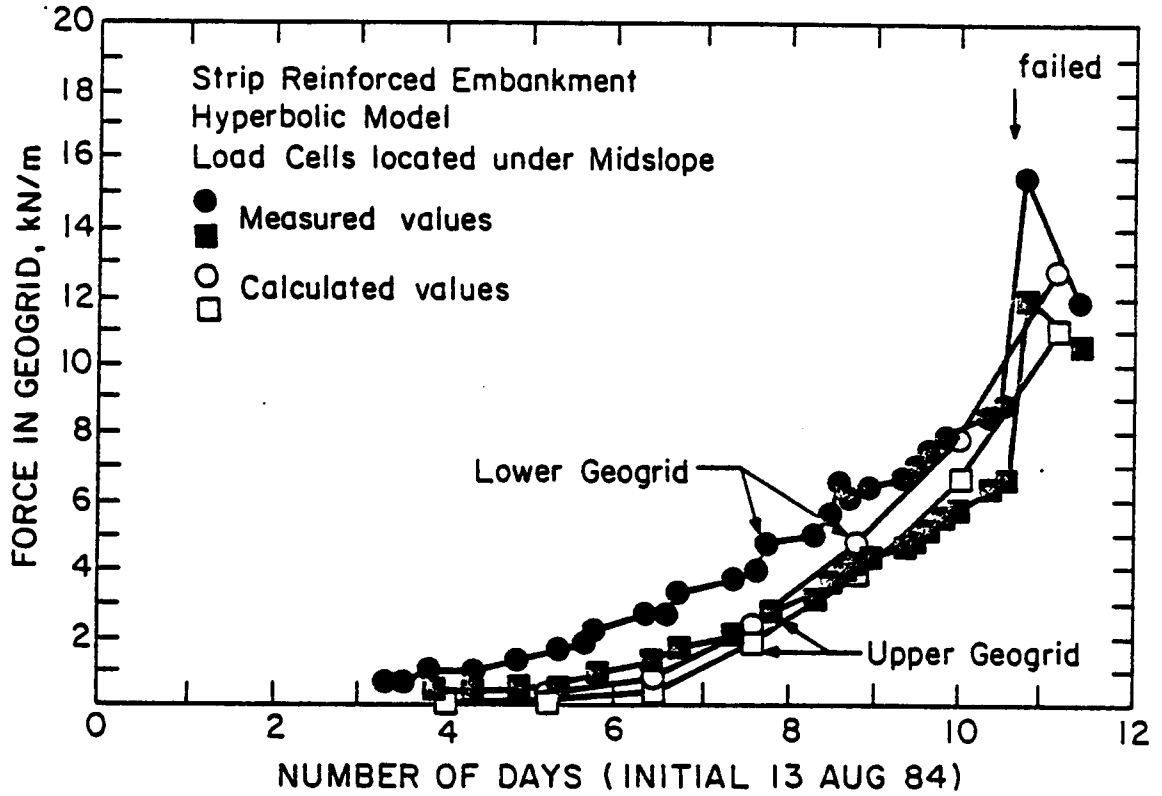

Figure 6.14 Measured geogrid forces in the strip reinforced embankment compared with calculated reinforcement forces using SSTIPN.

movements are quite large, but do not yet represent failed conditions, although the incremental movements are significant.

Finally, the calculated values of geogrid force are compared to the measured values in Figure 6.14. The calculated values underpredict the measured geogrid forces slightly through the entire analysis. It should be noted that geogrid forces do not occur in the analysis until the third load step due to constraints in the program. Thus forces which may have developed in the early stages of construction were not included in the calculated values. The calculated forces in the geogrid under the centerline were 20 and 16 kN/m for the lower and upper layers, about four to eight kN/m greater than the calculated values under the midslope.

6.7.4 Geocell Mattress Embankment

The soil parameters used for the analyses of the geocell mattress using SSTIPG were identical to those used in the SSTIPN analyses of the strip reinforced embankment except for the strength of the clay crust layer. The strength of the clay crust was taken as the mid-depth vane shear strength values reported by Busbridge et al. (1985). These strengths were about 75 percent of the strength of the clay crust at the strip reinforced embankment location.

The results of reinforced and unreinforced analyses of the geocell embankment are shown in Figures 6.15, 6.16 and 6.17. The calculated settlement behavior agrees with the measured values very well. As in the hyperbolic model analyses of the strip reinforced embankment, the forces

calculated in the geocell mattress did not reach failure values. However, large incremental settlements did occur in the analyses when the embankment height was increased to 5.2 m.

The calculated and measured values of horizontal deformation at the toe are compared in Figure 6.16. The agreement is reasonably good, with calculated values being somewhat greater than measured values at an embankment height of 3.6 m. At an embankment height of 4.4, the measured values of horizontal deformation are slightly larger than those calculated. These measured values represent conditions just prior to failure. Failure occurred in the field at an embankment height of 4.6 m. At the embankment heights shown in Figure 6.16, the reinforced and unreinforced analyses show minor differences in the horizontal deformation behavior. When the height in the analyses was increased to 5.2 m, the calculated difference between the reinforced and the unreinforced embankments became more pronounced, with movements at the toe of the unreinforced embankment being about 80 to 100 mm greater than corresponding movements in the reinforced embankment. The differences became significantly larger when the fill height was increased to 6.0 m.

Comparisons of the measured and calculated force in the geogrid are shown in Figure 6.17. Because a composite element was used to represent the geocell mattress, the program SSTIPG does not explicitly provide reinforcement forces. However, the force can be calculated from the strains which occur in any mattress element. it can be seen in Figure 6.17 that the calculated forces are less than those measured. The measured values have an initial force induced at 1.5 days, which was induced during con-

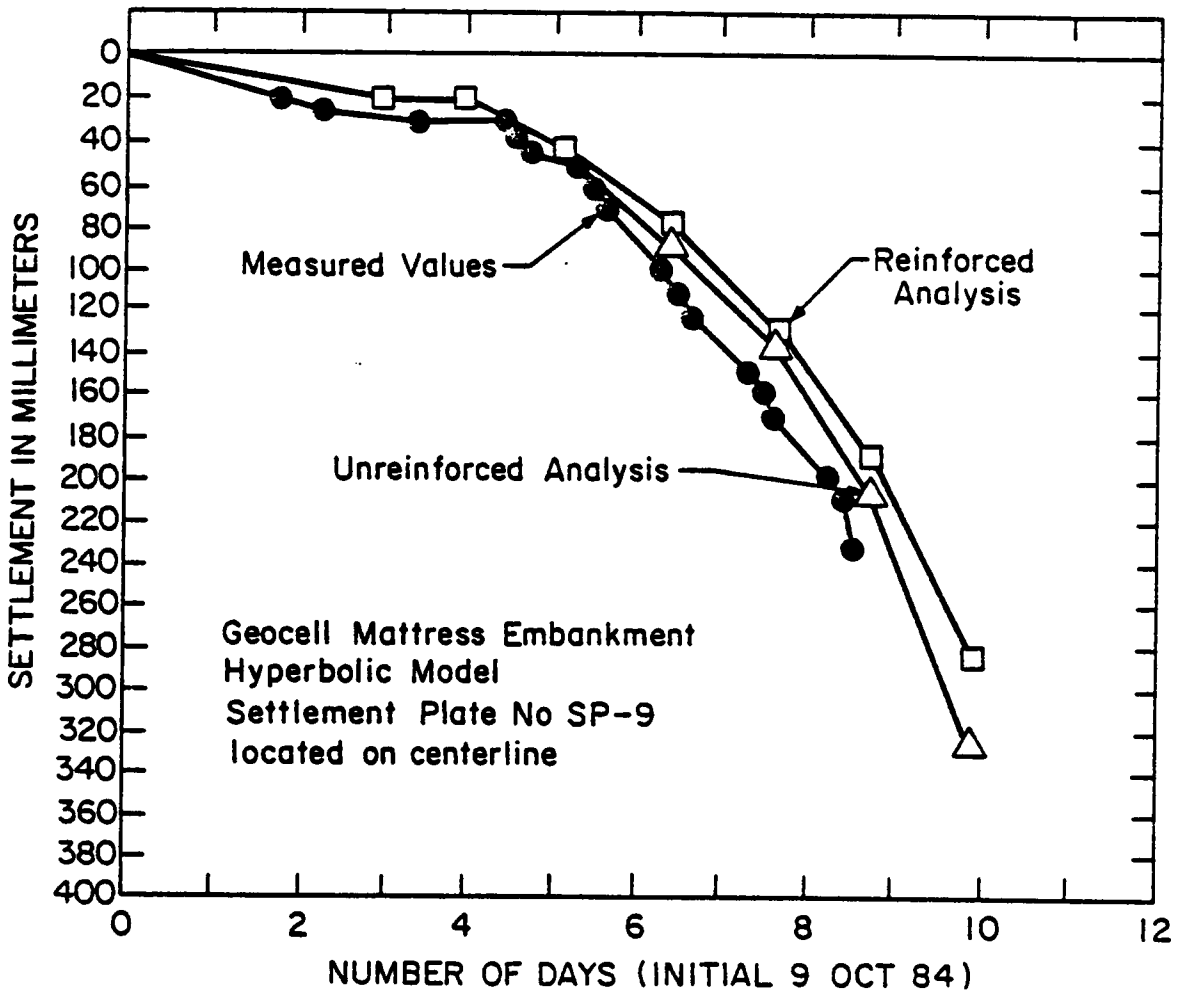

Figure 6.15 Measured settlement behavior of the geocell mattress embankment compared with calculated settlement using SSTIPG.

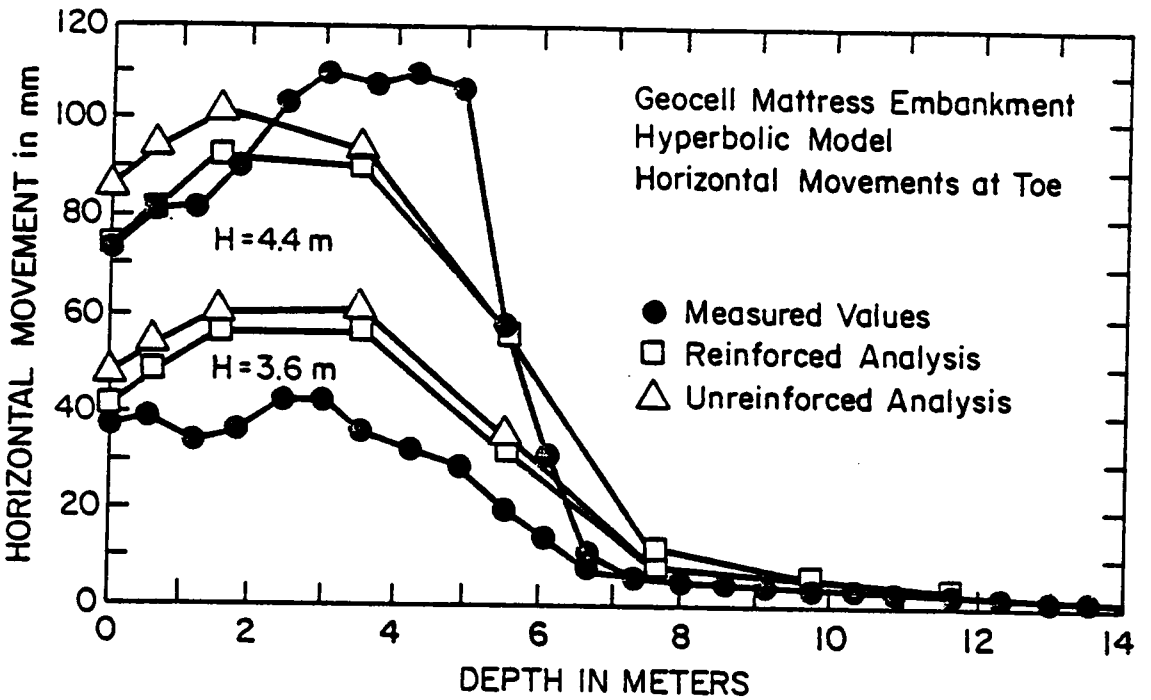

Figure 6.16 Measured horizontal movements at the toe of the geocell mattress compared with calculated horizontal movements using SSTIPG.

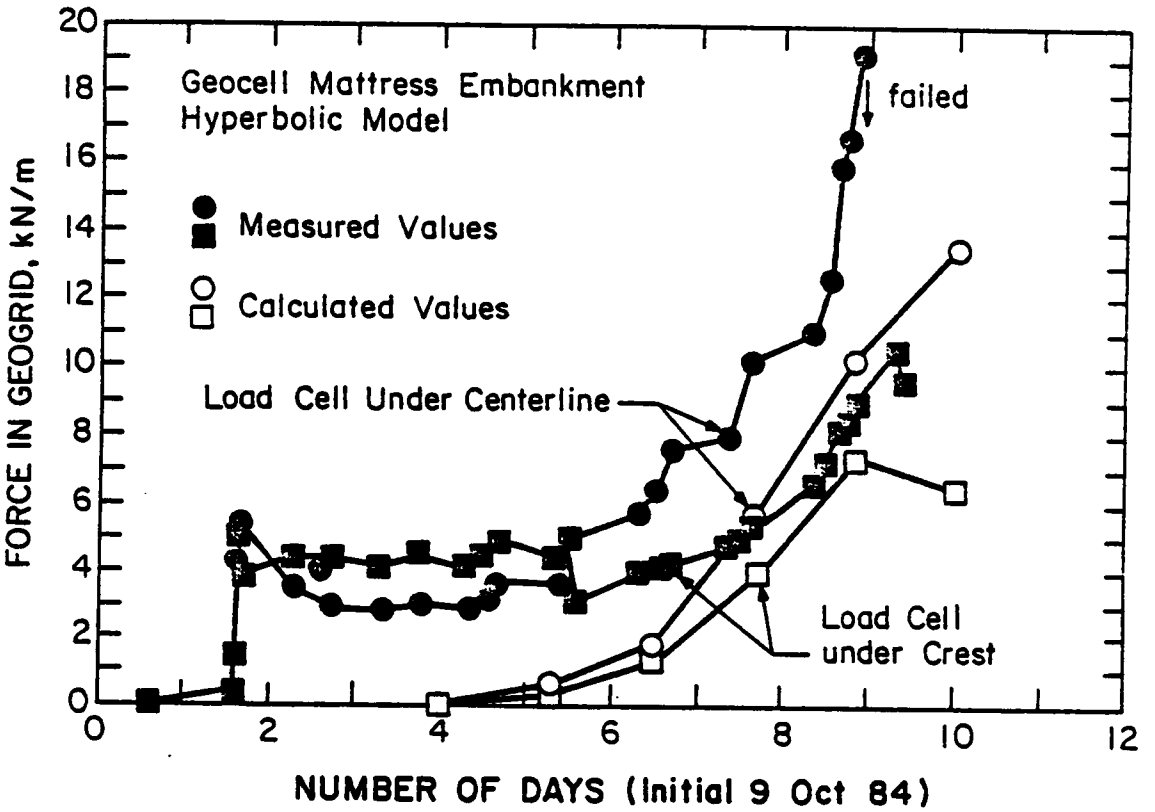

Figure 6.17 Measured geogrid forces in the geocell mattress compared with calculated reinforcement forces using SSTIPG.

struction of the mattress, and this force remains relatively constant until day five (fill height of 2.8 m). If the measured values are shifted to eliminate this initial prestress, the measured and calculated values would agree reasonably well. It may be seen that both the measured and the calculated values show the force at the centerline to be larger than the force under the crest, as would be expected.

The analyses performed do not shed much light on why the geocell mattress embankment failed at a height less than the control embankment. The analyses do show that distress was beginning to occur in the foundation soils at fill heights around 4.5 m. Coupling this with the known brittle behavior of highly sensitive soils, it is reasonable to conclude that failure might occur at any height above about 4.5 m.

6.8 Discussion

The results of the analyses performed using CON2D86 indicate that calculated behavior is very sensitive to the value of mean preconsolidation pressure P'_0 used in the analyses. A somewhat better prediction of settlement behavior was obtained when the P'_0 values used in the analysis were reduced, but this resulted in a less satisfactory prediction of horizontal movements. The forces in the geogrid predicted in these analyses matched measured values well at fill heights less than about four meters. Above this height the analyses showed considerably higher forces than measured in the field.

The results from analyses using the hyperbolic soil model showed remarkable agreement to the measured settlement data and reasonable agreement with the horizontal deformations. This tends to support the method used to determine the modulus numbers from undrained secant moduli. The calculated and measured geogrid forces also matched reasonably well, although the calculated forces were lower than the measured values in the early stages of the analyses. These results demonstrate that this soil model can accurately model the behavior of reinforced soil embankments under working conditions. The determination of a failure height from hyperbolic model analyses needs to be based on the stress levels in elements. On this basis, a continuous band of overstressed elements in the analyses appear to correspond well with the observed field behavior.

The differences obtained between measured and calculated horizontal movements are in agreement with results reported by Poulos (1972). In an analysis of a number of case histories, Poulos found that when good agreement between measured and calculated settlements was obtained, the predicted horizontal movements were greater than those measured. Among the reasons cited for the differences were: the difficulty of estimating Poisson's ratio of the soil; anisotropy, nonlinear stress-strain behavior and nonhomogeniety of the soil; and the neglect of certain factors in the analyses, such as the effect of embankment stiffness and foundation roughness. When changes in the above factors were made, Poulos found that the sensitivity of horizontal movement predictions was considerably more than that of the settlement predictions. The effects of Poisson's ratio,

anisotropy and nonhomogeniety appeared to be the most significant factors.

All the reinforced analyses showed higher geogrid forces under the centerline than under the midslope or crest, and it is felt that similar behavior almost certainly occurred in the field trials. In the CON2D86 analyses, the maximum geogrid load occurred under the centerline and had values of 24 to 29 kN/m for analysis A and about 70 kN/m for analysis B. In analysis B the embankment failed when the height was increased to 6.0 m, which matched the field behavior, and these forces are believed to be representative of the field behavior. The maximum calculated forces in the strip reinforced analysis from SSTIPN were 20 kN/m in the lower layer and 16 kN/m in the upper layer, also occurring under the centerline. These forces are smaller than those determined using CON2D86, as a result of the smaller deformations calculated in these analyses.

Any interpretation of the force mobilized in the geogrid at failure must take account of the orientation of the geogrid when failure occurs. On one hand the orientation at failure can be considered to be horizontal. For this condition, results of stability analyses indicate that a geogrid force of 55 to 60 kN/m-width would be mobilized at failure. In the finite element analyses, the reinforcement force acts in an essentially horizontal direction. The forces calculated at a location consistent with the observed failure surface were about 65 to 70 kN/m at an embankment height of 6.0 m. These results appear to be in good agreement with the stability analyses, and suggest that at failure the mobilized force in

the geogrid was near 60 kN/m. This is a reasonable value based on the load-strain data shown in Figure 6.4.

The calculated behavior of a reinforced embankment is a direct function of the reinforcement modulus input into the analysis. In this study only one modulus value was used. This value is believed to provide a reasonable representation of the field behavior of the geogrid.

6.9 Summary and Conclusions

The goal of the study of the St. Alban embankments was to ascertain if accurate predictions of reinforced embankment behavior could be made using straightforward interpretations of soil data. The analyses performed in this study were accomplished with minimal fine-tuning of the soil parameters. The results of the analyses performed suggest that the behavior of reinforced embankments on sensitive soils can be modelled reasonably well using finite element techniques.

CHAPTER VII

SUMMARY

The studies described herein have been concerned with the development and application of analytical techniques to reinforced soil foundations and embankments over weak soils. The primary analytical employed tool was the finite element method.

During this study an existing finite element computer program was modified for applications to reinforced soil structures. The computer program, CON2D86, was developed for the analysis of stresses, displacements, and consolidation of soil masses. The capability of modelling reinforcement was added through the use of bar elements having axial stiffness but no flexural stiffness. In addition, the program was rewritten to adopt the efficiencies of structured programming, to eliminate errors and unused statements, and to provide additional documentation of the code. An axisymmetric version of the program (CONSAX86) was extended for analysis of reinforced soil structures through the addition of a membrane element which has radial stiffness but no flexural stiffness.

A simplified procedure for computing the bearing capacity of reinforced sand over soft clay was proposed and compared to laboratory model tests. Good agreement with available experimental results was obtained, and based on these comparisons the procedure appears to be suitable for estimating the ultimate bearing capacity of such systems. Additional verification of the proposed method, by comparison with laboratory model

studies and field cases, is desirable. In the meantime, it seems likely that the judicious use of factors of safety with the proposed method should result in satisfactory performance of reinforced foundations.

Finite element analyses of model tests of reinforced sand over weak soils showed good qualitative and fair quantitative agreement with the measured load-displacement behavior, and they agreed well with the observed modes of failure. The analyses show that the presence of the reinforcement reduces the shear stresses in the upper zones of the clay, resulting in increased load carrying capacity of the reinforced sand-clay system. Improved understanding of the effect of the compressibility of the sand and of the initial stresses inherent in compacted sand would provide greater confidences in the use of the finite element technique as a design tool. Currently, a design approach combining the finite element analyses and the proposed bearing capacity analysis technique developed herein should provide a reasonable engineering solution for reinforced sand overlying weak soils.

Two well documented and well instrumented reinforced embankments have analyzed during the course of this investigation. The study of Mohicanville Dike No. 2 included an evaluation of its performance during and shortly after construction, and finite element analyses of its behavior. The observed performance of the dike showed that it is feasible to stabilize embankments as high as 25 feet on weak foundations very effectively using a single layer of reinforcement near the base of the embankment. Comparison of the calculated and measured reinforcement forces indicates that finite element analyses which include the effects

of consolidation provide an effective means of estimating the amount of reinforcing force that would develop during construction, and the rate at which the force would decrease after construction as the foundation soils consolidate.

A study of the effects of ageing of the compacted clay fill on the behavior of Mohicanville Dike No. 2 were inconclusive. While laboratory studies showed that the compacted fill used at Mohicanville would gain strength and increase in stiffness with ageing, finite element analyses showed that increasing the strength and stiffness of the new fill did not change the computed results significantly. When increased strength and stiffness were used in the old fill under the reinforcement as well as the new fill above, the computed and measured behavior were in excellent agreement. However, it seems likely that some stiffening of the soils, perhaps the foundation as well as the embankment soils, did occur over the winter shutdown, probably as a result of consolidation and thixotropy, and that these changes in properties resulted in the changed behavior that was clearly evident in the early stages of the second construction season.

The analyses of the St. Alban test embankments were performed to determine if accurate predictions of reinforced embankment behavior could be made using straightforward interpretations of the soil data. The results of the analyses, for both the Cam Clay model and the hyperbolic model, were in good agreement with the field measurements. The measured geogrid forces, prior to failure of the embankments, were predicted well by the analyses, showing that working conditions can be modelled well by finite element analyses. The finite element analyses did not accurately

model the sudden failure of the brittle sensitive clay, but they did show a large zone of contiguous failed elements at the stage at which failure occurred.

The successful application of the finite element method to these cases shows that the method can be used with some confidence for future projects, as a valid and reliable engineering analysis tool.

7.1 Recommendations for Future Research

7.1.1 Reinforced Foundations.

The use of reinforcement to improve the supporting capacity of layers of sand over weak clay is still in its infancy. A limited number of model test studies have shown that reinforcement can increase the capacity of such systems. However, these model tests have been restricted to relatively small scale, and to a limited number of configurations of reinforcement placement, i.e., a single layer at the sand-clay interface. It appears that further model test studies are warranted, wherein the location, spacing and type of reinforcing are varied to ascertain the consequences of such changes. In conducting model tests, the instrumentation of the reinforcement to gather strain or load data would be desirable to obtain information on the mobilized forces in the reinforcement. This information would aid considerably in fostering improved understanding of the reinforcement-soil interaction mechanism.

Additional work is needed to verify the bearing capacity models proposed. As more experimental data, and perhaps field data, become available, such verification will be possible. The applicability of the general shear failure mechanism requires that the effect of reinforcement on the shear strength of a sand be quantified through experimental work.

7.1.2 Reinforced Embankments

The case history studies have shown that slope stability and finite element techniques can be used effectively in the design and analysis of reinforced embankments. However, questions remain about the behavior of reinforcement in embankments. Conflicting data in the literature concerning pullout resistance indicates that additional work is needed to clarify the effects of sand density and grain size, and geogrid mesh size and strength on the soil-reinforcement mechanism. Additional analyses of case histories are warranted as the data become available to check that slope stability procedures and the finite element method provide reliable and consistent results. The development of simplified design procedures having general applicability is desirable to promote the increased application of reinforcing for stabilizing embankments over weak soils.

REFERENCES

Akinmusuru, J. O. and Akinboldae, J. A. (1981). "Stability of loaded footings on reinforced soil. Journal of the Geotechnical Engineering Division, American Society of Civil Engineers. 107&colonGT6:819-827.

Andrawes, K. A., McGown, A., Wilson-Fahmy, R. F., and Mashhour, M. M. (1982). "The finite element method of analysis applied to soil geotextile systems." Proceedings, Second International Conference on Geotextiles. Las Vegas, Nevada. August 1-6. 3:695-700.

Atkinson, J. H., and Bransby, P. L. (1978). The Mechanics of Soils - An Introduction ot Critical State Soil Mechanics. McGraw-Hill, London.

Barksdale, R. D. and Prendergast, J. E. (1985). "A field study of the performance of a Tensar reinforced haul road." Report to the Tensar Corporation, Georgia Tech Research Project E20-674. Georgia Tech, Atlanta, GA.

Bell, J. R. (1980). "Design criteria for selected geotextile installations." First Canadian Symposium on Geotextiles. Calgary, Alberta, Canada. pp. 35-57.

Bell, J. R., Greenway, D. R. and Vischer, W. (1977). "Construction and analysis of a factic reinforced low embankment on muskeg." Proceedings, First International Conference on the Use of Fabrics and Geotechnics. Paris. pp.71-76.

Belloni, L. and Sembenelli, P. (1977). "Road embankments on compressible soils constructed with the aid of synthetic fabrics." (in French). Proceedings, First International Conference on the Use of Fabrics in Geotechnics. Paris, 20-22 April. 1:49-54.

Bender, D. A. and Barenberg, E. J. (1978). "Design and behavior of soil-fabric-aggregate systems." Transportation Research Board, Transportation Research Record 671, p 64-75.

Binquet, J. and Lee, K. L. (1975). "Bearing capacity tests on reinforced earth slabs." Journal of the Geotechnical Engineering Division, American Society of Civil Engineers. 101:GT12:1241-1255.

Bishop, A. W. (1955). "The use of the slip circle in the stability analysis of earth slopes." Geotechnique 5:1:7-17.

Bjerrum, L. (1972). "Embankments on soft ground." Proceedings, Specialty Conference on Performance of Earth and Earth-Supported Structures. American Society of Civil Engineers. Purdue University, Lafayette, Indiana. June 11-14. 2:1-54.

Booker, J. R. and Small, J. C. (1975). "An investigation of the stability of numberical solutions of Biot's equations of consolidation." International Journal for Solids and Structures, 11:907-917.

Boutrup, E. and Holtz, R. D. (1983). "Analysis of embankments on soft ground reinforced with geotextiles." Proceedings, Eigth European Conference on Soil Mechanics and Foundation Engineering. Helsinki. May 23-26. 2:469-472.

Bozozuk, M. (1963). "The modulus of elasticity of Leda clay from field measurements." Canadian Geotechnical Journal, 1:1:43-51.

Brakel, J., Coppens, M., Maagdenberg, A. C. and Risseeuw, P. (1982). "Stability of slopes constructed with polyester reinforcing fabric, test section at Almere, Holland, '79." Proceedings, Second International Conference on Geotextiles. Las Vegas, Nevada. August 1-6. 3:727-732.

Broms, B. B. (1977). "Polyester fabric as reinforcement in soil." Proceedings, First Internaltional Conference on the Use of Fabrics in Geotechnics. Paris. April 20-22. 1:129-135.

Brown, B. S. and Poulos, H. G. (1978). "Finite element analysis of reinforced embankments." Proceedings, Symposium on Soil Reinforcing and Stabilizing Techniques. Sydney, Austrailia. pp 233-252.

Burland, J. B. (1967). "Deformation of soft clay." Ph.D. Thesis, Cambridge University, England.

Busbridge, J. R., Chan, P., Milligan, V., La Rochelle, P. and Lefebvre, L. D. (1985). Draft Report on "The effect of geogrid reinforcement on the stability of embankments on a soft sensitive Champlain clay deposit." Prepared for the Transportation Development Centre, Montreal, Quebec by Golder Associates and Laval University.

Casagrande, A. (1936). "Characteristics of cohesionless soils affecting the stability of earth slopes." Journal of the Boston Society of Civil Engineers, January. Reprinted in Contributions to Soil Mechanics 1925-1940, BSCE. pp 257-276.

Casagrande, A., Hirschfeld, R. C. and Poulos, S. J. (1963). "Third Progress Report on Investigation of Stress-Deformation and Strength Characteristics of Compacted Clay." Soil Mechanics Series No. 70, Harvard University, Cambridge, Massachusetts. November.

Chang, C-S. and Duncan, J. M. (1977). "Analysis of consolidation of earth and rockfill dams." Report No. TE77-3 to U. S. Army Engineers Waterways Experiment Station. College of Engineering, University of California, Berkeley. September.

Chen, Z. (1984). Private communication to Dr. J. M. Duncan.

Christie, I. F. and El-Hadi, K. M. (1977). "Some aspects of the design of earth dams reinforced with fabric." Proceedings, First Internaltional Conference on the Use of Fabrics in Geotechnics. Paris. April 20-22. 1:99-103.

Christian, J. T. (1977). "Two- and three- dimensional consolidation." Chapter 12 in Numerical Methods in Geotechnical Engineering, Edited by C. S. Desai and J. T. Christian. McGraw-Hill, New York.

Christopher, B. R. and Holtz, R. D. (1984). "Geotextile Engineering Manual." Federal Highway Administration, National Highway Institute, Washington, D.C. 917 pages.

Collios, A., Delmas, P., Gourc, J. P. and Giroud. J. P. (1980). "Experience on soil reinforcement with geotextiles." The Use of Geotextiles for Soil Improvement, 80-177, ASCE National Convention, (Portland, Oregon, April, 17), 53-73.

Collins, S. A. (1986). "Analysis of instrumentation and evaluation of embankment performance: Mohicanville Dike No. 2." Report to the Huntington District Corps of Engineers, Huntington, West Virginia. June.

Collins, S. A., Rogers, W. and Sowers, G. F. (1982). "Report of Embankment Reanalysis - Mohicanville Dikes." Report for Department of the Army, Huntington District Corps of Engineers, Huntington, West Virginia, by Law Engineering Testing Company, July.

Dafalias, Y. F. and Herrmann, L. R. (1982). "Bounding surface formulation of soil plasticity." In Soil Mechanics - Transient and Cyclic Loads, ed. by Ziekiewicz, O. C. and Pande, G. W. John Wiley and Sons, New York. pages 253-282.

Davis, E. H. (1968). "Theories of plasticity and failure of soil masses." Chapter 6 in Soil Mechanics - Selected Topics, Ed. by I. K. Lee. Butterworths, London. pp. 341-380.

Dhowian, A. W. and Edil, T. B. (1980). "Consolidation behavior of peats." Geotechnical Testing Journal, 3:3:105-114.

D'Orazio, T. B. and Duncan, J. M. (1982). "CONSAX: A computer program for axisymmetric finite element analysis of consolidation." Report

No. UCB/GT/82-01, College of Engineering, Univerity of California, Berkeley. April.

Dove, J. E. (1986). "The design and construction of a large plane strain apparatus for testing reinforced soil specimans." Masters Thesis, Virginia Polytechnic Institue and State University, Blacksburg, VA. April.

Drucker, D. C., Gibson, R. E., and Henkel, D. J. (1957). "Soil mecahnics and work-hardening theories of plasticity." Transactions, American Society of Civil Engineers, 122:338-346.

Duncan, J. M. (1972). "Finite element analyses of stresses and movements in dams, excavations and slopes." State-of-the-Art Report, Symposium on Applications of the Finite Element Method in Geotechnical Eningeering, U. S. Army Waterways Experiment Station, Vicksburg, MS 1-4 May.

Duncan, J. M., and Chang, C-Y. (1970). "Nonlinear analysis of stress and strain in soils." Journal of the Soil Mechanics and Foundations Division, American Society of Civil Engineers, 96:SM5:1693-1653. September.

Duncan, J. M., Byrne, P., Wong, K. S. and Mabry, P. (1980). "Strength, stress-strain and bulk modulus parameters for finite element analysis of stresses and movements in soils." Geotechnical Engineering Research Report No. UCB/GT/80-01, Department of Civil Engineering, University of California, Berkeley. August.

Duncan, J. M., D'Orazio, T. B., Chang, C-S., Wong, K. S., and Namiq, L. (1981). "CON2D: A finite element computer program for analysis of consolidation." Report No. UCB/GT/81-01, College of Engineering, University of California, Berkeley. March.

Duncan, J. M., Low, B. K. and Schaefer, V. R. (1985). "STABGM: A computer program for slope stability analysis of reinforced embankments and slopes." Report No. VPI&SU/CE-GT-85-09. Department of Civil Engineering, Virginia Polytechnic Institute and State University. September.

Edil, T. B. and Dhowian, A. W. (1981). "At-rest lateral pressure of peat soils." Journal of the Geotechnical Engineering Division, American Society of Civil Engineers. 107:GT2:201-217.

Fowler, J. (1982). "Theoretical design considerations for fabric-reinforced embankments." Proceedings, Second International Conference on Geotextiles. Las Vegas, Nevada. August 1-6. 3:665-670.

Fowler, J., Leach, R. E., Peters, J. F. and Horz, R. C. (1983). "Mohicanville Reinforced Dike No. 2. - Design Memorandum."

Geotechnical Laboratory, U. S. Army Waterways Experiment Station, Vicksbury, Mississippi. September.

Fragazy, R. J. and Lawton, E. (1984). "Bearing capacity of reinforced sand subgrades." Journal of the Geotechnical Engineering Division, American Society of Civil Engineers. 110:GT10:1500-1506.

Giroud, J.-P. and Noiray, L. (1981). "Geotextile-reinforced unpaved road design." Journal of the Geotechnical Engineering Division, American Society of Civil Engineers. 107:GT9:1233-1254.

Giroud, J.-P., Ah-Line, C. and Bonaparte, R. (1984). "Design of unpaved roads and trafficked areas." Proceedings, Symposium on Polymer Grid Reinforcement in Civil Engineering. London. March 22-23. Paper No. 4.1.

Guido, V. A., Biesiadecki, G. L. and Sullivan, M. J. (1985a). "Bearing capacity of a geotextile-reinforced foundation." Proceedings, Eleventh International Conference on Soil Mechanics and Foundation Engineering. San Francisco. August 12-16. 3:1777-1780.

Guido, V. A., Chang, D. K. and Sweeney, M. A. (1985b). "Bearing capacity of shallow foundations reinforced with geogrids and geotextiles." Proceedings, Second Canadian Symposium on Geotextiles and Geomembranes, Edmonton, Alberta. September 23-24. p 71-77.

Haliburton, T. A., Fowler, J. and Langan, J. P. (1980). "Design and construction of fabric-reinforced embankment test section, Pinto Pass, Mobile, Alabama." Transportation Research Record 749. Transportation Research Board, National Academy of Sciences, Washington, D.C. pp27-34.

Haliburton, T. A., Lawmaster, J. D. and McGuffey, V. E. (1982). "Use of Engineering Fabric in Transportation Related Applications." Final Report under Contract No. DTFH-80-C-0094, Federal Highway Administration, National Highway Institute, Washington, D.C.

Hanna, A. M. and Meyerhof, G. G. (1980). "Design charts for ultimate bearing capacity of foundations on sand overlying soft clay." Canadian Geotechnical Journal. 17:2:300-303.

Herrmann, L. R. (1984). "Four node beam-membrane type element for two-dimensional modeling of Tensar geogrids for bearing capacity applications." Notes and FORTRAN routine for the SAC-2 Code, Department of Civil Engineering, University of California, Davis.

Herrmann, L. R. and Al-Yassin, Z. (1978). "Numerical analysis of reinforced soil systems." Proceedings, Symposium on Earth Reinforcement, American Society of Civil Engineers Annual Meeting, Pittsburg, PA. April 27.

Holtz, R. D. (1977). "Laboratory studies of reinforced earth using a woven polyester fabric." Proceedings, First International Conference on the Use of Fabrics in Geotechnics. Paris. April 20-22. 3:149-154.

Hwang, C. T., Morgenstern, N. R. and Murray, D. W. (1971). "On solution of plane strain consolidation problems by finite element methods." Canadian Geotechnical Journal, 8colon.1:109-118.

Ingold, T. S. (1982a). "An analytical study of geotextile reinforced embankments." Proceedings, Second International Conference on Geotextiles. Las Vegas, Nevada. August 1-6. 3:683-688.

Ingold, T. S. (1982b). "Some observations on the laboratory measurement of soil-geotextile bond." Geotechnical Testing Journal, GTJODJ, 5:3/4:57-67.

Ingold, T. S. (1983). "Laboratory pull-out testing of grid reinforcments in sand." Geotechnical Testing Journal, GTJODJ, 6:3:101-111.

Jarrett, P. M. (1984). "Evaluation of geogrids for construction of roadways over muskeg." Proceedings, Symposium on Polymer Grid Reinforcement in Civil Engineering. London. March 22-23. Paper No. 4.5.

Jewell, R. A. (1982). "A limit equilibrium design method for reinforced embankments on soft ground." Proceedings, Second International Conference on Geotextiles. Las Vegas, Nevada. August 1-6. 3:665-670.

Jewell, R. A. (1985). "Limit equilibrium analysis of reinforced soil walls." Proceedings, Eleventh Internaltional Conference on Soil Mechanics and Foundation Engineering. San Francisco. August 12-16. 3:1705-1708.

Jewell, R. A., Milligan, G. W. E., Sarsby, R. W. and Dubois, D. (1984). "Interaction between soil and geogrids." Proceedings, Symposium on Polymer Grid Reinforcement in Civil Engineering. London. March 22-23. Paper No. 1.3.

Jewell, R. A., Paine, N. and Woods, R. I. (1984). "Design methods for steep reinforced embankments." Proceedings, Symposium on Polymer Grid Reinforcement in Civil Engineering. London. March 22-23. Paper No. 3.1.

Jones, C. J. F. P., and Edwards, L. W. (1980). "Reinforced earth structures situated on soft foundation." Geotechnique 30:2:207-213.

Jones, C. J. F. P. (1985). Earth Reinforcement and Soil Structures. Butterworths, London.

Jurgenson, L. (1934). "The shearing resistance of soils." Journal of the Boston Society of Civil Engineers. July.

Kernighan, B. W. and Plauger, P. J. (1974). The Elements of Programming Style. McGraw-Hill, New York.

Kraft, L. M. and Helfrich, S. C. (1983). "Bearing capacity of shallow footing, sand over clay." Canadian Geotechnical Journal. 20:1:182-185.

Kroshus, J. B. and Varcoe, B. E. (1984). "Geogrid applications in the construction of oilfield pads and access areas in muskeg regions of northern Alberta." Proceedings, Symposium on Polymer Grid Reinforcement in Civil Engineering. London. March 22-23. Paper No. 4.4.

Lambe, T. W. and Whitman, R. V. (1979). Soil Mechanics. John Wiley and Sons. New York.

Landva, A. O. and La Rochelle, P. (1983). "Compressibility and shear characteristics of Radforth peats." Testing of Peats and Organic Soils, ASTM STP 820. P. M. Jarrett, Ed., American Society for Testing and Materials, pp. 157-191.

La Rochelle, P. and Lefebrve, G. (1971). "Sampling disturbance in Champlain clays." Sampling of Soil and Rock, ASTM STP 483, American Society for Testing and Materials. pp. 143-163.

La Rochelle, P., Trak, B., Tavenas, F. and Roy, M. (1974). "Failure of a test embankment on a sensitive Champlain clay desposit." Canadian Geotechnical Journal, 11:1:142-164.

Lee, K. L., Adams, B. D. and Vageron, J.-M. M. (1973). "Reinforced earth retaining walls." JSMFD, ASCE. 99:SM10::745-764.

Lefebrve, G. and La Rochelle, P. (1974). "The analyseis of slope failures in cemented Champlain clays." Canadian Geotechnical Journal, 11:1:89-108.

Lefebrve, G., Langlois, P., Lupien, C. and Lavallee, J.-G. (1984). "Laboratory testing and in situ behaviour of peat as embankment foundation." Canadian Geotechnical Journal, 21:2:322-337.

Leshchinsky, D. (1984). "Geotextile reinforced earth." Part I & II, Research Report Nos. CE 84-44/45. Department of Civil Engineering, University of Delaware, Newark, Delaware. July.

Leshchinsky, D. and Volk, J. C. (1985). "Stability charts for geotextile reinforced walls." Preprint, 64th Annual Meeting of the Transportation Research Board, Washington, D.C. January.

Low, B. K. (1985). "Analysis of the behavior of reinforced embankments on weak foundations." Thesis presented to the Unversity of California, Berkeley in partial fulfillment of the requirements for the degree of Doctor of Philosophy. 274 pages.

Low, B. K. and Duncan, J. M. (1985). "Analysis of the behavior of reinforced embankments on weak foundations." Report No. VPI&SU/CE-GT-85-09. Department of Civil Engineering, Virginia Polytechnic Institute and State University. September. California, Berkeley in partial fulfillment of the requirements for the degree of Doctor of Philosophy. 274 pages.

Maagdenberg, A. C. (1977). "Fabrics below sand embankments over weak soils, their technical specificaitons and their application in a test area." Proceedings, First International Conference on the Use of Fabrics in Geotechnics. Paris, 20-22 April. 1:49-54.

MacFarland, I. C. (1969). Muskeg Engineering Handbook. The Muskeg Subcommittee of the NRC Associate Committee on Geotechnical Development, University of Toronto Press, Toronto, Ont.

Majes, B. and Battelino, D. (1985). "Effect of surface reinforcing of soft soils." Proceedings, Eleventh International Conference on Soil Mechanics and Foundation Engineernig. San Francisco. August 12-16. 3:1729-1734.

Mayne, P. W. (1980). "Cam-clay predictions of undrained strength." Journal of the Geotechnical Engineering Division, American Society of Civil Engineers. 106:GT11:1219-1242.

McGown, A., Andrawes, K. Z. and Al-Husani, M. M. (1978). "Effect of inclusion properties on the behavior of sands." Geotechnique 28:3::327-346.

McGown, A., Andrawes, K. Z., Mashhour, M. M., and Myles. B. (1981). "Strain behavior of soil-fabric model embankments." Proceedings, Tenth International Conference on Soil Mechanics and Foundation Engineering. Stockholm. June 15-19. 3:739-744.

McGown, A., Paine, N. and DuBois, D. D. (1984). "Use of geogrid properties in limit equilibrium analysis." Proceedings, Symposium on Polymer Grid Reinforcement in Civil Engineering. London. March 22-23. Paper No. 1.4.

Meyerhof, G. G. (1974). "Ultimate bearing capacity of footings on sand layer overlying clay." Canadian Geotechnical Journal. 11:2:223-229.

Milligan, G. W. E. and Love, J. P. (1984). "Model testing of geogrids under an aggregate layer on soft ground." Proceedings, Symposium

on Polymer Grid Reinforcement in Civil Engineering. London. March 22-23. Paper No. 4.2.

Milligan, V. and La Rochelle, P. (1984). "Design methods for embankments over weak soils." Proceedings, Symposium on Polymer Grid Reinforcement in Civil Engineering. London. March 22-23. Paper No. 3.4.

Mitchell, J. K. (1960). "Fundamental aspects of thixotropy in soils." Journal of the Soil Mechanics and Foundations Division, American Society of Civil Engineers, 86:SM3:19-52. June.

Mitchell, R. J. (1970). "On the yielding and mechanical behavior of Leda clay." Canadian Geotechnical Journal, 7:3:297.

Murray, R. (1982). "Fabric reinforcement of embankments and cuttings." Proceedings, Second International Conference on Geotextiles. Las Vegas, Nevada. August 1-6. 3:707-713.

Pender, M. J. (1978). "A model for the behavior of overconsolidated soil." Geotechnique, 28:1:1-25.

Pilot, G., Trak, B. and La Rochelle, P. (1982). "Effective stress analysis of the stability of embankments on soft soils." Canadian Geotechnical Journal, 19:2:433-450.

Poran, C. J. (1985). "Bearing capacity of geogrid-reinforced granular-base overlying soft clay." Thesis presented to the Unversity of California, Davis in partial fulfillment of the requirements for the degree of Doctor of Philosophy.

Poulos, H. G. (1972). "Difficulties in prediction of horizontal deformations in foundations." Journal of the Soil Mechanics and Foundations Division, American Society of Civil Engineers, 98:SM8:843-848.

Poulos, H. G. (1972). Lecture Notes, CE 6500, Theoretical Soil Mechanics, Virginia Polytechnic Institute and State University, Fall Quarter.

Quigley, R. M. and Thompson, C. D. (1966). "The fabric of anisotropically consolidated marine clay." Canadian Geotechnical Journal. 3:2:

Reddy, J. N. (1984). An Introduction to the Finite Element Method. McGraw-Hill, New York.

Reed, M. B. (1984). "An invesitgation of numerical errors in the analysis of consolidation by finite elements." International Journal for Numerical and Analytical Methods in Geomechanics, 8:243-257.

Roscoe, K. H., Schofield, A. N. and Wroth, C. P. (1958). "On the yielding of soils." Geotechnique 8:1:25-53.

Roscoe, K. H., and Schofield, A. N. (1963). "Yielding of clays in states wetter than critical." Proceedings, Second European Conference on Soil Mechanics and Foundation Engineering, Wiesbaden. 1:47-54.

Roscoe, K. H., Schofield, A. N. and Thurairajah, A. (1963). "Yielding of soils in states wetter than critical." Geotechnique 13:3:211-240.

Roscoe, K. H. and Burland, J. B. (1968). "On the generalized stress-strain behavior of 'wet' clay." in Engineering Plasticity, Cambridge University Press, London. pp. 535-609.

Rowe, R. K., Booker, J. R. and Balaam, N. P. (1978). "Application of the initial stress method to soil-structure interaction." Internation Journal for Numerical Methods in Engineering. 12:5:873-880.

Rowe, R. K. (1982). "The analysis of an embankment constructed on a geotextile." Proceedings, Second International Conference on Geotextiles. Las Vegas, Nevada. August 1-6. 3:677-682.

Rowe, R. K. (1984). "Reinforced embankments: analysis and design." American Society of Civil Engineers, Journal of Geotechnical Engineering Division. 110:2:231-246.

Rowe, R. K., MacLean, M. D. and Barvary, A. K. (1984). "The observed behaviour of a geotextile-reinforced embankment constructed on peat." Canadian Geotechnical Journal, 21:2:289-304.

Rowe, R. K., MacLean, M. D. and Soderman, K. L. (1984). "Analysis of a geotextile-reinforced embankment constructed on peat." Canadian Geotechnical Journal, 21:3:563-576.

Rowe, R. K. and Soderman, K. L. (1984). "Comparison of predicted and observed behaviour of two test embankments." Geotextiles and Geomembranes 1:2:143-160.

Rowe, R. K. and Soderman, K. L. (1985). "An approximate method for estimating the stability of geotextile-reinforced embankments." Canadian Geotechnical Journal, 22:3:392-398.

Rowe, R. K., Ho, S. K. and Fisher, D. G. (1985). "Determination of soil-geotextile interface strength properties." Second Canadian Symposium on Geotextiles, Edmonton. September.

Sandhu, R. S. and Wilson, E. L. (1969). "Finite element analysis of seepage in elastic media." Journal of the Soil Mechanics and Foun-

dations Division, American Society of Civil Engineers, 83:SM4:641-652.

Sandhu, R. S., Liu, H. and Singh, K. J. (1977). "Numerical performance of some finite element schemes for ananlysis of seepage in porous elastic media." International Journal for Numerical and Analytical Methods in Geomechanics, 1:177-194.

Sarma, S. K. (1973). "Stability analysis of embankments and slopes." Geotechnique 23:3:423-433.

Schofield, A. N. and Wroth, C. P. (1968). Critical State Soil Mechanics. McGraw-Hill, London.

Seed, H. B. and Chan, C. K. (1957). "Thixotropic characteristics of compacted clay." Journal of the Soil Mechanics and Foundations Division, American Society of Civil Engineers, 83:SM4:1-35. November.

Seed, H. B., Mitchell, J. K. and Chan, C. K. (1960). "The strength of compacted cohesive soils." Proceedings, Research Conference on Shear Strength of Cohesive Soils. American Society of Civil Engineers. June.

Seed, R. B. and Duncan, J. M. (1983). "Soil-structure interaction effects of compaction-induced stresses and deflection." Department of Civil Engineering, University of California, Berkeley.

Tavenas, F., Chapeau, C., La Rochelle, P. and Roy, M. (1974). "Immediate settlements of three test embankments on Champlain clay." Canadian Geotechnical Journal, 11:1:109-141.

Tavenas, F. and Leroueil, S. (1980). "The behavior of embankments on clay foundations." Canadian Geotechnical Journal, 17:2:236-260.

Tavenas, F., Jean, P., Leblond, P. and Leroueil, S. (1983). "The permeability of natural soft clays, Part II: Permeability characteristics." Canadian Geotechnical Journal, 20:4:645.

Tcheng, Y. (1957). "Fondations superficielles en milieu stratifie." Proceedings, Fourth International Conference on Soil Mechanics and Foundation Engineering, London. 1:449-452.

Terzaghi, K. (1943). Theoretical Soil Mechanics. John Wiley & Sons. New York.

Terzaghi, K. and Peck, R. B. (1967). Soil Mechanics in Engineernig Practice. John Wiley & Sons. New York.

Trak, B., La Rochelle, P., Tavenas, F., Leroueil, S. and Roy, M. (1980). "A new approach to the stability analysis of embankments on sensitive clays. Canadian Geotechnical Journal, 17:4:526-584.

Trollope, D. H. and Chan, C. K. (1960). "Soil structure and the step-strain phenomenon." Journal of the Soil Mechanics and Foundations Division, American Society of Civil Engineers, 86:SM2:1-39. April.

Tumay, M. T., Antonini, M. and Arman, A. (1979). "Metal versus nonwoven fiber fabric earth reinforcement in dry sands: a comparative statistical analysis of model tests." Geotechnical Testing Journal, GTJODJ, 2:1:44-56.

University of California/Davis. (1984a). "Large-scale pull-out tests on Tensar SR2 geogrids." Progress Report to the Tensar Corporation, Atlanta, GA. Department of Civil Engineering. July.

University of California/Davis. (1984b). "Plate bearing tests on on Tensar SS1 geogrid reinforced granular base on weak clay subgrade." Progress Report to the Tensar Corporation, Atlanta, GA. Department of Civil Engineering. July. 30 pages.

Vermeer, P. A. and Verruijt, A. (1981). "An accuracy condition for consolidation by finite elements." International Journal for Numerical and Analytical Methods in Geomechanics, 5:1-14.

Vesic, A. S. (1973). "Bearing capacity of shallow foundations." Chapter 3 in Foundation Engineering Handbook, Edited by H. F. Winterkorn and H.-Y. Fang. Van Nostrand Reinhold, New York.

Vidal, H. (1969). "The principal of reinforced earth." Highway Research Board, Highway Research Record No. 282, p 1-16.

Volman, W., Krekt, L. and Risseiuw, P. (1977). "Reinforcement with fabrics, a new technique to inprove the stability of embankments on weak subsoils." (in French). Proceedings, First International Conference on the Use of Fabrics in Geotechnics. Paris, 20-22 April. 1:49-54.

Wager, O. (1968). "Stabilitetforbatrande sponkonstruckton for bankfyllningar." (A method for improvement of embankment stability by means of sheetpiling). Reprints and Preliminary Reports, No. 28, Swedish Geotechnical Institute, Stockholm, Sweden. pp. 21-24.

Wager, O. and Holtz, R. D. (1976). "Reinforcing embankments by short sheet piles and tie rods." Proceedings of the 1976 International Symposium on New Horizons in Construction Materials, Lehigh University. 1:177-186.

Weaver, W. and Johnston, P. R. (1984). Finite Element Analysis of Structures. Prentice-Hall, Englewood Cliffs, NJ. 403 pages.

Weber, W. G., Jr. (1969). "Performance of embankments constructed over peat." Journal of the Soil Mechanics and Foundations Division, American Society of Civil Engineers, 95:SM1:53-77.

Westergaard, H. M. (1938). "A problem of eleasticity suggested by a problem in soil mechanics: soft material reinforced by numerous strong horizontal sheets." Stephen Timoshenko 60th Anniversary Volume. Macmillan, New York.

White, G. W. (1967). "Glacial Survey of Wayne County, Ohio." Ohio Geological Survey Report Inv. 62.

Whitman, R. V. and Hoeg, K. (1965). "Development of plastic zone beneath a footing." Report by MIT, Department of Civil Engineering, Soils Publication No. 197 for U. S. Army Corps of Engineer Waterways Experiment Station, Vicksburg, Miss.

Wilson, E. L. (1970). "SAP-A structural analysis program." Report UC SESM 70-20, Department of Civil Engineering, University of California, Berkeley.

Wilson, E. L., Bathe, K. J. and Doherty, W. P. (1974). "Direct solution of large systems of linear equations." Computers and Structures, 4:363-372.

Wilson, S. A. (1970). "Suggested Method of Test for Moisture-Density Relations of Soils Using Harvard Compaction Apparatus." Special Procedures for Testing Soil and Rock for Engineeing Purposes. 5th Edition. ASTM Special Technical Publication 479. pp 101-103.

Appendix A

INSTRUMENTATION DATA FOR MOHICANVILLE DIKE NO. 2

This appendix contains a compilation of the instrumentation data collected at Mohicanville Dike No. 2 in Wayne County, Ohio. These data were collected at selected intervals during and following construction by personnel of the Huntington District Corps of Engineers. The types of data collected include readings from open tube, electric, and pneumatic piezometers; readings from strain gages on the steel reinforcement; readings from horizontal and vertical inclinometers; and surveys of settlement plates and surface monuments. The data presented here represents a fraction of the total data collected and were chosen to provide an accurate and complete set of data to which comparisons of analytical studies could be made.

Table A-1 presents a summary of the instrumentation used at Mohicanville and shows the distritubtion of the instruments among the various stations. Table A-2 traces the rise in embamkment height at the instrumented stations during construction. These data were developed from the periodic surveys made of the dike and from the daily readings taken by the construction observation personnel. Table A-3 summarized the measured reinforcement forces measured at the centerline of six stations through March 13, 1986. Tables A-4 and A-5 present the reinforcement forces measured upstream and downstream at Stations 6+55 and 9+00, respectively, for selected dates during and following construction.

Table A-6 summarizes information on the location of the piezometers and shows the elevation of the tips, what soil type the piezometer is tipped in and what piezometers may be paired. Table A-7 presents piezometric elevation data for selected dates. Table A-8 summarized the settlement plates measurements while Table A-9 summarizes the surface displacement monument elevations by date. Table A-9 presents information on the location, elevation, type and initial date of reading of the inclinometers at the site. Selected inclinometer data are presented in Tables A-10 through 21.

Table A-1. Instrumentation at Mohicanville Dike No. 2.

Instrument	Station 4+75	6+55	8+00	9+00	11+00	12+20	Total
Piezometers							
Open Tube	1	3		4		1	9
Electric	1	2		3		1	7
Pneumatic	4	8		7		4	23
							39
Inclinometers							
Vertical	1	3		3	1	1	9
Horizontal	1	1		1		1	4
Strain Gages on Steel	2	29	2	29 lower 10 upper	2	2	76
Settlements Plates	3	3		3		3	12
Surface Displacement Monuments	5	5	5	5	5		25

Table A-2. Average crest elevations at instrumented sections.

Date	Sta. 4+75	Date	Sta. 6+55	Date	Sta. 9+00	Date	Sta. 12+20
1984							
8/10-20	960.0	8/10-20	960.0	9/1-10	960.0	9/5-15	960.0
8/27-9/20	962.5	8/28-9/20	962.5	9/17-19	961.0	9/21-10/5	961.5
9/21	963.0	9/21-26	963.0	9/22-10/5	963.5	10/6-9	962.5
9/26	963.5	9/27	963.5	10/6-15	965.5	10/11	963.0
10/2	966.5	10/2-4	966.0	10/16	966.7	10/15	966.0
10/5-16	967.5	10/5-15	966.7	10/18	967.9	10/19	970.0
10/19	969.0	10/19	969.0	10/23-30	969.0	10/22-31	971.0
10/23-30	970.0	10/23-30	970.0	11/2	971.0	11/2	972.2
11/2	971.2	11/2	971.0				
1985							
6/4	971.2	6/4	971.0	6/4	971.0	6/4	972.2
6/5-17	972.3	6/5-17	971.8	6/5-17	971.9	6/5-17	973.3
6/20	973.6	6/20	973.5	6/20	973.2	6/20	974.1
6/21-25	974.3	6/21	974.6	6/21	974.0	6/25	974.6
6/27	975.7	6/25	975.7	6/25	975.2	6/26-27	976.2
6/27-30	977.5	6/27	975.9	6/27	975.4	6/28-30	976.8
7/1-9	978.3	6/27	977.4	6/27	976.7	7/1-9	979.1
7/11	979.1	6/28-30	978.4	6/28-30	978.4	7/11	978.2
7/12-15	979.4	7/1-9	979.6	7/1-9	979.2	7/12-15	981.4
7/17	981.8	7/11	980.4	7/11	981.3	7/17	982.1
7/23	982.5	7/12-15	981.2	7/12-15	982.3	7/23	982.7
7/31	983.0	7/17	982.7	7/17	982.8	7/31	983.2
9/4	983.04	7/23	983.5	7/23	983.6		
10/7	982.99	7/31	984.0	7/31	984.0		
1/21/86	982.92	9/4	983.94	9/4	983.85		
3/27	982.82	10/7	983.85	10/7	983.71		
		1/21/86	983.68	1/21/86	983.55		
		3/27	983.57	3/27	983.40		

Notes: 1. Two measurements on 6/27/85:
10:00 am for piezometers
6:00 pm for strain gages

2. Elevations for 9/4/85 and after come from surface monuments located 5 ft upstream.

Table A-3. Centerline reinforcement forces (in tons/ft).

Station 4 + 75			Station 6 + 55		
Date	Force	Crest Elev.	Date	Force	Crest Elev.
8/27/84	Installed	960.0	8/28/84	Installed	960.0
9/21	0.31	962.5	9/21	0.30	963.0
9/26	0.36	963.0	9/26	0.26	963.5
10/2	1.64	966.5	10/2	1.45	966.0
10/5	2.23	967.5	10/8	2.14	966.7
10/8	2.28	967.5	10/11	2.28	966.7
10/9	2.28	967.5	10/15	2.42	966.7
10/11	2.31	967.5	10/19	2.63	966.7
10/15	2.43	967.5	10/23	4.05	969.0
10/19	3.28	969.0	10/23	4.56	970.0
10/23	3.82	970.0	10/26	4.67	970.0
10/26	3.86	970.0	10/30	4.72	970.0
10/30	4.06	970.0	11/2	5.65	971.0
11/2	4.75	971.2	11/7	5.69	971.0
11/7	4.78	971.2	11/13	5.68	971.0
11/13	4.71	971.2	11/19	5.67	971.0
11/19	4.70	971.2	12/11	5.50	971.0
5/17/85	3.58	971.2	5/16/85	5.27	971.0
6/7	3.92	972.3	6/7	5.44	972.8
6/12	3.87	972.3	6/12	5.39	972.8
6/19	3.97	973.6	6/19	6.60	974.6
6/24	4.83	974.3	6/24	7.84	976.1
6/27	6.58	977.5	6/27	9.58	977.4
6/28	6.90	977.5	6/28	10.51	978.4
7/1	7.58	978.3	7/1	11.96	979.6
7/8	7.88	978.3	7/3	12.43	979.6
7/11	8.19	979.1	7/8	12.83	979.6
7/15	8.59	979.4	7/9	12.88	979.6
7/18	9.48	981.8	7/11	13.21	980.4
7/22	9.73	982.5	7/15	13.69	981.4
7/25	9.79	982.5	7/18	14.45	982.7
7/31	9.92	983.0	7/22	14.92	983.5
8/14	10.29	983.0	7/25	14.89	983.5
9/5	10.43	983.0	7/31	15.03	984.0
10/3	10.45	983.0	8/14	15.21	984.0
12/4	11.71	982.9	9/5	15.27	983.9
3/12/86	11.84	982.8	10/3	15.28	983.8
			12/4	15.22	983.7
			3/12/86	15.27	983.6

Note: Values from upstream gage.

Table A-3. Centerline reinforcement forces (cont.) (in tons/ft).

Station 11 + 00			Station 12 + 20		
Date	Force	Crest Elev.	Date	Force	Crest Elev.
9/21/84	Installed	960.0	9/21/84	Installed	960.0
9/25	-0.06		9/22	-0.02	961.5
9/26	-0.18		9/26	-0.03	961.5
10/3	0.04		10/3	-0.11	961.5
10/8	0.40		10/8	0.13	962.5
10/11	0.40		10/11	0.32	963.0
10/15	0.68		10/15	1.10	966.0
10/19	1.80		10/19	2.59	970.0
10/23	2.02		10/23	2.71	971.0
10/26	2.05		10/26	2.72	971.0
10/30	2.28		10/30	2.88	971.0
11/2	3.74	972.0	11/2	4.72	972.2
11/7	3.81	972.0	11/7	4.79	972.2
11/13	3.85	972.0	11/13	4.73	972.2
11/19	3.90	972.0	11/19	4.73	972.2
12/11	3.90	972.0	12/11	4.63	972.2
5/16/85	3.69	971.2	5/17/85	4.48	972.2
6/7	4.06	972.3	6/7	4.86	973.3
6/12	4.08	972.3	6/12	4.84	973.3
6/19	4.37	973.6	6/19	4.99	973.3
6/24	5.24	974.3	6/24	5.59	974.6
6/27	5.94		6/27	6.47	976.2
6/28	6.82	978.0	6/28	7.07	976.8
7/1	7.30	978.0 (8:00 am)	7/1	7.16	976.8 (8:00 am)
7/1	7.78	979.7 (5:15 pm)	7/1	8.31	979.1 (6:00 pm)
7/8	9.19		7/8	8.78	979.1
7/9	9.25		7/11	9.52	980.5
7/11	9.63	980.7	7/15	10.00	981.4
7/15	10.36		7/18	10.39	982.1
7/18	10.59	982.8	7/22	10.51	982.7
7/22	10.98	983.0	7/31	10.55	983.2
7/25	11.06		8/14	10.67	
7/31	11.26	983.5	9/5	10.70	
8/14	11.57		10/3	10.73	
9/5	11.65	983.29	12/4	10.74	
10/3	11.68	983.25	3/12/86	10.71	
12/4	11.61	983.08			
3/12/86	11.47	983.02			

Note: Values from upstream gage.

Note: Values from upstream gage.

Table A-3. Centerline reinforcement forces (cont.) (in tons/ft).

Station 8 + 00			Station 9 + 00				
Date	Force	Crest Elev	Date	Force			Crest Elev
				Upper	Lower	Total	
9/13/84	Install	960.0	9/18/84	Install			960.0
9/21	0.88	963.0	9/22	-0.15	Install	-0.15	961.0
9/26	1.24	963.0	9/26	-0.15	-0.09	-0.21	961.0
10/2	1.93	965.5	10/3	0.0	0.66	0.66	963.5
10/5	2.41	966.0	10/8	0.16	0.43	0.59	965.5
10/8	2.86	966.0	10/11	0.11	0.37	0.48	965.5
10/11	2.83	966.7	10/15	0.15	0.49	0.64	965.5
10/15	2.94	966.7	10/19	0.69	0.99	1.68	967.9
10/19	4.43	969.0	10/23	0.80	1.12	1.92	969.0
10/23	4.81	969.5	10/26	0.80	1.14	1.94	969.0
10/26	4.82	969.5	10/30	0.89	1.25	2.14	969.0
10/30	4.85	969.5	11/2	1.55	1.73	3.28	971.0
11/2	5.70	971.0	11/7	1.66	1.69	3.40	971.0
11/7	5.68	971.0	11/13	1.65	1.69	3.34	971.0
11/13	5.61	971.0	11/19	1.66	1.68	3.34	971.0
11/19	5.58	971.0					
5/16/85	5.41	971.0	5/17/85	2.03	1.25	3.28	971.0
6/7	5.81	971.9	6/7	1.66	1.02	2.68	971.9
6/12	5.77	971.9	6/12	1.70	0.99	2.69	972.5
6/19	6.75	974.4	6/19	2.35	1.26	3.61	974.6
6/24	7.94	975.9	6/24	3.38	1.86	5.24	976.1
6/27	9.35	976.7	6/27	4.33	2.41	6.74	977.6
6/28	10.47	978.2	6/28	5.13	3.01	8.14	978.6
7/1	11.18	978.2*	7/1	6.40	3.58	9.98	979.8
7/1	11.94	979.2*	7/8	7.95	4.29	12.24	979.8
7/2	12.35	979.2	7/9	8.03	4.29	12.32	979.8
7/3	12.84	979.2	7/11	8.60	4.59	13.19	979.8
7/8	13.11	979.2	7/15	9.57	5.14	14.71	980.5
7/9	13.16	979.2	7/18	10.17	5.34	15.51	981.4
7/11	13.83	981.5	7/22	10.40	5.41	15.81	983.1
7/15	15.03	982.0	7/25	10.52	5.38	15.90	983.6
7/22	15.99	983.2	7/31	10.74	6.36	16.10	984.0
7/31	16.11	984.0	8/14	11.06	5.27	16.39	984.0
8/14	16.25	983.9	9/5	11.09	4.94	16.03	983.8
9/5	16.27	983.8	10/3	11.17	4.57	15.74	983.7
10/3	16.19	983.7	12/4	11.11	3.72	14.83	983.6
12/4	16.05	983.6	3/12/86	11.26	3.04	14.30	983.4
3/12/86	15.94	983.5					

Note: Values from upstream gage.
* On 7/1 two readings were taken, at 8 am and 5 pm.

Table A-4. Reinforcement forces about centerline at Station 6+55 (in tons/ft).

Date	10/5/84	11/2	6/4/85	6/24	7/1	7/9	7/31	12/4	3/12/86
Elev.	966.7	971.0	971.0	976.1	980.0	980.0	983.5	984.0	983.6
Location									
70US	--	0.64	--	0.62	0.58	0.60	0.62	0.69	0.73
65US	0.29	0.76	--	0.77	0.94	1.01	1.12	1.46	1.56
60US	0.41	1.09	0.24	0.93	1.26	1.36	1.73	1.79	1.97
55US	1.15	2.37	1.91	2.60	2.81	3.11	3.47	3.64	3.77
50US	1.37	3.24	2.99	3.43	3.71	4.07	4.16	4.27	4.20
45US	1.63	4.30	3.76	4.13	4.49	4.89	5.46	4.64	4.22
40US	1.65	4.44	4.62	5.55	6.24	6.73	7.67	8.07	8.09
35US	1.24	3.70	3.51	4.37	5.50	6.08	7.17	6.65	6.17
30US	0.32	3.82	--	5.19	7.15	7.88	--	10.13	10.14
25US	1.05	3.26	2.60	4.31	7.02	7.66	9.48	9.70	9.59
20US	0.69	2.78	1.48	3.16	6.31	7.03	9.12	9.32	9.19
15US	1.60	4.80	4.38	6.68	10.33	10.9	12.74	12.89	12.89
10US	1.69	4.97	4.44	6.65	10.57	11.2	13.86	14.07	14.00
5US	1.96	5.35	4.91	7.35	11.18	11.9	14.03	14.28	14.27
CL	2.14	5.65	5.27	7.84	11.96	12.8	15.03	15.22	15.27
5DS	1.87	5.17	4.50	7.09	10.74	12.22	14.07	14.48	14.55
10DS	2.14	5.55	4.67	7.56	10.91	12.31	14.31	14.77	14.78
15DS	2.14	5.39	4.32	7.12	10.62	11.91	13.73	14.21	14.29
20DS	2.32	5.36	4.42	7.20	10.14	11.31	12.68	13.21	13.48
25DS	2.42	5.32	4.59	7.06	9.36	10.62	11.88	11.98	12.10
30DS	2.57	5.47	4.85	7.08	9.21	10.51	11.38	12.46	12.52
35DS	2.27	4.89	4.43	6.21	7.78	8.86	9.89	10.30	10.41
40DS	2.05	4.43	4.10	5.27	6.37	7.23	8.06	8.28	8.35
45DS	1.92	4.05	3.81	4.47	5.19	5.82	6.44	--	--
50DS	1.21	3.22	2.85	3.31	3.78	4.15	4.54	4.32	4.30
55DS	0.69	2.52	2.13	2.27	2.62	2.86	3.11	2.72	2.62
60DS	0.55	2.03	1.49	1.59	1.93	2.13	2.31	1.85	1.72
65DS	0.17	1.34	0.92	0.92	1.24	1.45	1.65	1.43	1.20
70DS	0.20	0.89	0.37	-0.11	0.06	0.04	-0.11	-1.40	-1.78

Table A-5. Reinforcement forces about centerline at station 9+00 (in tons/ft).

Lower Steel

Date	10/8/84	11/2	5/17/85	6/24	7/1	7/9	7/31	12/4	3/12/86
Elev.	965.5	971.0	971.0	975.2	979.2	979.2	984.0	983.6	983.4
Location									
70US	0.36	0.58	0.73	0.57	0.76	0.96	1.17	1.00	0.95
65US	0.35	0.62	0.29	0.45	0.68	0.87	0.98	0.76	0.74
60US	0.44	0.89	0.76	0.74	1.01	1.21	1.33	0.89	0.77
55US	0.54	1.06	0.74	0.68	1.13	1.41	1.59	0.83	0.46
50US	0.60	2.14	1.75	2.11	2.67	3.07	3.56	2.53	2.27
45US	0.76	3.13	2.62	3.30	3.65	3.99	4.38	3.94	3.72
40US	0.59	2.32	2.63	3.26	4.28	4.84	4.38	5.38	5.33
35US	--	1.14	2.86	3.94	5.41	6.12	5.48	6.95	7.00
30US	0.30	1.76	2.18	3.32	5.05	5.90	6.95	6.82	6.83
25US	0.23	1.28	1.83	2.82	4.76	5.74	6.87	7.13	7.10
20US	--	0.93	0.37	1.97	4.33	5.41	7.09	6.22	5.50
15US	0.33	1.94	2.23	3.42	6.25	7.43	9.574	9.44	9.39
10US	0.05	1.64	1.95	3.23	6.32	7.75	10.36	10.30	10.35
5US	0.00	1.43	1.43	3.58	6.39	8.02	10.89	11.42	11.75
CL	0.16	1.55	2.03	3.38	6.40	7.95	10.74	11.11	11.26
5DS	0.26	1.49	1.63	2.95	6.00	7.55	10.77	11.15	11.32
10DS	0.00	0.98	0.05	1.12	3.72	4.92	7.61	7.59	7.58
15DS	0.39	1.32	1.40	1.81	3.80	4.69	6.75	7.00	7.12
20DS	0.69	2.25	2.43	2.94	4.84	5.58	7.32	7.62	7.82
25DS	0.71	2.43	2.65	3.07	4.82	5.55	7.06	7.44	7.59
30DS	0.67	2.58	2.49	3.16	4.69	5.36	6.63	7.01	7.11
35DS	0.84	2.90	3.19	3.48	4.85	5.45	6.57	6.91	7.01
40DS	0.81	2.85	3.33	3.47	4.65	5.14	6.07	6.31	6.45
45DS	0.79	2.64	3.32	3.35	4.32	4.74	5.34	5.70	5.84
50DS	0.76	2.28	3.05	2.87	3.54	3.86	4.38	4.45	4.51
55DS	0.66	1.74	2.38	2.12	2.53	2.75	3.03	3.08	3.19
60DS	0.43	1.19	1.59	1.52	1.78	1.93	2.04	2.10	2.20
65DS	0.26	0.85	1.04	1.03	1.23	1.29	1.25	1.33	1.42
70DS	0.13	0.49	0.95	0.58	0.68	0.66	0.60	0.74	0.92

Table A-5. Reinforcement forces about centerline at station 9+00 (in tons/ft).

Upper Steel

Date	10/8/84	11/2	5/17/84	6/24	7/1	7/9	7/31	12/4	3/12/86
Elev.	965.5	971.0	971.0	975.2	979.2	979.2	984.0	983.6	983.4
Location									
70US	0.02	0.46	0.98	0.78	0.90	1.23	1.06	1.66	1.73
65US									
60US	-0.18	0.31	0.27	0.60	1.38	1.80	2.30	2.66	2.68
55US									
50US	-0.07	0.43	0.01	0.58	1.77	2.31	2.92	3.14	3.05
45US									
40US	-0.15	-0.30	-1.48	-1.12	0.13	0.77	1.48	0.18	-0.26
35US									
30US	0.60	1.36	0.72	0.88	1.98	2.57	3.43	2.41	2.04
25US									
20US	0.80	1.97	1.28	2.52	3.68	4.50	5.70	4.69	4.36
15US									
10US	0.64	2.33	--	3.01	4.53	5.42	6.75	4.93	4.08
5US									
CL	0.43	1.73	1.25	2.41	3.58	4.29	5.36	3.72	3.04
5DS									
10DS	1.36	3.50	3.41	4.58	5.65	6.30	7.32	6.15	5.70
15DS									
20DS	1.22	3.29	3.05	4.49	5.51	6.06	7.09	6.19	5.80
25DS									
30DS									
35DS									
40DS									
45DS									
50DS									
55DS									
60DS									
65DS									
70DS									

Table A-5. Reinforcement forces about centerline at station 9+00 (in tons/ft).

Total for both layers of steel.

Date	10/8/84	11/2	5/17/85	6/24	7/1	7/9	7/31	12/4	3/12/86
Elev.	965.5	971.0	971.0	975.2	979.2	979.2	984.0	983.6	983.4
Location									
70US									
65US	0.38	0.96	1.71	1.35	1.66	2.19	2.23	2.66	2.68
60US									
55US	0.26	1.20	1.03	1.34	2.39	3.01	3.63	3.55	3.45
50US									
45US	0.53	2.57	1.76	2.69	4.44	5.38	6.48	5.67	5.32
40US									
35US	0.44	2.02	1.15	2.14	4.41	5.61	6.96	5.56	5.07
30US									
25US	0.90	3.12	2.90	4.20	7.03	8.47	10.30	9.23	8.87
20US									
15US	0.80	2.90	1.65	4.49	8.01	9.91	12.76	10.81	9.86
10US									
5US	0.69	3.97	--	6.24	10.85	13.17	17.11	15.23	14.43
CL									
5DS	0.59	3.28	3.28	5.79	9.98	12.24	16.10	14.83	14.30
10DS									
15DS	1.36	4.48	3.46	5.70	9.37	11.22	14.93	13.74	13.28
20DS									
25DS	1.91	5.54	5.48	7.43	10.35	11.64	14.41	13.81	13.62
30DS									
35DS									
40DS									
45DS									
50DS									
55DS									
60DS									
65DS									
70DS									

Table A-6. Piezometer locations and elevations.

Number	Location	Tipped In	Tip Elevation	Paired With
D18	4+96, 78'US	Inoperative	945.9	
EP1	4+72, 10'US	Inoperative	924.9	PP9
EP2	6+52, 10'US	Found. Clay	925.9	PP10
EP3	8+95, 10'US	Found. Clay	930.2	PP11
EP4	12+23, 10'US	Found. Clay	924.6	PP12
EP5	6+52, 62'US	Found. Clay	930.8	PP21
EP6	8+95, 62'US	Found. Clay	928.7	PP22
EP7	6+52, 62'DS	Found. Clay	929.8	PP23
EP8	8+95, 62'DS	Found. Clay	930.0	
OP28	4+80, 10'US	Peat	945.9	PP5
OP29	6+44, 10'US	Peat	940.5	PP6
OP30	9+03, 10'US	Peat	938.2	PP7
OP31	12+16, 10'US	Peat	945.5	PP8
OP32	6+44, 62'US	Peat	946.1	PP17
OP33	9+03, 62'US	Old Emb. Clay	944.2	PP18
OP34	6+44, 62'DS	Peat	945.3	PP19
OP35	9+03, 62'DS	Peat	944.1	PP20
PP1	4+80, 10'US	Found. Clay	935.9	
PP2	6+44, 10'US	Old Emb. Clay	951.0	
PP3	8+95, 14'US	Old Emb. Clay	951.1	
PP4	12+16, 14'US	Old Emb. Clay	952.5	
PP5	4+59, 10'US	Peat	945.9	OP28
PP6	6+58, 10'US	Peat	938.9	OP29
PP7	9+03, 10'US	Peat	938.2	OP30
PP8	12+16, 10'US	Peat	924.9	OP31
PP9	4+72, 10'US	Found. Clay	924.9	EP1
PP10	6+52, 10'US	Found. Clay	925.9	EP2
PP11	8+95, 10'US	Found. Clay	930.2	EP3
PP12	12+23, 10'US	Found. Clay	924.6	EP4
PP13	4+72, 10'US	Found. Clay	912.9	
PP14	6+52, 10'US	Found. Clay	910.9	
PP15	8+95, 10'US	Found. Clay	910.2	
PP16	12+23, 10'US	Found. Clay	915.6	
PP17	6+44, 62'US	Peat	946.1	OP32
PP18	9+03, 62'US	Old Emb. Clay	944.2	OP33
PP19	6+44, 62'DS	Peat	945.3	OP34
PP20	9+03, 62'DS	Peat	944.1	OP35
PP21	6+52, 62'US	Found. Clay	930.8	EP5
PP22	8+95, 62'US	Found. Clay	928.7	EP6
PP23	6+52, 62'DS	Found. Clay	929.8	EP7
UD27	9+67, 144'DS	Peat	950.0	

Table A-7. Piezometric elevations selected by station and date.

Piezometer	Initial Reading	Date 10/4/84	11/2	5/15/85	6/27	7/1	7/23
Sta. 4+75							
OP28	959.7	967.6	973.7	957.4	972.5	975.8	978.2
PP1	956.9	965.0	970.0	964.3	969.5	973.0	977.0
PP5	958.6	966.0	971.1	965.5	969.7	971.9	973.8
PP9	954.9	955.2	957.0	955.6	957.2	958.6	958.6
PP13	952.8	952.1	952.1	952.8	952.8	953.0	952.6
Sta. 6+55							
EP2	955.7	959.6	964.2	958.5	963.8	968.0	971.4
EP5	956.9	959.4	961.7	959.9	961.9	963.0	963.9
EP7	958.3	958.8	964.6	961.8	964.6	966.2	967.4
OP29	957.7	965.1	971.9	967.4	973.8	977.4	980.0
OP32	958.4	962.4	963.6	960.7	961.4	961.6	962.8
OP34	959.4	961.0	966.2	962.8	963.6	963.7	963.9
PP2	965.5	969.5	972.9	966.7	971.5	974.5	975.2
PP6	957.4	962.0	968.2	964.7	971.4	975.2	977.7
PP10	956.4	958.2	965.8	963.0	969.0	972.7	975.3
PP14	955.7	955.7	957.5	956.6	958.4	959.8	959.8
PP17	959.9	962.0	963.4	960.4	961.3	961.6	961.6
PP19	955.7	961.9	967.0	964.0	964.9	965.0	965.4
PP21	954.3	960.6	962.6	960.3	962.2	963.3	964.0
PP23	958.3	958.9	964.4	961.4	964.4	965.9	966.7
Sta. 9+00							
EP3	965.7	968.3	978.9	979.1	984.1	987.7	994.0
EP6	960.0	963.2	966.4	966.1	967.9	969.3	972.3
EP8	957.8	959.6	966.2	966.5	968.4	969.7	970.8
OP30	960.0	963.4	968.4	962.3	965.1	967.6	969.5
OP33	957.6	956.9	957.7	957.2	956.9	956.8	956.2
OP35	960.6	962.9	968.2	964.7	966.2	966.6	967.1
PP3	959.9	959.9	961.3	959.4	960.8	961.9	961.9
PP7	962.0	963.1	967.7	962.2	965.3	967.5	969.6
PP11	965.3	967.1	977.5	976.8	983.0	987.4	994.6
PP15	959.3	963.3	974.3	974.1	979.6	983.2	988.4
PP18	955.7	956.0	956.9	956.4	956.3	956.3	955.5
PP20	959.6	960.7	965.8	962.8	964.2	964.6	965.3
PP22	960.5	962.4	965.4	963.3	966.7	967.5	970.5
UD27	954.5	954.5	954.9	955.3	955.2	955.2	955.3
Sta. 12+20							
EP4	953.0	953.3	952.7	--	--	--	--
OP31	959.1	956.3	960.2	956.1	958.4	960.1	960.6
PP4	961.7	962.4	965.2	962.2	962.9	964.4	964.5
PP8	955.0	955.4	958.7	956.8	957.8	959.7	960.3
PP12	954.1	954.4	956.4	954.1	956.3	958.3	658.5
PP16	949.7	949.7	949.5	950.2	950.4	950.4	950.0

Table A-7. Piezometric elevations selected by station and date (cont.).

Piezometer	Date 7/31	8/15	9/5	10/3	12/4	3/12/86
Sta. 4+75						
OP28	978.8	977.9	977.1	976.7	975.8	974.4
PP1	977.2	976.3	975.4	974.2	973.0	971.2
PP5	973.4	973.4	972.7	972.9	972.2	971.5
PP9	958.4	958.1	957.0	957.0	956.7	956.7
PP13	952.6	952.3	951.7	951.4	952.4	953.5
Sta. 6+55						
EP2	971.9	972.2	971.1	968.8	963.8	961.9
EP5	964.1	964.1	963.9	963.7	963.3	963.0
EP7	967.1	967.5	967.0	966.7	965.9	964.9
OP29	979.7	979.5	978.7	978.1	977.0	975.6
OP32	962.1	962.0	962.0	961.9	961.5	961.2
OP34	964.2	964.2	964.5	964.7	964.1	964.0
PP2	975.0	974.5	973.6	973.2	971.8	970.2
PP6	977.2	977.0	976.0	975.6	974.4	973.0
PP10	975.7	976.0	975.0	972.5	968.1	966.0
PP14	959.8	959.1	958.7	957.7	957.7	957.5
PP17	961.0	961.8	962.0	961.6	961.1	960.9
PP19	965.4	965.8	965.8	965.8	965.8	965.4
PP21	964.0	963.8	963.8	963.8	963.3	962.9
PP23	967.1	966.7	966.3	966.0	965.3	964.2
Sta. 9+00						
EP3	994.9	994.6	993.8	992.8	991.2	989.8
EP6	972.0	972.7	972.5	--	--	--
EP8	971.1	971.5	971.6	971.6	971.5	971.0
OP30	969.5	969.1	967.7	966.9	965.9	965.3
OP33	956.3	956.3	957.1	957.0	956.3	956.9
OP35	967.3	967.6	967.8	967.7	967.7	967.1
PP3	961.9	961.9	961.5	961.0	960.6	960.1
PP7	969.8	969.1	968.4	967.0	966.4	965.4
PP11	994.1	993.4	993.0	992.5	990.9	989.5
PP15	988.4	988.4	987.7	987.5	985.2	983.1
PP18	955.5	955.5	956.4	956.2	956.9	957.4
PP20	965.3	965.6	965.8	965.8	965.8	965.3
PP22	970.5	970.2	970.0	969.5	968.8	968.2
UD27	955.2	955.2	955.2	955.3	955.7	955.7
Sta. 12+20						
EP4	--	--	--	--	--	--
OP31	960.9	959.5	959.1	958.6	958.1	957.8
PP4	964.0	962.9	962.0	960.8	961.5	964.7
PP8	959.6	959.3	958.9	958.2	958.0	957.3
PP12	957.8	957.4	956.4	955.7	955.3	954.8
PP16	949.7	949.7	949.3	949.1	948.8	950.7

Table A-8. Settlement plate movements, settlement in feet.

Settlement Plate	Location	Initial Elev.	Settlement, ft 10/4/84	11/2	5/15/85	6/27	7/1
SP-1	4+75 60'DS	961.08	0.03	0.13	0.32	0.34	0.31
SP-2	6+55 60'DS	961.36	0.04	0.19	0.59	0.64	0.63
SP-3	9+00 60'DS	962.07	--	0.13	0.44	0.46	0.44
SP-4	12+20 60'DS	961.24	--	0.04	0.20	0.21	0.21
SP-5	4+75 60'US	960.99	0.04	0.07	0.23	0.22	0.21
SP-6	6+55 60'US	960.79	0.05	0.09	0.25	0.26	0.23
SP-7	9+00 60'US	962.51	--	0.06	0.23	0.26	0.28
SP-8	12+20 60'US	961.28	--	0.04	0.13	0.10	0.10
SP-9	4+75 10'US	961.09	0.04	0.12	0.29	0.22	0.25
SP-10	6+55 10'US	961.17	0.06	0.14	0.39	0.42	0.45
SP-11	9+00 10'US	962.42	--	0.16	0.52	0.64	0.73
SP-12	12+20 10'US	961.22	--	0.11	0.29	0.28	0.31

Settlement Plate	Settlement, ft 7/9	7/31	8/13	9/4	10/7	1/22/86	4/8
SP-1	0.31	0.31	0.31	0.34	0.33	0.40	0.43
SP-2	0.65	0.67	0.68	0.75	0.76	0.92	1.00
SP-3	0.47	0.50	0.52	0.58	0.61	0.75	0.75
SP-4	0.22	0.21	0.21	0.24	0.26	0.33	0.35
SP-5	0.20	0.22	0.22	0.24	0.24	0.29	0.29
SP-6	0.23	0.29	0.29	0.33	0.33	0.41	0.41
SP-7	0.28	0.31	0.33	0.36	0.39	0.49	0.51
SP-8	0.09	0.13	0.12	0.15	0.14	0.18	0.17
SP-9	0.26	0.36	0.39	0.41	0.45	0.53	0.58
SP-10	0.53	0.68	0.73	0.80	0.84	1.02	1.12
SP-11	0.83	1.03	1.08	1.18	1.25	1.46	1.58
SP-12	0.32	0.42	0.42	0.47	0.48	0.57	0.62

Table A-9. Elevations of surface displacement monument by date.

Monument & Location			Elevation on							
			Initial	11/8	5/16	7/1	7/31	10/9	1/4	3/27
D-1	4+75	30'DS	975.21					75.18	75.09	75.09
D-2	4+75	105'DS	958.80	58.79	58.80	58.78	58.80	58.76	58.83	58.94
D-3	6+55	30'DS	974.94					74.84	74.64	74.56
D-4	6+55	105'DS	958.61	58.59	58.58	58.57	58.61	58.57	58.65	58.75
D-5	7+50	30'DS	974.83					74.74	74.58	74.52
D-6	7+50	105'DS	957.93	57.90	57.86	57.83	57.86	57.83	57.94	58.02
D-7	9+00	30'DS	974.91					74.84	74.63	74.50
D-8	9+00	105'DS	961.40	61.39	61.30	61.31	61.37	61.31	61.33	61.37
D-9	11+00	30'DS	975.54					75.49	75.35	75.28
D-10	11+00	105'DS	959.00	59.00	58.97	58.97	59.00	59.00	59.02	59.04
U-1	4+75	5'US	983.04					82.99	82.92	82.82
U-2	4+75	30'US	975.57					75.53	75.45	75.42
U-3	4+75	105'US	964.86	64.86	64.80	64.79	64.79	64.78	64.78	64.88
U-4	6+55	5'US	983.94					83.85	83.68	83.57
U-5	6+55	30'US	975.37					75.31	55.16	75.11
U-6	6+55	105'US	962.63	62.64	62.68	62.69	62.71	62.71	62.75	62.81
U-7	7+50	5'US	983.26					83.18	82.99	82.91
U-8	7+50	30'US	975.46					75.39	75.25	75.18
U-9	7+50	105'US	962.78	62.79	62.76	62.77	62.80	62.82	62.87	62.96
U-10	9+00	5'US	983.85					83.77	83.55	83.41
U-11	9+00	30'US	975.59					75.53	75.34	75.24
U-12	9+00	105'US	961.22	61.22	61.17	61.18	61.18	61.18	61.24	61.37
U-13	11+00	5'US	983.29					83.25	83.08	83.02
U-14	11+00	30'US	974.74					74.72	74.59	74.55
U-15	11+00	105'US	962.60	62.61	62.57	62.59	62.59	62.60	62.60	62.61

Table A-10. Inclinometer information.

Number	Location	Direction	Elevation	Initial Reading
I-1	6+62, 117' US	Vertical	961.04	10/13/84
I-4*	9+42, 85' DS	Vertical	962.76	
I-5	6+87, 103' DS	Vertical	958.24	10/ 5/84
I-6	12+03, 128' US	Vertical	958.89	10/ 9/84
I-7	6+52, 60' US	Vertical	967.04	10/ 3/84
I-8	9+03, 60' US	Vertical	970.92 (10/23) 967.67 (6/20/85)	10/18/84
I-9	9+03, 41' US	Vertical	974.00	10/18/84
I-10	4+75, 93' US	Horizontal	959.25	9/27/84
I-11	6+55, 93' US	Horizontal	959.26	9/27/84
I-12	9+00, 93' US	Horizontal	959.25	10/ 8/84
I-13	12+20, 93' US	Horizontal	959.21	10/11/84
I-14	9+14, 150' US	Vertical	961.32	6/ 5/85
I-15*	9+50, 102' DS	Vertical	959.10	6/17/85

* I-4 was destroyed in June, 1985 and replaced with I-15.

Table A-11. Horizontal movements at inclinometer I-1 in feet.

Depth	6/6/85	6/17/85	7/23/85	3/13/86
3	0.070	0.067	0.018	-0.021
5	0.055	0.055	0.003	-0.032
7	0.043	0.042	-0.009	-0.040
9	0.040	0.039	-0.010	-0.040
11	0.034	0.033	-0.014	-0.046
13	0.029	0.027	-0.018	-0.053
15	0.032	0.031	-0.013	-0.055
17	0.032	0.031	-0.011	-0.054
19	0.033	0.032	-0.008	-0.055
21	0.035	0.034	-0.005	-0.053
23	0.033	0.032	-0.005	-0.055
25	0.026	0.025	-0.011	-0.061
27	0.024	0.023	-0.012	-0.062
29	0.022	0.020	-0.014	-0.064
31	0.019	0.018	-0.016	-0.065
33	0.018	0.017	-0.015	-0.065
35	0.019	0.017	-0.014	-0.063
37	0.019	0.018	-0.011	-0.059
39	0.022	0.021	-0.005	-0.052
41	0.022	0.021	-0.002	-0.044
43	0.025	0.024	0.010	-0.014
45	0.026	0.026	0.018	0.004
47	0.038	0.037	0.034	0.028
49	0.037	0.037	0.034	0.032
51	0.026	0.026	0.025	0.042

Note: (1) Positive values are movements in the downstream direction.

(2) Initial reading was on October 13, 1984.

Table A-12. Horizontal movements at inclinometer I-5 in feet.

Depth	6/6/85	6/21/85	7/23/85	3/13/86
2	0.195	0.205	0.239	0.311
4	0.182	0.193	0.232	0.307
6	0.167	0.177	0.224	0.302
8	0.175	0.186	0.238	0.317
10	0.187	0.197	0.253	0.335
12	0.177	0.186	0.248	0.329
14	0.147	0.154	0.222	0.300
16	0.104	0.111	0.184	0.260
18	0.071	0.078	0.155	0.229
20	0.059	0.065	0.142	0.214
22	0.056	0.062	0.136	0.206
24	0.054	0.059	0.129	0.195
26	0.054	0.059	0.123	0.187
28	0.053	0.057	0.115	0.175
30	0.049	0.053	0.099	0.151
32	0.038	0.040	0.067	0.102
34	0.022	0.024	0.039	0.059
36	0.013	0.014	0.020	0.034
38	0.007	0.008	0.010	0.015
40	0.005	0.006	0.008	0.010
42	0.004	0.005	0.005	0.007
44	0.002	0.004	0.004	0.004
46	0.002	0.003	0.003	0.004
48	0.000	0.001	0.001	0.001
50	0.000	0.000	0.001	0.001

Note: (1) Positive values are movements in the downstream direction.

(2) Initial reading was on October 5, 1984.

Table A-13. Horizontal movements at inclinometer I-6 in feet.

Depth	6/6/85	6/21/85	7/23/85	3/13/86
2	0.014	0.013	0.012	0.017
4	0.011	0.010	0.004	0.010
6	0.008	0.007	-0.003	0.003
8	0.005	0.004	-0.009	-0.004
10	0.004	0.002	-0.012	-0.007
12	0.003	0.000	-0.011	-0.006
14	0.002	0.000	-0.009	-0.004
16	0.003	0.001	-0.007	-0.002
18	0.003	0.003	-0.004	-0.000
20	0.004	0.003	-0.000	0.000
22	0.004	0.003	-0.000	0.001
24	0.003	0.003	-0.000	0.001
26	0.003	0.002	0.000	0.001
28	0.003	0.002	0.000	0.001
30	0.003	0.002	0.000	0.001
32	0.002	0.001	0.000	0.001
34	0.002	0.000	0.000	0.001
36	0.001	0.000	0.000	0.001
38	0.000	0.000	0.000	0.000
40	0.000	0.000	0.000	0.000
42	0.000	0.000	0.000	0.000
44	0.000	0.000	0.000	0.000
46	0.000	0.000	0.000	0.000

Note: (1) Positive values are movements in the downstream direction.

(2) Initial reading was on October 9, 1984.

Table A-14. Horizontal movements at inclinometer I-7 in feet.

Depth	6/5/85	6/21/85	7/23/85	3/13/86
2	0.029	0.022	0.035	0.080
4	0.047	0.042	0.059	0.082
6	0.052	0.048	0.066	0.066
8	0.039	0.033	0.045	0.035
10	0.025	0.018	0.022	0.002
12	0.012	0.004	0.000	-0.029
14	0.002	-0.006	-0.018	-0.057
16	-0.009	-0.018	-0.037	-0.084
18	-0.020	-0.030	-0.056	-0.112
20	-0.028	-0.040	-0.073	-0.138
22	-0.036	-0.048	-0.089	-0.163
24	-0.037	-0.049	-0.095	-0.174
26	-0.036	-0.048	-0.098	-0.183
28	-0.035	-0.046	-0.101	-0.189
30	-0.037	-0.046	-0.102	-0.196
32	-0.038	-0.046	-0.104	-0.202
34	-0.038	-0.046	-0.106	-0.219
36	-0.039	-0.047	-0.109	-0.216
38	-0.039	-0.047	-0.109	-0.219
40	-0.037	-0.045	-0.106	-0.216
42	-0.031	-0.038	-0.098	-0.208
44	-0.020	-0.028	-0.082	-0.188
46	-0.006	-0.013	-0.046	-0.141
48	-0.000	-0.006	-0.022	-0.078
50	0.002	0.000	-0.013	-0.037
52	0.003	0.001	-0.007	-0.014
54	0.003	0.002	-0.005	-0.010
56	0.003	0.002	-0.003	-0.008
58	0.003	0.002	-0.002	-0.006
60	0.002	0.002	-0.000	-0.005
62	0.001	0.002	-0.000	-0.003

Note: (1) Positive values are movements in the downstream direction.

(2) Initial reading was on October 3, 1984.

Table A-15. Horizontal movements at inclinometer I-8 in feet.

Depth	6/5/85	6/21/85	7/23/85	3/13/86
2	0.008	-0.001	0.011	0.031
4	0.099	0.042	0.050	0.098
6	0.085	0.037	0.036	0.115
8	0.072	0.023	0.010	0.071
10	0.075	0.012	-0.014	0.030
12	0.070	0.004	-0.034	-0.002
14	0.051	-0.002	-0.052	-0.029
16	0.028	-0.020	-0.078	-0.069
18	0.020	-0.032	-0.098	-0.108
20	0.024	-0.041	-0.113	-0.140
22	0.024	-0.047	-0.127	-0.161
24	0.005	-0.053	-0.141	-0.185
26	-0.019	-0.068	-0.163	-0.217
28	-0.033	-0.081	-0.181	-0.257
30	-0.038	-0.085	-0.191	-0.276
32	-0.047	-0.094	-0.205	-0.302
34	-0.061	-0.101	-0.217	-0.324
36	-0.076	-0.107	-0.227	-0.349
38	-0.083	-0.111	-0.233	-0.366
40	-0.074	-0.104	-0.228	-0.367
42	-0.067	-0.099	-0.223	-0.362
44	-0.062	-0.093	-0.217	-0.355
46	-0.060	-0.089	-0.213	-0.349
48	-0.068	-0.085	-0.208	-0.345
50	-0.086	-0.082	-0.202	-0.337
52	-0.088	-0.083	-0.198	-0.335
54	-0.063	-0.079	-0.189	-0.326
56	-0.040	-0.071	-0.179	-0.301
58	-0.045	-0.078	-0.179	-0.287
60	-0.036	-0.064	-0.157	-0.265
62	-0.012	-0.042	-0.113	-0.215
64	0.015	-0.017	-0.045	-0.118
66	0.018	-0.009	-0.028	-0.053
68	0.011	-0.008	-0.023	-0.043
70	0.003	-0.007	-0.019	-0.038
72	-0.002	-0.006	-0.016	-0.033
74	-0.002	-0.006	-0.013	-0.029
76	0.001	-0.004	-0.009	-0.024
78	0.011	-0.000	-0.004	-0.015
80	0.019	0.003	-0.000	-0.008

Note: (1) Positive values are movements in the downstream direction.

(2) Initial reading was on October 18, 1984.

Table A-16. Horizontal movements at inclinometer I-9 in feet.

Depth	6/5/85	6/21/85	7/23/85	3/13/86
2	-0.300	-0.230	-0.186	-0.141
4	-0.232	-0.164	-0.127	-0.106
6	-0.106	-0.045	-0.008	0.007
8	-0.003	0.017	0.044	0.093
10	0.031	0.024	0.035	0.096
12	0.027	0.014	0.011	0.060
14	0.008	-0.008	-0.027	0.006
16	-0.017	-0.035	-0.067	-0.051
18	-0.044	-0.059	-0.104	-0.106
20	-0.069	-0.084	-0.139	-0.156
22	-0.080	-0.092	-0.158	-0.192
24	-0.066	-0.076	-0.152	-0.203
26	-0.047	-0.063	-0.151	-0.209
28	-0.041	-0.065	-0.166	-0.231
30	-0.043	-0.067	-0.178	-0.260
32	-0.052	-0.079	-0.197	-0.294
34	-0.068	-0.096	-0.221	-0.333
36	-0.080	-0.103	-0.233	-0.363
38	-0.081	-0.100	-0.234	-0.378
40	-0.083	-0.105	-0.244	-0.390
42	-0.097	-0.118	-0.256	-0.414
44	-0.108	-0.126	-0.267	-0.436
46	-0.114	-0.128	-0.268	-0.444
48	-0.113	-0.124	-0.261	-0.439
50	-0.103	-0.113	-0.245	-0.421
52	-0.088	-0.097	-0.218	-0.387
54	-0.072	-0.082	-0.187	-0.339
56	-0.062	-0.074	-0.168	-0.300
58	-0.058	-0.070	-0.151	-0.263
60	-0.055	-0.066	-0.138	-0.229
62	-0.050	-0.061	-0.123	-0.206
64	-0.044	-0.048	-0.082	-0.161
66	-0.029	-0.030	-0.040	-0.077
68	-0.016	-0.021	-0.025	-0.036
70	-0.011	-0.018	-0.020	-0.027
72	-0.008	-0.015	-0.016	-0.021
74	-0.010	-0.016	-0.017	-0.021
76	-0.015	-0.020	-0.020	-0.023
78	-0.019	-0.020	-0.019	-0.022
80	-0.010	-0.010	-0.010	-0.010

Note: (1) Positive values are movements in the downstream direction.

(2) Initial reading was on October 18, 1984.

Table A-17. Vertical settlement at inclinometer I-10 in feet.

Dist.	10/16/84	6/7/85	7/23/85	3/13/86
90	0.05	0.29	0.27	0.24
85	0.12	0.41	0.38	0.34
80	0.06	0.29	0.26	0.20
75	0.04	0.27	0.22	0.15
70	0.03	0.26	0.22	0.18
65	0.02	0.27	0.24	0.19
60	0.01	0.27	0.24	0.23
55	0.00	0.27	0.25	0.25
50	0.00	0.27	0.27	0.28
45	0.00	0.27	0.28	0.31
40	0.00	0.26	0.29	0.32
35	0.00	0.26	0.28	0.33
30	0.01	0.23	0.28	0.33
25	0.01	0.22	0.28	0.35
20	0.02	0.22	0.29	0.37
15	0.01	0.21	0.29	0.38
10	0.01	0.21	0.30	0.40
5	0.00	0.23	0.32	0.45
CL	0.01	0.24	0.36	0.47
5	0.01	0.25	0.36	0.47
10	0.00	0.24	0.33	0.42
15	0.02	0.23	0.32	0.41
20	0.02	0.23	0.32	0.40
25	0.02	0.23	0.31	0.39
30	0.02	0.25	0.32	0.37
35	0.02	0.27	0.32	0.35
40	0.02	0.27	0.31	0.33

Note: (1) Positive values are settlement.

(2) Initial reading was on September 27, 1984.

Table A-18. Vertical settlement at inclinometer I-11 in feet.

Dist.	6/7/85	6/26/85	7/23/85	3/13/86
90	0.51	0.53	0.45	0.55
85	0.62	0.66	0.60	0.68
80	0.55	0.57	0.58	0.62
75	0.51	0.55	0.43	0.63
70	0.48	0.54	0.51	0.66
65	0.46	0.53	0.50	0.70
60	0.44	0.52	0.50	0.76
55	0.42	0.51	0.52	0.80
50	0.40	0.50	0.53	0.86
45	0.38	0.49	0.54	0.89
40	0.37	0.49	0.56	0.95
35	0.35	0.48	0.58	0.99
30	0.33	0.47	0.60	1.01
25	0.30	0.45	0.61	1.03
20	0.29	0.45	0.62	1.05
15	0.26	0.44	0.62	1.04
10	0.26	0.43	0.62	1.04
5	0.24	0.42	0.62	1.03
CL	0.23	0.40	0.62	0.98
5	0.20	0.37	0.60	0.89
10	0.15	0.34	0.53	0.80
15	0.15	0.34	0.47	0.76
20	0.14	0.34	0.45	0.74
25	0.14	0.34	0.45	0.77
30	0.15	0.34	0.40	0.82
35	0.17	0.33	0.39	0.60
40	0.20	0.38	0.38	0.59

Note: (1) Positive values are settlement.

(2) Initial reading was on September 27, 1984.

Table A-19. Vertical settlement at inclinometer I-12 in feet.

Dist.	10/23/84	6/17/85	7/23/85	3/13/86
90	0.018	0.25	0.20	0.15
85	0.064	0.31	0.25	0.21
80	0.038	0.31	0.24	0.22
75	0.031	0.34	0.26	0.28
70	0.030	0.36	0.31	0.37
65	0.036	0.40	0.39	0.51
60	0.046	0.43	0.45	0.66
55	0.055	0.47	0.54	0.77
50	0.060	0.49	0.61	0.86
45	0.065	0.50	0.65	0.97
40	0.065	0.51	0.69	1.04
35	0.062	0.51	0.73	1.12
30	0.060	0.51	0.75	1.17
25	0.056	0.51	0.79	1.22
20	0.056	0.51	0.82	1.26
15	0.055	0.52	0.86	1.32
10	0.056	0.53	0.89	1.35
5	0.060	0.54	0.92	1.40
CL	0.065	0.56	0.96	1.43
5	0.074	0.57	0.96	1.43
10	0.075	0.56	0.91	1.35
15	0.078	0.56	0.87	1.30
20	0.083	0.56	0.85	1.24
25	0.087	0.55	0.81	1.15
30	0.093	0.56	0.78	1.09
35	0.117	0.55	0.75	1.02
40	0.120	0.54	0.70	0.94

Note: (1) Positive values are settlement.

(2) Initial reading was on October 10, 1984.

Table A-20. Vertical settlement at inclinometer I-13 in feet.

Dist.	10/23/84	6/7/85	7/23/85	3/13/86
90	0.02	0.16	0.15	0.10
85	0.07	0.20	0.20	0.14
80	0.05	0.19	0.20	0.16
75	0.03	0.17	0.17	0.13
70	0.02	0.18	0.18	0.16
65	0.02	0.22	0.23	0.23
60	0.02	0.20	0.22	0.24
55	0.02	0.25	0.28	0.32
50	0.04	0.25	0.30	0.36
45	0.04	0.30	0.37	0.45
40	0.05	0.29	0.40	0.48
35	0.05	0.28	0.41	0.52
30	0.05	0.30	0.43	0.54
25	0.05	0.30	0.44	0.57
20	0.05	0.27	0.44	0.56
15	0.05	0.27	0.44	0.57
10	0.05	0.25	0.43	0.54
5	0.04	0.26	0.45	0.55
CL	0.05	0.25	0.44	0.54
5	0.05	0.26	0.44	0.53
10	0.04	0.27	0.42	0.48
15	0.03	0.24	0.36	0.40
20	0.03	0.20	0.33	0.37
25	0.03	0.22	0.34	0.34
30	0.03	0.22	0.34	0.30
35	0.03	0.21	0.29	0.23
40	0.04	0.19	0.26	0.18

Note: (1) Positive values are settlement.

(2) Initial reading was on October 11, 1984.

Table A-21. Horizontal movements at inclinometer I-14 in feet.

Depth	6/21/85	7/3/85	7/23/85	3/13/86
3	-0.007	-0.030	-0.070	-0.105
5	-0.004	-0.028	-0.068	-0.112
7	-0.004	-0.027	-0.066	-0.112
9	-0.003	-0.025	-0.062	-0.107
11	-0.003	-0.024	-0.060	-0.105
13	-0.003	-0.022	-0.057	-0.104
15	-0.003	-0.021	-0.056	-0.106
17	-0.003	-0.020	-0.055	-0.109
19	-0.004	-0.020	-0.054	-0.111
21	-0.004	-0.020	-0.053	-0.110
23	-0.003	-0.019	-0.052	-0.108
25	-0.002	-0.018	-0.050	-0.104
27	-0.002	-0.017	-0.048	-0.100
29	-0.002	-0.017	-0.047	-0.099
31	-0.002	-0.016	-0.047	-0.099
33	-0.002	-0.016	-0.046	-0.099
35	-0.002	-0.015	-0.044	-0.098
37	-0.002	-0.014	-0.042	-0.095
39	-0.001	-0.014	-0.041	-0.094
41	-0.001	-0.013	-0.040	-0.094
43	-0.001	-0.013	-0.039	-0.093
45	-0.001	-0.012	-0.039	-0.093
47	-0.000	-0.011	-0.038	-0.093
49	0.000	-0.011	-0.036	-0.090
51	0.000	-0.009	-0.034	-0.086
53	0.000	-0.008	-0.031	-0.081
55	0.000	-0.008	-0.030	-0.077
57	0.000	-0.007	-0.028	-0.074
59	0.000	-0.007	-0.027	-0.071
61	0.000	-0.006	-0.024	-0.067
63	0.000	-0.006	-0.023	-0.064
65	0.000	-0.006	-0.021	-0.060
67	0.000	-0.004	-0.015	-0.047
69	0.000	-0.003	-0.009	-0.029
71	0.000	-0.001	-0.005	-0.012
73	0.000	-0.000	-0.002	-0.006
75	0.000	0.000	-0.000	-0.002
77	0.000	0.000	-0.000	-0.001
79	0.000	0.000	-0.000	-0.001
81	0.000	0.000	-0.000	-0.000

Note: (1) Positive values are movements in the downstream direction.

(2) Initial reading was on June 5, 1985.

Table A-22. Horizontal movements at inclinometer I-15 in feet.

Depth	7/3/85	7/1285	7/23/85	3/12/65
2	0.043	0.056	0.127	0.203
4	0.045	0.056	0.197	0.212
6	0.048	0.080	0.134	0.234
8	0.050	0.084	0.140	0.257
10	0.051	0.087	0.146	0.275
12	0.052	0.091	0.151	0.289
14	0.054	0.095	0.158	0.302
16	0.057	0.100	0.165	0.314
18	0.058	0.103	0.171	0.325
20	0.060	0.106	0.176	0.335
22	0.061	0.109	0.177	0.343
24	0.061	0.111	0.180	0.351
26	0.062	0.112	0.182	0.356
28	0.062	0.114	0.188	0.367
30	0.063	0.116	0.192	0.376
32	0.063	0.115	0.191	0.377
34	0.060	0.112	0.183	0.375
36	0.058	0.110	0.180	0.372
38	0.057	0.108	0.177	0.369
40	0.056	0.106	0.174	0.364
42	0.051	0.104	0.167	0.353
44	0.050	0.097	0.159	0.343
46	0.046	0.092	0.151	0.332
48	0.041	0.082	0.135	0.302
50	0.035	0.069	0.113	0.249
52	0.028	0.055	0.089	0.190
54	0.021	0.038	0.060	0.125
56	0.012	0.019	0.028	0.056
58	0.006	0.009	0.011	0.018
60	0.002	0.004	0.006	0.008
62	0.002	-0.001	0.000	0.000
64	0.000	0.000	0.000	-0.002
66	0.000	0.000	0.000	-0.002
68	0.000	0.000	0.000	-0.000

Note: (1) Positive values are movements in the downstream direction.

(2) Initial reading was on June 17, 1985.

Appendix B

MEMBRANE PLATE ELEMENT

This appendix describes the derivation of the stiffness matrix for a membrane plate element having only axial (radial) stiffness under axially symmetric conditions.

Consider the element shown in Figure B-1, which is subjected to only radial forces which result in only radial and tangential displacements. A local coordinate system is adopted, as shown in Figure B-1. Using an isoparametric element, the displacements can be defined as

$$u = N_1 u_1 + N_2 u_2 \qquad [B.1]$$

where N_1 and N_2 are shape functions for the element and are equal to

$$N_1 = \frac{1}{2}(1 - L) \qquad [B.2a]$$

$$N_2 = \frac{1}{2}(1 + L) \qquad [B.2b]$$

In an analogous manner, the radius can be written as

$$r = N_1 r_1 + N_2 r_2 \qquad [B.3]$$

The strain can be obtained by differentiating Equation B.1 so that

$$\{\varepsilon\} = \begin{Bmatrix} \varepsilon_r \\ \varepsilon_\theta \end{Bmatrix} = \begin{Bmatrix} \dfrac{\partial u}{\partial r} \\ \dfrac{u}{r} \end{Bmatrix} = [B]\{q\} \qquad [B.4]$$

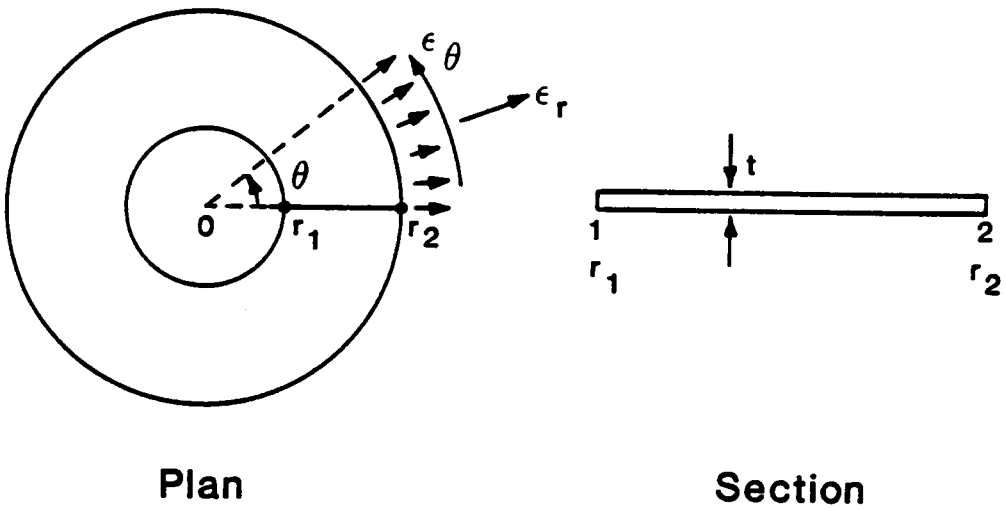

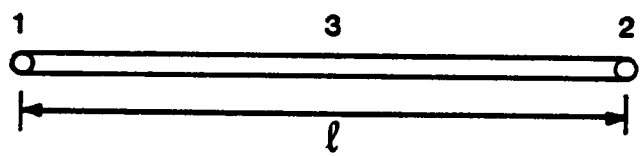

Define Local Coordinate: $L = \frac{r - r_3}{\ell/2}$

r_3 = Midpoint Coordinate: $r_3 = \frac{r_1 + r_2}{2}$

Figure B-1 Axially symmetric membrane plate element: plan view, section view, and local coordinate system.

Now the strain terms ε_r and ε_θ can be obtained from

$$\varepsilon_r = \frac{\partial u}{\partial r} = \frac{\partial u}{\partial L} \times \frac{\partial L}{\partial r} = \frac{1}{l}(-u_1 + u_2) \qquad [B.5]$$

and

$$\varepsilon_\theta = \frac{1}{r}\left(\frac{1}{2}(1 - L)u_1 + \frac{1}{2}(1 + L)u_2\right) \qquad [B.6]$$

We can therefore write

$$\begin{Bmatrix} \varepsilon_r \\ \varepsilon_\theta \end{Bmatrix} = \begin{Bmatrix} \frac{\partial u}{\partial r} \\ \frac{u}{r} \end{Bmatrix} = \begin{bmatrix} \frac{-1}{l} & \frac{+1}{l} \\ \frac{(1 - L)}{2r} & \frac{(1 + L)}{2r} \end{bmatrix} \begin{Bmatrix} q_1 \\ q_2 \end{Bmatrix} \qquad [B.7]$$

The stiffness matrix is

$$[K] = \int [B]^T [C][B] r dr dz d\theta \qquad [B.8]$$

where

$$[B] = \begin{bmatrix} \frac{-1}{l} & \frac{+1}{l} \\ \frac{(1 - L)}{2r} & \frac{(1 + L)}{2r} \end{bmatrix} \begin{Bmatrix} q_1 \\ q_2 \end{Bmatrix} \qquad [B.9]$$

and where $d\theta$ = 1 radian, dz = t (thickness) rdr = $\frac{l}{2}$ r dL. Integrating from L = -1 to +1 This becomes

$$[K] = \int_{-1}^{+1} [B]^T [C][B] r dL \qquad [B.10]$$

where [B] is given in Eqn. [B.9]

Substituting Eqn [B.3] into Eqn [B.10], and performing the matrix multiplication and the indicated integration, the stiffness matrix is found to be

$$[K] = \frac{EI}{(1+\nu)(1-2\nu)} \begin{bmatrix} C_{11} & C_{12} \\ C_{21} & C_{22} \end{bmatrix} \qquad [B.11]$$

where

E = Young's Modulus

ν = Poisson's ratio

l = length of the element

$$C_{11} = \frac{1}{2}\frac{(1-\nu)}{l^2} - \frac{(1+2\nu)}{l} + \frac{(1-\nu)}{4}\left(\frac{1}{l} + 2\frac{(r_1+r_2)}{l^2} + \frac{(r_1+r_2)^2}{l^3}\right)\log\left(\frac{r_2}{r_1}\right)$$

$$C_{12} = -\frac{1}{2}\frac{(1-\nu)}{l^2} + \frac{(1-\nu)}{4}\left(\frac{1}{l} - \frac{(r_1+r_2)^2}{l^3}\right)\log\left(\frac{r_2}{r_1}\right)$$

$$C_{21} = C_{12}$$

$$C_{22} = \frac{1}{2}\frac{(1-\nu)}{l^2} + \frac{(1+2\nu)}{l} + \frac{(1-\nu)}{4}\left(\frac{1}{l} - 2\frac{(r_1+r_2)}{l^2} + \frac{(r_1+r_2)^2}{l^3}\right)\log\left(\frac{r_2}{r_1}\right)$$

Equation [B.11] was coded into a FORTRAN subroutine and added to the axisymmetric program CONSAX (D'Orazio and Duncan 1982). This provided the ability to model axisymmetric reinforced foundation problems. The bevhavior of this element was verified by comparison to results using

theoretical elasticity equation presented by Timoshenko and Goodier (1951).

Equation [B.11] shows the stiffness to be a function of E, Young's modulus and ν, Poisson's ratio. As derived, these values are for an isotropic medium. Geogrids exhibit different strength and stiffness characteristics in the longitudinal and the transverse directions. The larger of the two stiffness values can be termed the the major stiffness (modulus) and the other as the minor stiffness (modulus). Applications involving geogrid reinforcing materials and other bidirectional modulus materials require the development of a single, equivalent modulus for use in Equation [B.11]. Such a modulus was developed in the manner outlined below.

The computer program SSTIPG, developed by Low and Duncan (1985), contains a composite reinforcing-soil element which employs different stiffness values for the reinforcement in perpendicular directions. A segment of a circle was modelled using this program, assuming zero soil strength and using various major and minor reinforcement stiffness values. A parametric study was performed of the displacement resulting from the application of uniform radial loads applied to the outer radius of the circle segment. These displacements were compared to the theoretical displacement values obtainable for isotropic materials using the relationships presented by Timoshenko and Goodier (1951):

$$\frac{u}{r} = \frac{1}{E}\sigma(1 - \nu) \qquad [B.12]$$

where

u = radial displacement

r = radius at point of concern

σ = applied radial stress at radius r.

Computed results using the program SSTIPG for equal major and minor moduli matched Equation [B.12] very well. Next, the minor modulus was reduced to some fraction of the major modulus to simulate the bidirectional stiffness of geogrids. The resulting displacements were then compared with those obtained using equal values of modulus in both directions.

If Equation [B.12] is solved for E, and Poisson's ratio is set equal to zero, a reasonable assumption for geogrids, we can obtain

$$E = \frac{\sigma}{\frac{u}{r}} \qquad [B.13]$$

u can be renamed Δr, the change in radius, and r renamed r_o, the original radius. Now an equivalent modulus is defined as

$$\overline{E} = \frac{\sigma}{\frac{\overline{\Delta r}}{r_o}} \qquad [B.14]$$

where $\overline{\Delta r}$ is the average change in radius computed when different stiffness values are used in perpendiular directions. If we maintain the same stress, σ and initial radius, r_o in Equations [B.13] and [B.14] and find the ratio $\frac{\overline{E}}{E}$, we obtain

$$\frac{\overline{E}}{E} = \frac{\frac{u}{r}}{\frac{\overline{\Delta r}}{r}} \qquad [B.15]$$

Values of $\overline{\Delta r}$ were determined by performing a parametric study using SSTIPG in which values of the minor modulus were taken as some fraction of the major modulus. From this study, the curve in Figure B.2 was developed, in which the equivalent modulus divided by the major modulus is shown to be a function of the ratio of the minor and major moduli. This curve was found to be independent of the major modulus value and is applicable to any bidirectional stiffness material with Poisson's ratio equal to zero.

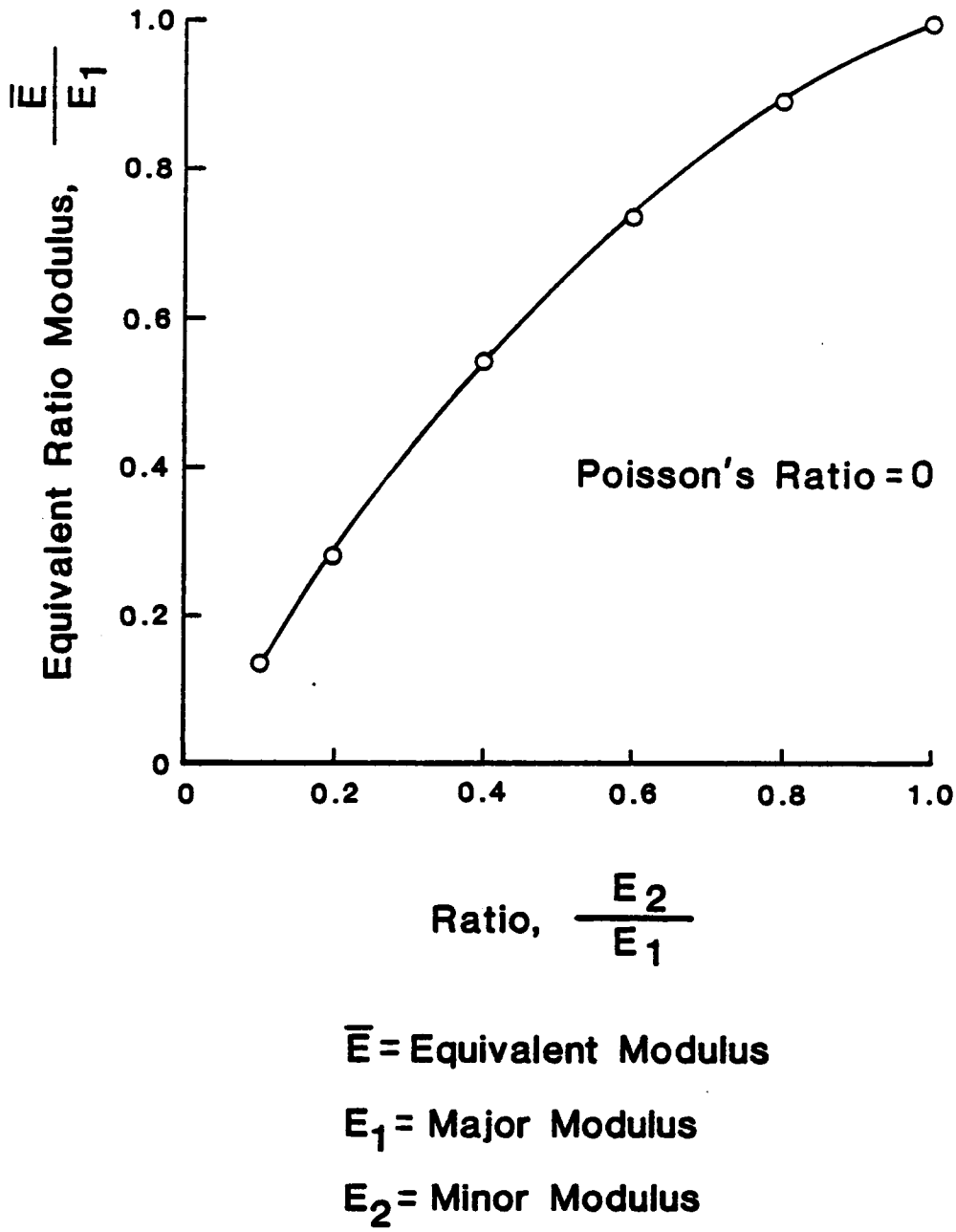

Figure B-2 Relationship between equivalent modulus and the ratio of the major and minor modulus values for bi-directional geogrids.

Appendix C

USER'S GUIDE FOR PROGRAM CON2D86

C.1 Introduction

The program CON2D86 is a plane strain finite element computer program for analysis of stresses, displacements and consolidation in saturated and partly saturated earth masses. The program can be used to analyze consolidation in embankment dams during and after construction, and in foundation soils subject to surface loads imposed by fills, buildings and storage tanks. The program treats the coupled problem of deformation and fluid flow, and can be used to calculate movements and pore pressures under undrained, partly drained and fully drained conditions. Reinforced soil structures can be analyzed using bar elements.

CON2D86 was originally developed by Chang and Duncan (1977) and was later modified by Duncan et al. (1981). The program follows the general programming concepts and solution techniques developed by Wilson (1970) and Bathe and Wilson (1976). The present version incorporates a bar element to model reinforcement, and provides enhanced source code documentation and efficiency.

C.2 Program Operation

C.2.1 Systems and Sign Convention

The global coordinate system is a right handed X-Y system with X increasing to the right and Y increasing vertically.

Soil element and interface normal stresses are positive in compression and negative in tension. The soil stresses are all effective stresses. Positive pore pressures are compressive. Total stresses are obtained by adding pore pressures at the center of elements to the effective soil stresses.

Bar element forces are output in a local coordinate system. Axial force is positive if the member is in compression and negative if in tension.

C.2.2 Storage Allocation

Dynamic storage allocation (Bathe and Wilson 1976) is used within the program and storage is allocated at the time of execution. The storage can be readily adjusted through the COMMON (A) statement in the source code. Storage requirements are checked immediately after reading the control data, and if insufficient, an error message printed detailing the minimum storage requirements for the problem and execution is halted.

The equation-solving subroutines use only one-half of the full banded stiffness matrix. Secondary storage (disk or tape storage) is used to

minimize the amount of core storage required by solving the equations by blocks (Wilson et al. 1974). The smaller the number of equations per block, the greater is the required number of transfers between core and secondary storage, and the more costly is the solution procedure. Thus, the more storage allocation exceeds the minimum value, the larger is the number of equations per block, and hence the shorter is the solution time.

C.2.3 Element Types

CON2D86 has three types of elements as follows:

1. Soil elements are four-to-eight variable node, two-dimensional, isoparametric elements as described by Bathe and Wilson (1976). Each node may also have a pore pressure degree-of-freedom. Any number of nodes from four to eight can be specified for each element. Triangular shaped elements can be formed by superimposing nodes. The nodal point numbers must be specified in the order I, II, III, IV, V, VI, VII, VIII as shown in the upper part of Figure C-1. For an element with fewer than eight nodes, the nodal point numbers of the omitted nodes are set equal to zero, as shown in the bottom of Figure C-1. For triangular elements, the nodal point number III must be equal to the nodal point number IV.

2. Bar elements are two node elements with axial stiffness only (no flexural or shear resistance), and may be used to connect any two nodal points.

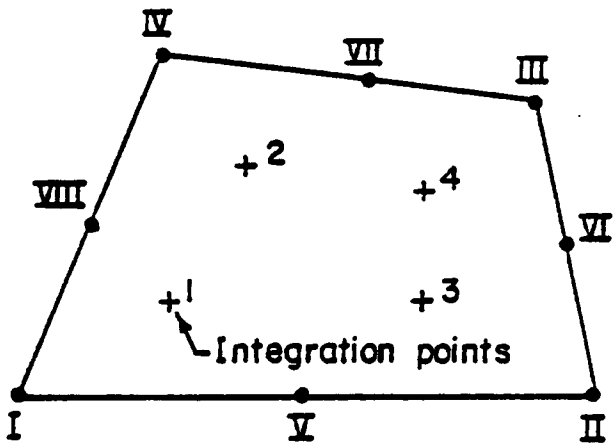

Note: Node I must be in lower left corner of element.

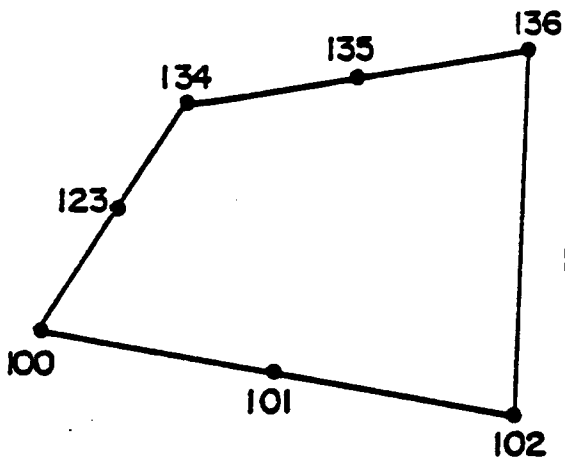

NEL = 7

I	II	III	IV	V	VI	VII	VIII
100	102	136	134	101	0	135	123

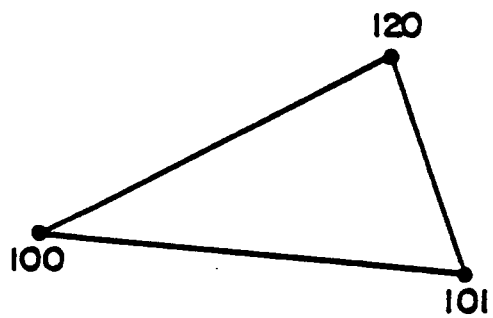

NEL = 4

I	II	III	IV	V	VI	VII	VIII
100	101	120	120	0	0	0	0

Figure C-1 Nodal point numbering for two-dimensional elements.

3. Linkage elements may be used to represent interfaces between a structure and adjacent soil or between zones within a soil mass. As shown in Figure C-2, a linkage element connects two nodal points called I and J, which may have identical coordinate values. The stiffness of the linkage element represents the properties of a section of the interface. The length and orientation of the section of the interface represented by the linkage element are defined by two nodal points called NI and NJ. The orientation of the interface in along the line NI-NJ. The shear direction is parallel to NI-NJ, and the normal direction is perpendicular to NI-NJ. The length of the section of the interface is one-half of the distance from NI to NJ. The examples of linkage element numbering shown in Figure C-3 illustrate how the orientations of linkage elements and the lengths of sections of the interface they represent are defined in terms of nodes I, J, NI and NJ.

C.2.4 Meshes

A example mesh for analysis of an embankment dam is shown in Figure C-4. The nodal points are numbered from left to right across each level. Elements are numbered in the same way, with the element numbers increasing from left to right in each layer and from the bottom up. For accurate displacements, stresses, and pore pressures, embankment meshes should have six or more layers of elements above the foundation.

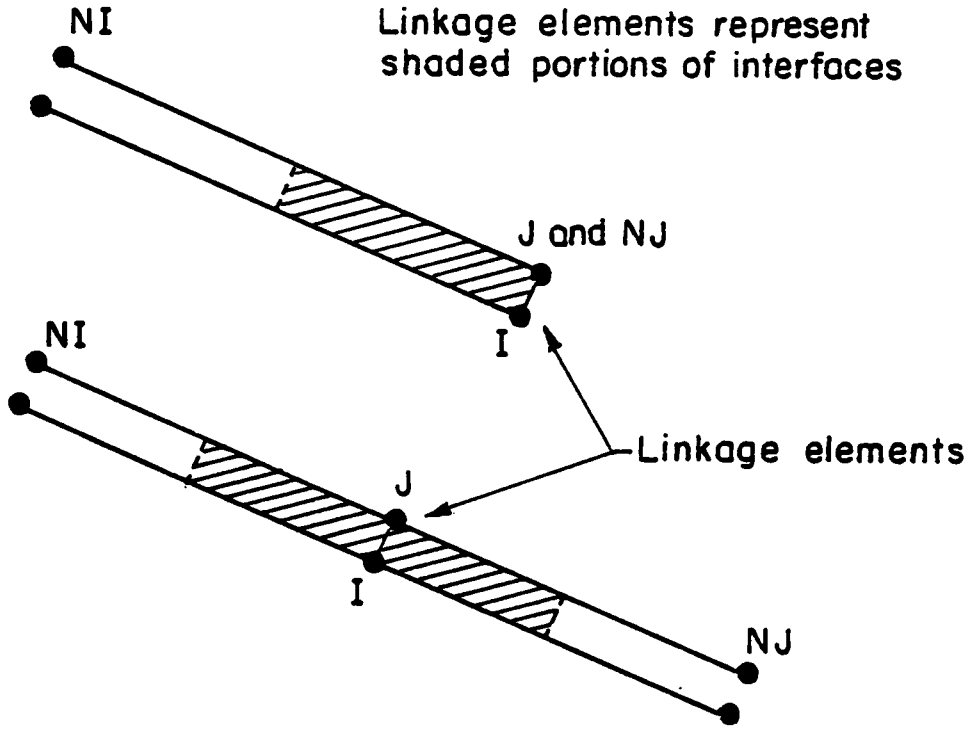

LINKAGE ELEMENTS CONNECT NODE I WITH NODE J

LENGTH = $\frac{1}{2}$ DISTANCE FROM NI TO NJ

SHEAR DIRECTION PARALLEL TO LINE FROM NI TO NJ

NORMAL DIRECTION PERPENDICULAR TO LINE FROM NI TO NJ

Figure C-2 Nodal point numbering conventions for linkage elements.

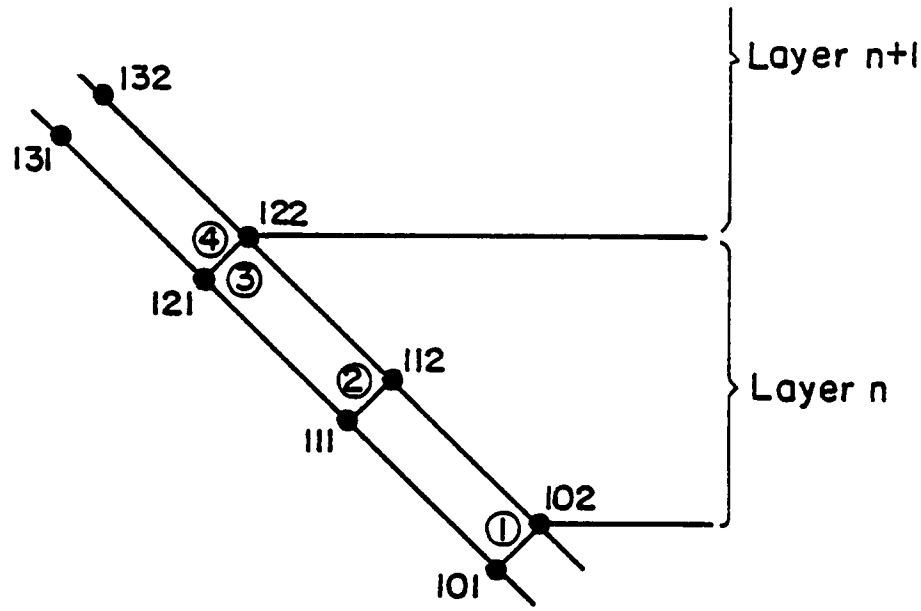

Linkage Element	I	J	NI	NJ
1	101	102	112	102
2	111	112	122	102
3	121	122	122	112
4	121	122	132	122

Linkage element ③ represents half of interface from node 112 to node 122, and would be added to mesh with layer n. Linkage element ④ represents half of interface from node 122 to node 132, and would be added to mesh with layer n + 1.

Nodes 101 and 102, 111 and 112, etc., may have same coordinates.

Figure C-3 Linkage element example.

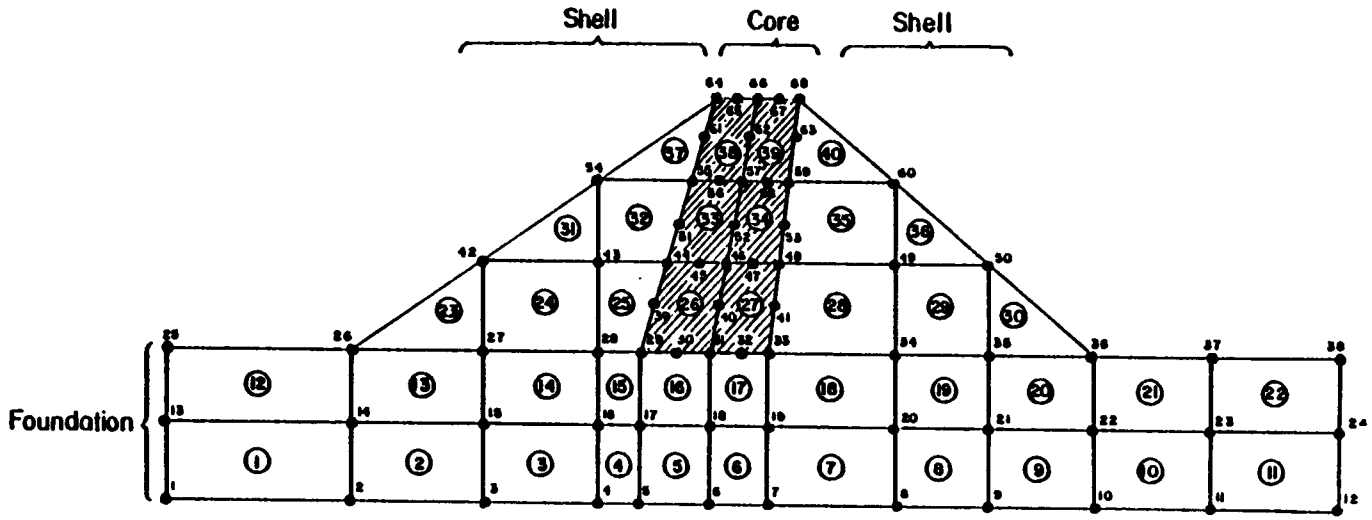

Note: Example mesh. More elements required for accurate results.

Figure C-4 Example mesh for an embankment dam.

Pre-existing elements in any configuration may be included within or beneath the embankment. As shown in Figure C-5, the pre-existing part of the mesh may be beneath the embankment, adjacent to the embankment, or entirely within the final geometry of the complete embankment, and it may consist of more than one part. The initial stresses, displacement, and pore pressures may be generated by earlier analyses with CON2D86 or by hand calculations. The strains in the pre-existing part can be set equal to zero by the program, or non-zero values can be read in by the user, at the user's option.

C.2.5 Increments

An increment may consist of the placement of a layer on an embankment, or of an application of loads to a mesh. Placement of a layer of fill is simulated by applying forces to represent the weight of the added layer. The layer being placed is assigned very small modulus values to simulate the fact that a newly added layer of uncompacted fill on an embankment has very low stiffness. Each element in the newly placed layer is assigned stresses consistent with the overburden pressure at its center. The strains in the newly placed elements are set equal to zero, and taken as the reference state of strain. For accurate results, it is best to add only one layer of elements at a time, and in general, six or more layers of elements in the mesh will provide reasonably accurate results.

A layer to be added in an increment is defined by specifying the first and last elements to be added [NOMEL(LN,1) and NOMEL(LN,2)], the first

Embankments with Preexisting Parts

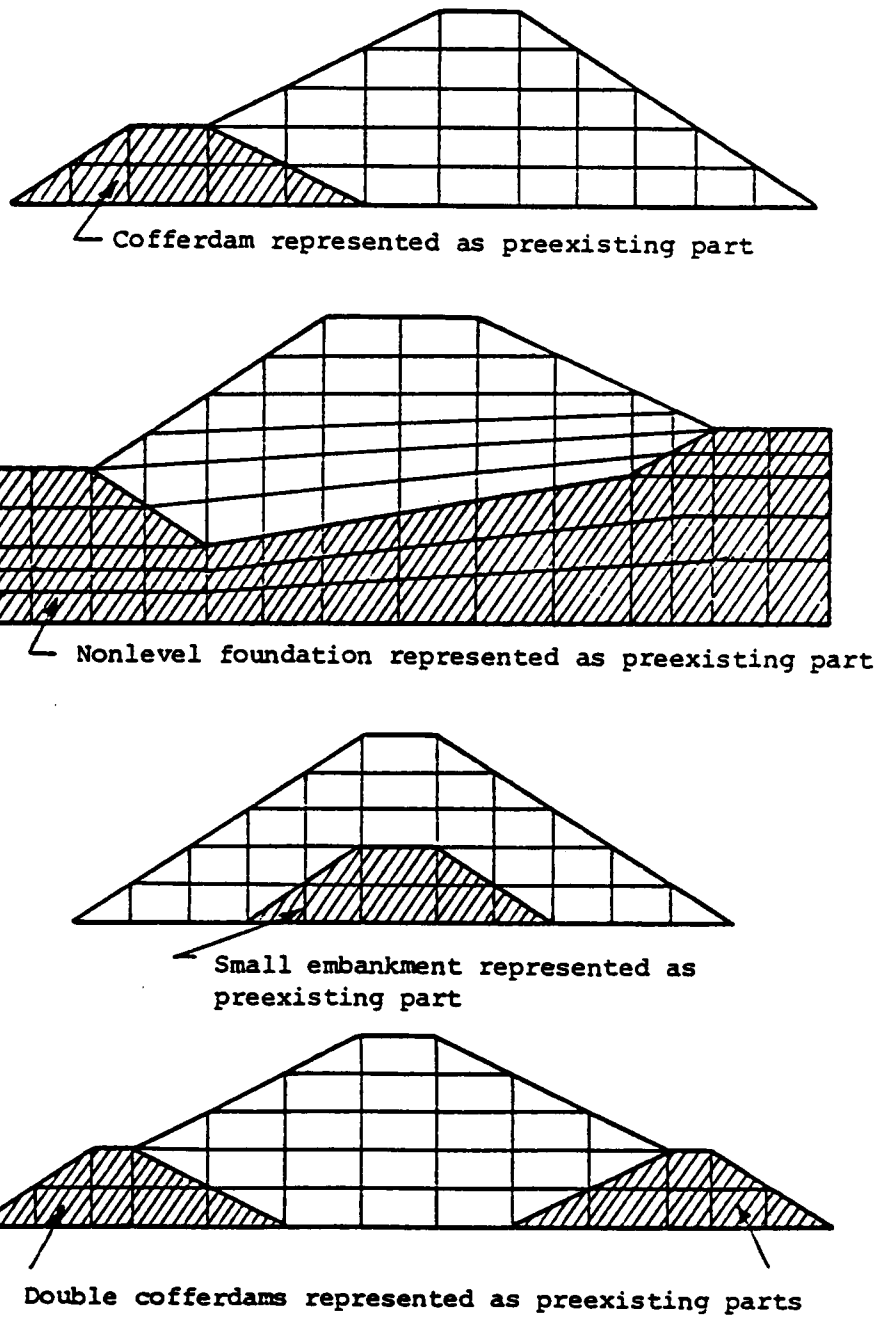

Figure C-5 Example meshes for embankment with pre-existing parts.

and layer nodal points to be added [NOMNP(LN,1) and NOMNP(LN,2)], and by data which define the position of the surface of the newly added layer, as shown in Figure C-6. The program assumes that all of the elements between and including those specified as the first and last are being added, and the same is true for nodal points. Therefore meshes must be numbered so that this convention is followed.

The surface of the new layer is specified by four nodes [NPHUMP(LN,1 to 4)] which define what is called the humped surface. This surface defines the top of the newly placed layer for purposes of calculating overburden pressures in newly placed elements. To the left of the first nodal point and to the right of the last nodal point which define the surface, the surface is assumed to be level.

The nodal points having pore pressure degrees of freedom and which are on the surface of the layer are specified in NOMNP. All of the nodes between NOMNP(LN,3) and NOMNP(LN,4) are assumed to be on the surface of the layer and are assigned zero initial pore pressures.

Loads applied to a mesh may be specified in terms of nodal point forces or boundary pressures. Nodal point forces have units of force per unit length, because the two-dimensional mesh represents a slice of unit thickness through the embankment.

Distributed loads are input by specifying two nodal points (I and J) on one side of an element and the pressures (PRESI and PRESJ) at these nodes. As shown in Figure C-7, the sign convention is such that, with I on the left and J on the right, the load is directed toward the observer.

Quantity	Specifies	Value For LN = 1	LN = 2
NOMEL(LN,1)	First added element	1	10
NOMEL(LN,2)	Last added element	9	15
NOMNP(LN,1)	First added nodal point	1	26
NOMNP(LN,2)	Last added nodal point	25	35
NOMNP(LN,3)	First nodal point to be assigned zero pore pressure	20	31
NOMNP(LN,4)	Last nodal point to be assigned zero pore pressure	22	33
NPHUMP(LN,1)	First nodal point on humped surface	1	17
NPHUMP(LN,2)	Second	16	29
NPHUMP(LN,3)	Third	25	35
NPHUMP(LN,4)	Fourth nodal point on humped surface	12	25

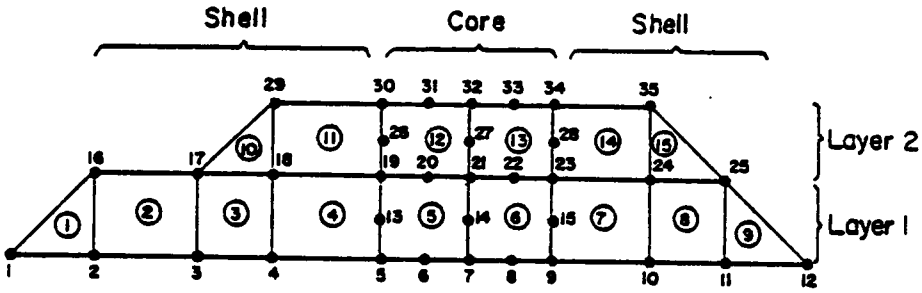

Note: Nodal points which are assigned pore pressure degrees of freedom, and which are at the top of a layer, should be defined in NOMNP so they will be assigned zero pore pressures initially. The humped surface defines the upper boundary of the new layer for purposes of calculating initial stresses in the elements.

Figure C-6 Example data for construction layers.

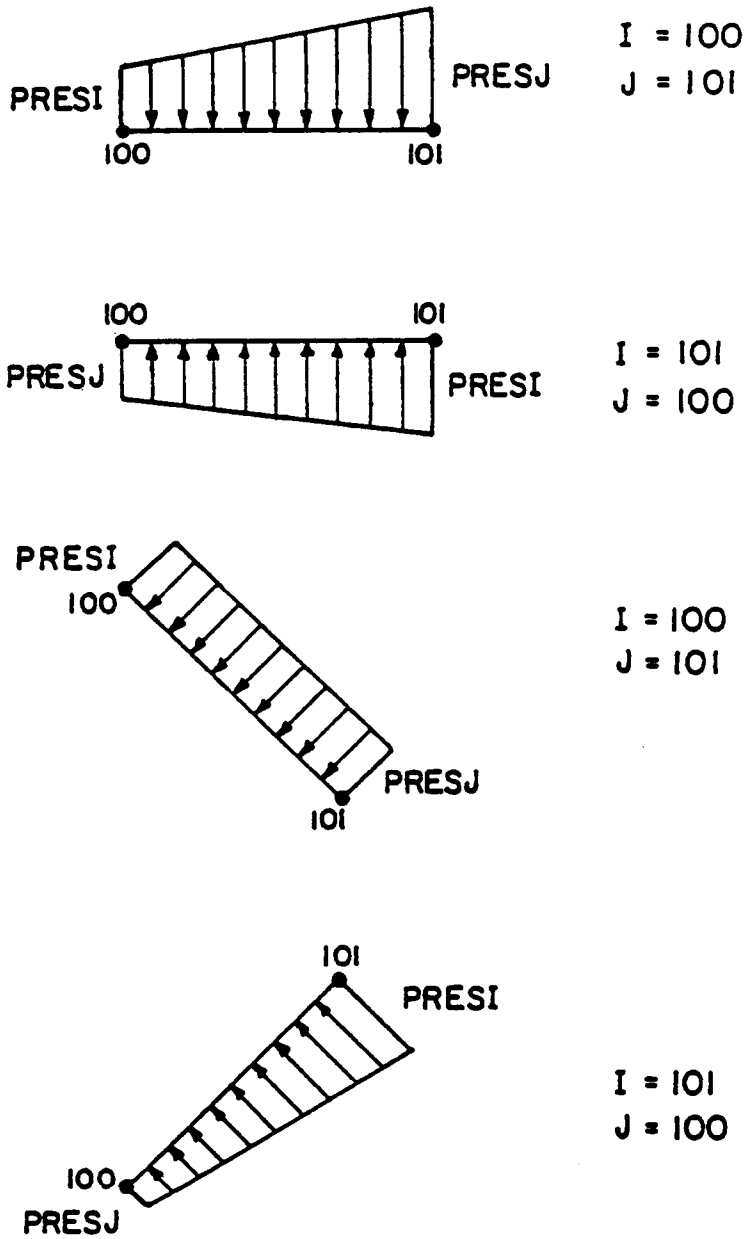

Figure C-7 Example data for distributed loads..

The data required to describe changes in the reservoir level on the upstream side of a dam are illustrated in Figure C-8. Within the shell, elements are subjected to a reduction in effective unit weight when they are submerged below a rising reservoir, and an increase in effective unit weight when they emerge above a falling reservoir.

The changes in water pressure along the shell/core boundary are calculated within the program using the information specified in NUMSWP(I), LEVOLD and NEWLEV. Because these data are specified in terms of nodal point numbers, each water level elevation must coincide with the elevation of a nodal point on the shell/core boundary. Because of the sign convention used in the program, downstream must be in the positive x-direction (to the right).

C.3 Program Organization

The main program (CON2D86) reads and prints the control data and monitors all operations by calling the subroutines in the specified order.

1. Subroutine LAYOUT controls the subroutines which read the input data. Subroutine LAYOUT calls INPTNP to read and print nodal point data, MATIN to read and print soil material property data, BARIN to read and print bar element data, LINKIN to read and print linkage element data, PREXIN to read and print pre-existing element data, ELEMIN to read and print soil element data, and CLBAND to calculate the bandwidth for the problem. Storage requirements are calculated and if

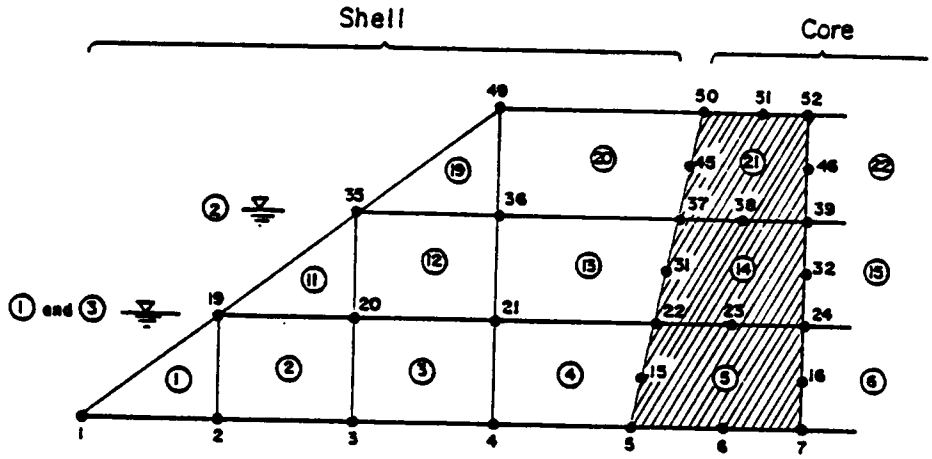

Data specifying nodal points on shell/core boundary:
NUMNPF = 7 (total number)
NPF(I) = 5, 15, 22, 31, 37, 45, 50 (list of nodal points)

Data specifying water level positions and affected elements and nodal points.

Quantity	Specifies	Value For Stage 1	Stage 2	Stage 3
NUMBYP	Number of elements submerged or drained	4	3	3
DELGAM	Change in unit wt. for these elements	Neg.	Neg.	Pos.
NBYEL(I)	List of elements submerged or drained	1,2,3,4	11,12,13	11,12,13
LEVOLD	Nodal point at elev. of old water level	5	22	37
NEWLEV	Nodal points at new water level, on shell/ core boundary	22	37	22
ISIGN	Direction of water pressure (ISIGN = 1 for pressure in x-direction. ISIGN = -1 for pressure in -x-direction.)	1	1	1

Figure C-8 Example data for changes in reservoir level.

the problem requires more storage, a message is printed and execution halted.

2. Subroutine INITL reads and/or calculates the initial values of stresses, strains, displacements and pore pressures for pre-existing elements and added layer elements.

3. Subroutine FORMB establishes the strain-displacement matrix for the soil elements by calling BMATPS, which forms the strain-displacement matrix for a four- to eight-node isoparametric, quadrilateral element. BMATPS calls JACOBI to form the Jacobian, which calls SHAPE to calculate the shape functions.

4. Subroutine CALBLK reads the control data for each increment and determines the number of elements and nodal points being analyzed, the number of elements and nodal points in the pre-existing part and added layers, the number of equations, the number of equations in each block, and the number of blocks for each increment.

5. Subroutine FVECT calculates nodal point forces due to weights of added elements, or due to buoyancy forces and reads and prints concentrated load data and boundary pressure data.

6. Subroutine ELSTFF formulates the stiffness matrix for each element. ELSTFF call STST to form the stress-strain relationship for the soil elements and calls MODIFY to modify the load vector for each time

step. STST calls POICAL and LAMCAL to compute the current values of Poisson's ratio and lambda, calls ELAST to calculate the elastic part of the stress-strain relationship, and calls CAMCLY to calculate the elasto-plastic stress-strain relationship. ELSTFF calls QK to calculate the current compressibility and permeability of the pore fluid in each element.

7. Subroutine ADDSTF forms the global stiffness matrix. The soil element stiffness values are read from tape and the stiffness values for bar and linkage elements are found by calling BRSTIF and LKSTIF.

8. Subroutine TRIAFAC triangulizes the global stiffness matrix.

9. Subroutine REDVK back substitutes and solves the equations for displacement and pore pressure.

10. Subroutine RESULT calculates the current values of stress and strain. RESULT calls OUTPUT to print out the results.

C.4 Data Input Guide

C.4.1 Control Data

C.4.1.1 Heading Data (72A)

HEAD Title for program identification.

C.4.1.2 First Control Data Data

NUMELT Total number of soil elements in the complete mesh.

NUMNPT Total number of nodal points in the complete mesh.

NUMMAT Number of different soil material types.

NUMCEL Number of soil elements in the pre-existing part.

NUMCNP Number of nodal points in the pre-existing part.

NLAY Number of construction layer increments.

NFORCE Number of load increments after construction.

NUMSWP Total number of nodal points on the shell/core boundary at which changes in water pressure will occur during any of the steps of the analysis.

C.4.1.3 Second Control Data Data

NBRELT Total number of bar elements in the complete mesh.

NBRMAT Number of different bar material types.

NUMCBR Number of bar elements in the pre-existing part.

NLKELT Total number of linkage elements in the complete mesh.

NLKMAT Number of different linkage material types.

NUMCLK Number of linkage elements in the pre-existing part.

C.4.2 Nodal point and boundary condition data.

N Nodal point number.

X(N) X-coordinate (+ to the right).

Y(N) Y-coordinate (+ up).

ID(N,1) Boundary condition code for displacement in the x-direction.

ID(N,2) Boundary condition code for displacement in the y-direction.

ID(N,3) Boundary condition code for pore pressure.

Nodal points must be read in sequence. If nodal point data are omitted, the coordinates of a series of nodal points are generated automatically at equal spacing between those specified. The boundary condition codes for the generated nodal points are set equal to the boundary condition codes for the previous nodal point. The first and last points must be specified.

The boundary condition code convention is as follows:

Quantity	Condition	Code

x displacement	always zero	ID (N,1) = 1
	may be non-zero	ID (N,1) = 0
y displacement	always zero	ID (N,2) = 1
	may be non-zero	ID (N,2) = 0
pore pressure	always zero	ID (N,3) = 1
	may be non-zero	ID (N,3) = 0

C.4.3 Material Property Data

C.4.3.1 Units Conversion Data

PATM Atmospheric pressure expressed in the system of units used in the problem.

GAMAW Unit weight of water expressed in the system of units used.

For example:

Length off	Unit Weight	Cohesion	Stiffness	Atmospheric Pressure	Unit weight of Water
ft	ton/ft	ton/ft	ton/ft	1.058	0.0312
ft	kip/ft	kip/ft	kip/ft	2.116	0.0624
ft	lb/ft	lb/ft	lb/ft	2116.2	62.4
m	ton/m	ton/ft	ton/ft	10.33	1.00
M	kN/m	kN/m	kN/m	101.3	9.807
cm	kg/cm	kg/cm	kg/cm	1.033	0.001
in	lb/in	psi	lb/in	14.70	0.0361

C.4.3.2 Soil Material Properties

9 lines of data are required for each material.

M Material type number (MATNO).

EMPR(M,1) Permeability code (PCODE).

0.0 - for a material which is to be assumed infinitely permeable, for example, the granular shell material in a zoned earth dam.

1.0 - for a material which is not infinitely permeable, for example, the core material in a zoned earth dam.

EMPR(M,2) Unit weight (moist unit weight), γ (GAMMAW).

EMPR(M,3) Cam clay soil parameter, κ (KAPPA).

EMPR(M,5) Intercept, p_r (effective stress) (PRINTR).

EMPR(M,6) Slope, $M_{triaxial}$ (effective stress) (MTRIAX).

EMPR(M,9) Horizontal saturated permeability, k_{hs} (PERMX).

EMPR(M,10) Vertical saturated permeability, k_{vs} (PERMZ).

EMPR(M,11) Degree of saturation at which the water begins to move freely, S_f (SF).

EMPR(M,12) Initial void ratio, e_o (VOID).

EMPR(M,13) Initial degree of saturation, S_o (SATURN).

EMPR(M,14) Pressure at which break in slope occurs, p'_{break} (PBREAK).

EMPR(M,15) Intercept after break, p_r (PRINTR).

EMPR(M,16) Slope after break, $M_{triaxial}$ (MTRIAX).

EMPR(M,17) Preconsolidation pressure, P'_p (mean normal stress) (PO). (PO).

EMPR(M,18) Tensile strength, σ_t (TENSTR).

The above values of initial void ratio, initial degree of saturation, and preconsolidation pressure are used only for material properties of elements that are not preexisting. The values of these properties for preexisting elements are submitted in line 9b.

Second through fifth lines:

These data describe as many as 16 points on the p'_o -λ curve for the material.

Second and third lines:

EMPR(M,31) Pressure, p'_o corresponding to the first λ point.

EMPR(M,32) Pressure, p'_o corresponding to the second λ point.

etc. continue for as many points as needed to dexcribe the $p'_o - \lambda$ curve. Two lines are required even in the case where the $p'_o - \lambda$ curve is defined by eight or fewer points. If eight or fewer points are used, the second line is blank.

Fourth and fifth lines:

EMPR(M,47) Slope, λ of the first point.

EMPR(M,48) Slope, λ of the second point.

etc. Two lines are required even in the case where the $p'_o - \lambda$ curve is defined by eight or fewer points. If eight or fewer points are used, the second line is blank.

Sixth through ninth lines:

These lines describe as many as 16 points on the p'-v curve for the material.

Sixth and seventh lines:

EMPR(M,63) Mean normal pressure, p' corresponding to the first point.

EMPR(M,64) Mean normal pressure, p' corresponding to the second point.

etc. Two lines are required even in the case where the p'-v curve is defined by eight or fewer points. If eight or fewer points are used, the second line is blank.

Eighth and ninth lines:

EMPR(M,79) Poisson's ratio corresponding to the first point.

EMPR(M,80) Poisson's ratio corresponding to the second point.

etc. Two lines are required even in the case where the $p'_0 - v$ curve is defined by eight or fewer points. If eight or fewer points are used, the second line is blank.

C.4.4 Bar Element Data

If NBRELT = 0, these data are omitted.

C.4.4.1 Material Property Data

N Material type number.

PROPBR(N,1) E, elastic modulus.

PROPBR(N,2) A, area of bar.

PROPBR(N,3) Weight/length ratio.

C.4.4.2 Bar Element Data

One line of data for each bar element.

M Element number.

INPBR(M,1) Material type number.

INPBR(M,2) Nodal point number for node I.

INPBR(M,3) Nodal point number for node J.

C.4.4.3 Initial bar force data.

One line of data for each bar element.

N Bar element number.

STBTOT Initial force in pre-existing bar element number N.

C.4.5 Linkage Element Data

If NLKELT = 0, these data are omitted.

C.4.5.1 Material Property Data

N Material type number.

PROPLK(N,3) Cohesion of linkage material.

PROPLK(N,4) Friction angle of linkage material.
Note: PROPLK(N,1) and PROPLK(N,2) are the normal and shear stiffness of the link and are set in the program.

C.4.5.2 Linkage Element Data

One line of data for each linkage element.

M Element number.

INPLK(M,1) Material type number.

INPLK(M,2) Nodal point number for node I.

INPLK(M,3) Nodal point number for node J.

NI Nodal point number for node NI.

NJ Nodal point number for node NJ.
Definition of points I, J, NI, and NJ, and example data are shown in Figures C-2 and C-3.

C.4.5.3 Pre-existing Linkage Element Data

If NUMCLK = 0, these data are omitted.
Use as much data as required for NUMCLK linkage elements.

LINKC(1) Element number of first pre-existing element number.

LINKC(2) Element number of second pre-existing element number.

LINKC(N) Etc. for N pre-existing elements.

C.4.5.4 Pre-existing Linkage Element Stress Data

If NUMCLK = 0, these data are omitted.
Use one lind of data for each pre-existing linkage element.

N Element number.

STRSLK(N,1) Initial normal linkage stress.

STRSLK(N,2) Initial shear linkage stress.

C.4.6 Pre-existing Element and Nodal Point Data

C.4.6.1 Pre-existing Soil Element Data

If NUMCEL = 0, these data are omitted. Use as much data as required for NUMCEL elements.

ICEL Number of first pre-existing element.

JCEL Number of second pre-existing element.
Element numbers are generated in sequence between those specified, and one sequence of elements is defined by each line of data. For an isolated pre-existing element, ICEL and JCEL are the same, describing a sequence of one. Use one lind of data per sequence or series of elements.

C.4.6.2 Pre-existing Nodal Point Data

If NUMCNP = 0, these data are omitted. Use as much data as required for NUMCNP elements.

ICNP Number of first pre-existing nodal point.

JCNP Number of second pre-existing nodal point.
Nodal point numbers are generated in sequence between those specified, and one sequence of nodal points is defined by each line of data. For an isolated pre-existing nodal point, ICNP and JCNP are the same, describing a sequence of one. Use one line of data per sequence or series of nodal points.

C.4.7 Soil Element Data

One line of data for each element.

M Element number.

NELNP(N) Number of nodes in this element (4-8).

MTYPE(N) Material type number.

INP(N,1) Nodal point number I.

INP(N,2) Nodal point number II.

INP(N,3) Nodal point number III.

INP(N,4) Nodal point number IV.

INP(N,5) Nodal point number V.

INP(N,6) Nodal point number VI.

INP(N,7) Nodal point number VII.

INP(N,8) Nodal point number VIII.

Soil element data must be read in sequence. The nodal point numbers must be specified in the order I,II,III,IV,V, VI,VII,VIII as shown in the upper part of Figure C-1. For an element with fewer than eight nodes, the nodal point numbers of the omitted nodes must be specified as zero. For triangular elements, the nodal point number III must be equal to the nodal point number IV, as shown at the bottom of Figure C-1. The locations of the integration points, where pore pressures are calculated, are also shown in Figure C-1.

N = 1 for the first soil element.
N = 2 for the second soil element.
etc.

C.4.8 Construction Layer Element and Nodal Point Data

One line of data for each construction layer.
If NLAY = 0, these data are omitted.

LN Construction layer number. Layer numbers increase upward from the bottom.

NOMEL(LN,1) Smallest soil element number of the newly placed elements in this layer.

NOMEL(LN,2) Largest soil element number of the newly placed elements in this layer.

NOMEL(LN,3) Smallest bar element number of the newly placed bar elements in this layer.

NOMEL(LN,4) Largest bar element number of the newly placed bar elements in this layer.

NOMNP(LN,1) Smallest nodal point number of the newly placed nodal points in this layer.

NOMNP(LN,2) Largest nodal point number of the newly placed nodal points in this layer.

NOMNP(LN,3) Smallest nodal point number on the new boundary surface with pore pressure degree of freedom.

NOMNP(LN,4) Largest nodal point number on the new boundary surface with pore pressure degree of freedom.

NPHUMP(LN,1) First nodal point on the humped surface.

NPHUMP(LN,2) Second nodal point on the humped surface.

NPHUMP(LN,3) Third nodal point on the humped surface.

NPHUMP(LN,4) Fourth nodal point on the humped surface.

Do not use vertical segments in the humped surface, because this will result in division by zero. See Figure C-6 for an example of construction layer data input format.

C.4.9 Stress, Strain, Displacement and Pore Pressure Data for Pre-existing Part.

If NUMCEL = 0, these data are omitted.

C.4.9.1 Control Data

NMODE Strain code of input data.
0 = stresses, displacements, pore pressures, and strains are to be read.
1 = stresses, displacements, and pore pressures are to be read and strains are set equal to zero.

C.4.9.2 Initial Stress and Property Data for Soil Elements.

NUMCEL linde of data are needed unless generation procedure is used.

N Element Number.

STRESS(N,1) σ'_x

STRESS(N,2) σ'_y

STRESS(N,3) σ'_z

STRESS(N,4) τ_{xy}

STRESS(N,5) Pore pressure at center of element.

VOID(N) Initial void ratio, e_o

SATURN(n) Initial degree of saturation, S_o

PO(N) Preconsolidation mean stress, P_o

Compressive stresses are positive. The x and y coordinates are in the plane of the analysis, z is normal to the plane.

If initial stress and property data are omitted, the program assigns the initial stress and properties of the immediately preceding element to the omitted elements.

C.4.9.3 Initial Displacement and Pore Pressure Data

Need NUMCNP lines of data (if generation is not used).

N Nodal point number

U(N) Initial pore pressure at node N.

DISP(N,1) Initial X-displacement.

DISP(N,2) Initial Y-displacement.

If initial displacements and pore pressure data are omitted, the program assigns the initial displacement and pore pressures of the node that immediately precedes the omitted nodes. Data for the first and last nodes must be input.

C.4.9.4 Initial Strain Data

If NMODL = 1, these data are omitted. Otherwise NUMCEL line of data are required (if generation is not used).

N Element number

STRAIN(N,1) Initial value of ε_x

STRAIN(N,2) Initial value of ε_y

STRAIN(N,3) Initial value of ε_z

STRAIN(N,4) Initial value of τ_{xy}.

If initial strain are needed, generation of in between data can be program assigns the initial strain of the node that immediately precedes the omitted nodes. Data for the first and last nodes must be input.

C.4.9.5 Specified Water Pressure Boundary Data

If NUMSWP = 0, these data are omitted. Otherwise use as many as required for NUMSWP nodal points.

NSWP(1) First nodal point

NSWP(2) Second nodal point

NSWP(N) Nth nodal point

These nodes are those on the shell/core boundary at which changes in water pressure will occur at any of the steps of the analysis. These nodal points should be specified in the order from the botton of the mesh to the top.

C.4.10 Layer, Force and Time Increment Data

Need (NLAY + NFORCE) sets of data, each consisting of the following 8 lines of data.

C.4.10.1 Newly Placed Bar Element Data

If NBRELT = 0, these data are omitted.

First Data

NBREL Number of newly placed bar elements in this step.

Second Data: If NBREL = 0, these data are omitted. Otherwise use as many lines of data as required for NBREL newly placed bar elements.

NUMBR(1) First newly placed bar element

NUMBR(2) Second newly placed bar element

etc. Continue on for NBREL number of lines of data.

0

C.4.10.2 Newly Placed Linkage Element Data

If NLKELT = 0, these data are omitted.

First Data

NLKEL Number of newly placed linkage elements in this step.

Second Data: If NLKEL = 0, these data are omitted. Otherwise use as many lines of data as required for NLKEL newly placed bar elements.

NUMLK(1) First newly placed bar element

NUMLK(2) Second newly placed bar element

etc. Continue on for NLKEL number of lines of data.

C.4.10.3 Layer and Load Case Control Data

NUMFC Number of nodal point forces in this load case.

NUMPC Number of distributed loads in this load case.

NUMBWP Number of nodal points subjected to a change in static water pressure in this load case. (This number must be equal to or less than NUMSWP on the first control data line.

NUMBYP The number of elements which, during this load case, are submerged below a rising reservoir or which emerge above a falling reservoir.

NEWLAY 0 if there are no newly added elements in this step, greater than 0 if there are new elements added.

C.4.10.4 Buoyancy Force Data

If NUMBYP = 0, these data are omitted.

First Data

DELGAM Change in unit weight due to submergence or drawdown.

DELGAM = $\gamma_w - \gamma_m$ for submerged elements. This value is negative.

DELGAM = $\gamma_m + \gamma_w - \gamma_{sat}$ for elements which were below water before drawdown and are above water after. This value is positive.

Second Data

NBYEL(1) Element number of first element which is submerged beneath a rising water level or exposed above a falling water level.

NBYEL(2) etc.

C.4.10.5 Nodal Point Force Data

If NUMFC = 0, these data are omitted. Otherwise need NUMFC lines of data.

N Nodal point number where force is applied

FX(N) X-component of force applied at N (+ to right).

FY(N) Y-component of force applied at N (+ up).

C.4.10.6 Distributed Load Data

If NUMPC = 0, these data are omitted. Otherwise need NUMPC lines of data.

INODE Nodal point number at I

JNODE Nodal point number at J

PRESI Normal pressure at nodal point I

PRESJ Normal pressure at nodal point J

Definition of points I and J, and examples of data for distributed load cases are shown in Figure C-7.

C.4.10.7 Reservoir Level Change Data

If NUMBWP = 0, these data are omitted.

First Data

ISIGN ISIGN = 1 if water pressure acts in +x direction on structure. ISIGN = -1 if water pressure acts in -x direction.

LEVOLD Nodal point number at the same elevation as the old water level (before this load case).

NEWLEV Nodal point number at the same elevation as the new water surface.

These data define changes in boundary pressure due to rising or falling water level. See Figure C-8 for an example of data for a change in reservoir level.

C.4.10.8 Time Period Data

NSTEP Every load step is divided into NSTEP parts, each of which is analyzed separately, to improve computational accuracy.

NTIME Length of time interval encompassed by this loading increment.

Whenever it is desired to obtain output for various times with no changes in loading, water levels or other conditions, save consolidation, another set of these data must be input.

Appendix D

USER'S GUIDE FOR PROGRAM CONSAX86

D.1 Introduction

The program CONSAX86 is an axisymmetric finite element computer program for analysis of stresses, displacements and consolidation in saturated and partly saturated earth masses. The program can be used to analyze consolidation in soil mechanics problems that have an axisymmetric geometry. The program treats the coupled problem of deformation and fluid flow, and can be used to calculate movements and pore pressures under undrained, partly drained and fully drained conditions. Reinforced soil structures can be analyzed using membrane elements (see Appendix B).

CONSAX86 was originally developed by Chang and Duncan (1977) and was later modified by D'Orazio and Duncan (1982). The program follows the general programming concepts and solution techniques developed by Wilson (1970) and Bathe and Wilson (1976). The present version incorporates a membrane element to model reinforcement, and provides enhanced source code documentation and efficiency.

D.2 Program Operation

D.2.1 Systems and Sign Convention

The global coordinate system is a right handed R-Z system with R increasing to the right and Z increasing vertically.

Soil element and interface normal stresses are positive in compression and negative in tension. The soil stresses are all effective stresses. Positive pore pressures are compressive. Total stresses are obtained by adding pore pressures at the center of elements to the effective soil stresses.

Membrane element forces are output in a local coordinate system. Radial force is positive if the member is in compression and negative if in tension.

D.2.2 Storage Allocation

Dynamic storage allocation (Bathe and Wilson 1976) is used within the program and storage is allocated at the time of execution. The storage can be readily adjusted through the COMMON (A) statement in the source code. Storage requirements are checked immediately after reading the control data, and if insufficient, an error message printed detailing the minimum storage requirements for the problem and execution is halted.

The equation-solving subroutines use only one-half of the full banded stiffness matrix. Secondary storage (disk or tape storage) is used to

minimize the amount of core storage required by solving the equations by blocks (Wilson et al. 1974). The smaller the number of equations per block, the greater is the required number of transfers between core and secondary storage, and the more costly is the solution procedure. Thus, the more storage allocation exceeds the minimum value, the larger is the number of equations per block, and hence the shorter is the solution time.

D.2.3 Element Types

CONSAX86 has three types of elements as follows:

1. Soil elements are four-to-eight variable node, two-dimensional, isoparametric elements as described by Bathe and Wilson (1976). Each node may also have a pore pressure degree-of-freedom. Any number of nodes from four to eight can be specified for each element. Triangular shaped elements can be formed by superimposing nodes. The nodal point numbers must be specified in the order I, II, III, IV, V, VI, VII, VIII as shown in the upper part of Figure D-1. For an element with fewer than eight nodes, the nodal point numbers of the omitted nodes are set equal to zero, as shown in the bottom of Figure D-1. For triangular elements, the nodal point number III must be equal to the nodal point number IV.

2. Membrane elements are two node elements with radial stiffness only (no flexural or shear resistance), and may be used to connect any two nodal points.

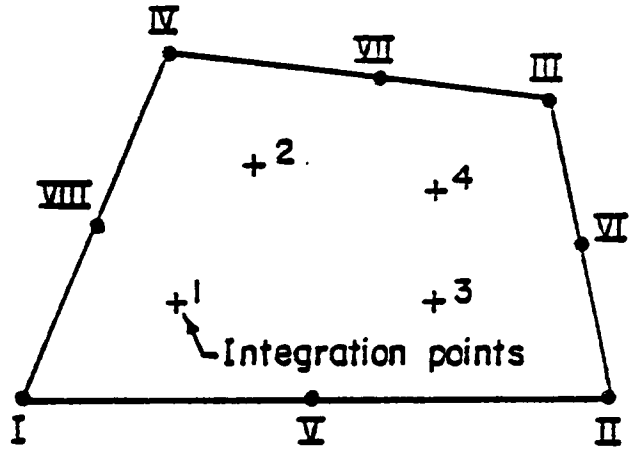

Note: Node I must be in lower left corner of element.

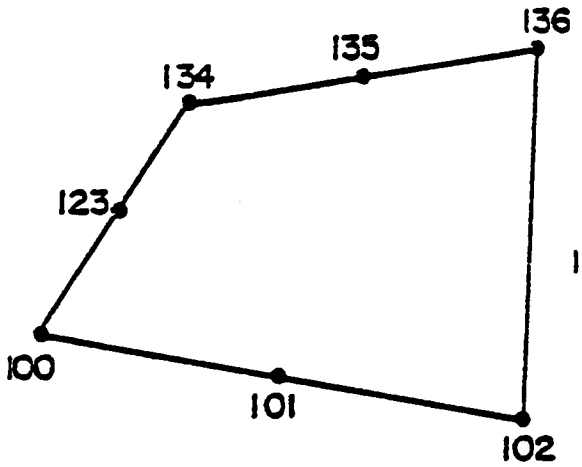

NEL = 7

I	II	III	IV	V	VI	VII	VIII
100	102	136	134	101	0	135	123

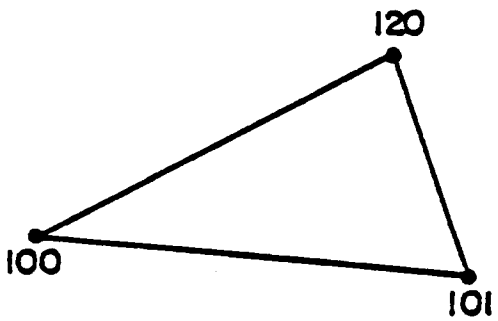

NEL = 4

I	II	III	IV	V	VI	VII	VIII
100	101	120	120	0	0	0	0

Figure D-1 Nodal point numbering for two-dimensional elements.

3. Linkage elements may be used to represent interfaces between a structure and adjacent soil or between zones within a soil mass. As shown in Figure D-2, a linkage element connects two nodal points called I and J, which may have identical coordinate values. The stiffness of the linkage element represents the properties of a section of the interface. The length and orientation of the section of the interface represented by the linkage element are defined by two nodal points called NI and NJ. The orientation of the interface in along the line NI-NJ. The shear direction is parallel to NI-NJ, and the normal direction is perpendicular to NI-NJ. The length of the section of the interface is one-half of the distance from NI to NJ. The examples of linkage element numbering shown in Figure D-3 illustrate how the orientations of linkage elements and the lengths of sections of the interface they represent are defined in terms of nodes I, J, NI and NJ.

D.2.4 Meshes

A example mesh for analysis of a tank foundation is shown in Figure D-4. The nodal points are numbered from left to right across each level. Elements are numbered in the same way, with the element numbers increasing from left to right in each layer and from the bottom up. For accurate displacements, stresses, and pore pressures, loads should be applied in six or more increments.

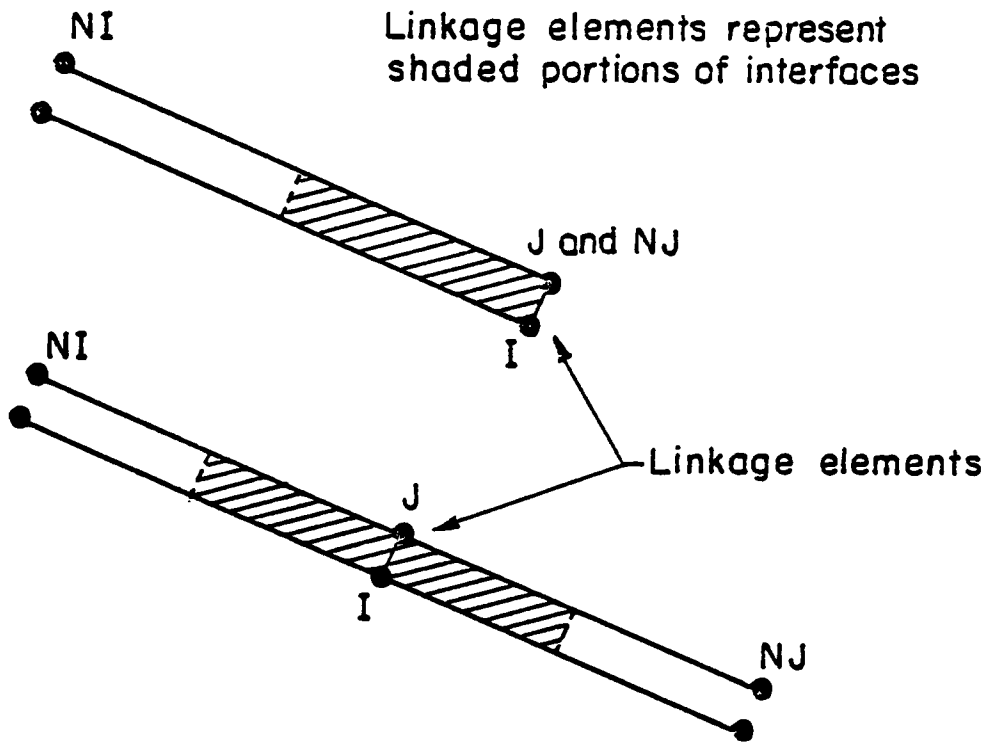

LINKAGE ELEMENTS CONNECT NODE I WITH NODE J

LENGTH = $\frac{1}{2}$ DISTANCE FROM NI TO NJ

SHEAR DIRECTION PARALLEL TO LINE FROM NI TO NJ

NORMAL DIRECTION PERPENDICULAR TO LINE FROM NI TO NJ

Figure D-2 Nodal point numbering conventions for linkage elements.

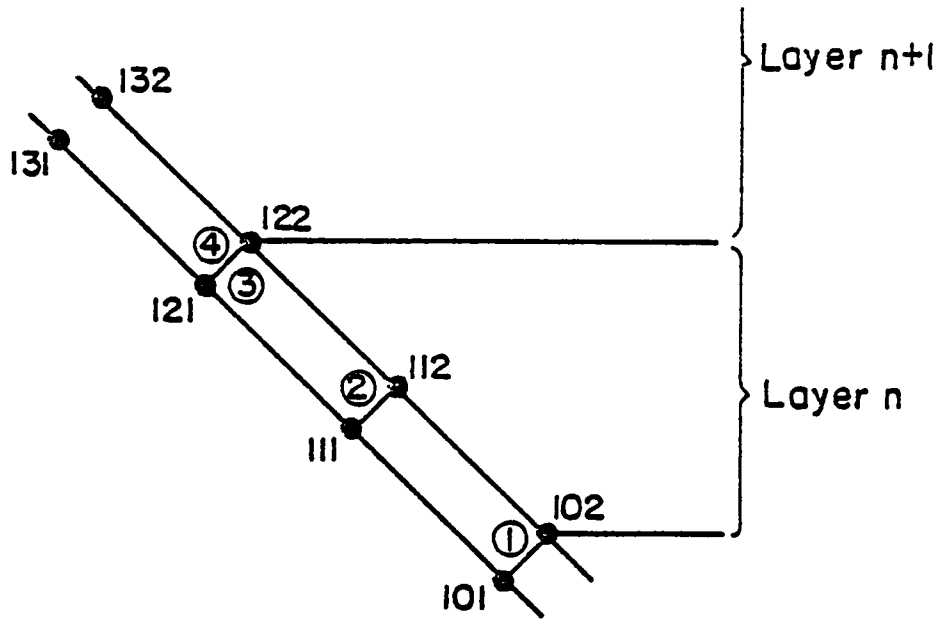

Linkage Element	I	J	NI	NJ
1	101	102	112	102
2	111	112	122	102
3	121	122	122	112
4	121	122	132	122

Linkage element ③ represents half of interface from node 112 to node 122, and would be added to mesh with layer n. Linkage element ④ represents half of interface from node 122 to node 132, and would be added to mesh with layer n + 1.

Nodes 101 and 102, 111 and 112, etc., may have same coordinates.

Figure D-3 Linkage element example.

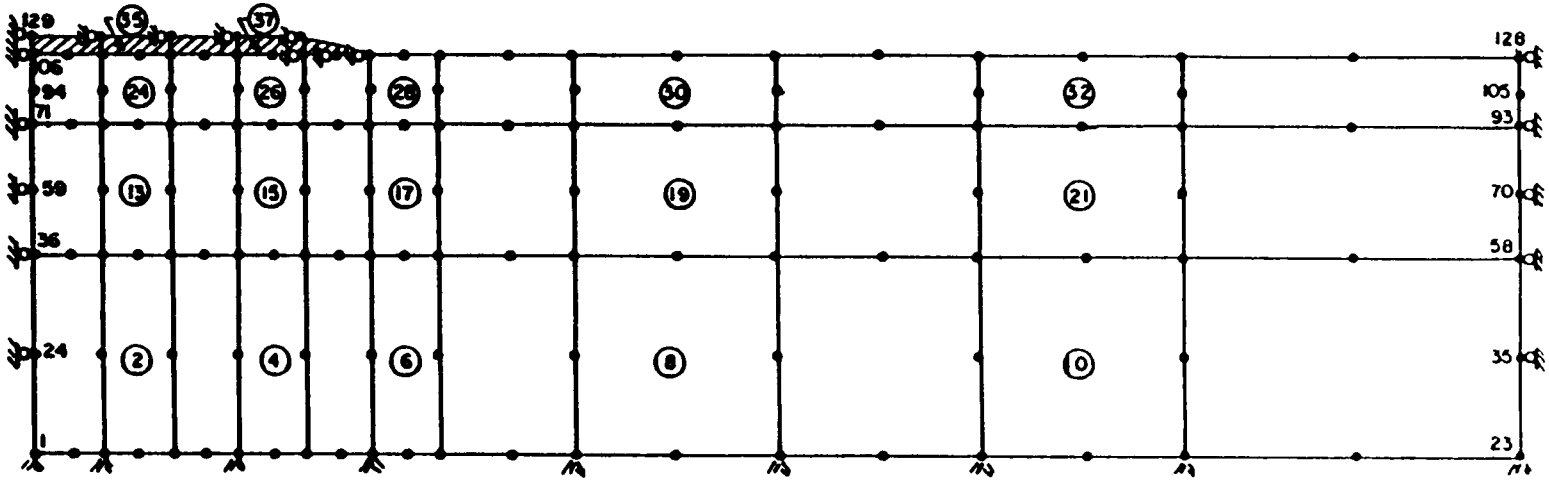

Elements 1-33, clay soil of finite permeability - elements with mid-side nodes are used

Elements 34-38, sandy soil of infinite permeability - elements without mid-side nodes are used

Figure D-4 Example mesh for tank foundation.

Pre-existing elements in any configuration may be included within or beneath the embankment. As shown in Figure D-5, the pre-existing part of the mesh may be beneath the embankment, adjacent to the embankment, or entirely within the final geometry of the complete embankment, and it may consist of more than one part. The initial stresses, displacement, and pore pressures may be generated by earlier analyses with CONSAX86 or by hand calculations. The strains in the pre-existing part can be set equal to zero by the program, or non-zero values can be read in by the user, at the user's option.

D.2.5 Increments

An increment may consist of the placement of a layer of fill on a foundation, or of an application of loads to a mesh. Placement of a layer of fill is simulated by applying forces to represent the weight of the added layer. The layer being placed is assigned very small modulus values to simulate the fact that a newly added layer of uncompacted fill has very low stiffness. Each element in the newly placed layer is assigned stresses consistent with the overburden pressure at its center. The strains in the newly placed elements are set equal to zero, and taken as the reference state of strain. For accurate results, it is best to add only one layer of elements at a time, and in general, six or more layers of elements in the mesh will provide reasonably accurate results.

A layer to be added in an increment is defined by specifying the first and last elements to be added [NOMEL(LN,1) and NOMEL(LN,2)], the first

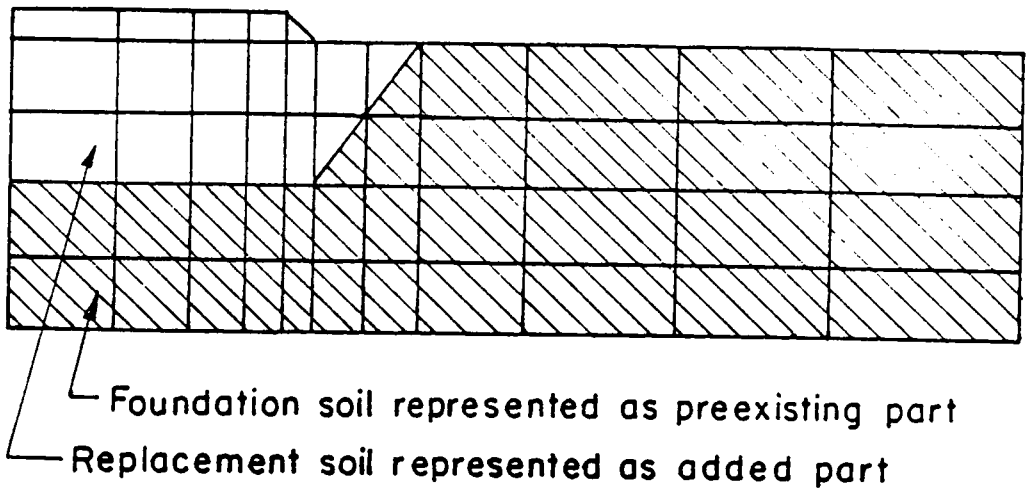

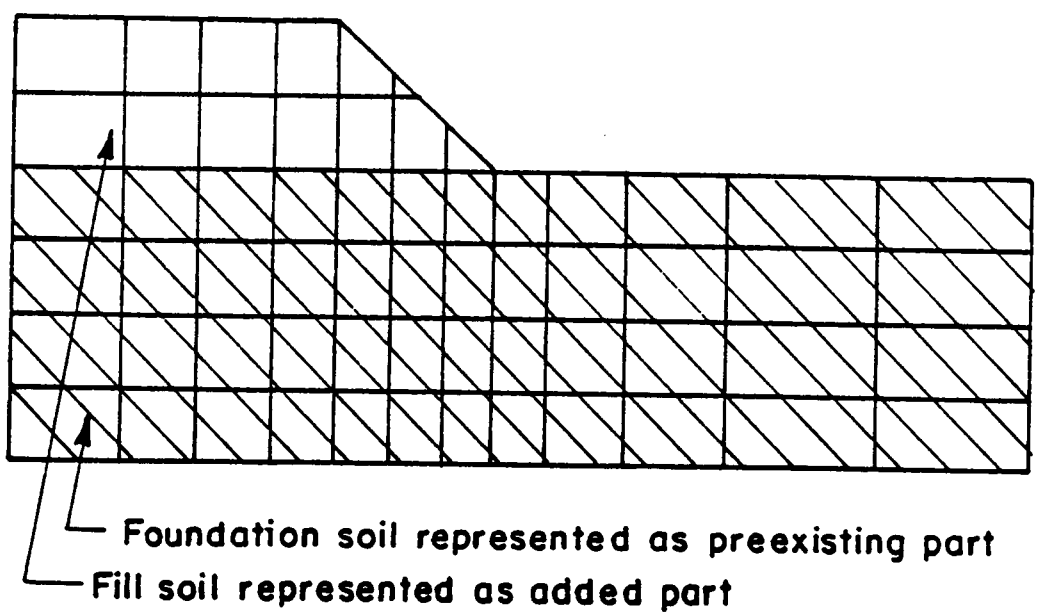

Figure D-5 Example meshes with pre-existing parts.

and layer nodal points to be added [NOMNP(LN,1) and NOMNP(LN,2)], and by data which define the position of the surface of the newly added layer, as shown in Figure D-6. The program assumes that all of the elements between and including those specified as the first and last are being added, and the same is true for nodal points. Therefore meshes must be numbered so that this convention is followed.

The surface of the new layer is specified by four nodes [NPHUMP(LN,1 to 4)] which define what is called the humped surface. This surface defines the top of the newly placed layer for purposes of calculating overburden pressures in newly placed elements. To the left of the first nodal point and to the right of the last nodal point which define the surface, the surface is assumed to be level.

The nodal points having pore pressure degrees of freedom and which are on the surface of the layer are specified in NOMNP. All of the nodes between NOMNP(LN,3) and NOMNP(LN,4) are assumed to be on the surface of the layer and are assigned zero initial pore pressures.

Loads applied to a mesh may be specified in terms of nodal point forces or boundary pressures. Nodal point forces have units of force, and each force acts over a length equal to 2π times the radial coordinate of the nodal point.

Distributed loads are input by specifying two nodal points (I and J) on one side of an element and the pressures (PRESI and PRESJ) at these nodes. As shown in Figure D-7, the sign convention is such that, with I on the left and J on the right, the load is directed toward the observer.

Quantity	Specifies	Value For LN = 1	Value For LN = 2
NOMEL(LN,1)	First added element	1	10
NOMEL(LN,2)	Last added element	9	15
NOMNP(LN,1)	First added nodal point	1	26
NCMNP(LN,2)	Last added nodal point	25	35
NOMNP(LN,3)	First nodal point to be assigned zero pore pressure	20	31
NCMNP(LN,4)	Last nodal point to be assigned zero pore pressure	22	33
NPHUMP(LN,1)	First nodal point on humped surface	1	17
NPHUMP(LN,2)	Second	16	29
NPHUMP(LN,3)	Third	25	35
NPHUMP(LN,4)	Fourth nodal point on humped surface	12	25

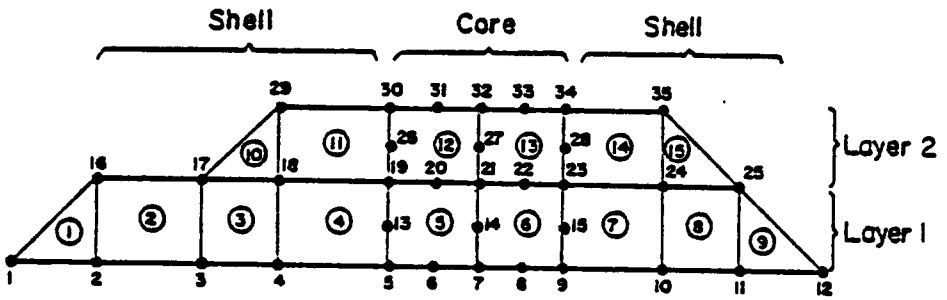

Note: Nodal points which are assigned pore pressure degrees of freedom, and which are at the top of a layer, should be defined in NOMNP so they will be assigned zero pore pressures initially. The humped surface defines the upper boundary of the new layer for purposes of calculating initial stresses in the elements.

Figure D-6 Example data for construction layers.

In this option, the program automatically calculates the radii of points I and J and assigns the appropriate nodal point forces.

The data required to specify a constant non-zero pore pressure condition is shown in Figure D-8. In this figure, the seepage from and the expansion of a borehole due to water pressure is modeled. The number of nodal points that have a constant non-zero pore pressure is NUMSWP. The value of constant pore pressure is maintained for the duration of the load case. A value of NUMBWP = 1 indicates that there are nodal points that have a constant non-zero pore pressure for this load case.

D.3 Program Organization

The main program (CONSAX86) reads and prints the control data and monitors all operations by calling the subroutines in the specified order.

1. Subroutine LAYOUT controls the subroutines which read the input data. Subroutine LAYOUT calls INPTNP to read and print nodal point data, MATIN to read and print soil material property data, MEMBIN to read and print membrane element data, LINKIN to read and print linkage element data, PREXIN to read and print pre-existing element data, ELEMIN to read and print soil element data, and CLBAND to calculate the bandwidth for the problem. Storage requirements are calculated and if the problem requires more storage, a message is printed and execution halted.

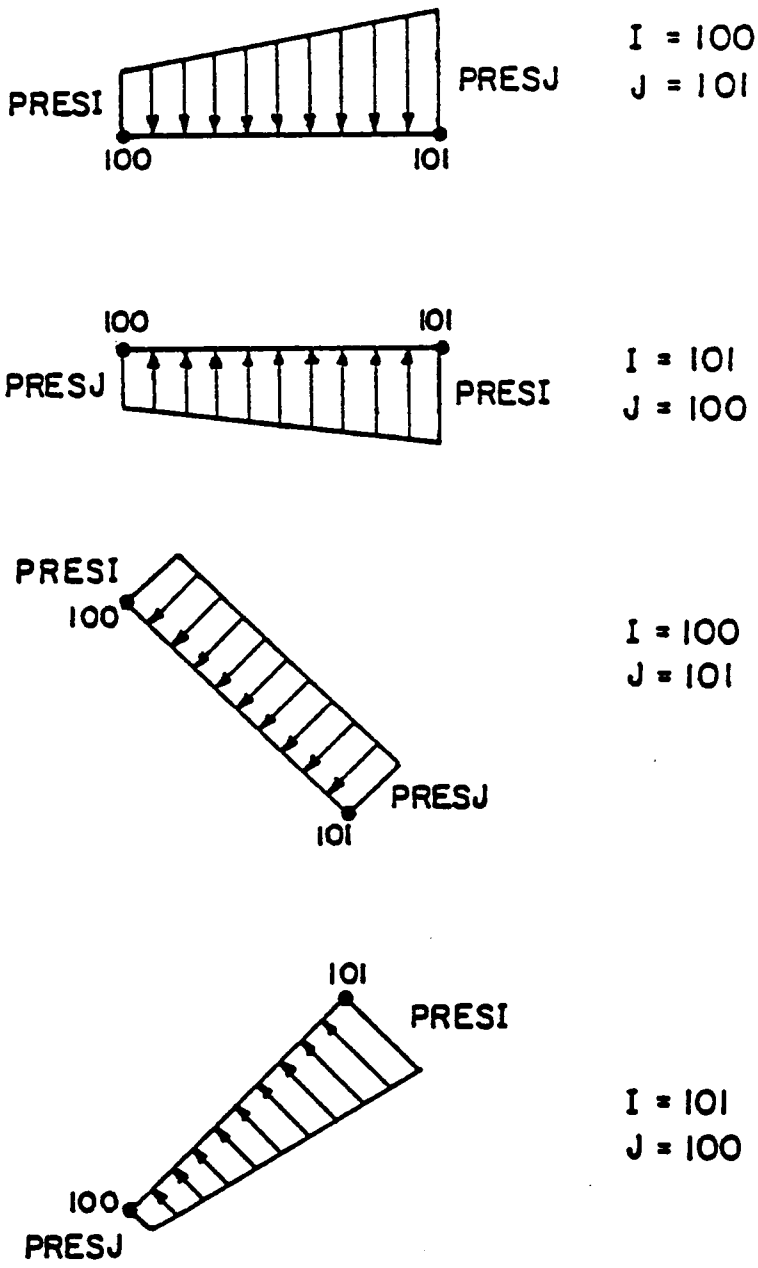

Figure D-7 Example data for distributed loads.

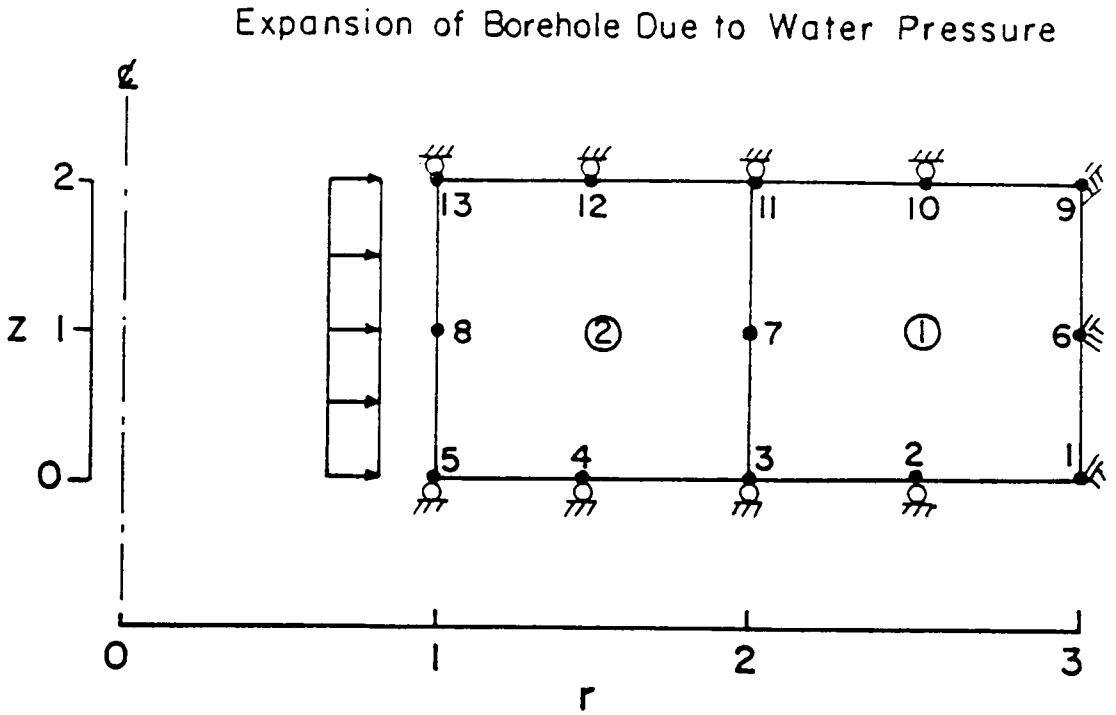

NUMSWP = 3
NUMPC = 2
NUMBWP = 1

I	J	PRESI	PRESJ
5	8	100	100
8	13	100	100

NPSWP	PFPR
5	100
8	100
13	100

Figure D-8 Example data for constant non-zero pore pressure.

2. Subroutine INITL reads and/or calculates the initial values of stresses, strains, displacements and pore pressures for pre-existing elements and added layer elements.

3. Subroutine FORMB establishes the strain-displacement matrix for the soil elements by calling BMATAX, which forms the strain-displacement matrix for a four- to eight-node isoparametric, quadrilateral element. BMATAX calls JACOBI to form the Jacobian, which calls SHAPE to calculate the shape functions.

4. Subroutine CALBLK reads the control data for each increment and determines the number of elements and nodal points being analyzed, the number of elements and nodal points in the pre-existing part and added layers, the number of equations, the number of equations in each block, and the number of blocks for each increment.

5. Subroutine FVECT calculates nodal point forces due to weights of added elements and reads and prints concentrated load data and boundary pressure data.

6. Subroutine ELSTFF formulates the stiffness matrix for each element. ELSTFF call STST to form the stress-strain relationship for the soil elements and calls MODIFY to modify the load vector for each time step. STST calls POICAL and LAMCAL to compute the current values of Poisson's ratio and lambda, calls ELAST to calculate the elastic part of the stress-strain relationship, and calls CAMCLY to calculate the

elasto-plastic stress-strain relationship. ELSTFF calls QK to calculate the current compressibility and permeability of the pore fluid in each element.

7. Subroutine ADDSTF forms the global stiffness matrix. The soil element stiffness values are read from tape and the stiffness values for membrane and linkage elements are found by calling MBSTIF and LKSTIF.

8. Subroutine TRIAFAC triangulizes the global stiffness matrix.

9. Subroutine REDVK back substitutes and solves the equations for displacement and pore pressure.

10. Subroutine RESULT calculates the current values of stress and strain. RESULT calls OUTPUT to print out the results.

D.4 Data Input Guide

D.4.1 Control Data

D.4.1.1 Heading Data (72A)

HEAD Title for program identification.

D.4.1.2 First Control Data

NUMELT Total number of soil elements in the complete mesh.

NUMNPT Total number of nodal points in the complete mesh.

NUMMAT Number of different soil material types.

NUMCEL Number of soil elements in the pre-existing part.

NUMCNP Number of nodal points in the pre-existing part.

NLAY Number of construction layer increments.

NFORCE Number of load increments after construction.

NUMSWP Total number of nodal points that have a constant non-zero pore pressure during any of the steps of the analysis.

D.4.1.3 Second Control Data

NMBELT Total number of membrane elements in the complete mesh.

NMBMAT Number of different membrane material types.

NUMCMB Number of membrane elements in the pre-existing part.

NLKELT Total number of linkage elements in the complete mesh.

NLKMAT Number of different linkage material types.

NUMCLK Number of linkage elements in the pre-existing part.

D.4.2 Nodal point and boundary condition data.

N Nodal point number.

R(N) R-coordinate (+ to the right).

Z(N) Z-coordinate (+ up).

ID(N,1) Boundary condition code for displacement in the r-direction.

ID(N,2) Boundary condition code for displacement in the z-direction.

ID(N,3) Boundary condition code for pore pressure.

Nodal points must be read in sequence. If nodal point data are omitted, the coordinates of a series of nodal points are generated automatically at equal spacing between those specified. The boundary condition codes for the generated nodal points are set equal to the boundary condition codes for the previous nodal point. The first and last points must be specified.

The boundary condition code convention is as follows:

Quantity	Condition	Code
r displacement	always zero	ID (N,1) = 1
	may be non-zero	ID (N,1) = 0
z displacement	always zero	ID (N,2) = 1
	may be non-zero	ID (N,2) = 0
pore pressure	always zero	ID (N,3) = 1
	may be non-zero	ID (N,3) = 0

D.4.3 Material Property Data

D.4.3.1 Units Conversion Data

PATM Atmospheric pressure expressed in the system of units used in the problem.

GAMAW Unit weight of water expressed in the system of units used.

For example:

off Length	Unit Weight	Cohesion	Stiffness	Atmospheric Pressure	Unit weight of Water
ft	ton/ft	ton/ft	ton/ft	1.058	0.0312
ft	kip/ft	kip/ft	kip/ft	2.116	0.0624
ft	lb/ft	lb/ft	lb/ft	2116.2	62.4
m	ton/m	ton/ft	ton/ft	10.33	1.00
M	kN/m	kN/m	kN/m	101.3	9.807
cm	kg/cm	kg/cm	kg/cm	1.033	0.001
in	lb/in	psi	lb/in	14.70	0.0361

D.4.3.2 Soil Material Properties

9 lines of data are required for each material.

M Material type number (MATNO).

EMPR(M,1) Permeability code (PCODE).
0.0 - for a material which is to be assumed infinitely permeable, for example, the granular shell material in a zoned earth dam.
1.0 - for a material which is not infinitely permeable, for example, the core material in a zoned earth dam.

EMPR(M,2) Unit weight (moist unit weight), γ (GAMMAW).

EMPR(M,3) Cam clay soil parameter, κ (KAPPA).

EMPR(M,5) Intercept, p_r (effective stress) (PRINTR).

EMPR(M,6) Slope, $M_{triaxial}$ (effective stress) (MTRIAX).

EMPR(M,9) Horizontal saturated permeability, k_{hs} (PERMX).

EMPR(M,10) Vertical saturated permeability, k_{vs} (PERMZ).

EMPR(M,11) Degree of saturation at which the water begins to move freely, S_f (SF).

EMPR(M,12) Initial void ratio, e_o (VOID).

EMPR(M,13) Initial degree of saturation, S_o (SATURN).

EMPR(M,14) Pressure at which break in slope occurs, p'_{break} (PBREAK).

EMPR(M,15) Intercept after break, p_r (PRINTR).

EMPR(M,16) Slope after break, $M_{triaxial}$ (MTRIAX).

EMPR(M,17) Preconsolidation pressure, P'_p (mean normal stress) (PO). (PO).

EMPR(M,18) Tensile strength, σ_t (TENSTR).

The above values of initial void ratio, initial degree of saturation, and preconsolidation pressure are used only for material properties of elements that are not preexisting. The values of these properties for preexisting elements are submitted in data 9b.

Second through fifth lines of data:

These data describe as many as 16 points on the p'_o -λ curve for the material.

Second and third lines of data:

EMPR(M,31) Pressure, p'_o corresponding to the first λ point.

EMPR(M,32) Pressure, p'_o corresponding to the second λ point.

etc. continue for as many points as needed to dexcribe the $p'_o - \lambda$ curve. Two lines of data are required even in the case where the $p'_o - \lambda$ curve is defined by eight or fewer

points. If eight or fewer points are used, the second line is blank.

Fourth and fifth lines of data:

EMPR(M,47) Slope, λ of the first point.

EMPR(M,48) Slope, λ of the second point.

etc. Two lines of data are required even in the case where the $p'_o - \lambda$ curve is defined by eight or fewer points. If eight or fewer points are used, the second line is blank.

Sixth through ninth lines of data:

These lines describe as many as 16 points on the p'-v curve for the material.

Sixth and seventh lines of data:

EMPR(M,63) Mean normal pressure, p' corresponding to the first point.

EMPR(M,64) Mean normal pressure, p' corresponding to the second point.

etc. Two lines are required even in the case where the p'-v curve is defined by eight or fewer points. If eight or fewer points are used, the second line is blank.

Eighth and ninth lines of data:

EMPR(M,79) Poisson's ratio corresponding to the first point.

EMPR(M,80) Poisson's ratio corresponding to the second point.

etc. Two lines of data are required even in the case where the $p'_o - v$ curve is defined by eight or fewer points. If eight or fewer points are used, the second line is blank.

D.4.4 Membrane Element Data

If NMBELT = 0, these data are omitted.

D.4.4.1 Material Property Data

N Material type number.

PROPMB(N,1) Elastic modulus of the membrane.

PROPMB(N,2) Poisson's ratio of the membrane.

D.4.4.2 Membrane Element Data

One line of data for each membrane element.

M Element number.

INPMB(M,1) Material type number.

INPMB(M,2) Nodal point number for node I.

INPMB(M,3) Nodal point number for node J.

D.4.4.3 Initial Membrane Force Data

One line of data for each membrane element.

N Membrane element number.

SMBTOT Initial force in pre-existing membrane element number N.

D.4.5 Linkage Element Data

If NLKELT = 0, these data are omitted.

D.4.5.1 Material Property Data

N Material type number.

PROPLK(N,3) Cohesion of linkage material.

PROPLK(N,4) Friction angle of linkage material.
Note: PROPLK(N,1) and PROPLK(N,2) are the normal and shear stiffness of the link and are set in the program.

D.4.5.2 Linkage Element Data

One line of data for each linkage element.

M Element number.

INPLK(M,1) Material type number.

INPLK(M,2) Nodal point number for node I.

INPLK(M,3) Nodal point number for node J.

NI Nodal point number for node NI.

NJ Nodal point number for node NJ.
Definition of points I, J, NI, and NJ, and example data are shown in Figures D-2 and D-3.

D.4.5.3 Pre-existing Linkage Element Data

If NUMCLK = 0, these data are omitted.
Use as many line of data as required for NUMCLK linkage elements.

LINKC(1) Element number of first pre-existing element number.

LINKC(2) Element number of second pre-existing element number.

LINKC(N) Etc. for N pre-existing elements.

D.4.5.4 Pre-existing Linkage Element Stress Data

If NUMCLK = 0, these data are omitted.
Use one line of data for each pre-existing linkage element.

N Element number.

STRSLK(N,1) Initial normal linkage stress.

STRSLK(N,2) Initial shear linkage stress.

D.4.6 Pre-existing Element and Nodal Point Data

D.4.6.1 Pre-existing Soil Element Data

If NUMCEL = 0, these data are omitted. Use as many lines of data as required for NUMCEL elements.

ICEL Number of first pre-existing element.

JCEL Number of second pre-existing element.
Element numbers are generated in sequence between those specified, and one sequence of elements is defined by each line. For an isolated pre-existing element, ICEL and JCEL are the same, describing a sequence of one. Use one line per sequence or series of elements.

D.4.6.2 Pre-existing Nodal Point Data

If NUMCNP = 0, these data are omitted. Use as many lines of data as required for NUMCNP elements.

ICNP Number of first pre-existing nodal point.

JCNP Number of second pre-existing nodal point.
Nodal point numbers are generated in sequence between those specified, and one sequence of nodal points is defined by each line of data. For an isolated pre-existing nodal point, ICNP and JCNP are the same, describing a sequence of one. Use one line per sequence or series of nodal points.

D.4.7 Soil Element Data

One line of data for each element.

M Element number.

NELNP(N) Number of nodes in this element (4-8).

MTYPE(N) Material type number.

INP(N,1) Nodal point number I.

INP(N,2) Nodal point number II.

INP(N,3) Nodal point number III.

INP(N,4) Nodal point number IV.

INP(N,5) Nodal point number V.

INP(N,6) Nodal point number VI.

INP(N,7) Nodal point number VII.

INP(N,8) Nodal point number VIII.

Soil element data must be read in sequence. The nodal point numbers must be specified in the order I,II,III,IV,V, VI,VII,VIII as shown in the upper part of Figure D-1. For an element with fewer than eight nodes, the nodal point numbers of the omitted nodes must be specified as zero. For triangular elements, the nodal point number III must be equal to the nodal point number IV, as shown at the bottom of Figure D-1. The locations of the integration points, where pore pressures are calculated, are also shown in Figure D-1.

N = 1 for the first soil element.
N = 2 for the second soil element.
etc.

D.4.8 Construction Layer Element and Nodal Point Data.

One line of data for each construction layer.
If NLAY = 0, these data are omitted.

LN Construction layer number. Layer numbers increase upward from the bottom.

NOMEL(LN,1) Smallest soil element number of the newly placed elements in this layer.

NOMEL(LN,2) Largest soil element number of the newly placed elements in this layer.

NOMEL(LN,3) Smallest membrane element number of the newly placed membrane elements in this layer.

NOMEL(LN,4) Largest membrane element number of the newly placed membrane elements in this layer.

NOMNP(LN,1) Smallest nodal point number of the newly placed nodal points in this layer.

NOMNP(LN,2) Largest nodal point number of the newly placed nodal points in this layer.

NOMNP(LN,3) Smallest nodal point number on the new boundary surface with pore pressure degree of freedom.

NOMNP(LN,4) Largest nodal point number on the new boundary surface with pore pressure degree of freedom.

NPHUMP(LN,1) First nodal point on the humped surface.

NPHUMP(LN,2) Second nodal point on the humped surface.

NPHUMP(LN,3) Third nodal point on the humped surface.

NPHUMP(LN,4) Fourth nodal point on the humped surface.

Do not use vertical segments in the humped surface, because this will result in division by zero. See Figure D-6 for an example of construction layer data input format.

D.4.9 Stress, Strain, Displacement and Pore Pressure Data for Pre-existing Part.

If NUMCEL = 0, these data are omitted.

D.4.9.1 Control Data

NMODE Strain code of input data.
0 = stresses, displacements, pore pressures, and strains are to be read.
1 = stresses, displacements, and pore pressures are to be read and strains are set equal to zero.

D.4.9.2 Initial Stress and Property Data for Soil Elements.

NUMCEL lines of data are needed unless generation procedure is used.

N Element Number.

STRESS(N,1) σ'_r

STRESS(N,2) σ'_z

STRESS(N,3) σ'_θ

STRESS(N,4) τ_{rz}

STRESS(N,5) Pore pressure at center of element.

VOID(N) Initial void ratio, e_o

SATURN(n) Initial degree of saturation, S_o

PO(N) Preconsolidation mean stress, P_o

Compressive stresses are positive. The r and z coordinates are in the plane of the analysis, θ is normal to the plane.

If initial stress and property data are omitted, the program assigns the initial stress and properties of the immediately preceding element to the omitted elements.

D.4.9.3 Initial Displacement and Pore Pressure Data.

Need NUMCNP lines of data (if generation is not used).

N Nodal point number

U(N) Initial pore pressure at node N.

DISP(N,1) Initial R-displacement.

DISP(N,2) Initial Z-displacement.

If initial displacements and pore pressure data are omitted, the program assigns the initial displacement and pore pressures of the node that immediately precedes the omitted nodes. Data for the first and last nodes must be input.

D.4.9.4 Initial Strain Data.

If NMODL = 1, these data are omitted. Otherwise NUMCEL lines of data are required (if generation is not used).

N Element number

STRAIN(N,1) Initial value of ε_r

STRAIN(N,2) Initial value of ε_z

STRAIN(N,3) Initial value of ε_θ

STRAIN(N,4) Initial value of γ_{rz}

If initial strain are needed, generation of in between data can be program assigns the initial strain of the node that immediately precedes the omitted nodes. Data for the first and last nodes must be input.

D.4.10 Layer, Force and Time Increment Data

Need (NLAY + NFORCE) sets of data, each consisting of the following 8 lines of data.

D.4.10.1 Newly Placed Membrane Element Data. (skip if NMBELT = 0).

First Data

NMBEL Number of newly placed membrane elements in this step.

Second Data: If NMBEL = 0, these data are omitted. Otherwise use as many lines of data as required for NMBEL newly placed membrane elements.

NUMMB(1) First newly placed membrane element

NUMMB(2) Second newly placed membrane element

etc. Continue on for NMBEL number of lines of data.

0

D.4.10.2 Newly Placed Linkage Element Data. (skip if NLKELT = 0).

First Data

NLKEL Number of newly placed linkage elements in this step.

Second Data: If NLKEL = 0, these data are omitted. Otherwise use as many lines of data as required for NLKEL newly placed membrane elements.

NUMLK(1) First newly placed membrane element

NUMLK(2) Second newly placed membrane element

etc. Continue on for NLKEL number of lines of data.

D.4.10.3 Layer and Load Case Control Data

NUMFC Number of nodal point forces in this load case.

NUMPC Number of distributed loads in this load case.

NUMBWP 0 if there are no points that have a constant non-zero pore pressure in this load case. 1 if there are points that have a constant non-zero pore pressure in this load case.

NEWLAY 0 if there are no newly added elements in this step, greater than 0 if there are new elements added.

D.4.10.4 Nodal Point Force Data

If NUMFC = 0, these data are omitted. Otherwise need NUMFC lines of data.

N Nodal point number where force is applied

FR(N) R-component of force applied at N (+ to right).

FZ(N) Z-component of force applied at N (+ up).

D.4.10.5 Distributed Load Data

If NUMPC = 0, these data are omitted. Otherwise need NUMPC lines of data.

INODE Nodal point number at I

JNODE Nodal point number at J

PRESI Normal pressure at nodal point I

PRESJ Normal pressure at nodal point J
Definition of points I and J, and examples of data for distributed load cases are shown in Figure D-7.

D.4.10.6 Constant Pore Pressure Data

If NUMBWP = 0, these data are omitted. Otherwise need NUMBWP lines of data.

NPSWP(I) Nodal point number at which pore pressure remains constant

PFPR(I) Pore pressure at the nodal point.

D.4.10.7 Time Period Data

NSTEP Every load step is divided into NSTEP parts, each of which is analyzed separately, to improve computational accuracy.

NTIME Length of time interval encompassed by this loading increment.

Whenever it is desired to obtain output for various times with no changes in loading, water levels or other conditions, save consolidation, another set of these data must be input.

The vita has been removed from the scanned document